UNIVERSITE DE STRASBOURG

Ecole de doctorale des Sciences de la Vie et de la santé

Thèse de doctorat

Présentée par

Ahmad KOBIITA

Soutenue le : 12 Février 2016

En vue de l'obtention du grade de
Docteur de l'Université de Strasbourg I
Discipline : Sciences du vivant
Spécialité : Aspects Moléculaires et Cellulaires de la Biologie

"Shifting eating creates a misalignment of peripheral and central circadian clocks, which leads to a metabolic syndrome"

" Un décalage de l'alimentation déclenche une asynchronie entre l'horloge circadienne centrale et les horloges périphériques et engendre un syndrome métabolique "

Thèse dirigée par: **Pr. Pierre CHAMBON**, IGBMC, Illkirch, France
Rapporteur externe: **Pr. Walter WAHLI**, Lee Kong Chian School of Medicine, Singapore
Rapporteur externe: **Pr. Filippo RIJLI**, Institute Friedrich Miescher, Basel, Switzerland
Examinateur: **Pr. Romeo RICCI**, IGBMC, Illkirch, France

"Early to bed and early to rise, makes a man healthy, wealthy and wise"

Benjamin Franklin (1706-1790)

Table of contents……1

Acknowledgments

First of all, I would like to express my sincere gratitude to Professor Pierre CHAMBON to give me the opportunity to work and learn under his supervision and for his valuable guidance, discussions and encouragement during my PhD.

I also would like to thank Dr Daniel METZGER for his support during my PhD.

I would like to thank Pr Walter WAHLI and Pr Filippo RIJLI for accepting to be the external referees and Pr Romeo RICCI for accepting to be the internal referee of my thesis work.

Big thanks to all members of CHAMBON/METZGER lab especially to Atish, Laetitia, Manohar, Nisha, and Jacky for their useful discussion and their support during my PhD.

I also would like to thank Valérie for her assistance.

Big thanks to the personnel of IGBMC-ICS care facilities.

I am especially grateful to my parents, my two sisters and my friends for fully supporting me in all these years.

Résumé en Français

Depuis sa création, la vie sur terre est rythmée par le cycle circadien qui en 24 heures correspond à l'alternance du jour et de la nuit. La rotation de la terre autour de son axe soumet la majeure partie de la surface terrestre à une alternance de clarté et d'obscurité. Le comportement et la physiologie de la plupart des êtres vivants sur la terre sont affectés en conséquence. Chez les mammifères, chaque cellule possède une horloge moléculaire circadienne qui assure l'alternance régulière de périodes d'activité et de repos d'environ 12 heures. En effet, la plupart des animaux chassent au moment où ils sont actifs et leur aptitude à apercevoir leur proie la plus grande. Par contre d'autres, comme les souris, cherchent à être à l'abri et à éviter d'être aperçus par les prédateurs. L'apport de nourriture étant circadien, de nombreux aspects de la physiologie, la glycémie et l'homéostasie sont également liés à la régulation circadienne. Une propriété importante des rythmes circadiens est qu'ils ne dépendent pas directement de l'alternance du jour et de la nuit, mais sont gouvernés par une horloge endogène qui est capable de conserver une période proche de 24 heures.

En 1971, Konopka et Benzer ont été les premiers à identifier des gènes jouant un rôle dans l'horloge circadienne chez la drosophile. Après cette découverte, une dizaine de gènes impliqués dans la genèse de l'horloge circadienne furent identifiés. Les produits de ces gènes forment des boucles d'auto-activation et d'auto-inhibition transcriptionelles et traductionnelles permettant ainsi la formation d'une période rythmique d'environ 24h. Ces gènes sont exprimés au sein de l'horloge centrale située dans les neurones du noyau suprachiasmatique (NSC) et dans toutes les cellules des tissues de la périphérie. Au niveau moléculaire, les éléments clé du système de l'horloge sont les protéines Clock (Circadian Locomotor Output Cycles Kaput) et Bmal1 (Brain and Muscle Arnt-like Protein 1). Ces dernières agissent comme des facteurs de transcription en se fixant sur la boite régulatrice E (E-Box) de la région promotrice des gènes ''horloges'' Period (Per1, Per2) et Cryptochrome (Cry1, Cry2). Lorsque l'expression des protéines Per et Cry atteint un certain niveau dans le cytoplasme, ces deux protéines se dimérisent et se transloquent dans le noyau en empêchant la fixation du dimère Clock/Bmal1, et en conséquence inhibent leur propre expression. Par ailleurs, l'expression du gène Bmal1 est régulée par l'intermédiaire des facteurs de transcription appartenant à la famille des récepteurs nucléaires orphelins. Il s'agit de RORs (α, β et γ) et de RevErbs (α et β), qui se fixent sur les séquences ROREs (Retinoic acid-related Orphan receptor Response Elements) présentes sur le

promoteur du gène Bmal1. Le récepteur nucléaire RevErbα est un nouveau venu dans l'oscillateur moléculaire qui réprime à son tour l'expression de Bmal1 et par conséquence sa propre expression.

En fait, cette horloge tourne dans des conditions très déterminées, tout en restant synchronisée avec son environnement. Une question très importante est de comprendre comment cette synchronisation est établie entre l'individu et le monde extérieur ?? Cela suggère l'existence d'une voie de signalisation d'entrée par laquelle les stimuli externes (lumière ou autres) ajustent la période de l'horloge interne afin que sa phase reste synchronisée avec son environnement extérieur et d'une autre voie de sortie (vers les organes périphériques) par laquelle cette horloge est capable de générer une réponse optimale de l'ensemble des fonctions physiologiques de l'organisme.

Deux propriétés fondamentales caractérisent l'activité de l'horloge circadienne:

• La rythmicité de son activité est endogène et proche de 24 heures.

• Elle doit être synchronisée par des signaux externes (par exemple la lumière)

Chez les mammifères, dans les conditions normales, la lumière est le puissant synchronisateur de l'horloge. En effet une brève exposition à la lumière durant la nuit est capable d'induire l'expression immédiate des gènes de l'horloge tels Per1 et Per2, ce qui suggère la présence d'un lien direct par lequel la lumière contrôle l'oscillateur de l'horloge centrale NSC.

Des travaux réalisés au cours ces dernières années ont mis en évidence d'autres synchroniseurs que la lumière qui agissent sur l'horloge circadienne. De fait la nourriture agit comme un nouveau et un puissant facteur de contrôle des horloges périphériques. L'équipe d'U.Schibler à Genève a démontré que la nourriture est capable d'entraîner les rythmes du système circadien périphérique chez la souris. En déplaçant l'horaire de l'alimentation chez celle-ci, l'inversion la prise de nourriture de la phase ''active'' à la phase de ''repos'' (Restricted Feeding : RF) entraîne l'horloge périphérique et sans avoir d'effet sur l'horloge centrale (NSC), ce qui conduit à un découplage entre les deux horloges. Ainsi, les horloges périphériques suivent le rythme imposé par les apports de nourriture, alors que les NSC suivent le rythme imposé par la lumière.

Ces études de découplage entre les horloges centrales et périphériques indiquent que les deux synchronisateurs, la lumière et la nourriture, peuvent agir indépendamment l'un de l'autre. Dans

de telles conditions, les horloges périphériques peuvent être en permanence décalées par rapport à l'horloge centrale, ce qui pourra perturber l'homéostasie des fonctions corporelles et déclencher à long terme des perturbations du cycle vielle-sommeil, du métabolisme (syndrome métabolique, obésité, diabète de type II) et du comportement. Ainsi un certain nombre de données ont montré qu'un défaut de synchronisation de l'horloge circadienne peut être induit observé chez les personnes engagées dans une activité décalée ou nocturne et dont le régime alimentaire est décalé.

Au cours de mon travail de thèse, j'ai adressé plusieurs questions concernant au niveau moléculaire la compréhension de ces perturbations métaboliques consécutives à un régime alimentaire décalé dans le cadre d'un travail posté.

En effet, un décalage de phase pour l'accès à la nourriture (RF), de la phase ''active'' à la phase de ''repos'' chez la souris, décalait les horloges périphériques de 12 heures par rapport à l'horloge centrale. Toutefois le mécanisme moléculaire d'inversion de l'horloge circadienne par l'apport décalé de nourriture dans les organes périphériques restait inconnu.

Durant ma thèse, j'ai montré au niveau moléculaire que les altérations métaboliques induites par l'inversion de phase pour l'alimentation exercent une grande influence sur l'expression des éléments essentiels des horloges périphériques. En effet déplacer l'heure d'accès à l'alimentation de la phase ''active'' (ZT(*Zeitgeber*) 12-ZT0) à la phase de repos (ZT0-ZT12) crée de fait un état de « jeûne » de 12 heures chez la souris. Nous avons donc étudié les paramètres métaboliques pendant cette période. Nous avons constaté que le passage de l'horloge circadienne initiale à la nouvelle horloge circadienne sous le régime RF comporte deux phases distinctes: (i) la rupture de l'horloge circadienne initiale, et (ii) la génération et le maintien d'une nouvelle horloge circadienne décalée de 12 heures.

Pendant les premières heures du régime alimentaire décalé, nous avons remarqué une diminution du taux de glucose sanguin et une rapide chute au niveau de la production d'insuline. La poursuite de la baisse d'insuline permet l'activation de la lipolyse. Suite à cette activation, une augmentation accrue au niveau des acides gras libres (Free fatty-acid : FFA) survient dans le sang. Cette augmentation aberrante des acides gras libres (FFA) conduit à une surexpression pendant la phase de repos du récepteur nucléaire PPARα dont ils sont des ligands naturels. De plus, des souris portant des mutations sélectives de PPARα dans le foie (hépatocytes) et l'intestin (cellules épithéliales) ont montré que l'augmentation précoce de l'activité de RevErbα

durant la phase de repos est dépendante de celle de PPARα. Des analyses « ChIP » poussées ont montré que la fixation de PPARα sur un élément de liaison DR2 présent dans le promoteur de RevErbα était en fait à l'origine de son expression précoce pendant la phase de repos. L'ensemble de ces résultats suggèrent un rôle essentiel de PPARα durant le régime alimentaire décalé qui pourrait, dans les organes périphériques étudiés, déclencher l'expression précoce de RevErbα, ce qui en décalant l'horloge circadienne, entraînait un décalage complet des horloges périphériques par rapport à l'horloge centrale. En outre, l'hypoinsulinémie conduit à une augmentation de l'activité du glycogène synthase kinase 3β (GSK3ß) qui, en stabilisant la protéine RevErbα, augmente son niveau pendant la phase ''active''.

Des études avaient montré que le régime alimentaire décalé (RF), provoquait l'apparition d'un nouveau pic additionnel de corticostérone pendant la période de repos (ZT0), de manière non contrôlée par l'horloge centrale (NSC) et dont le mécanisme d'apparition était inconnu. La biosynthèse de cette hormone se fait en plusieurs étapes. La CRH (Corticotropin-Releasing Hormone), synthétisée dans les noyaux paraventriculaires (NPV) de l'hypothalamus, est libérée dans le système porte hypothalamo-hypophysaire, Ce qui induit la synthèse de l'hormone adrénocorticotrope ACTH (Adrenocorticotrophin hormone), puis sa sécrétion dans la circulation générale. L'ACTH stimule ensuite la synthèse de glucocorticoïdes par le cortex surrénalien.

L'axe de signalisation Adénosine monophosphate cyclique (cAMP) - protéine kinase A (PKA)-Response Element-binding protein (CREB) (AMPc/PKA/CREB) joue un rôle essentiel dans la production physiologique de corticostérone au début de la phase ''active'' de la souris (ZT12) au travers de la transactivation de nombreux gènes impliqués dans la synthèse de la corticostérone. J'ai donc étudié le rôle de cet axe dans la production du ''nouveau'' pic de cortisone chez la souris. J'ai trouvé qu'une augmentation de l'activation de CREB en pCREB dans les glandes surrénales durant le régime alimentaire décalé RF, activait l'expression de différents gènes-cibles de CREB, y compris ceux qui sont impliqués dans la synthèse de la corticostérone (Cyp11a, Cyp11b, Hsd3b, Prkar2b, and Adcy5).

Dans un deuxième temps, nous avons confirmé que l'horloge centrale circadienne n'est pas affectée pendant le régime alimentaire RF, même après un régime de longue durée (RF90/90 jours). En fait, nous n'avons détecté, ni le récepteur nucléaire PPARα, ni le récepteur du glucagon dans le NCS, récepteurs qui jouent un rôle déterminant dans la chaîne d'événements

métaboliques conduisant au décalage de l'horloge circadienne périphérique. Nous avons donc suggéré que c'est l'absence de ces deux récepteurs qui immunise l'horloge centrale contre le décalage provoqué dans les organes périphériques par un régime alimentaire décalé.

Au cours d'un régime alimentaire décalé de longue durée, nous avons constaté que l'expression de certain "gènes contrôlés par les horloges périphériques" (clock-controlled genes: CCGs) impliqués dans l'homéostasie et dans le métabolisme, est décalée de 12 heures chez les souris RF par rapport aux phases de repos et d'activité contrôlées par horloge centrale (NSC), de telle sorte que l'expression périphérique de gènes normalement exprimés durant la « phase d'activité » s'effectue au cours de la « phase de repos » et vice-versa, créant ainsi l'apparition progressive d'un syndrome métabolique pendant un régime alimentaire décalé (RF) de longue durée.

Pendant les 18 premiers mois de mon travail de thèse, nous avons exploré au niveau moléculaire, l'impact du microbiote intestinal sur le fonctionnement de l'horloge circadienne et l'homéostasie des cellules de l'épithélium intestinal.

Une seule couche de Cellules Epithéliales Intestinales (CEI) forme la barrière physique qui sépare le reste du corps des quelque 100.000 milliards de micro-organismes qui constituent le microbiote intestinal essentiellement composé de bactéries normalement non pathogènes, dites commensales, qui vivent en étroite symbiose avec leur hôte. De nombreuses études portant sur des souris élevées stérilement (Germ-free mice) ou dépourvues de microbiote (AIMD : antibiotic-induced microbiota-depleted) par traitement antibiotique ont révélé que la colonisation de l'intestin par les bactéries est bénéfique pour l'équilibre physiologique (homéostasie) de leur hôte en contrôlant de nombreux processus au niveau de l'épithélium intestinal (absorption intestinale, immunité innée, prolifération cellulaire, activités métaboliques, etc,).

Des travaux réalisés au cours des 15 dernières années avaient révélé la nature du dialogue moléculaire qui sous-tend la symbiose hôte-microbiote, en démontrant qu'il nécessitait l'interaction entre des composés provenant du microbiote et des récepteurs appartenant au groupe des « Toll-like receptors » (TLRs) localisés à la surface des CEI. La question posée était : comment ces interactions entre TLRs et composés provenant de bactéries commensales pouvaient-elles contrôler, au niveau moléculaire, de nombreuses fonctions physiologiques des CEI ? J'ai démontré que l'expression des gènes TLRs est sélectivement déclenchée par un

rouage de l'horloge circadienne, le gène RORα, qui est exprimé au début de la phase circadienne d'activité. Ainsi, grâce à l'activation rythmique du rouage RORα, les signaux arythmiques émis par le microbiote sont « convertis » en une signalisation rythmique par les TLRs, qui stimulent sélectivement l'expression des gènes caractéristiques de la période d'activité. Ceci jusqu'au moment où l'horloge circadienne atteint la phase de repos, le rouage RervErbα, de l'horloge réprime la synthèse des TLRs et autorise l'expression sélective des gènes contrôlant l'homéostasie pendant la période de repos, ainsi que la production de glucocorticoïdes par les cellules de la partie terminale de l'intestin grêle, l'iléon.

En effet, le bon fonctionnement de cette horloge dans les cellules de l'épithélium intestinal nécessite la présence de microorganismes non pathogènes qui vivent dans le tube digestif en étroite symbiose avec leur hôte. En l'absence de microbiote, la désorganisation de l' « axe » microbiote-TLRs-horloge circadienne se traduit dans les CEI par l'altération de l'expression des gènes codant pour les protéines qui constituent les rouages de l'horloge circadienne, et aussi par l'altération de l'expression des gènes qui présentent normalement un profil d'expression circadien. Il y a augmentation de l'expression des gènes qui sont exprimés durant la phase de repos au détriment de ceux exprimés pendant la phase d'activité. De plus la surproduction de glucocorticoïdes par l'iléon entraine l'apparition d'un syndrome de type pré-diabétique.

En conclusion, notre étude a révélé des mécanismes moléculaires jusqu'alors inconnus qui sous-tendent l'extraordinaire symbiose entre le microbiote et l'épithélium intestinal, en démontrant comment des signaux du microbiote agissent en se liant aux TLRs des CEI pour contrôler le bon fonctionnement de leur horloge circadienne qui, elle-même, joue un rôle crucial dans le maintien de l'homéostasie intestinale. Enfin la découverte d'une liaison directe entre le microbiote intestinal, le cycle circadien et l'équilibre physiologique de l'épithélium intestinal ouvre de nouvelles perspectives concernant l'origine et la physiopathologie des affections intestinales et (ou) systémiques qui sont liées à des altérations du microbiote et (ou) du cycle circadien, notamment chez les personnes travaillant en horaires décalées.

Abbreviations

AMPK: Adenosine monophosphate-activated protein kinase
AVP: Arginine vasopressin
Bmal1: Brain and muscle aryl hydrocarbon receptor nuclear translocator (ARNT)-like
cAMP: Cyclic adenosine monophosphate
CC: Circadian clock
CKI: Caseine kinase I
Clock: Circadian locomotor output cycles kaput
CRE: cAMP responsive element
CREB: cAMP Response Element-binding protein
Cry: Cryptochrome
DBS: DNA binding sequence
DMH: Dorsomedial nucleus of the hypothalamus
DBP: D site of albumin promoter
DR2: Direct repeat 2
Elovl6: Elovl fatty acid elongase 6
FAA: Food-antipatory activity
FFA: Free fatty acids
FAS: Fatty acid synthase
G6pc: Glucose-6-phosphatase, catalytic subunit
GABA: Gamma aminobutyric acid
GK: Glucokinase
Glut2: Glucose transporter 2
GSK3β: Glycogen synthase kinase 3 beta
HFD: High-fat diet
HLF: Hepatic leukemia factor
HPA: Hypothalamic–pituitary–adrenal
INS: Insulin
LDL: Low-density lipoprotein
mRNA: messenger ribonucleic acid
NAD: Nicotinamide adenine dinucleotide
NAMPT: Nicotinamide phosphoryl-transferase
Pepck: Phosphoenolpyruvate carboxykinase 2
Per: Period
PGC1: Peroxisome proliferator-activated receptor gamma coactivator1
PPARα: Peroxisome proliferator-activated receptor alpha
PPARγ: Peroxisome proliferator-activated receptor gamma
RF: Restricted Feeding
ROR: Retinoic acid-related orphan receptor
RORE: RevErb/ROR Response element
SCN: Suprachiasmatic nucleus of the hypothalamus
SIRT: Sirtuin
Srebp1c: Sterol regulatory element binding transcription factor 1
TEF: Thyrotroph embryonic factor
TG: Triglycerides
VIP: Vasoactive intestinal peptide
WAT: White adipose tissue

WT: Wild type
ZT: Zeitgeber time

Introduction

1- Circadian rhythms

By definition, a rhythm is a change that is repeated with similar pattern during a certain period. Finding food and avoiding predators and inclement weather are the daily functions of wild animals. Some animals hunt their prey when they have the greatest ability to see (day), but others in contrary, as mice, need to avoid predators and thus are active mainly during the night. In any case, these adaptations lead to a strong circadian behavioral rhythmicity. Most processes in our body oscillate in a daily rhythmic fashion. In humans, sleep-wake cycles are the most obvious circadian manifestations of behavior (Achermann and Borbély, 2003, Borbély, 1982). These include cerebral activity, metabolism, energy homeostasis, heart rate, blood pressure, body temperature, and hormone secretion. These daily variations are connected to changes in the environment, such as regular and predictable day/night cycles, due to the fact that the Earth rotates on itself. Life has evolved and diversified through the process of natural selection to be adapted to almost every environment cues. The existence of daily rhythms in plants and animals is known for a long time, and Androsthenes Thasius described the concept of living rhythm early in the 4th century BC. He observed that leaves of certain plants (especially *Tamarindus Indicus*) did not occupy the same day and night position.

The first scientific publication related to biological clocks appeared in from 1729, when Jean-Jacques d'Ortous Mairan observed the opening and closure of *Mimosa Pudica* leaves during the day and the night, even when the plant was kept in constant darkness. Thereafter, the observations of physiological or behavioral rhythms have accumulated during centuries. “Clock genetics” began in 1971 with the discovery by Ron Konopka and Seymour Benzer of the period (per) locus in Drosophila (Konopka and Benzer, 1971). In the early 20th century, circadian oscillations have been demonstrated in animals. When mice or rats are placed in constant light conditions (continuous light or darkness), the pace of locomotor activity was retained (Pittendrigh CS et al., 1976).

However, Jurgen Aschoff observations of human subjects without any external timing cue (light) for weeks revealed an unexpected finding. All individuals displayed body temperature and urine production rhythms of nearly 24 hours, and when living isolated from all

environmental cues continue to have a functioning rhythm with a period greater than 24 hours (25,9h), thereby indicating the existence of an internal biological clock (Aschoff, 1965).

2- The molecular mechanism of circadian clocks in mammals

The molecular core clock in mammals, expressed both in brain and peripheral tissues, comprises a series of transcription–translation feedback loops that result in cascades of gene expression. The mechanism of the core clock in mammals is the heterodimeric transcription factor complex of Clock and Bmal1, which activates transcription of the Period (Per) genes and Cryptochrome (Cry) genes via E-box DBS in their promoters. The Per-Cry repressive complex translocates into the nucleus to inhibit Clock-Bmal1 transactivation activity, resulting in the repression of the Per and Cry genes (Joseph Bass, 2012).

An additional feedback loop, involves the nuclear receptors RevErbα and retinoic acid-related orphan receptor RORα. Clock-Bmal1 activates RevErbα transcription, resulting in daily fluctuations of RevErbα, which, in turn, represses Bmal1. RORα, another nuclear receptor and component of the clock machinery, competes with RevErbα for the binding to the Bmal1 promoter RORE DBS, and activates its transcription. Therefore, the two nuclear receptors, RevErbα and RORα, act as a new regulatory loop. They play a crucial role for a proper timing of the core clock machinery **(Figure 1)** (Joseph Bass, 2012).

There is a large number of genes including key regulators for cell cycle and metabolism are controlled by the components of circadian clock [the so called clock-controlled genes (CCGs)] as the heterodimer Bmal1-Clock, RevErbα, RORα that suggests to contribute to the transcriptional output of the circadian clock, which are important to maintain normal cellular functions in peripheral tissues (Robles and Mann, 2013, Asher and Sassone-Corsi, 2015).

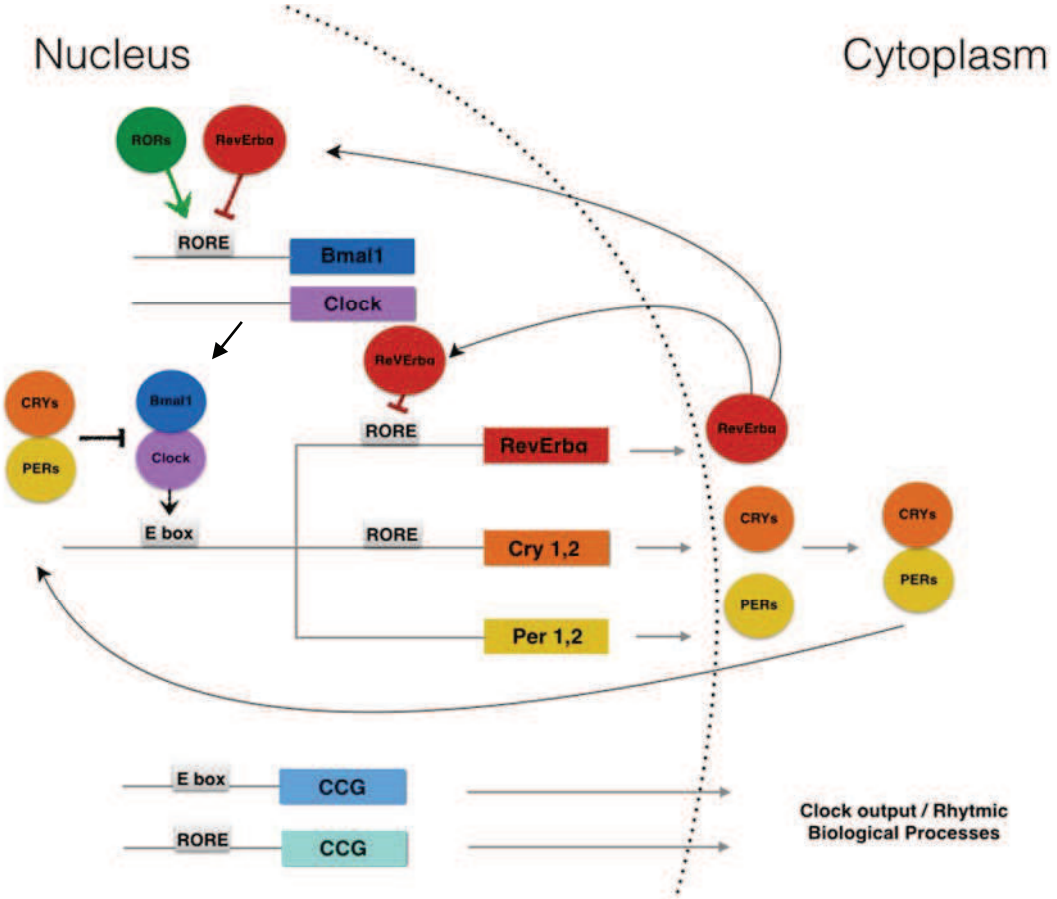

Figure 1: Transcriptional-translational feedback loops of the mammalian circadian clock. The positive elements of the loop (Bmal1/Clock) dimerize to active the rhythmic transcription of RevErbα, Crys (Cry1 and Cry2) and Pers (Per1 and Per2) genes through E-box enhancer elements. Cry-Per proteins interact with Bmal/Clock to negatively regulate Clock/Bmal1-mediated transcription. RevErbα protein accumulation leads to periodic repression of Bmal1 and of its own gene expression (CCGs: clock-controlled genes).

The auto regulatory feedback loops described above take approximately 24 hours to complete a cycle and constitute a circadian molecular clock. Furthermore, clock proteins are modified in a post-translational manner by phosphorylation, acetylation, SUMOylation and ubiquitination, resulting in multiple layers of regulation to the core clock machinery. During the "active" phase, Per-Cry is degraded through the ubiquitylation of Cry by the FBXL3 complex. For example, phosphorylation of Per1 and Per2 by casein kinase 1 (CK1δ or CKlε) can modulate the period of circadian gene expression, and RevErbα has been shown to be stabilized when phosphorylated by the glycogen synthase kinase 3 (GSK3β) (Yin L et al., 2006).

Further circuits are generated through additional clock-controlled transcription factors such as DBP, TEF and HLF proteins, whose expression is E-box dependent, and E4BP4, whose

expression is RORE-dependent. Finally, E-box, RORE, and D-box can explain variable rhythms of CCGs, which control tissue-specific functions **(Figure 2)** (Ripperger and schibler, 2006) (Le Martelot et al., 2009) (Asher and Schibler, 2011).

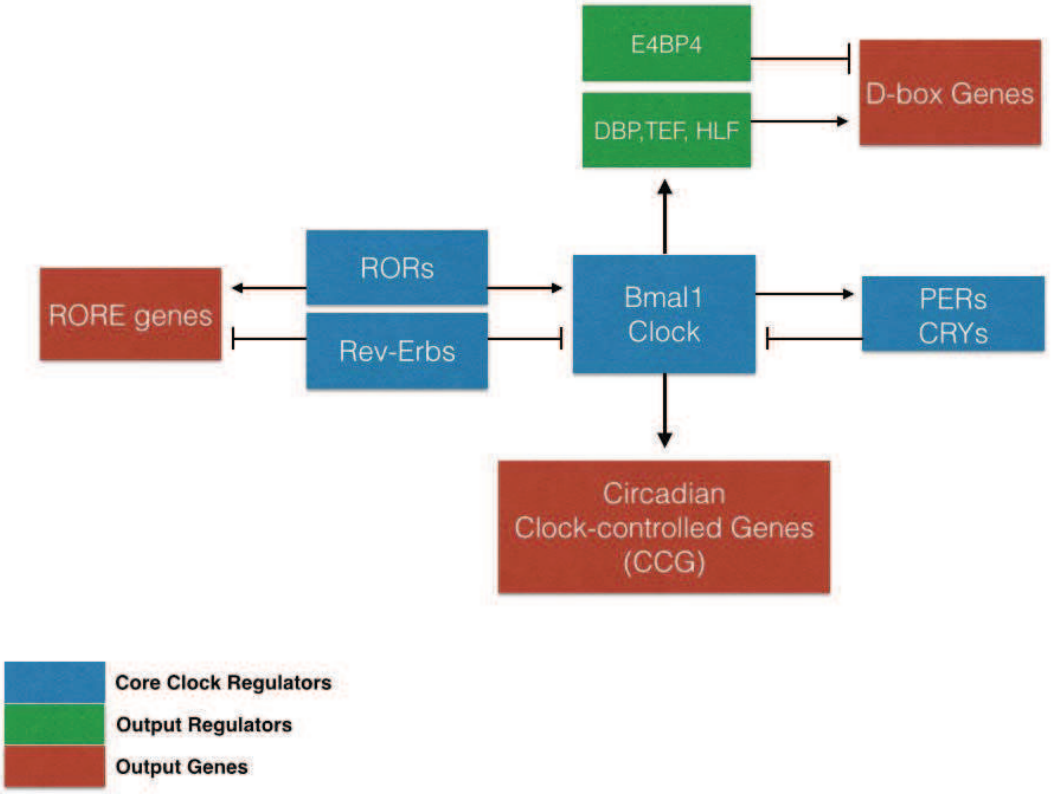

Figure 2: The generation of different phases by the moleclar clock. The molecular clock in peripheral organs consists of two interlocked feedback loops. The major and essential loop involves the transcriptional activation of Period (Per1 and Per2) and Cryptochrome (Cry1, Cry2) genes by the transcription factors Clock and Bmal1, and the autorepression of Per and Cry genes by their own protein products. Another feedback loop is established through negatively and positively acting nuclear orphan receptors: the activators RORs compete with the repressors Rev-Erbs for the binding on the RORE DBS of the Bmal1 gene. Further phases are generated through additional clock-controlled transcription factors such as DBP TEF HLF whose expression is E box dependent, and E4BP4, whose expression is RORE dependent, (output regulators). The major and accessory feedback loops can therefore regulate widely different phases of genes encoding metabolic enzymes and modulators (output genes) involved in rhythmic metabolism.

3- Central and peripheral circadian clocks in mammals

a- The Suprachiasmatic nucleus of the hypothalamus (SCN): the master circadian clock synchronizer

The suprachiasmatic nucleus of the hypothalamus (SCN) is a small, but extremely complex structure in the hypothalamus. Various studies of evidence show that the SCN regulates circadian rhythms, physiological and behavioral rhythms (Rusak and Zucker, 1979). Since the 1970s, lesion experiments in mammals have demonstrated its importance as a central circadian clock (Richter 1965, Moore and Eichler, 1972, Rusak, 1977). The definitive proof that's SCN is the master synchronizer of behavior came when Ralph and colleagues have demonstrated that the behavioral rhythms of an SCN lesioned animal can be restored by transplantation of a donor SCN and exhibit the same period length of the donor animal (Ralph et al., 1990; Ralph and Menaker, 1988). In addition, in absence of SCN, different metabolites and hormones patterns lost their rhythmicity in blood. Plasma glucose, corticosterone, insulin and glucagon became completely arrhythmic by an SCN lesion in intact rats under ad libitum feeding conditions **(Figure 3)** (Kalsbeek et al., 2010).

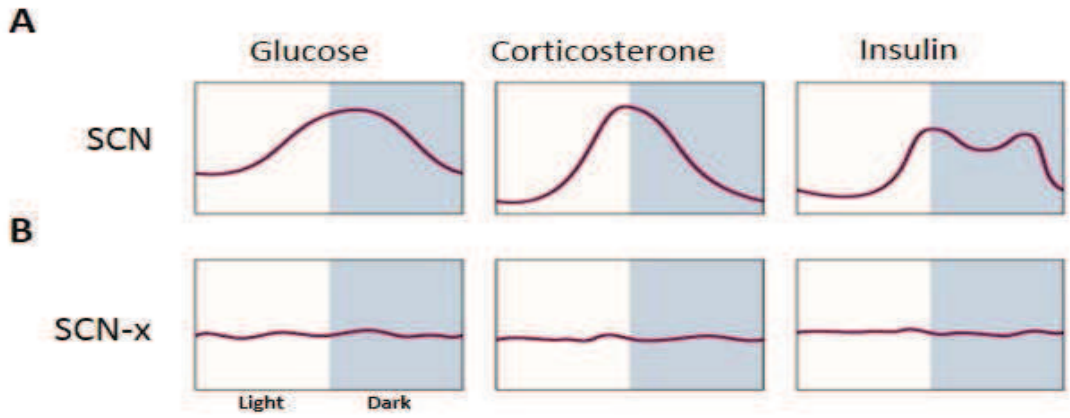

Figure 3: Daily rhythms in basal plasma glucose, corticosterone and insulin concentrations in presence (A) and absence of SCN (B) under 12 hour light/dark cycle and Ad *libitum* feeding condition (SCN-x: SCN lesion) (Adapted from Kalsbeek et al., 2010).

Following these important studies, it was established that in many species of mammals, the SCN control and coordinate many physiological and behavioral circadian functions (Hastings and Herzog, 2004). In mice, the SCN contains approximately ~20,000 neurons, and about ~50,000 neurons in humans, which have a cell-autonomous circadian oscillator. It is subdivided

into two main anatomic-functional subparts; these designations were originally defined according to the expression of neuropeptides:

1- A ventromedial core consists of two types of neurons expressing the neuropeptides VIP (Vasoactive intestinal peptide) and GRP (Gastrin-releasing peptide).
2- A dorsomedial shell consists of neurons expressing the neuropeptide AVP (vasopressin).

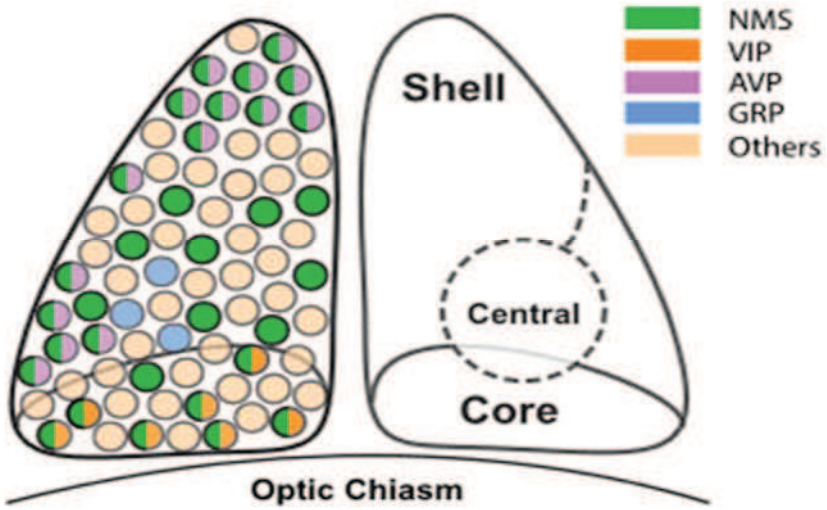

Figure 4: The neuropeptide distribution in the SCN neurons. The suprachiasmatic nucleus (SCN) in the hypothalamus is divided into two major anatomical and functional subdivisions: a ventrolateral 'core' and a dorsomedial 'shell'. (**NMS***: neuropeptide neuromedin S,* ***VIP***: vasoactive *intestinal peptide,* ***AVP****: arginine vasopressin,* ***GRP****: Gastrin Releasing peptide)* (Adapted from Lee et al., 2015).

Several studies have indicated the presence of a large number of neurotransmitters in the SCN, which play an important role for the entrainment of the clock and for the control of different rhythms (**Figure 4**). VIP signaling in particular seems key to maintaining synchrony among SCN neurons. Mice lacking VIP or its receptor display erratic free-running behavior and the rhythms of individual neurons within a single SCN are no longer held in uniform phase (Harmar et al., 2002; Colwell et al., 2003). More recently, Joseph Takahashi lab has found that the NMS (neuropeptide neuromedin S) neurons define a subset of SCN that dictate and generate SCN network synchrony and in vivo circadian rhythms through intercellular synaptic transmission (Lee et al., 2015).

b- Peripheral circadian clocks

Since the late 1990s, several teams have shown that in mammals most brain structures outside of the SCN, and even isolated cells express the molecular clock. Daily oscillation of clock genes have been observed in vitro in rat fibroblast cultures (Balsalobre et al., 1998), but in vivo, in peripheral tissues such as liver, muscle, kidneys, lungs (Abe et al., 2002; Yamazaki et al., 2000; Zylka et al., 1998). Such studies have suggested that most cells have molecular circadian clocks. The molecular mechanism of peripheral clocks was studied and based on the same molecular mechanism as in neurons of SCN (Yagita et al., 2001). Many studies on the expression of clock gene oscillations in peripheral cells have used the fibroblast culture as a model (Balsalobre et al., 1998; Welsh et al., 2004). They showed that each cell has its own molecular circadian clock. However, fibroblasts can be resynchronized by adding various factors such as a change of the culture medium, adding serum to the medium (Balsalobre et al., 1998) or the glucocorticoid dexamethasone (Balsalobre et al., 2000). An ex vivo study in 2004 has shown that the oscillations of a number of peripheral tissues such as liver, kidney and lungs persisted as long as those of the SCN **(Figure 5)** (Yoo et al., 2004).

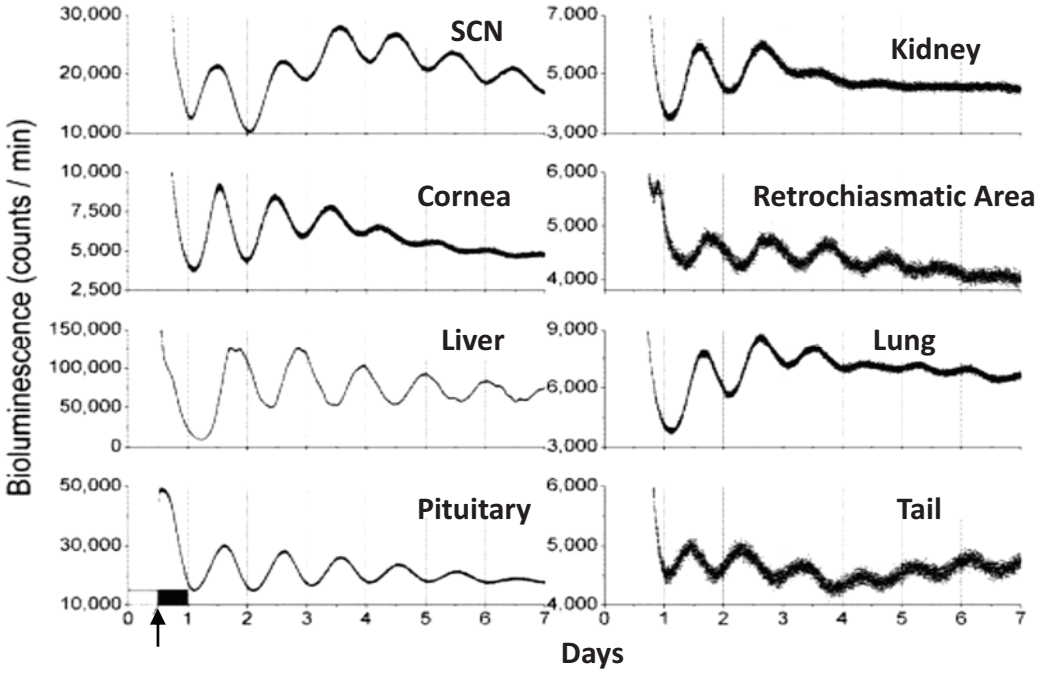

Figure 5: The expression of the core circadian clock genes reflects the presence of circadian oscillators in almost every tissue in the body. Representative records of bioluminescence showing circadian profiles of mPer2 expression from various tissues from mPer2 Luc knocking animals. Tissues were explanted just before lights off (arrow). Light output (in counts per min) is plotted against previous light onset (Adapted from Yoo et al., 2004).

4- Phenotypic effects of circadian clock mutations

The molecular mechanism underlying the mammalian clockwork has been mostly studied in the mouse. The internal circadian system could be altered by a mutation of one or more clock genes, which lead to a disruption of the animal rhythms, and even in some cases to a total arrhythmia, associated to various physiological abnormalities **(TABLE 1)** (Ko CH and Takahashi JS, 2006).

Gene	Circadian phenotype	References	Associated physiological abnormality	References
Clock∆19	Semi-dominant, 4 hours longer period followed by loss-of-circadian activity rhythm in constant darkness (DD)	Vitaterna et al. 1994	Hyperphagic & Obese Abnormal gluconeogenesis Hypersensitive to chemotherapeutic agent Enhanced response to cocaine Mania phenotype Decreased duration of sleep time	Gorbacheva et al. 2005 ;Rudic et al 2004 ;McClung et al 2005 ;Turek et al 2005
Clock Null mutant	0.5 hour shorter period	DeBruyne et al 2006	None Determined	_
Per1 Null mutant	0-0.5 hour shorter period/ some animals lose circadian activity rhythm in DD	Zheng et al 2001;Cermakian et al 2001	Lack of sensitization to cocaine	Abarca et al 2002
Per2 Per2tm1Brd Null mutant	1.5 hour shorter period and tendency for loss of circadian rhythm	Bae et al 2001;Zheng et al 1999	Increased tumor development following genotoxic stress Hyper-sensitization to cocaine Improper alcohol intake Early onset of sleep	Abarca et al 2002;Fu et al 2002;Toh et al 2001
Per1 & Per2 Double null mutant	Complete loss of circadian activity rhythm in DD	Zheng et al 2001 ; Bae et al 2001	None Determined	_
Cry1 Null mutant	1 hour shorter period	Van der Horst et al 2000 ; Vitaterna et al 1999	None Determined	_

Gene	Circadian phenotype	References	Associated physiological abnormality	References
Cry2 Null mutant	1 hour longer period	Thersher et al 1998	None Determined	_
Cry1 & Cry2 Double null mutant	Complete loss of circadian activity rhythm in DD	Van der Horst et al 2000 ; Vitaterna et al 1999	Delayed hepatocyte re-generation Resistant to chemotherapeutic agent's toxicity I	Gorbacheva et al 2005;Fu et al 2002;Matsuo et al 2000
RevErbα (Nr1d1) Null mutant	0.5 hour shorter period/ Altered photic entrainment	Preitner et al 2002	None Determined	_
RORa mutant	0.5 hour shorter period	Sato et al 2004	Cerebellar ataxia Abnormal bone metabolism	Meyer et al 2000 ;Steinmayr et al 1998
VIP Null mutant	Abnormal entrainment to light cycles Dissociated circadian wheel-running rhythms in DD Reduced amplitude in behavioral rhythms in DD	Aton et al 2005; Colwell et al 2003	Impaired temporal regulation of metabolism and feeding	Bechtold et al 2008
VIP Receptor2 Null mutant	Abnormal entrainment to light cycles Dissociated circadian wheel-running rhythms in DD Reduced amplitude in behavioral rhythms in DD Impaired responses to light	Aton et al 2005; Harmar et al 2002	Impaired temporal regulation of metabolism and feeding	Bechtold et al 2008

Table1: Mouse circadian mutants and observed circadian and physiological phenotypes (Adapted from Caroline H Ko and Takahashi JS, 2006).

5- External cues entrain circadian clocks

a- Light-entrainment of the master SCN circadian clock

The different body oscillators have to be periodically synchronized to the environment. The light-entrained master central circadian clock (CC) in the SCN not only controls the diurnal alternance of the active phase and the rest phase, but also synchronizes the ubiquitous peripheral CCs with these phases to maintain homeostasis **(Figure 6)**.

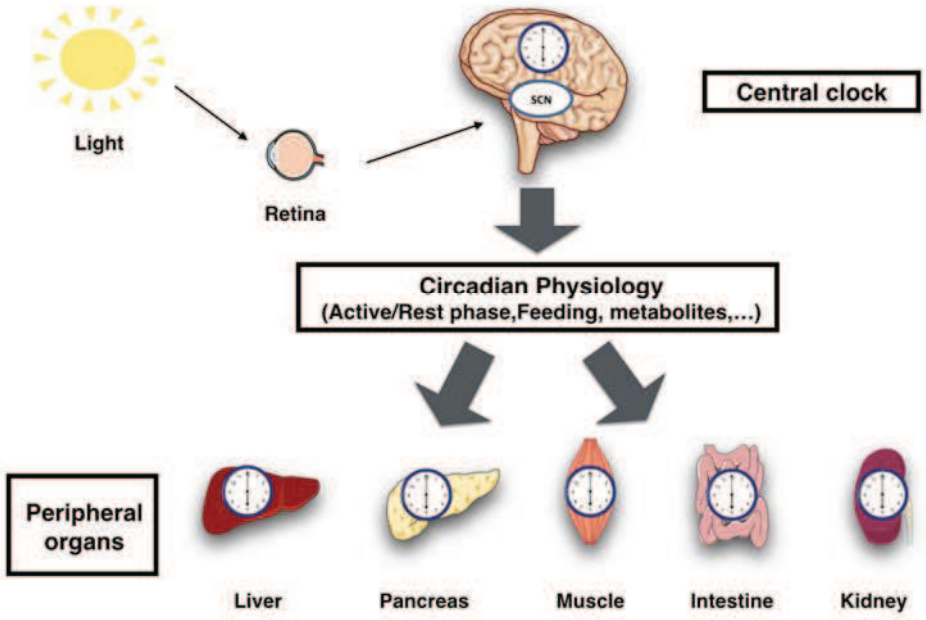

Figure 6: Light entrains the master clock in the suprachiasmatic nucleus (SCN), which in turn synchronizes extra-SCN and peripheral clocks.

Light enters the eye and activates different types of photoreceptors in retina. Of note, for more than 150 years, rods and cones have been considered to be the only photoreceptor cells in the retina. More recently, in 2002, intrinsically photosensitive retinal ganglion cells (*ip*RGCs) have been discovered melanopsin-expressing ganglion cells (non-vision pathway). The discovery of a group of blind humans who were unable to form images (absence of rods and cones), but were capable of detecting light for regulation of melatonin secretion, provided an evidence of an additional photoreceptive system in the retina through melanospsin (Berson et al., 2002, Hattar et al., 2002). Interestingly, Melanopsin knock-out mice only displayed mild phase-shifting phenotypes and the SCN clock can be photoentrained (Ruby et al., 2002, Panda et al., 2002). In addition, when a melanopsin knock-out allele was bred into Rd mice (lack of rods and cones),

the resulting mutants completely lost their circadian photoentrainement and the activity in the presence of a light-dark cycle (Panda et al., 2003, Hattar et al., 2003). This clearly demonstrated that the circadian photoperception is a property generated by the activity of rods and cones cells, in combination with melanopsin-expressing ganglion cells. Photic signals transmitted from the retina to SCN neurons lead to an influx of Ca^{2+} in postsynaptic neurons, which through activation of protein kinase A (PKA) stimulates the activity of the cAMP response element binding protein (CREB) (De Cesare D et al., 2000), which is a transcription factor that induces the transcription of the Per1 and Per2 clock genes. Moreover, it has been shown that a pulse of light during the second half of the night, can immediately induce the expression of components of SCN CC as Per1 and Per2, proteins accumulate precociously, which results in a phase advance (Shearman et al., 1997, Albrecht et al., 1997).

Thus, the light-induced CREB-dependent increase in expression of Per genes, provides an explanation of how a light input can influence the function of neurons of the SCN CC.

b- Feeding-entrainment of circadian clocks of peripheral cell /tissues

Feeding and peripheral circadian clocks (PCCs) are tightly interconnected, as the feeding time can act as a potent entraining timing signal (cue) or "*Zeitgeber*" for PCC. It has been reported that PPC gene expression tissues such as liver, pancreas, intestine, kidney and heart, can be shifted by 12 hours when the food is exclusively provided during the day time (the "rest" phase in mice) and prevented during the night time (the "active" phase in mice) [the so-called Restricted Feeding (RF)], whereas the SCN central circadian clock remaining unchanged (Damiola et al., 2000). Importantly, a 12-hour RF-regime can entrain a rhythmic circadian clock in peripheral tissues of a SCN-ablated animals which are arrhythmic (Krieger et al., 1977).

What are then the signals, which arise from feeding and entrain peripheral clocks? They could be the food itself, food-induced metabolites, or hormones whose secretion is controlled by feeding or its absence? A possibility is that feeding rhythms drive variations in glucose levels. The glucose metabolism is indeed well known to participate in all major biochemical functions in all cell types. Following carbohydrate-rich meals, glucose is converted into glycogen, which is stored in the liver to serve as a rapidly available "fuel" to mobilize glucose for brain and other tissues after feeding. Glycogenolysis is the primary mechanism by which glucose is made available. Hepatic gluconeogenesis and glycogenolysis represent the main pathway by which nutrient homeostasis is maintained over diurnal periods of feeding and fasting. Circadian variations of glucagon and insulin hormones control these biochemical processes. Interestingly

enough, the molecular mechanism through by which glucose may affect the function of circadian clock components has not been investigated.

Interestingly, not only the time of feeding could control the circadian peripheral clock, but the meal composition may also plays a crucial role in this control. In mice, a High fat diet (HFD) regime affects not only the activity, but also the cycling of clock genes and of their clock controlled targets. Recently, it has been reported that consumption of a HFD produces widespread alterations in circadian transcriptional and metabolic profiles in peripheral tissues (Kohsaka et al., 2007) (Eckel-Mahan et al., 2013).

6- Nuclear receptors and circadian clocks

Nuclear receptors (NRs) represent a large superfamily of genes encoding receptors composed of 48 members in human and 49 in mice, which play diverse aspects involved in different biological pathways, such as energy metabolism, immunology and tissue homeostasis (Yang et al., 2006). A large number of these receptors, including both isoform α and β of RevErbs, RORs (α, β, γ) and all three PPARs (α, β, γ) are expressed in mice in a circadian manner at least at the transcript level (Yang et al., 2006). They represent a complex array of extracellular signals into transcriptional responses, many of which specifically regulate the expression of target genes. Their primary function is to mediate in target cells the transcriptional response to hormones such as the sex steroids, adrenal steroids (glucocorticoids) and retinoid ligands, as well as a variety of additional metabolic ligands. Glucocorticoids (GC) hormones might play a role in the synchronization of circadian peripheral clocks (Le Minh et al., 2001). Indeed, the level of GC displays a robust circadian rhythm. GCs are belong to a group of steroid hormones released by adrenal gland cortex that are involved in multiple functions, including inflammation, metabolism, and neurological functions. These hormones activate the glucocorticoid receptor (GR), which in glucocorticoid-responsive elements +GRE within promoter of Per genes. Although a treatment of cultured cells in vitro with dexamethasone (a synthetic GR agonist) is able to synchronize their circadian clocks, mice bearing a hepatocyte-specific knockout of the GR gene tuned their circadian liver clocks more rapidly to inverted feeding cycles than wild-type mice upon RF regime (Le Minh et al., 2001). Of note, it has been shown that GR interacts with and repressed by Cry 1 and 2 (Lamia et al., 2011).

PPARs (Peroxisome Proliferator-Activated Receptors) play a crucial role at the gene level in the regulation of mammalian metabolism, including Fatty acid oxidation and lipogenesis (Kersten et al., 2000). Three major isoforms of PPAR encoded by different genes have been

identified: PPARα, PPARβ and PPARγ. The activation of target gene transcription depends directly on the binding of the free Fatty acid (FFA) to the receptor. PPARα is predominantly expressed in adipose tissue, liver, intestine, kidney, heart and skeletal muscle. During fasting and starvation period, when the carbohydrates stock has been used, the body switches to mobilizing its fat stores as a source of energy. At this point, the role of PPARα is crucial in the hepatic response to fasting by regulating genes with direct roles in ketogenesis, as shown by using gene knockout mice models and from transcriptomic analyses. More recently, it has been demonstrated that PPARα could be connected with the circadian clock machinery through a direct binding on the DR2 DBS of RevErbα gene, which acts on the core circadian clocks (Duez et al., 2008).

7- Circadian clocks and metabolic factors are tightly linked

The circadian clock machinery is controlled by transcriptional feedback loops in which clock components act through binding directly to DNA response elements. Interestingly, the same elements are present throughout the genome and regulate the expression of clock-controlled genes (CCGs) (Ueda et al., 2005). Recent genome wide transcriptome analyses in the SCN, liver and adrenal gland of mice, revealed the expression of 10% of the cell transcripts is regulated in a circadian fashion. Among these transcripts, key regulators of glucose and lipid metabolism are present (Ueda et al., 2002; Lowrey and Takahashi 2004; Hughes et al., 2009). The availability of genetic models of circadian alteration provided new opportunities to dissect the relationship between circadian clocks and metabolic systems. One of the first alteration to be studied was that of the Clock gene. It has been shown that a Clock mutation induced changes in glucose homeostasis including impairments in glucose tolerance, insulin secretion, PEPCK and Glycogen Synthase 2 (E-box) mRNA expression, as well as and increased insulin sensitivity (Kennaway et al., 2007) (Doi et al., 2010). Homozygous Clock mutant mice exhibited a dampened feeding pattern with increase food intake during the “rest” phase, which contributed to gain weight by fat excess. Clock mutant mice displayed multiple metabolic alterations including hyperglycemia, hypertriglyceridemia and hepatic steatosis. Moreover, a Clock mutation altered the diurnal rhythms of CC genes and of some of metabolic genes in mice brain (Turek et al., 2005). Gluconeogenesis was suppressed by a deletion of Bmal1 and mice became more to sensitive exogenous insulin (Rudic et al., 2004). In addition, a liver deletion of Bmal1 in mice induced a hypoglycemia during the “rest” phase, and normal total body fat as compared to the Wt mice (Lamia et al., 2008).

Metabolic sensors and circadian clock components

Most cells in mammalian body use glucose as their major source of energy. Glucose molecules are broken down within cells in order to produce adenosine triphosphate (ATP) molecules, the energy molecules that power numerous cellular processes. The maintenance of constant plasma glucose levels is therefore crucial to prevent from many metabolic disorders. The connection between the circadian clocks and metabolism is tightly dependent on the role of metabolic sensors that regulate the clock machinery.

AMPK and circadian clocks

AMP-activated protein kinase (AMPK) is one of the metabolic sensors that have been reported to transmit energy-dependent signals to the circadian clock. In the liver, it is activated in response to prolonged fasting. AMPK has been found to directly phosphorylate CKIε, resulting in increased CKIε activity and degradation of mPER2. In addition it has been shown that AMPK phosphorylates and destabilizes mCRY1, leading to altered circadian rhythms (Lamia et al., 2009) (Feng and Lazar, 2012).

SIRT1 and circadian clocks

SIRT1 (Sirtiun 1) has emerged as a key metabolic sensor that directly links nutrient signals to metabolic homeostasis. SIRT1 is a NAD+-dependent protein deacetylase that governs many physiological processes, and has recently been found to play a key role in the control of the circadian rhythms in which circadian control is coupled to metabolism (Asher et al. 2008; Nakahata et al., 2009; Ramsey et al., 2009). In 2008, two studies from the laboratories of Ueli Schibler (Asher et al., 2008) and Paolo Sassone-Corsi (Nakahata et al., 2008) have demonstrated that SIRT1 activity is intimately linked with the hepatic circadian clock. They have shown that the circadian SIRT1 activity modulates the expression of circadian clock-controlled genes by deacetylating Per2 and Bmal1. Deacetylation of Bmal1 affects its transcriptional activity (Nakahata et al., 2008) and that of Per2 to alter its stability (Asher et al. 2008). Furthermore, SIRT1 ablation resulted in an increase in DBP and Per2 mRNA (Storch et al., 2002). Nicotinamide phosphoribosyltransferase (Nampt) is the rate-limiting enzyme in NAD+ biosynthesis and Clock and Bmal1 directly activate the Nampt promoter, leading to circadian activity of NAMPT and of cellular NAD+ levels (Nakahata et al., 2009; Ramsey et al., 2009).

It has also been shown that SIRT1 in the brain governs the central SCN circadian clock by activating transcription of the two major circadian clock components, Bmal1 and Clock (Chang et al., 2013). The discovery of circadian-directed sirtuin activity suggests that metabolites such as NAD^+ could be themselves playing an important role in the cellular link between metabolism and the circadian clocks (Paolo Sassone-Corsi, 2014).

8- Microbiota and circadian clocks

"Bacteria" is a word that gives us a wrong impression of representing something dirty, contaminated or infected. We however live in a world filled with bacteria; they are everywhere and colonize our human body from birth. Bacteria reside on the skin, in the mouth and gut level; they constitute what is called the skin, oral and the intestinal flora. In intestine, it is also name the intestinal microbiota. It comprises 10^{14} microbial cells, around 100 times more cells than the human body itself. The intestinal epithelium has the delicate function to absorb nutrients, while being simultaneously a potential line of defense against the environment. A single layer of intestinal epithelial cells (IEC) provides a physical barrier that separates the commensal bacteria in the intestinal lumen from the underlying lamina propria and the rest of the body. IECs also express Toll like Receptors (TLRs) and are thus a part of the innate immune system, both as a physical barrier and as a first-line pathogen recognition system (Abreu, 2010).

TLRs play an important role in host defense against microbial infection. Stimulation of TLRs by their cognate pathogen-associated microbial patterns (PAMPs) initiates signaling cascades leading to the activation of transcription factors, such as AP-1 and NF-κB (Hooper et al., 2001). Significant progress has been made over the past years in the understanding of TLR function (Rakoff-Nahoum et al., 2004). The contribution of the microbiota in regulation of physiology is vast and complex associated with intestinal disorders as well as with diseases such as obesity (Ley et al., 2005; Turnbaugh et al., 2006). Studies on Germ-Free (GF) and antibiotic-induced microbiota-depleted (AIMD) mice have revealed that gut colonization by the microbiota is beneficial in many respects for mammalian host homeostasis unveiled that commensal bacteria are recognized by IEC Toll-like receptors (TLRs), thus providing a new perspective on host-commensal symbiosis and raising the question of how the interaction of commensal bacterial products (PAMPs) with TLR members of the pattern recognition receptors (PRRs) could control at the molecular level many homeostatic processes in IECs (Abreu, 2010). Several intestinal functions (e.g., nutrient absorption, cell proliferation, motility, metabolic activities)

are known to be rhythmically regulated in a circadian manner (Hussain and Pan, 2009), and it has been shown that core components of the circadian clock could be functional in mouse small intestine in which the expression of some TLR genes may also vary around the circadian day (Froy and Chapnik, 2007). Moreover, it has been recently shown that the composition of the microbiota undergoes diurnal oscillations in both mice and humans (Thaiss et al., 2014), and that these oscillations are disturbed in mice by a genetic mutation in the clock system, as well as in jet-lag experiments (Thaiss et al., 2014) (Asher and Sassone-Corsi P, 2015). The question, which remained to be investigated, was how the gut clock interplays with metabolic pathways, and is the microbiota controlling the gut clock or vice versa?

References

1. Abe M, Herzog ED, Yamazaki S, Straume M, Tei H, Sakaki Y, Menaker M, Block GD. Circadian rhythms in isolated brain regions. J Neurosci. 2002;22:350–356
2. Abreu MT (2010) Toll-like receptor signalling in the intestinal epithelium: how bacterial recognition shapes intestinal function. Nat Rev Immunol 10: 131–144. doi: 10.1038/nri2707
3. Achermann P and Borbély AA (2003) Mathematical models of sleep regulation. Frontiers in Bioscience 8: 683-693.
4. Albrecht, U., Sun, Z. S., Eichele, G., Lee, C. C. A differential response to two putative mammalian circadian regulators, mper1 and mper2, to light. Cell 91: 1055-1064, 1997.
5. AschoffJ (1965) Circadian rhythms in man. Science 148:1427–1432
6. Asher G, Gatfield D, Stratmann M, Reinke H, Dibner C, Kreppel F, Mostoslavsky R, Alt FW, Schibler U. (2008). SIRT1 regulates circadian clock gene expression through PER2 deacetylation. Cell 134, 317–328.
7. Asher, G., and Schibler, U. (2011). Crosstalk between components of circadian and metabolic cycles in mammals. Cell Metab. 13, 125–137.
8. Asher, G., and Sassone-Corsi, P. (2015). Time for food: the intimate interplay between nutrition, metabolism, and the circadian clock. Cell 161, 84–92.
9. Balsalobre A, Damiola F & Schibler U (1998). A serum shock induces circadian gene expression in mammalian tissue culture cells. Cell 93 929–937.
10. Balsalobre A, Brown SA, Marcacci L, Tronche F, Kellendonk C, Reichardt HM, Schutz G & Schibler U (2000). Resetting of circadian time in peripheral tissues by glucocorticoid signaling. Science 289 2344–2347.
11. Bass J Circadian topology of metabolism (2012) .Nature 491 (7424), 348-356
12. Berson DM, Dunn FA, Takao M. Phototransduction by retinal ganglion cells that set the circadian clock. Science. 2002;295:1070–3.
13. Borbély AA (1982) A two process model of sleep regulation. Human Neurobiolgy 1:195-204
14. Chang H. C., Guarente L. (2013). SIRT1 mediates central circadian control in the SCN by a mechanism that decays with aging. Cell 153, 1448–1460. 10.1016/j.cell.2013.05.027.
15. Colwell C, Michel S, Itri J, Rodriguez W, Tam J, Lelievre V, Hu Z, Liu X, Waschek J. Disrupted circadian rhythms in VIP- and PHI-deficient mice. Am J Physiol Regul Integr Comp Physiol.2003;285:R939–R949.
16. Damiola F., Le Minh,N., Preitner,N., Kornmann,B., Fleury-Olela,F. and Schibler,U. (2000) Restricted feeding uncouples circadian oscillators in peripheral tissues from the central pacemaker in the suprachiasmatic nucleus. Genes Dev., 14, 2950–2961.
17. De Cesare D, Sassone-corsi P. Transcriptional regulation by cyclic AMP-responsive factors. Prog Nucleic Acid Res Mol Biol. 2000;64:343-69.
18. Doi M, Takahashi Y, Komatsu R, Yamazaki F, Yamada H, Haraguchi S, Emoto N,Ok uno Y, Tsujimoto G, Kanematsu A, et al. 2010. Salt-sensitive hypertension in circadian

clock-deficient Cry-null mice involves dysregulated adrenal Hsd3b6. Nat Med 16: 67–74.
19. Duez H, Staels B (2008) Rev-erb α gives a time cue to metabolism. FEBS Lett 582(1): 19–25.
20. Eckel-Mahan KL, Patel VR, de Mateo S, Ceglia NJ, Sahar SS, Dilag S, Dyar KA, Orozco-Solis R, Baldi P, and Sassone-Corsi P. Reprogramming of the Circadian Clock by Nutritional Challenge Cell, 2013 December 19,155(7), 1464-1478
21. Feng D, Lazar MA (2012) Clocks, metabolism, and the epigenome. Mol Cell 47(2):158–167.
22. Froy, O., and Chapnik, N. (2007). Circadian oscillation of innate immunity components in mouse small intestine. Mol. Immunol. 44, 1954–1960.
23. Hattar S, Liao HW, Takao M, Berson DM, Yau KW. Melanopsin-containing retinal ganglion cells: architecture, projections, and intrinsic photosensitivity. Science. 2002;295:1065–70.
24. Hattar S, Lucas RJ, Mrosovsky N, Thompson S, Douglas RH, Hankins MW, Lem J, Biel M, Hofmann F, Foster RG, Yau KW. Melanopsin and rod-cone photoreceptive systems account for all major accessory visual functions in mice. Nature. 2003;424:76–81.
25. Harmar A, Marston H, Shen S, Spratt C, West K, Sheward W, Morrison C, Dorin J, Piggins H, Reubi J, et al. The VPAC(2) receptor is essential for circadian function in the mouse suprachiasmatic nuclei. Cell. 2002;109:497–508.
26. Hastings MH & Herzog ED 2004 Clock genes, oscillators, and cellular networks in the suprachiasmatic nuclei. Journal of Biological Rhythms 19 400–413.
27. Hooper, L.V., Wong, M.H., Thelin, A., Hansson, L., Falk, P.G., and Gordon, J.I. (2001). Molecular analysis of commensal host-microbial relationships in the intestine. Science *291*, 881–884.
28. Hughes ME, DiTacchio L, Hayes KR, Vollmers C, Pulivarthy S, et al. Harmonics of circadian gene transcription in mammals. PLoS Genet. 2009;5:e1000442.
29. Hussain, M.M., and Pan, X. (2009). Clock genes, intestinal transport and plasma lipid homeostasis. Trends Endocrinol. Metab. *20*, 177–185.
30. Kalsbeek A, Bruinstroop E, Yi CX, Klieverik LP, La Fleur SE, Fliers E. Hypothalamic control of energy metabolism via the autonomic nervous system. Ann. N. Y. Acad. Sci. 2010;1212:114–129.
31. Kennaway DJ, Owens JA, Voultsios A, Boden MJ, Varcoe TJ. Metabolic homeostasis in mice with disrupted Clock gene expression in peripheral tissues. Am. J. Physiol. Regul. Integr. Comp. Physiol.2007;293:R1528–R1537.
32. Kersten S, Desvergne B, Wahli W (2000) Roles of PPARs in health and disease. Nature 405(6785):421–424.
33. Ko, C.H. & Takahashi, J.S. (2006) Molecular components of the mammalian circadian clock. Human Molecular Genetics, 15, R271-277.

34. Kohsaka A, Laposky AD, Ramsey KM, Estrada C, Joshu C, Kobayashi Y, Turek FW, Bass J. High-fat diet disrupts behavioral and molecular circadian rhythms in mice. Cell Metab. 2007; 6:414–421.
35. Konopka RJ and Benzer S (1971) Clock mutants of Drosophila melanogaster. Proc Natl Acad Sci U S A 68:2112-2116.
36. Krieger DT, Hauser H, Krey LC. Suprachiasmatic nuclear lesions do not abolish food-shifted circadian adrenal and temperature rhythmicity. Science. 1977;197:398–9.
37. Lamia KA, Storch KF, Weitz CJ (2008) Physiological significance of a peripheral tissue circadian clock. Proc Natl Acad Sci USA 105:15172–15177.
38. Lamia KA, Sachdeva UM, DiTacchio L, Williams EC, Alvarez JG, Egan DF, Vasquez DS, Juguilon H, Panda S, Shaw RJ, Thompson CB, Evans RM. (2009) AMPK regulates the circadian clock by cryptochrome phosphorylation and degradation. Science 326:437–440. doi: 10.1126/science.1172156
39. Lamia KA, Papp SJ, Yu RT, Barish GD, Uhlenhaut NH, Jonker JW, Downes M, Evans RM (2011). Cryptochromes mediate rhythmic repression of the glucocorticoid receptor. Nature 2011;480:552–556. doi: 10.1038/nature10700.
40. Lee I. T., Chang A. S., Manandhar M., Shan Y., Fan J., Izumo M., et al. . (2015). Neuromedin s-producing neurons act as essential pacemakers in the suprachiasmatic nucleus to couple clock neurons and dictate circadian rhythms. Neuron 85, 1086–1102. 10.1016/j.neuron.2015.02.006.
41. Le Martelot G, Claudel T, Gatfield D, Schaad O, Kornmann B, Lo Sasso G, Moschetta A, Schibler U. 2009. REV-ERBalpha participates in circadian SREBP signaling and bile acid homeostasis. PLOS Biology 7:e1000181. doi: 10.1371/journal.pbio.1000181.
42. Le Minh N, Damiola F, Tronche F, Schütz G, Schibler U (2001) Glucocorticoid hormones inhibit food-induced phase-shifting of peripheral circadian oscillators. EMBO J 20(24):7128–7136.
43. Ley R., Backhed F., Turnbaugh P., Lozupone C., Knight R., Gordon J. (2005) Obesity alters gut microbial ecology. Proc Natl Acad Sci U S A 102: 11070–11075.
44. Lowrey PL, Takahashi JS. Mammalian circadian biology: elucidating genome-wide levels of temporal organization. Annu. Rev. Genom. Hum. Genet. 2004;5:407–441.
45. Moore, R. Y., and Eichler, V. B., 1972, Loss of circadian adrenal corticosterone rhythm following suprachiasmatic lesions in the rat, Brain Res. 42: 201–206.
46. M.R. Ralph, M. Menaker. A mutation of the circadian system in golden hamsters Science, 241 (1988), pp. 1225–1227
47. M.R. Ralph, R.G. Foster, F.C. Davis, M. Menaker.Transplanted suprachiasmatic nucleus determines circadian period. Science, 247 (1990), pp. 975–978.
48. Nakahata Y, Kaluzova M, Grimaldi B, Sahar S, Hirayama J, Chen D, Guarente LP, Sassone-Corsi P. (2008). The NAD+-dependent deacetylase SIRT1 modulates CLOCK-mediated chromatin remodeling and circadian control. Cell 134, 329–340.
49. Nakahata Y, Sahar S, Astarita G, Kaluzova M, Sassone-Corsi P. (2009). Circadian control of the NAD+ salvage pathway by CLOCK-SIRT1. Science 324, 654–657.

50. Panda S, Sato TK, Castrucci AM, Rollag MD, DeGrip WJ, et al. Melanopsin (Opn4) requirement for normal light-induced circadian phase shifting. Science. 2002;298:2213–6.
51. Panda S, Provencio I, Tu DC, Pires SS, Rollag MD, Castrucci AM, Pletcher MT, Sato TK, Wiltshire T, Andahazy M, Kay SA, Van Gelder RN, Hogenesch JB. Melanopsin is required for non-image-forming photic responses in blind mice. Science. 2003;301:525–527.
52. Pittendrigh, C.S., Daan, S.: A functional analysis of circadian pacemakers in nocturnal rodents. I. The stability and lability of spontaneous frequency. J. comp. Physiol.106, 223–252 (1976)
53. Rakoff-Nahoum, S., Paglino, J., Eslami-Varzaneh, F., Edberg, S., and Medzhi- tov, R. (2004). Recognition of commensal microflora by toll-like receptors is required for intestinal homeostasis. Cell 118, 229–241.
54. Ramsey K, Yoshino J, Brace CS, Abrassart D, Kobayashi Y, Marcheva B, Hong HK, Chong JL, Buhr ED, Lee C, et al. (2009). Circadian clock feedback cycle through NAMPT-mediated NAD+ biosynthesis. Science 324, 651–654.
55. Richter, C. P., 1965, Biological Clocks in Medicine and Psychiatry, Charles C. Thomas, Publisher, Springfield, Ill.
56. Ripperger, U. Schibler. Rhythmic CLOCK-BMAL1 binding to multiple E-box motifs drives circadian Dbp transcription and chromatin transitions. Nat. Genet., 38 (2006), pp. 369–374
57. Robles, MS & Mann, M. (2013) Proteomic approaches in circadian biology. in Handbook of experimental pharmacology: Circadian Clocks. pp. 389-407. Handbook of Experimental Pharmacology.
58. Ruby NF, Brennan TJ, Xie X, Cao V, Franken P, et al. Role of melanopsin in circadian responses to light. Science. 2002;298:2211–3.
59. Rudic RD, et al. (2004) BMAL1 and CLOCK, two essential components of the circadian clock, are involved in glucose homeostasis. PLoS Biol 2:e377.
60. Rutter J, Reick M, Wu LC, McKnight SL (2001) Regulation of Clock and NPAS2 DNA binding by the redox state of NAD cofactors. Science 293: 510–514.
61. Rusak, B., 1977. The role of the suprachiasmatic nuclei in the generation of Circadian rhythm in the golden hamster, Mesocricetus auratus, J. Comp. Physiol. 118: 145–164.
62. Rusak B, Zucker I (1979) Neural regulation of circadian rhythms. Physiol Rev 59:449–526.
63. Takahashi JS, Hong HK, Ko CH, McDearmon EL. The genetics of mammalian circadian order and disorder: implications for physiology and disease. Nat. Rev. Genet. 2008;9:764–775.
64. Thaiss CA, et al. (2014). Transkingdom control of microbiota diurnal oscillations promotes metabolic homeostasis. Cell 159(3):514–529.
65. Turek F.W, C. Joshu, A. Kohsaka, E. Lin, G. Ivanova, E. McDearmon, A. Laposky, S. Losee-Olson, A. Easton, D.R. Jensen, et al. Obesity and metabolic syndrome in circadian Clock mutant mice. Science, 308 (2005), pp. 1043–1045.

66. Turnbaugh P., Ley R., Mahowald M., Magrini V., Mardis E., Gordon J. (2006) An obesity-associated gut microbiome with increased capacity for energy harvest. Nature 444: 1027–1031.
67. Sassone-Corsi P. The Time of Your Life. Cerebrum. 2014 Jul-Aug; 2014: 11.
68. Shearman, L. P., Zylka, M. J., Weaver, D. R., Kolakowski, L. F., Jr., Reppert, S. M. Two period homologs: circadian expression and photic regulation in the suprachiasmatic nuclei. Neuron 19: 1261-1269, 1997.
69. Storch, K. F., Lipan, O., Leykin, I., Viswanathan, N., Davis, F. C., Wong, W. H., et al. (2002). Extensive and divergent circadian gene expression in liver and heart. Nature, 417, 78–83.
70. Ueda HR, Chen W, Adachi A, Wakamatsu H, Hayashi S, Takasugi T, Nagano M, Nakahama K, Suzuki Y, Sugano S, et al.: A transcription factor response element for gene expression during circadian night. Nature 2002, 418:534-539.
71. Ueda HR, Hayashi S, Chen W, Sano M, Machida M, Shigeyoshi Y, Iino M, Hashimoto S: System-level identification of transcriptional circuits underlying mammalian circadian clocks. Nat Genet 2005, 37:187-192.
72. Welsh DK, Yoo SH, Liu AC, Takahashi JS & Kay SA 2004 Bioluminescence imaging of individual fibroblasts reveals persistent, independently phased circadian rhythms of clock gene expression. Current Biology 14 2289–2295.
73. Yamazaki S, Numano R, Abe M, Hida A, Takahashi R, Ueda M, Block GD, Sakaki Y, Menaker M & Tei H 2000 Resetting central and peripheral circadian oscillators in transgenic rats. Science 288 682–685.
74. Yang X, Downes M, Yu RT, Bookout AL, He W, Straume M, Mangelsdorf DJ, Evans RM. 2006. Nuclear receptor expression links the circadian clock to metabolism. Cell 126: 801–810.
75. Yagita K, Tamanini F, van Der Horst GT & Okamura H 2001 Molecular mechanisms of the biological clock in cultured fibroblasts. Science 292 278–281.
76. Yin L., Wang J., Klein P. S., Lazar M. A. Nuclear receptor Rev-Erb alpha is a critical lithium-sensitive component of the circadian clock. Science. 2006;311:1002–5.
77. Yoo SH, Yamazaki S, Lowrey PL, Shimomura K, Ko CH, Buhr ED, Siepka SM, Hong HK, Oh WJ, Yoo OJ et al. 2004 PERIOD2::LUCIFERASE real-time reporting of circadian dynamics reveals persistent circadian oscillations in mouse peripheral tissues. PNAS 101 5339–5346.
78. Zylka MJ, Shearman LP, Weaver DR, Reppert SM. Three period homologs in mammals: differential light responses in the suprachiasmatic circadian clock and oscillating transcripts outside of brain.Neuron. 1998;20:1103–1110.

Aim of the thesis

Under physiological conditions, the light-entrained master central circadian clock (CC), which is located in the suprachiasmatic nucleus (the SCN CC), synchronizes the ubiquitous peripheral clocks (PCCs). It also generates in the laboratory mouse a diurnal alternance of phases of ‘’activity‘’ (during the dark period) and ‘’rest’’ (during the light period), both of which are at the origin of rhythmic variations of genes expression. This phase alternance is essential to maintain a metabolic and behavioral homeostasis. In marked contrast with mice, in most vertebrates the period of ‘’activity’’ take place during the light period (the light period of the day) while the period of ‘’rest’’ take place during the dark period of the day (the night). The central circadian clock has evolved as a time keeping schedule for our body to optimize the timing of metabolic events according to physiological needs and environmental cues. Under homeostatic conditions, the peripheral circadian clocks and the metabolism are intimately linked, and a perturbation of this coupling creates pathologies. Time of feeding acts as a powerful “*Zeitgeber*” (time cue) for peripheral clocks in rodents. Interestingly, it has been demonstrated that by shifting the feeding time, from the “active” phase, to the “rest” phase, [the so-called Restricted Feeding (RF)], shifts by 12 hours the expression pattern of the circadian core components in peripheral organs within 7-10 days, whereas they retain their normal pattern of expression in the SCN CC, thereby creating a misalignment between the two clocks (SCN CC and PCCs). Most interestingly, such “RF” mice develop with time a cohort of metabolic pathologies including diabetes, obesity and metabolic syndrome. We have addressed during my thesis work some of the questions, which deal with the systemic metabolic and behavioral effects of shifting the time of feeding in relation with alterations of both the peripheral and central circadian clocks:

1- Deciphering the identity of the molecular signals, which orchestrate a shift of peripheral CCs upon Restricted Feeding (RF).
2- How is the SCN master central clock immunized against RF-induced metabolic perturbations? How does the RF-induced circadian misalignment between the peripheral circadian clocks (PCCs) and the SCN master central clock (SCN CC) create a metabolic syndrome-like pathology?
3- How the microbiota provide molecular cues for the circadian control of intestinal epithelial cell (IEC) homeostasis.

Publication 1: Shifting the feeding of mice to the rest phase creates metabolic alterations, which, on their own, shift the peripheral circadian clocks by 12 hours. Mukherji A*, **Kobiita A***, Chambon P (2015). **Proc Natl Acad Sci USA, 10.1073/pnas.1519735112. (*Co-First author)**

Publication 2: Shifting eating to the circadian rest phase misaligns the peripheral clocks with the master SCN clock and leads to a metabolic syndrome. Mukherji A, **Kobiita A**, Damara M, Misra N, Meziane H, Champy MF, and Chambon P (2015)**. ProcNatl Acad Sci USA, 10.1073/pnas.1519807112.**

Publication 3: Homeostasis in intestinal epithelium is orchestrated by the circadian clock and microbiota cues transduced by TLRs. Mukherji A, **Kobiita A**, Ye T, and Chambon P. (2013). **Cell 153, 812–827.**

Shifting the feeding of mice to the rest phase creates metabolic alterations, which, on their own, shift the peripheral circadian clocks by 12 hours

Atish Mukherji[a,1], Ahmad Kobiita[a,1], and Pierre Chambon[a,b,2]

[a]Institut de Génétique et de Biologie Moléculaire et Cellulaire, CNRS UMR7104, INSERM U964; and [b]University of Strasbourg Institute for Advanced Study, Collège de France, Illkirch 67404, France

Contributed by Pierre Chambon, October 9, 2015 (sent for review September 2, 2015; reviewed by Gerard Karsenty and Paolo Sassone-Corsi)

The molecular mechanisms underlying the events through which alterations in diurnal activities impinge on peripheral circadian clocks (PCCs), and reciprocally how the PCCs affect metabolism, thereby generating pathologies, are still poorly understood. Here, we deciphered how switching the diurnal feeding from the active to the rest phase, i.e., restricted feeding (RF), immediately creates a hypoinsulinemia during the active phase, which initiates a metabolic reprogramming by increasing FFA and glucagon levels. In turn, peroxisome proliferator-activated receptor alpha (PPARα) activation by free fatty acid (FFA), and cAMP response element-binding protein (CREB) activation by glucagon, lead to further metabolic alterations during the circadian active phase, as well as to aberrant activation of expression of the PCC components nuclear receptor subfamily 1, group D, member 1 (*Nr1d1*/*RevErbα*), Period (*Per1* and *Per2*). Moreover, hypoinsulinemia leads to an increase in glycogen synthase kinase 3β (GSK3β) activity that, through phosphorylation, stabilizes and increases the level of the RevErbα protein during the active phase. This increase then leads to an untimely repression of expression of the genes containing a RORE DNA binding sequence (DBS), including the *Bmal1* gene, thereby initiating in RF mice a 12-h PCC shift to which the CREB-mediated activation of *Per1*, *Per2* by glucagon modestly contributes. We also show that the reported corticosterone extraproduction during the RF active phase reflects an adrenal aberrant activation of CREB signaling, which selectively delays the activation of the PPARα–RevErbα axis in muscle and heart and accounts for the retarded shift of their PCCs.

shifted eating | shifted peripheral circadian clocks | metabolic alterations | RevErbα | PPARα

Pioneering studies (1, 2) have established that switching the feeding time in mice from the "active" phase [dark period of the light-dark (L/D) cycle] to the "rest" phase (light period), i.e., restricted feeding (RF), overrides the suprachiasmatic nucleus (SCN) circadian clock (CC)-derived signals and acts as a "zeitgeber" for peripheral CCs (PCCs), leading to a 12-h shift in the time at which components of PCCs are expressed. Numerous studies have shown that under homeostatic conditions, the functions of PCCs and metabolism are tightly linked and that perturbations in their interactions leads to pathologies, e.g., obesity and metabolic syndrome (3–5).The identity of some of the molecular pathways that couple PCCs to metabolism are known (3–5), but it is largely unknown how environmental cues, e.g., altered feeding schedules, may directly perturb the expression of individual CC components (5–7), thereby leading to obesity and a metabolic syndrome-like pathology (5). Assuming that specific metabolic perturbations generated by switching the feeding time could selectively affect the time of expression of some of the CC core components, we looked for both metabolic and PCC alterations at early RF times. We report here a comprehensive temporal analysis, and we found that the shift of PCCs on RF is directly linked, at the molecular level, to metabolic reprogramming that directly impinges on CC component expression.

Results

RF Leads to a Starvation-Like State Characterized by Metabolic and CC Alterations. We initially observed that on RF, gastric emptying is severely delayed (Fig. S1*B*), thereby creating a "starvation-like state." This observation led us to investigate the effect of a 24-h starvation on metabolic parameters, which revealed reductions in glucose and insulin (INS) and increases of ketone bodies (βOHB; β-hydroxybutyrate) and free fatty acid (FFA) (Fig. S1 *A* and *E*), whereas concomitant transcript analyses showed an increase and altered pattern of expression for Period 1 and 2 (*Per1* and *Per2*) and nuclear receptor subfamily 1, group D, member 1 (*Nr1d1*/*RevErbα*), but not of aryl hydrocarbon receptor nuclear translocator-like protein 1 (*ARNTL1*/*Bmal1*), cryptochrome 1 (*Cry1*) and a nuclear Factor, interleukin 3 regulated (*NFIL3*/*E4BP4*) (Fig. S1 *C* and *D*). We therefore posited that RF could be accompanied by metabolic changes that could affect PCCs.

Analyzing the RF effect on these parameters during the RF first day (RF1; Fig. 1*A*) indicated INS and triglyceride (TG) decreases, whereas glucose, FFA, and glucagon increased (Fig. 1*B*). Looking at CC component expression during RF1 showed that *Per1*, *Per2*, and *RevErbα* transcripts increased between *"Zeitgeber"* (ZT) 20 and ZT4 (food withdrawal at ZT12), whereas *Bmal1*, *Cry1*, and *E4BP4* were unaltered (Fig. 1*C* and Fig. S1 *F*–*I*). Of note, using luciferase reporter mice, Saini et al. (8) observed a similar pattern of expression for *Per2*, *RevErbα*, and *Bmal1* in RF livers. That early RF metabolic changes were similar to those generated under starvation and that RF and starvation altered the same CC components prompted us to investigate how metabolic alterations may impair PCC during RF.

Significance

Under homeostasis, peripheral circadian clocks (CCs) and metabolism are intimately linked, as pathologies occur on perturbation of their coupling. In mice, shifting the feeding time from the phase of activity (night) to the phase of rest (day) is known to act as a time cue for peripheral CCs, leading to a 12-hour shift of the time at which their CC components are expressed. However, the molecular mechanisms that underlie this shift are largely unknown. Here, we reveal both the origin and the identity of the metabolic signals that are generated on shifting eating to the rest phase and how these signals directly alter the expression of CC components to generate the shift that ultimately leads to metabolic syndrome-like pathology.

Author contributions: A.M., A.K., and P.C. designed research; A.M. and A.K. performed research; A.M., A.K., and P.C. analyzed data; and A.M. and P.C. wrote the paper.

Reviewers: G.K., Columbia University, NY; and P.S.-C., University of California, Irvine.

The authors declare no conflict of interest.

[1]A.M. and A.K. contributed equally to this work.

[2]To whom correspondence should be addressed. Email: chambon@igbmc.fr.

This article contains supporting information online at www.pnas.org/lookup/suppl/doi:10.1073/pnas.1519735112/-/DCSupplemental.

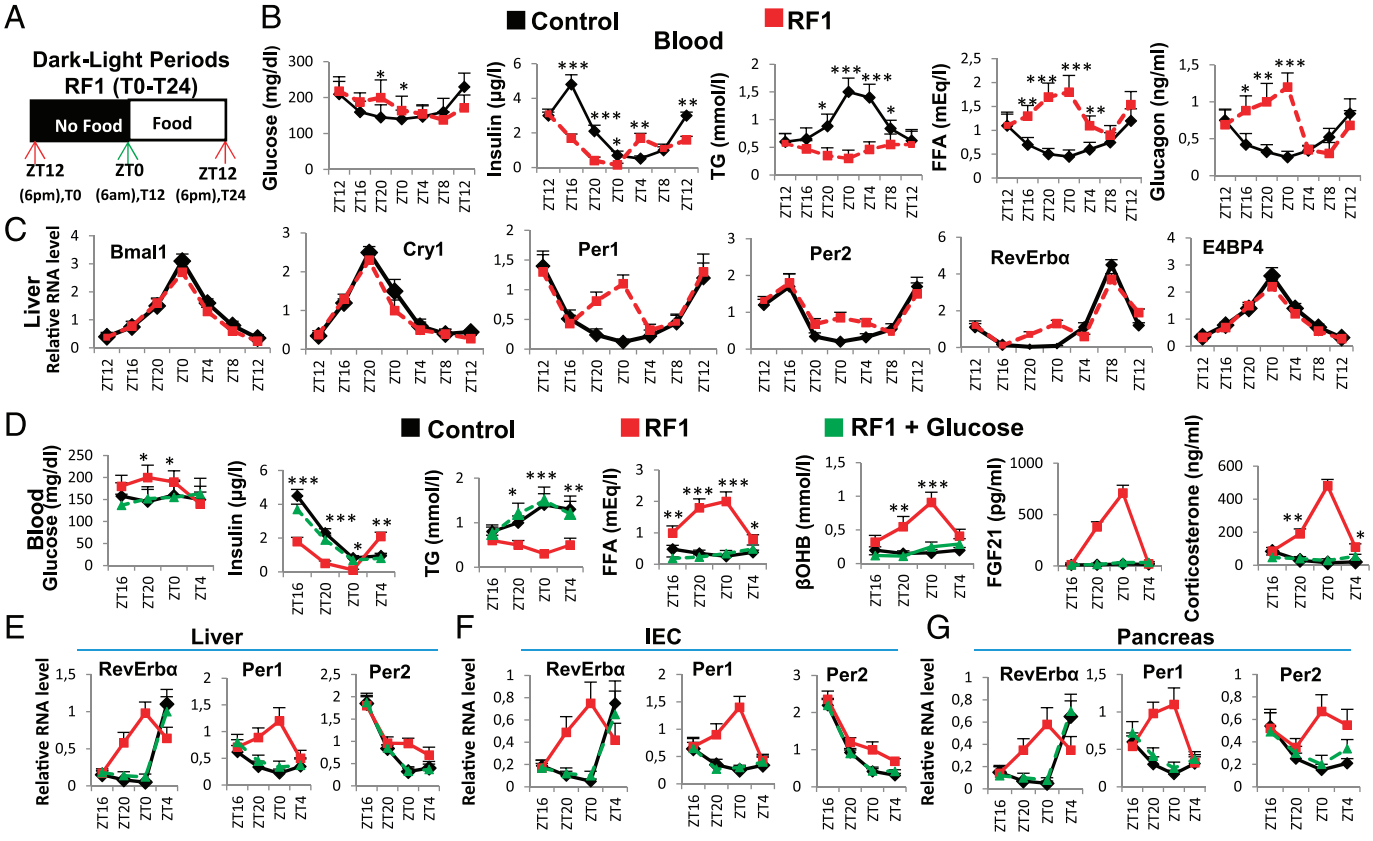

Fig. 1. RF initiation induces metabolic and CC alterations. (*A*) Schematic representation of the RF1 experiment. (*B*) Levels of blood components in control and RF1 mice. (*C*) RNA transcript levels of CC components in RF1 liver. (*D*) Levels of blood components in control, RF1, and RF1 intraperitoneally glucose administered (RF1+Glucose) mice. (*E*–*G*) RNA transcript levels of genes as indicated in liver (*E*), IEC (*F*), and pancreas (*G*) of control, RF1, and RF1+Glucose mice. All values are mean ± SEM. $*P < 0.05$, $**P < 0.01$, $***P < 0.001$.

Glucose Administration Prevents Metabolic and PCC Alterations During the RF Initial Phase. A starvation-induced decrease in blood glucose reduces INS and increases glucagon and FFA levels, thereby activating gluconeogenesis and β-oxidation (9, 10). We therefore posited that maintaining blood glucose may prevent metabolic and PCC alterations during early RF. Indeed, glucose administration to RF mice (RF glucose mice) prevented INS decrease and a rise in FFA, corticosterone, βOHB, and fibroblast growth factor 21 (FGF21) (Fig. 1*D*). Notably, there was no increase of *Per1*, *Per2*, and *RevErbα* in the liver, intestinal epithelial cells (IECs), and pancreas of RF glucose mice (Fig. 1 *E*–*G*), supporting our hypothesis that the initial RF CC alterations originate from an altered metabolism.

An Early Insulin Decrease Triggers Increased Lipolysis, FFA Release, and Aberrant PPARα Signaling in RF Mice. A decrease in blood INS triggers adipose tissue lipolysis and release of FFA, which acts as a ligand for peroxisome proliferator-activated receptor alpha (PPARα) (11). Importantly, FFA-liganded PPARα (see Fig. 3*A*) is known to activate transcription of a number of target genes containing a direct repeat 1 (DR1) DNA binding sequence (DBS) (11), and to activate its own transcription by binding to its own DR1 DBS (11). Accordingly, expression of *PPARα* and of its target genes was increased in RF liver and IECs between ZT16 and ZT0 (Fig. 2*B* and Fig. S2 *B*, *C*, and *F*), and ChIP assays demonstrated a concomitant increase in PPARα binding to its own DR1-DBS and to those of its target genes (Fig. 2*C*). We previously demonstrated that, in absence of Bmal1, PPARα could induce *RevErbα* transcription through binding to the DR2 DBS of the *RevErbα* promoter (12). As RevErbα transcripts increased in RF mice (when no Bmal1 activity could be detected; see above), we speculated that PPARα could also contribute to this RF increase in *RevErbα* expression. Indeed, PPARα was recruited to *RevErbα* DR2 DBS during early RF (ZT20–ZT0), but not in control animals (Fig. 2*D*). Moreover, selective *PPARα* mutations in liver ($PPAR\alpha^{hep-/-}$) and IECs ($PPAR\alpha^{iec-/-}$) demonstrated that the early RF increases in *RevErbα*, *HMGCS2*, *FGF21*, and *FIAF* transcripts were dependent on PPARα (Fig. S2 *D* and *E* and Fig. 3*A*). Importantly, glucose administration to RF mice inhibited PPARα binding to its own promoter and to the DR1 DBSs in its target genes, as well as to the *RevErbα* DR2 DBS (Fig. S2 *J* and *K*), leading to a reduction in their expression during RF (Fig. 1 *E*–*G* and Fig. S2*I*). Of note, these early RF-induced expressions of *PPARα* and of its target genes were not affected in $Bmal1^{hep-/-}$ and $Bmal1^{iec-/-}$ mutants (Fig. S2 *G* and *H*).

PPARα and RevErbα Are Instrumental in RF-Induced Breaking of Existing PCCs. As RF early metabolic alterations did affect the expression of *Per1*, *Per2*, and *RevErbα*, we analyzed the transcript of CC components after RF for 4, 8, 15, 30, and 90 d. In liver and IECs, all of them were shifted after RF4, but it took 8 d to achieve the same shifts in muscle and heart (see below). Importantly, once established these shifts were stable as long as RF was not interrupted, whereas the "original circadian active and rest phases" remained unchanged throughout the RF period (13).

Analysis of CC shifts in liver and IECs during the first 108 RF hours (Fig. 4*A* and Fig. S3*A*) revealed that they occurred in two steps. The first phase (broken clock; compare Fig. 3 *B* and *C*) was triggered by metabolic alterations occurring during the active phase (ZT12–ZT0) through (*i*) an increase of FFA-liganded PPARα that activated aberrant *RevErbα* expression (Figs. 3*C* and 4*A* and Fig. S3*A*) mediated by its binding to the *RevErbα* DR2 DBS (Fig. 4*D*). This RevErbα increased expression then repressed during the ac-

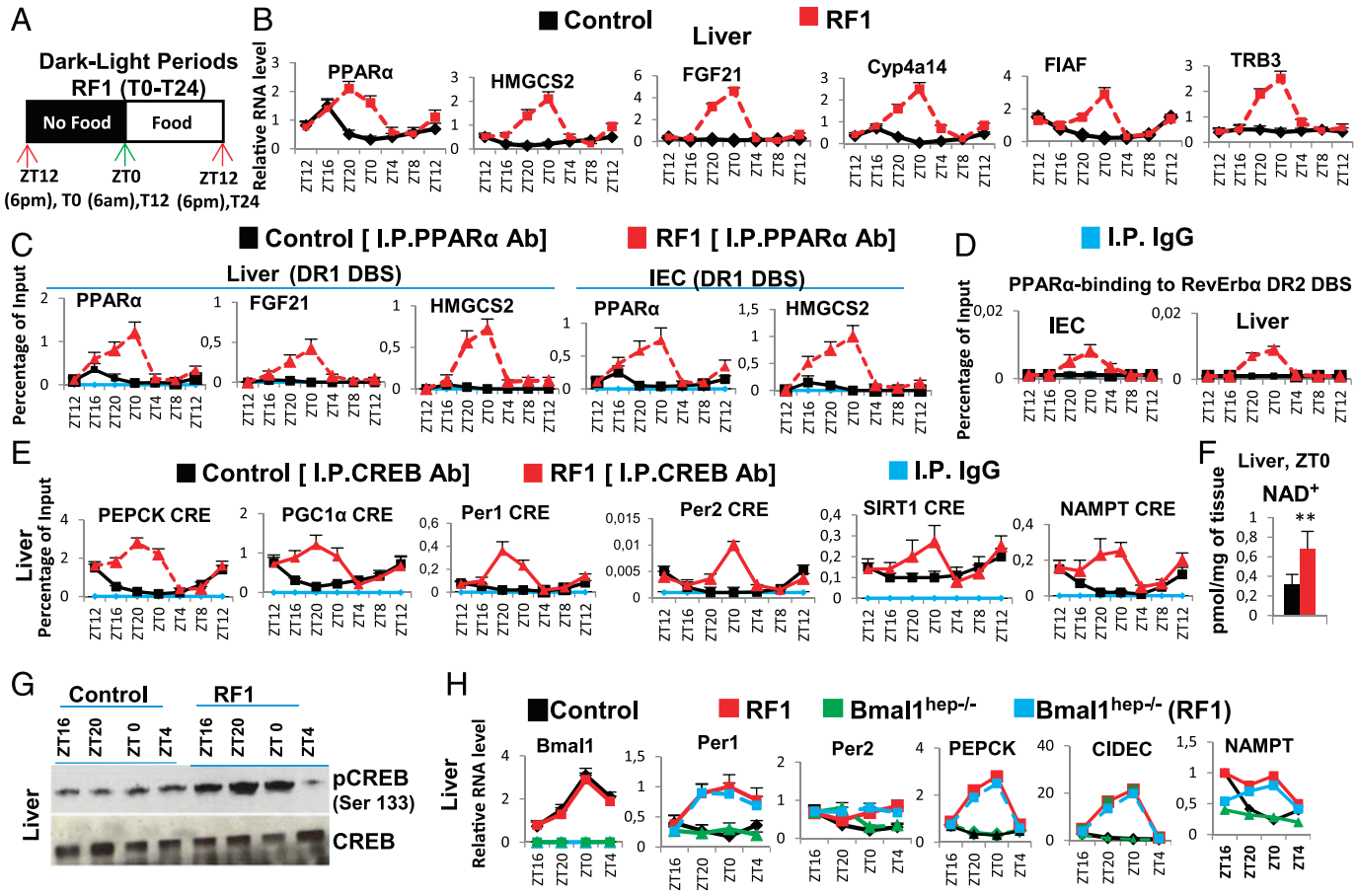

Fig. 2. RF-induced aberrant activations of PPARα and CREB signaling play a critical role in metabolic and CC alterations. (*A*) Schematic representation of the RF1 experiment. (*B*) RNA transcript levels of genes, as indicated, in RF1 liver. (*C*) ChIP-qPCR assays to analyze PPARα recruitment to DR1 DBS-containing genes in liver of control and RF1 mice. (*D*) ChIP-qPCR assays to analyze PPARα recruitment to the RevErbα DR2 DBS in liver and IEC of control and RF1 mice. (*E*) ChIP-qPCR assays to analyze CREB binding to CRE DBSs present in the indicated genes in control and RF1 liver. (*F*) NAD^+ levels in control and RF1 liver. (*G*) Immunoblot analyses of control and RF1 liver with indicated antibodies. (*H*) RNA transcript levels of genes as indicated in liver of control and RF1 mice, with or without selective mutation of Bmal1 ($Bmal1^{hep-/-}$). All values are mean ± SEM. $^{**}P < 0.01$.

tive phase the expression of RORα/RevErbα response element (RORE)-containing genes (Fig. 4 *A* and *B* and Fig. S3 *A* and *B*), and (*ii*) a simultaneous pCREB increase that activated *Per1*, *Per2* expression (Fig. 4*A* and Figs. S3*A*, S4*C*, and S5*A*). Importantly, besides these *Per1*, *Per2*, and *RevErbα* transcript alterations during RF1 night, there was no changes in the profile of other CC components (*Bmal1*, *Cry1*, and *E4BP4*; Fig. 4*A* and Fig. S3*A*). In contrast, the expression of all CC components was altered during RF2 (compare RF1 and RF2 in Fig. 4*A* and Fig. S3*A*), because (*i*) during the active phase, the levels of *Bmal1*, *Cry1*, and *E4BP4* transcripts were diminished, (*ii*) during the rest phase (ZT0–ZT12), there was a decrease in *RevErbα* transcripts that were abnormally expressed during the active phase, and (*iii*) the physiological ZT8–ZT12 expression of *Per2* transcripts disappeared, whereas both *Per1* and *Per2* transcripts were modestly expressed during the ZT20–ZT4 period (Fig. 4*A* and Fig. S3*A*).

ChIP assays were performed in RF liver and IECs to explore the basis for these aberrant expressions of PCC components. It is known that *RevErbα* expression is controlled by Bmal1 (3) and, in addition, that the *RevErbα* promoter contains a DR2 DBS to which RevErbα binds to trigger its autorepression, whereas the binding of FFA-liganded PPARα to the same element enhances *RevErbα* expression (12, 14) (Fig. 3*C*). As $PPAR\alpha^{hep-/-}$ and $PPAR\alpha^{iec-/-}$ mutants (Fig. S2 *D* and *E*) together with $Bmal1^{hep-/-}$ and $Bmal1^{iec-/-}$ mutants (Fig. S2 *G* and *H*) revealed the Bmal1-independent critical role of PPARα in *RevErbα* early expression in RF mice, we analyzed PPARα binding on the *RevErbα* DR2 DBS in RF tissues. Remarkably, this binding was only detected in RF mice during the ZT16–ZT0 period of the first two RF nights (Fig. 4*D*; see below), thereby leading to aberrant *RevErbα* transcription during the active phase (Figs. 3*C* and 4*A* and Fig. S3*A*).

As expected (9), RF hypoinsulinemia also decreased pAKT, thereby activating glycogen synthase kinase 3β (GSK3β) which, in turn, through phosphorylation, increases the amount of RevErbα (steps 8–11 in Fig. 3*A* and Fig. S3*C*) (13). ChIP assays (Fig. 4*B* and Fig. S3*B*) performed to investigate the consequence of this active phase RevErbα expression revealed a time-restricted (ZT8–ZT12) RevErbα binding to *Bmal1*, *Cry1*, and *E4BP4* RORE DBS (3) in both control and RF mice during the RF1 rest phase (Fig. 4*B* and Fig. S3*B*). In contrast, during the active phase of RF2, RevErbα was recruited on these RORE DBSs between ZT20 and ZT4, which resulted in their repression during the active phase (Fig. 4*B*, Fig. S3*B*, and see steps 1–3 in Fig. 3*C*).

The Shifted Expression of Bmal1 Generates Shifted PCCs. As Bmal1-dependent transcription of *Per1*, *Per2*, and *RevErbα* is known to drive CCs (3–5), ChIP assays were performed to analyze its contribution in initiating the RF PCC shift. In control mice, ChIP assays showed a rest phase (ZT4–ZT12) Bmal1 binding to the E-Box DBS of *Per1*, *Per2*, and *RevErbα* (Fig. 4*C* and Fig. S4*A*) (15). Strikingly, on RF1 night, no Bmal1 binding could be detected on the E-box of these genes when they were initially

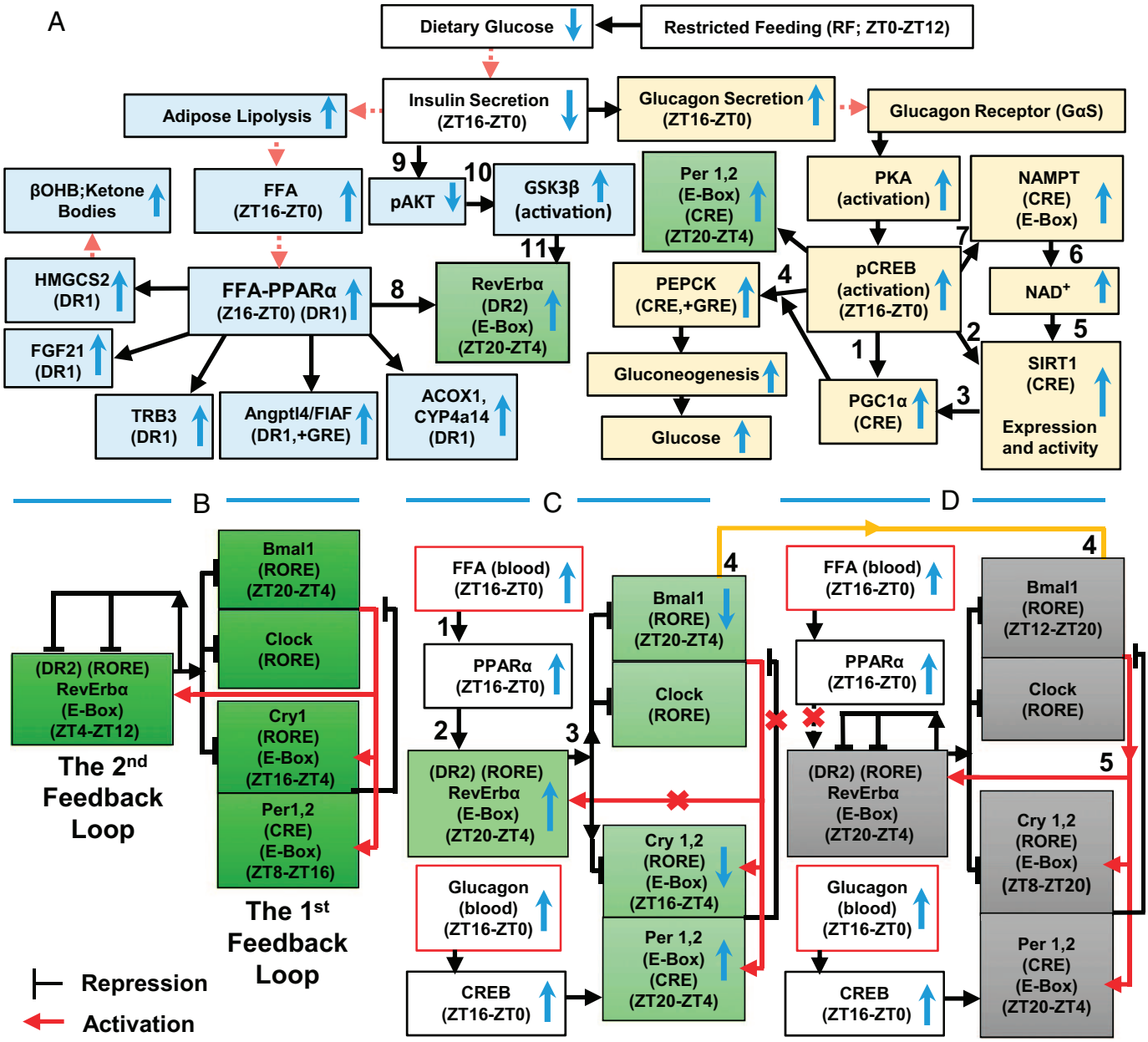

Fig. 3. A schematic representation of how RF-induced metabolic alterations induce a shift of PCCs. (*A*) Metabolic alterations induced by RF. The up and down blue arrows correspond, respectively, to increases and decreases of indicated components during RF. The red arrowheads indicate components present in the blood. (*B*) The two interlocked feedback loops constituting the normal CC oscillator. (*C*) The early phase of peripheral CC disruption. The up and down blue arrows correspond to increases and decreases of indicated components in RF, respectively. Red crosses represent RF-induced impairments. (*D*) The late phase of reconstruction of a new shifted PCC.

aberrantly expressed (Fig. 4*C* and Fig. S4*A*), due to PPARα binding on the *RevErbα* DR2 DBS and CREB recruitment on the CRE present in *Per1* and *Per2* genes (Fig. 4*D* and Figs. S4*C* and S5*A*). Remarkably, no Bmal1 binding to these E-Boxes could be observed during the ZT4–ZT12 period of RF2, due to the repression on *Bmal1* exerted by RevErbα aberrantly expressed during the RF2 night (Fig. 4 *A* and *B* and Fig. S3 *A* and *B*). Importantly, refeeding RF mice (at ZT0) reduced the FFA blood level and consequently decreased PPARα binding on the *RevErbα* DR2 DBS (Fig. 4*D*), thus reducing *RevErbα* expression (see ZT4 of RF3; Fig. 4*A* and Fig. S3*A*).This resulted in a derepression of *Bmal1* expression that was delayed to the ZT12–ZT20 period of RF3, thereby initiating the PCC shift (Fig. 4*A* and Fig. S3*A*; see Fig. 3 *C* and *D*).

During the second phase of the RF CC shift (Fig. 4*A* and Fig. S3*A*), the now shifted *Bmal1* expression progressively restored the Bmal1-dependent expression of *RevErbα*, *Per1*, and *Per2* during the ZT20–ZT4 period (Fig. 4 *A* and *C* and Figs. S3*A* and S4*A*; see Fig. 3*D*). Importantly, this Bmal1-dependent *RevErbα* synthesis during the ZT20–ZT4 period (Fig. 4*C* and Fig. S4*A*) not only prevented further binding of PPARα on the *RevErbα* DR2 DBS (making its transcription independent of metabolism), but also started to repress itself through binding to its own RORE and DR2 DBS (Fig. 4*E* and Fig. S3*B*). This pattern of *RevErbα* expression (ZT20–ZT4) with a zenith at ZT0 instead of ZT8 in WT mice was then repeated on the subsequent RF days, thereby creating an RF permanently shifted temporal window (ZT12–ZT20) for the RORα/γ-dependent expression of RORE

DBS-containing genes (3). Indeed, the new ZT12–ZT20 period of *Bmal1*, *Cry1*, and *E4BP4* expression in RF mice was first detected on RF3 and subsequently repeated on the following nights (Fig. 4*A* and Figs. S3*A* and S5*B*), whereas Per1 and Per2 expression was not stabilized before RF5. Importantly, in contrast with its decreased binding to *RevErbα* DR2 DBS during the ZT16–ZT0 period of RF3 and RF4, PPARα binding to its own DR1 DBS, as well as to that of the *HMGCS2* gene, was unaltered during the same period (Fig. S4*B*). Most notably, the selective mutation of *RevErbα* in either liver (*RevErbα*$^{hep-/-}$) or IECs (*RevErbα*$^{iec-/-}$) prevented the RF CC shift in these tissues, but not the RF-induced metabolic alterations (Fig. S5 *C*–*G*).

An Increased Glucagon Secretion Results in an Activation of CREB Signaling During RF. Glucagon maintains blood glucose through gluconeogenesis, which is initiated by glucagon receptor-mediated activation of protein kinase A (PKA), which then activates CREB (10). Thereafter, pCREB triggers the expression of genes involved

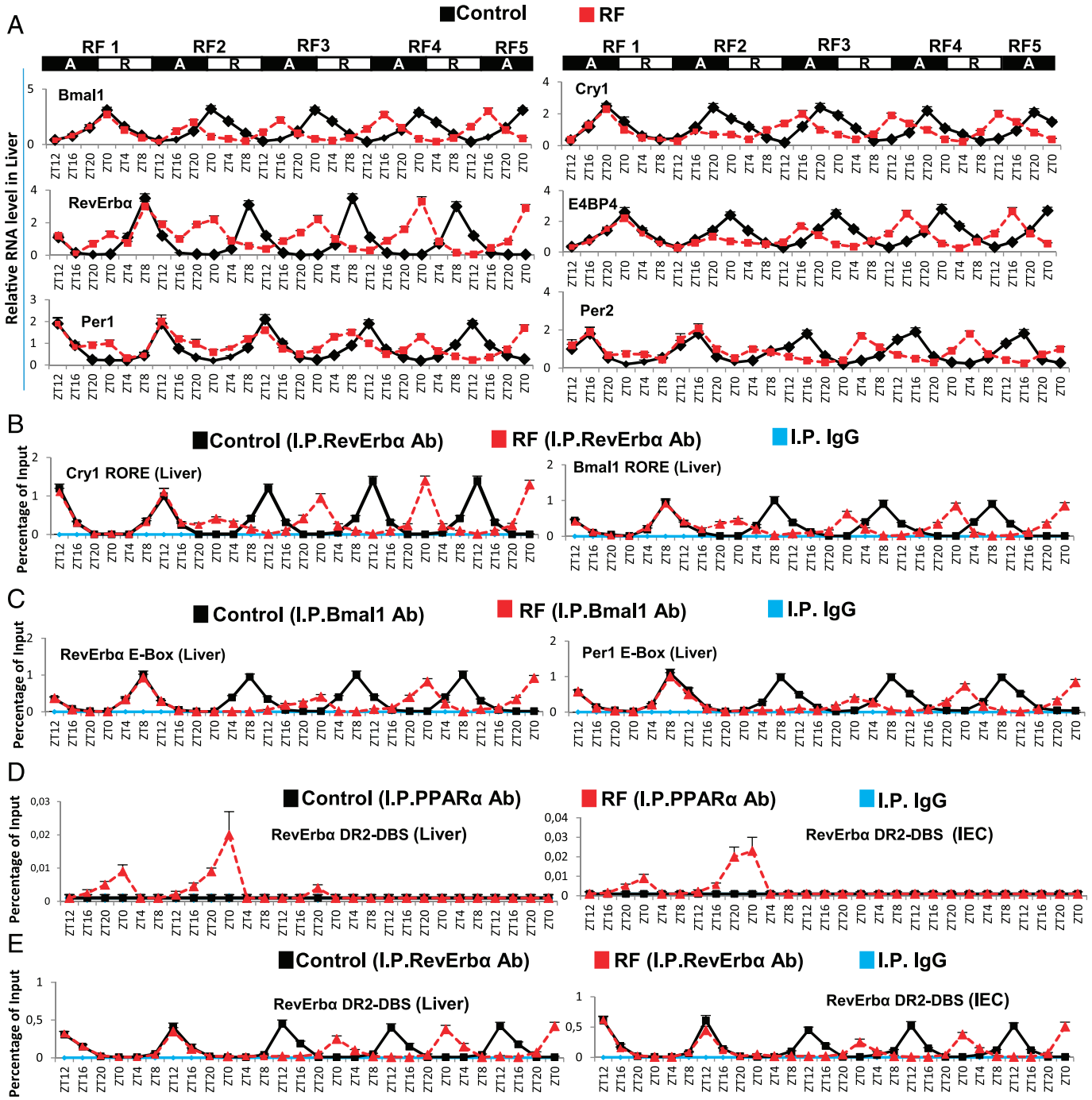

Fig. 4. RevErbα is instrumental in the RF-induced CC shift. (*A*) RNA transcript levels of indicated CC components in the liver during the first 108 h of RF. Black boxes (A) represent the active phase and white boxes (R) the rest phase. (*B*) ChIP-qPCR assays to analyze RevErbα recruitment (in control and RF liver) to the RORE DBS present in Bmal1 and Cry1 genes. (*C*) ChIP-qPCR assays to analyze Bmal1 recruitment (in control and RF liver) to the E-Box DBS present in RevErbα and Per1 genes. (*D*) ChIP-qPCR assays to analyze PPARα recruitment to the RevErbα DR2-DBS in control and RF liver and IEC. (*E*) ChIP-qPCR assays to analyze RevErbα recruitment to the RevErbα DR2-DBS in control and RF liver and IEC. All values are mean ± SEM.

in gluconeogenesis (steps 1–4 in Fig. 3*A*) (10). In keeping with the RF glucagon surge, there was indeed a pCREB increase (Fig. 2*G* and Fig. S6*D*) that led to increased expressions of CRE-containing genes (Fig. 2*E* and Fig. S6 *B, C,* and *E*; see Fig. 3*A*). NAD^+ is increased in RF liver (Fig. 2*F*) and plays a critical role in the sirtuin1 (SIRT1)-mediated activation of peroxisome proliferator-activated receptor gamma coactivator 1-alpha (PGC1α) (10). These RF NAD^+ and NAMPT [nicotinamide phosphoribosyltransferase; the rate limiting enzyme in the salvage pathway (4, 5)] increases were concomitant (Fig. S6 *B* and *C*). Note that this RF-induced increase in *NAMPT* expression persisted in the selective $Bmal1^{hep-/-}$ and $Bmal1^{iec-/-}$ mutants (Fig. 2*H* and Fig. S6*H*), even though Bmal1 is known to control its circadian expression (4, 5). Instead, we found that these *NAMPT* increases were related to an increased CREB binding to a CRE DBS (TGACGTCA) located in the *NAMPT* promoter (Fig. 2*E* and Fig. S6*E*; 7 in Fig. 3*A*). Moreover, ChIP analyses revealed an enhanced CREB binding to the CRE located in the *Per1* and *Per2* gene promoters (Fig. 2*E* and Fig. S6*E*) (16), which led to its increased expression during RF1 (see above). As expected, glucose administration to RF mice also prevented the RF-induced CREB activation (Fig. S6*G*), as well as the increased expressions of its target genes (Fig. 1 *E–G* and Fig. S6 *I* and *J*). Inhibiting the PKA activity by H-89 administration (17) during RF1 also prevented RF-induced CREB activation (Fig. S6*F*), as well as the increased expressions of its target genes (Fig. S6*K*), thus supporting the conclusion that the RF-induced CREB activation plays a critical role in the increased gluconeogenesis and CC alterations that occur on RF.

We next explored the relative contributions of FFA-PPARα-RevErbα and glucagon-CREB-Per1 and Per2 pathways in achieving the complete RF CC shift (Fig. 3 *C* and *D*). Notably, on RF4, there was no aberrant expression of *RevErbα* in selective $PPARα^{hep-/-}$ and $PPARα^{iec-/-}$ mutant mice (Fig. S7 *A* and *B*). However, the CREB-dependent ZT20–ZT4 increase in *Per1* and *Per2* expression persisted in these mutants (Fig. S7 *A* and *B*), which resulted after 8 RF days in a 4 days-delayed shift of all CC components in PPARα-ablated liver and IECs (Fig. S7 *C* and *D*), thus demonstrating that CREB activation plays an ancillary role in the RF CC shift, the major role being played by the PPARα-induced aberrant expression of RevErbα (Fig. 3*C*).

An Increased CREB Activity in Adrenal Glands of RF Mice Leads to Extra-Corticosterone Production. RF is known to induce during the ZT20–ZT4 period an extra peak of corticosterone production in an adrenal-dependent (Fig. S8*E*) (18), but SCN-independent, manner (21). However, the mechanism involved in this RF extra-corticosterone production has not been elucidated. As cAMP-PKA-CREB signaling plays, at ZT12, a critical role in physiological corticosterone production through transactivation of the numerous genes involved in corticosterone synthesis (22, 23), we investigated the role of CREB in extra-corticosterone production. We found, on RF1 night (Fig. S8*A*) in adrenal glands, increases in pCREB level (Fig. 5*C*), as well as in transcripts of various CREB target genes (Fig. S8 *B* and *C*), including those involved in corticosterone synthesis (*Cyp11a*, *Cyp11b*, *Hsd3b*, *Prkar2b*, and *Adcy5*; Fig. S8*D*). To support the role played by an increased CREB activity in RF extra-corticosterone production, the PKA activity was inhibited by H-89 administration (17), which prevented the RF-induced CREB binding to CREs present in *Cyp11a*, *Cyp11b*, and *Hsd3b* genes (Fig. S8*F*) and their ZT20–ZT4 transcription (Fig. 5*D*), thereby reducing the corticosterone blood level (Fig. S8*I*).

A Retarded RF-Induced CC Shift in Muscle and Heart Reflects a Delayed Activation of PPARα. It has been reported that the RF CC shift was delayed in muscles and heart (1) and that this delay could be overcome by adrenalectomy (Adx) (18), but how corticosterone could possibly retard the CC shift in muscle and heart was unknown. We posited that a retarded activation of PPARα (relative to other tissues such as liver and IECs; see above) in muscle and heart could be at the origin of this delay. Of note, it was reported (19) that a PPARβ-dependent synthesis of phosphatidylcholine 18:0/18:1 in the liver was a prerequisite for PPARα activation in muscle and heart (but not in liver; see below). Most interestingly, we found that the liver expression of *PPARβ*, which was repressed on RF1, was restored by Adx or administration of the glucocorticoid antagonist RU486 (Fig. 5 *A* and *B*). Moreover, we also found that within the *PPARβ* promoter there is a negative glucocorticoid receptor (GR) response element (IR2 nGRE) (20), which suggested to us that the RF1 extra-corticosterone surge (ZT20–ZT4; Fig. S8*G*) could account for the RF1 repression of *PPARβ* expression. Accordingly, we found that Adx or RU486 administration, by preventing the RF1 repression of *PPARβ* in the liver, led to an early activation of PPARα in muscle and heart and consequently to a stimulation of *RevErbα* expression in these tissues during RF1, thereby accelerating the pace of the CC shift in these tissues (Fig. 5 *A* and *B* and Fig. S7 *I* and *J*; see Fig. 5 *E* and *F*). Moreover, we found that this "extra-corticosterone"-dependent *PPARβ* repression was relieved by RF4 because the liver *PPARβ* expression shifted on RF4 from ZT20–ZT4 to ZT4–ZT12 (Fig. S7*L*) and therefore escaped the extra-corticosterone–dependent repression, which led to a gradual increase in *PPARα* level (in muscle and heart), and consequently to a shift in *RevErbα* expression (Fig. S7 *E–I* and Fig. 5 *E–G*).

Discussion

Shifting in the Mouse Eating from the Active Phase to the Rest Phase Induces Alterations of Two Metabolic Pathways That Unequally Generate a 12-Hour Shift of PCCs. Here we demonstrated that on RF, the shift of PCCs involves two distinct phases: (*i*) breaking the existing PCCs (Fig. 3*C*) and (*ii*) generating shifted PCCs (Fig. 3*D*). The breaking phase originates from the fasting imposed during the active phase, which by reducing INS secretion triggers an untimely increases in glucagon and FFA (Fig. 3 *A* and *C*). Importantly, in RF tissues (liver, IECs), these alterations impinge on CCs during the active phase through (*i*) the FFA-PPARα–dependent RevErbα expression and (*ii*) the glucagon-CREB–dependent Per1 and Per2 expression (Fig. 3*A*). Most notably, we found that glucose administration to RF mice by preventing the reduction in INS prevented the metabolic and subsequent PCC alterations (Fig. 1 *D–G*), thus establishing that a fasting state is in fact at the origin of the RF CC shift. Importantly, at the onset of RF, the PPARα-dependent aberrant *RevErbα* synthesis during the active phase breaks the existing PCCs through RORE-mediated repression of *Bmal1* synthesis (see steps 1–3 in Fig. 3*C*). The postfeeding reduction in FFA-PPARα levels then leads to a decrease in *RevErbα*, an essential event that derepresses *Bmal1* expression but also permanently shifts it to the ZT12–ZT20 period (step 4 in Fig. 3 *C* and *D*). Subsequently, through controlling the E-Box–mediated expression of *Per1*, *Per2*, and *RevErbα*, this shifted Bmal1 expression enables the emergence of a shifted repaired CC (step 5 in Fig. 3*D*). Notably, this whole process progressively restores a separation of 12 hours between the zenith and nadir of expression of all CC components, thus creating an RF peripheral CC oscillator, which is similar to that seen in non-RF mice, but shifted at the RNA level by 8 hours for the Bmal1, Cry1, RevErbα, and E4BP4 CC components, whereas Per1 and Per2 are shifted by 12 hours.

Importantly, we found that selective mutation of *PPARα* in liver and IECs delayed by 4 days the completion of their RF CC shift (Fig. S7 *A–D*). In these PPARα-mutant tissues, these shifts were achieved by CREB-dependent *Per1* and *Per2* activation. Therefore, it is the PPARα–RevErbα axis, which by perturbing the second loop of the CC oscillator (Fig. 3 *B* and *C*), efficiently drives the RF CC shift, whereas the CREB–Per1 and Per2 axis plays an ancillary role.

The RF-Generated Extra-Corticosterone Production Delays PPARα Activation in Muscle and Heart, Thereby Retarding the CC Shift in These Tissues. Our study unveiled that the underlying basis for the RF extra-corticosterone production (18, 21) (Fig. S8*G*) can be ascribed to an aberrant increase in adrenal CREB activity, which induces the adrenal expression of corticosterone synthesizing genes (Fig. S8*D*). Importantly, this RF-induced increase in adrenal CREB activity is accompanied by a surge in adrenocorticotropic hormone (ACTH) secretion (Fig. S8*H*), which is known to increase the cAMP-PKA–dependent CREB activity (22). Interestingly, this RF extra-ACTH-corticosterone surge temporally coincides with an RF blood increase in the liver-derived growth factor FGF21 (Fig. 1*D*

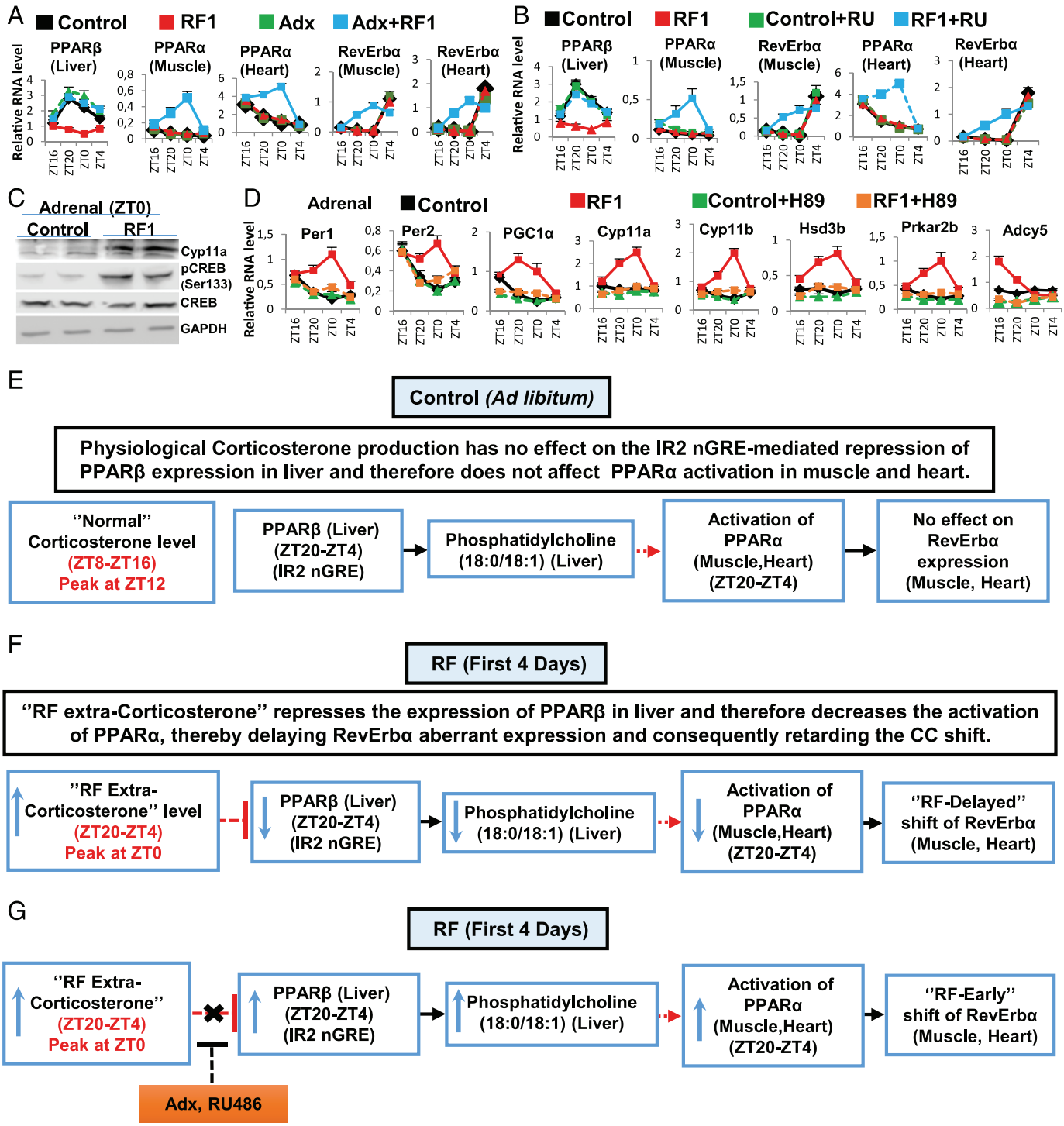

Fig. 5. RF-induced PPARα activation is delayed in muscle and heart. (*A*) RNA transcript levels of genes, as indicated, in control and RF1 mice on adrenalectomy (Adx). (*B*) RNA transcript levels of genes, as indicated, in control and RF1 mice with or without RU486 (RU) administration. (*C*) Immunoblot analyses of adrenal glands in control and RF1 mice with indicated antibodies. (*D*) RNA transcript levels of genes as indicated in the adrenal glands of control and RF1 mice treated with or without the PKA inhibitor (H-89). (*E*) Physiological corticosterone production has no effect on PPARβ expression in liver, which controls the activity of PPARα in muscle and heart. (*F*) A schematic representation of how RF extra-corticosterone production delays the CC shift in muscle and heart. (*G*) A schematic representation of how adrenalectomy (Adx) or inhibition of corticosterone signaling by RU486 leads to an RF-induced early CC shift in muscle and heart. All values are mean ± SEM.

and Fig. S2*F*), which was recently found to increase the hypothalamic corticotropin-releasing hormone (CRH) and pituitary ACTH secretion and, subsequently, corticosterone production (24). Thus, the RF-dependent increase in the FGF21 level provides a rationale for the previously reported suprachiasmatic nucleus (SCN)-independent corticosterone production during RF (21).

The delayed CC shift in tissues of RF *PPARα* mutants (see above) suggested to us that the delayed CC shift in muscle and heart, previously reported to be lagging behind that of liver (1), could reflect a delayed activation of *PPARα*. As this delay disappeared in ADX mice, it was ascribed to the RF extra-corticosterone production (18). Interestingly, PPARα activation in muscle and heart is dependent on the expression of *PPARβ* in liver (19), which reaches its zenith at ZT20–ZT4 (Fig. 5*E*). Notably, we found that, during early RF, the *PPARβ* promoter that contains an IR2 nGRE DBS (20) is repressed in liver by extra-corticosterone–liganded GR, thus accounting for the delayed activation of PPARα in muscle and heart (Fig. S7 *E–H* and Fig. 5 *F* and *G*) and also providing a rationale for the glucocorticoid-dependent inertia (18) of their RF CC shift.

Methods

Mice and Treatments. Eight- to 12-wk-old C57BL6/J male WT and adrenalectomized mice (Charles River Laboratories) were used. Control mice were provided food and water ad libitum, under 12-h light (6:00 AM–6:00 PM) and 12-h dark (6:00 PM–6:00 AM) conditions. RF mice were provided food during the entire light period (1). Breeding, maintenance, and experimental manipulations were approved by the Animal Care and Use Committee of IGBMC/ICS.

Statistics. Data are represented as mean ± SEM of at least three independent experiments and were analyzed by SyStat and Microsoft Excel statistics software using the Student *t* test (RNA transcripts) and one-way ANOVA (blood metabolic analysis). $P < 0.05$ was considered significant.

ACKNOWLEDGMENTS. We thank the staffs of animal house facilities in Institut de Génétique et de Biologie Moléculaire et Cellulaire (IGBMC)/Institut Clinique de la souris (ICS) for help and Marie-France Champy (ICS) for help in metabolic analysis. This work was supported by the Centre national de la recherche scientifique (CNRS), Institut national de la santé et de la recherche médicale (INSERM), University of Strasbourg Institute for Advanced Studies, and the Association pour la Recherche à l'IGBMC (ARI). A.M. and A.K. were supported by fellowships from ARI.

1. Damiola F, et al. (2000) Restricted feeding uncouples circadian oscillators in peripheral tissues from the central pacemaker in the suprachiasmatic nucleus. *Genes Dev* 14(23): 2950–2961.
2. Stokkan KA, Yamazaki S, Tei H, Sakaki Y, Menaker M (2001) Entrainment of the circadian clock in the liver by feeding. *Science* 291(5503):490–493.
3. Asher G, Schibler U (2011) Crosstalk between components of circadian and metabolic cycles in mammals. *Cell Metab* 13(2):125–137.
4. Bass J, Takahashi JS (2010) Circadian integration of metabolism and energetics. *Science* 330(6009):1349–1354.
5. Asher G, Sassone-Corsi P (2015) Time for food: The intimate interplay between nutrition, metabolism, and the circadian clock. *Cell* 161(1):84–92.
6. Vollmers C, et al. (2009) Time of feeding and the intrinsic circadian clock drive rhythms in hepatic gene expression. *Proc Natl Acad Sci USA* 106(50):21453–21458.
7. Asher G, et al. (2010) Poly(ADP-ribose) polymerase 1 participates in the phase entrainment of circadian clocks to feeding. *Cell* 142(6):943–953.
8. Saini C, et al. (2013) Real-time recording of circadian liver gene expression in freely moving mice reveals the phase-setting behavior of hepatocyte clocks. *Genes Dev* 27(13):1526–1536.
9. Saltiel AR, Kahn CR (2001) Insulin signalling and the regulation of glucose and lipid metabolism. *Nature* 414(6865):799–806.
10. Altarejos JY, Montminy M (2011) CREB and the CRTC co-activators: Sensors for hormonal and metabolic signals. *Nat Rev Mol Cell Biol* 12(3):141–151.
11. Kersten S, Desvergne B, Wahli W (2000) Roles of PPARs in health and disease. *Nature* 405(6785):421–424.
12. Mukherji A, Kobiita A, Ye T, Chambon P (2013) Homeostasis in intestinal epithelium is orchestrated by the circadian clock and microbiota cues transduced by TLRs. *Cell* 153(4):812–827.
13. Mukherji A, et al. (2015) Shifting eating to the circadian rest phase misaligns the peripheral clocks with the master SCN clock and leads to a metabolic syndrome. *Proc Natl Acad Sci USA*, 10.1073/pnas.1519807112.
14. Duez H, Staels B (2008) Rev-erb α gives a time cue to metabolism. *FEBS Lett* 582(1): 19–25.
15. Koike N, et al. (2012) Transcriptional architecture and chromatin landscape of the core circadian clock in mammals. *Science* 338(6105):349–354.
16. Travnickova-Bendova Z, Cermakian N, Reppert SM, Sassone-Corsi P (2002) Bimodal regulation of mPeriod promoters by CREB-dependent signaling and CLOCK/BMAL1 activity. *Proc Natl Acad Sci USA* 99(11):7728–7733.
17. Mao T, et al. (2011) PKA phosphorylation couples hepatic inositol-requiring enzyme 1α to glucagon signaling in glucose metabolism. *Proc Natl Acad Sci USA* 108(38): 15852–15857.
18. Le Minh N, Damiola F, Tronche F, Schütz G, Schibler U (2001) Glucocorticoid hormones inhibit food-induced phase-shifting of peripheral circadian oscillators. *EMBO J* 20(24): 7128–7136.
19. Liu S, et al. (2013) A diurnal serum lipid integrates hepatic lipogenesis and peripheral fatty acid use. *Nature* 502(7472):550–554.
20. Surjit M, et al. (2011) Widespread negative response elements mediate direct repression by agonist-liganded glucocorticoid receptor. *Cell* 145(2):224–241.
21. Krieger DT, Hauser H, Krey LC (1977) Suprachiasmatic nuclear lesions do not abolish food-shifted circadian adrenal and temperature rhythmicity. *Science* 197(4301): 398–399.
22. Spiga F, Liu Y, Aguilera G, Lightman SL (2011) Temporal effect of adrenocorticotrophic hormone on adrenal glucocorticoid steroidogenesis: Involvement of the transducer of regulated cyclic AMP-response element-binding protein activity. *J Neuroendocrinol* 23(2):136–142.
23. Mueller M, et al. (2007) Differential regulation of glucocorticoid synthesis in murine intestinal epithelial *versus* adrenocortical cell lines. *Endocrinology* 148(3):1445–1453.
24. Bookout AL, et al. (2013) FGF21 regulates metabolism and circadian behavior by acting on the nervous system. *Nat Med* 19(9):1147–1152.
25. Schuler M, Dierich A, Chambon P, Metzger D (2004) Efficient temporally controlled targeted somatic mutagenesis in hepatocytes of the mouse. *Genesis* 39(3):167–172.
26. Cima I, et al. (2004) Intestinal epithelial cells synthesize glucocorticoids and regulate T cell activation. *J Exp Med* 200(12):1635–1646.
27. Greten FR, et al. (2004) IKKbeta links inflammation and tumorigenesis in a mouse model of colitis-associated cancer. *Cell* 118(3):285–296.

Supporting Information

Mukherji et al. 10.1073/pnas.1519735112

SI Methods

Mice. Hepatocyte-specific ablation of Bmal1 (Bmal1$^{hep-/-}$), PPARα (PPARα $^{hep-/-}$), RevErbα (RevErbα $^{hep-/-}$), and PPARβ (PPARβ $^{hep-/-}$) was achieved by crossing floxed female mice with albumin-CreERT^2 floxed male mice (25), and subsequent tamoxifen injection for 5 d. IEC-selective mutants of Bmal1 (Bmal1$^{iec-/-}$), PPARα (PPARα$^{iec-/-}$), and RevErbα (RevErbα$^{iec-/-}$) were derived by crossing floxed female mice with Villin-Cre floxed male mice (12). Bmal1 floxed mice were obtained from Jackson Laboratories [B6.129S4 (Cg)-Arntl^{tm1Weit}/J], and all other floxed mice were generated and maintained in Institut de Génétique et de Biologie Moléculaire et Cellulaire (IGBMC)/Institut Clinique de la souris (ICS). Genotyping was performed by PCR on genomic DNA isolated from mouse tails. All experiments were performed under light-dark (L/D) conditions, with ZT0 being the start of the light period (6:00 AM) and ZT12 the start of the dark period (6:00 PM). Mice were killed at 4-h interval starting from ZT12 or ZT0. Food was removed from the RF cages at 6:00 PM and reintroduced at 6:00 AM. Food intake was measured (in 12 control and 20 RF mice) by continuously measuring the weight of the food supplied for individual animals (individual pellets weighing 20 mg). Overall food intake was measured by determining the amount of the consumed per week per mouse. All mice were fed the normal laboratory chow diet.

IEC Isolation. IECs were isolated using a modification of a nonenzymatic protocol (12, 26, 27). Briefly, ∼5- to 6-cm-long pieces of distal ileum were excised and placed in Petri dishes containing cold HBSS with 0.2% horse serum. Blood vessels and associated fat were removed, and the intestine was opened longitudinally, gently cleared of feces, and extensively washed on ice in HBSS with 1 mM DTT to remove mucus. The intestinal segments were placed in fresh PBS with 30 mM EDTA and shaken at 50 × *g* (37 °C for 10 min). The supernatant was transferred into a fresh tube and centrifuged (500 × *g*, 5 min at 4 °C), and the pellet was either immediately processed for subsequent analysis or snap frozen and stored at −70 °C for future use. The viability and purity of samples were checked by trypan blue dye exclusion and by measuring the relative transcript levels of alkaline phosphatase and Villin.

RNA Transcript Determination. Freshly isolated IECs, liver, pancreas, adrenal glands, muscles (gastrocnemius), and heart (left ventricle) samples were used for RNA isolation using TRI reagent (Molecular Research Center). Subsequent to the verification of RNA quality (gel electrophoresis), 1 μg total RNA (determined spectrophotometrically) was reverse transcribed using random hexamers and SuperScript II reagents (Invitrogen) as per the manufacturer's instructions. The synthesized cDNA was used for qRT-PCR with SYBRgreen (QIAGEN) and expressed relative to the hypoxanthine phosphoribosyltransferase (HPRT) levels, as previously described (12). Primer sequences are available on request. For transcript determination, four control and four RF mice were killed at each time point, and each experiment were replicated three times.

Protein Immunoblots. Immunoblots from isolated IECs, liver, and adrenal glands were performed following standard SDS/PAGE procedures. Proteins were visualized following ECL (Pierce), and images were captured using CCD. The primary antibodies for CREB1 (Sc-25785, H-74), PPARα (Sc-9000, H-98), and pCREB-1 Ser133 (Sc-101663) were from Santa Cruz Biotechnology, whereas the Cyp11a (SH-A11435) and GAPDH antibodies were from NovateinBio and Millipore, respectively. pAkt Ser473 (4060), Akt (4685), pGSK3β Ser9 (5558), GSK3β (12456), and pRevErbα Ser55/59 (2129) were obtained from Cell Signaling Technology. Bmal1 (ab93806) antibodies was obtained from abcam.

NAD$^+$ Measurement. NAD$^+$ measurement was performed from the liver extracts of control and RF1 mice (six mice per group) using the NAD/NADH colorimetric assay kit (ab65348; abcam), per the manufacturer's instructions.

FGF21 Measurement. FGF21 was assayed from the plasma samples obtained from the retro-orbital blood of control and RF1 mice (eight mice per group), using the FGF21 quantikine ELISA kit (R&D; MF2100) per the manufacturer's instructions.

ChIP Assays. ChIP was performed as previously reported (12, 15) with some minor modifications. Briefly, isolated IEC suspension in PBS was cross-linked with 1% formaldehyde for 15 min at room temperature; cross-linking was stopped with the addition of 2 M glycine (0.125 M final concentration) at room temperature for 5 min. Cells were pelleted, and 500 μL lysis buffer was added in the presence of protease inhibitors (Roche) on ice. For liver samples, identical lobes of liver from different groups of mice were disrupted using a dounce homogenizer; samples were then cross-linked and processed as described above. For adrenal glands, 12 adrenal glands were pulled and homogenized for each antibody per time point. Following cell lysis, the samples were sonicated (Bioruptor; Diagenode) to generate fragments of average length of 200–500 bp. Cellular debris were removed by centrifugation at 4 °C for 10 min (10,000 × *g*), and supernatant was precleared with Protein A/G-Sepharose (Roche) beads and preblocked with salmon DNA and BSA for 60 min at 4 °C. Beads were pelleted and discarded; 10% of the lysate was stored from each sample as the source of Input, and the remaining lysate was diluted eight times (five times for adrenal glands) in dilution buffer [16.7 mM Tris·HCl, pH 8.1, 0.01% (wt/vol) SDS, 1.1% (vol/vol) Triton X-100,1.2 mM EDTA, 16.7 mM NaCl, protease inhibitor mixture], in the presence of different primary antibodies for 14 h at 4 °C, on a flip-flop rocker. Protein A/G-Sepharose beads (90 μL; preblocked with salmon DNA and BSA) were then added for 90 min at 4 °C. Immunecomplexes were recovered by centrifugation at 500 × *g* for 1 min. Beads were washed extensively at 4 °C in low salt buffer [20 mM Tris·HCl, pH 8.1, 0.1% (wt/vol) SDS, 1% (vol/vol) Triton X-100, 2 mM EDTA, 150 mM NaCl], in high salt buffer [20 mM Tris·HCl, pH 8.1, 0.1% (wt/vol) SDS, 1% (vol/vol) Triton X-100, 2 mM EDTA, 500 mM NaCl], and in LiCl buffer [10 mM Tris·HCl, pH 8.1, 250 mM LiCl, 1% (vol/vol) Nonidet P-40, 1% (wt/vol) sodium deoxycholate, 1 mM EDTA], and finally in 1 mL TE buffer (10 mM Tris·HCl, pH 8.0, 1 mM EDTA). The bound chromatin was released from the beads by intermittent vortexing at room temperature in 200 μL elution buffer [1 (wt/vol) SDS and 100 mM $NaHCO_3$]. One milliliter of 10 mg/mL RnaseA and 5 M NaCl (200 mM final concentration) was added to the eluate and incubated overnight at 65 °C and then treated with Proteinase K for 1 h at 55 °C; DNA was purified using the QIAGEN PCR purification kit in a final volume of 50 μL. The qPCR was done using this eluted DNA and SYBRgreen reagent (QIAGEN). PCR cycles were verified to be within the linear range of amplification. Primer sequences are available on request. Antibodies used in ChIP assays were as follows: CREB-1 (H74x, sc-25785x; Santa Cruz Biotechnology), PPARα (ab2779, 3B6/PPAR; abcam), and Bmal1 (ab3350; abcam).

Plasma Metabolic Analysis. Blood glucose, insulin, glucagon, ACTH, corticosterone, TG, FFA, and βOHB (ketone bodies) levels were

measured from control and RF mice (eight mice per group per time point) at indicated ZTs. Blood glucose levels were determined on blood collected from the tail vein using a handheld Accu-check active glucometer (Roche). For all other measurements, blood was collected by retro-orbital puncture in EDTA-coated vials, plasma was separated, and measurements were done in the metabolomics unit of the IGBMC/ICS. For the experiments involving glucose administration to RF mice, following food withdrawal at ZT12, glucose (2 g/kg) was i.p. administered to one group of RF mice (RF+Glucose) at ZT15. The RF+Glucose mice were provided food at ZT0 (6:00 AM), simultaneously with the RF mice.

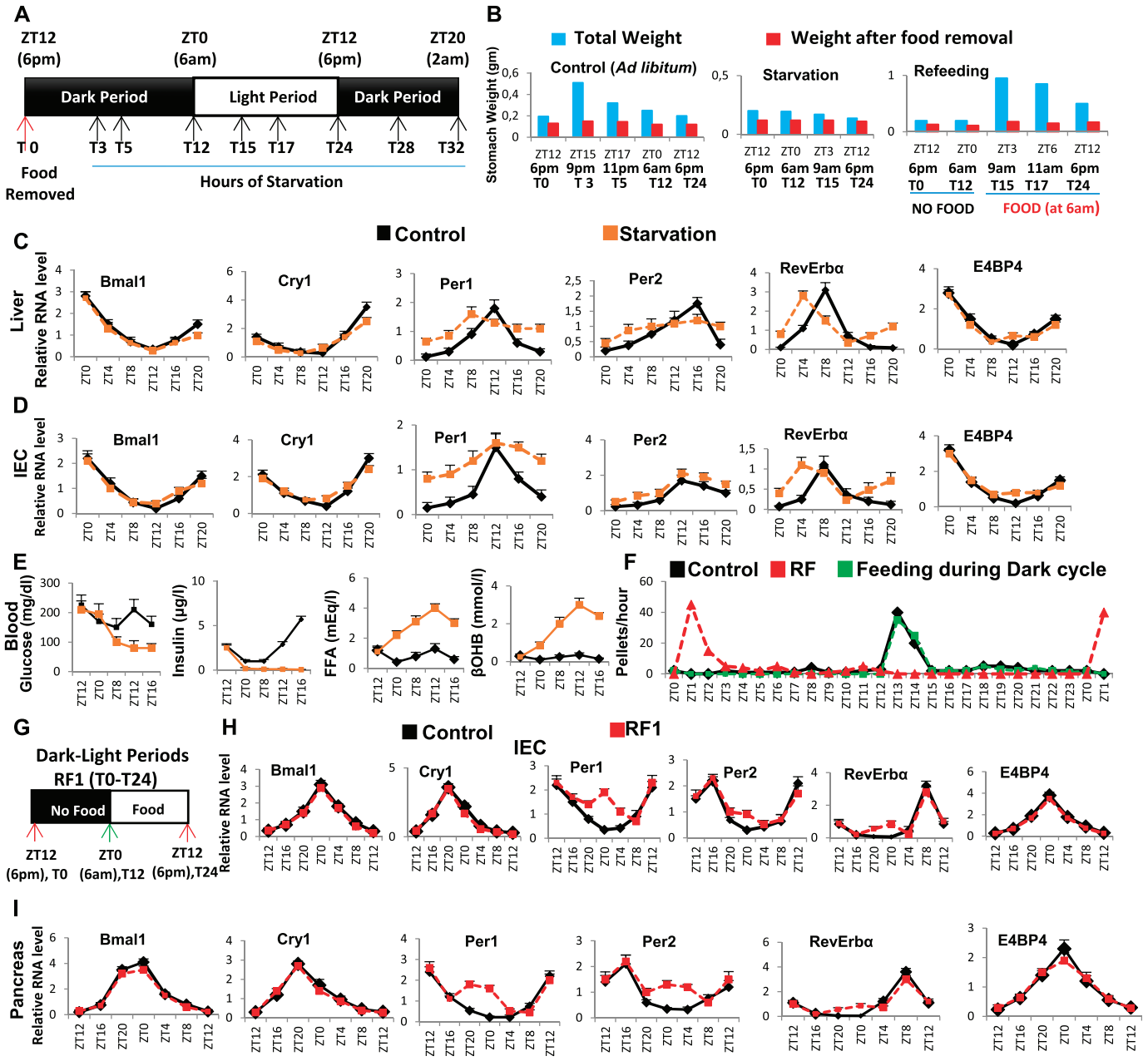

Fig. S1. Metabolic features during early RF resemble those of a state of starvation. (*A*) Schematic representation of the starvation experiment. Food was removed at 6:00 PM (ZT12/T0) and mice were starved for 32 h. The control group received food ad libitum. The black boxes represent the dark period of the normal dark-light (D/L) cycle, whereas the white box represents the light period. (*B*) Weight of the stomach before and after food removal in control and starved mice, as well as in mice refed at 6:00 AM (ZT0/T12) after 12 h of starvation (T0–T12). (*C* and *D*) RNA transcript levels of CC components in RF liver (*C*) and IECs (*D*) in control and starved mice. (*E*) Levels of blood components, as indicated, in control and starved mice. (*F*) Measurement of feeding activity (number of pellets consumed per hour) in control and RF mice, as well as in mice fed exclusively during dark cycle of D/L period. (*G*) Schematic representation of D/L periods during the RF1. Food was removed from the RF cages at 6:00 PM (ZT12/T0) and was reintroduced after 12 h at 6:00 AM (ZT0/T12; indicated with a green arrow) and present until T24 (6:00 PM). The black box represents the dark period (T0–T12, no food), whereas the white box represents the light period (T12–T24, with food) of the L/D cycle. (*H* and *I*) RNA transcript levels of CC components in IECs (*H*) and pancreas (*I*) of control and RF1 mice. All values are mean ± SEM.

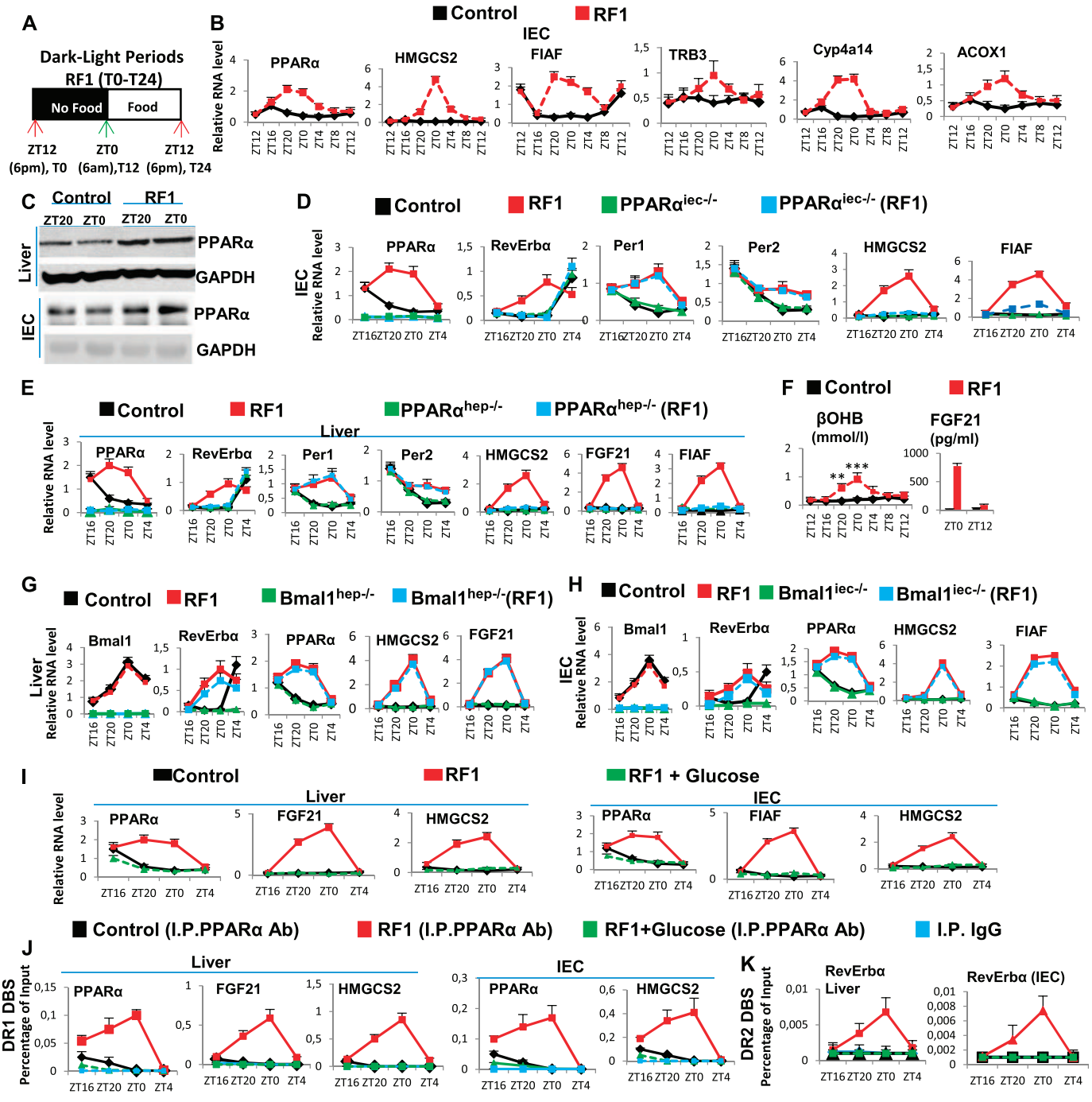

Fig. S2. Early RF induces temporally aberrant PPARα signaling. (*A*) A schematic representation of the RF1 experiment. (*B*) RNA transcript levels of indicated genes in IECs of control and RF1 mice. (*C*) Immunoblot analyses to evaluate the levels of PPARα in liver and IECs of control and RF1 mice. (*D*) RNA transcript analysis of genes, as indicated, in IECs of control and RF1 mice with or without an IEC-selective mutation of PPARα (PPARα$^{iec-/-}$). (*E*) RNA transcript analysis of genes, as indicated, in liver of control and RF1 mice with or without a liver-selective mutation of PPARα (PPARα$^{hep-/-}$). (*F*) Levels of ketone bodies (βOHB) and FGF21 in RF1 blood. (*G*) RNA transcript analysis of genes, as indicated, in liver of control and RF1 mice with or without a liver selective mutation of Bmal1 (Bmal1$^{hep-/-}$). (*H*) RNA transcript analysis of genes, as indicated, in IECs of control and RF1 mice with or without an IEC-selective mutation of Bmal1 (Bmal1$^{iec-/-}$). (*I*) RNA transcript levels of indicated genes in liver and IECs of control and RF1 and RF1+Glucose mice. (*J*) ChIP-qPCR assays in liver and IECs of control, RF1, and RF1+Glucose mice to analyze the PPARα recruitment to the DR1 DBSs present in the indicated genes. (*K*) As in *J*, but to analyze the PPARα recruitment to the RevErbα DR2 DBS. All values are mean ± SEM. $^{**}P < 0.01$, $^{***}P < 0.001$.

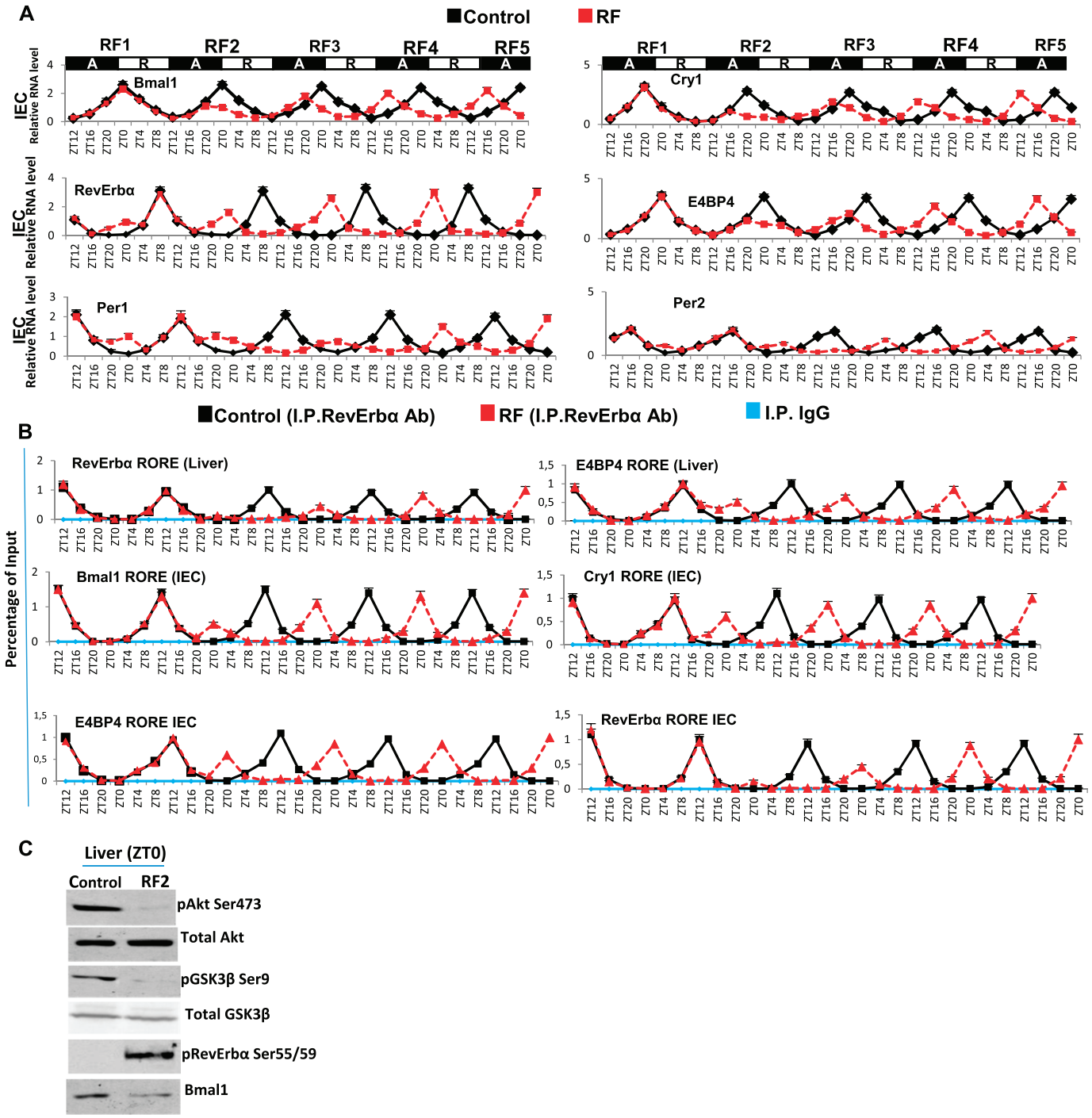

Fig. S3. Temporal analysis of the RF-induced PCC shift. (*A*) RNA transcript levels of indicated CC components in IECs during the RF first 108 h. Black boxes (A) represent the active phase, and white boxes (R) the rest phase. (*B*) ChIP-qPCR assays to analyze RevErbα recruitment to the RORE DBSs present in genes, as indicated, in control and RF liver and IECs. (*C*) Immunoblot analyses in liver of control and RF2 mice (at ZT0), with indicated antibodies. All values are mean ± SEM.

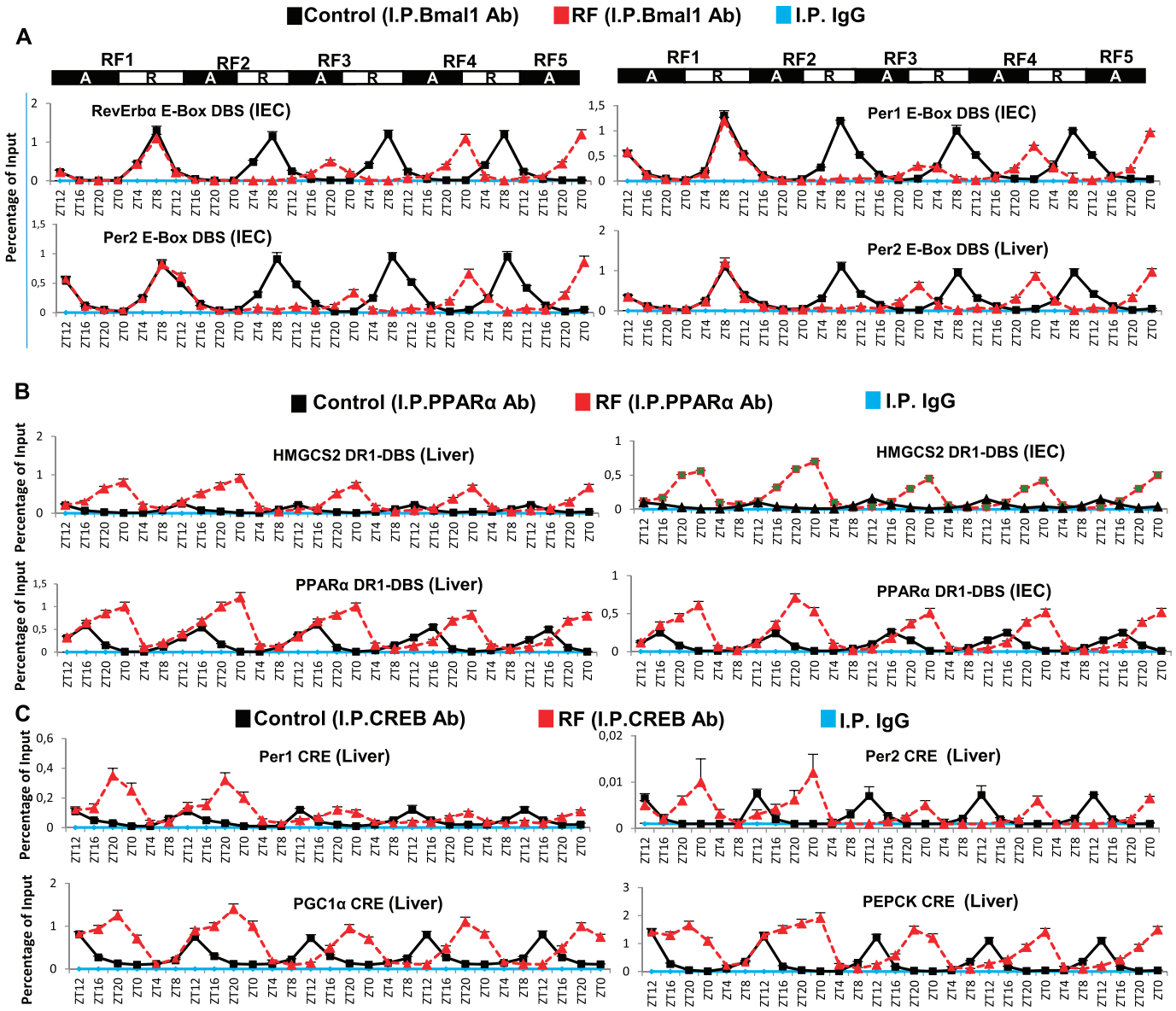

Fig. S4. The shift of Bmal1 expression plays a critical role in regenerating a new CC on restricted feeding. (*A*) ChIP-qPCR assays to analyze Bmal1 recruitment to the E-Box DBSs present in the RevErbα, Per1, and Per2 genes in IECs, as well as to the Per2 E-Box DBS in liver during the first 108 RF hours. (*B*) ChIP-qPCR assays in liver and IECs to analyze PPARα recruitment to the DR1 DBSs present in the PPARα and HMGCS2 genes during the first 108 RF hours. (*C*) ChIP-qPCR assays in liver to analyze the CREB recruitment to the CRE DBSs present in genes, as indicated. All values are mean ± SEM.

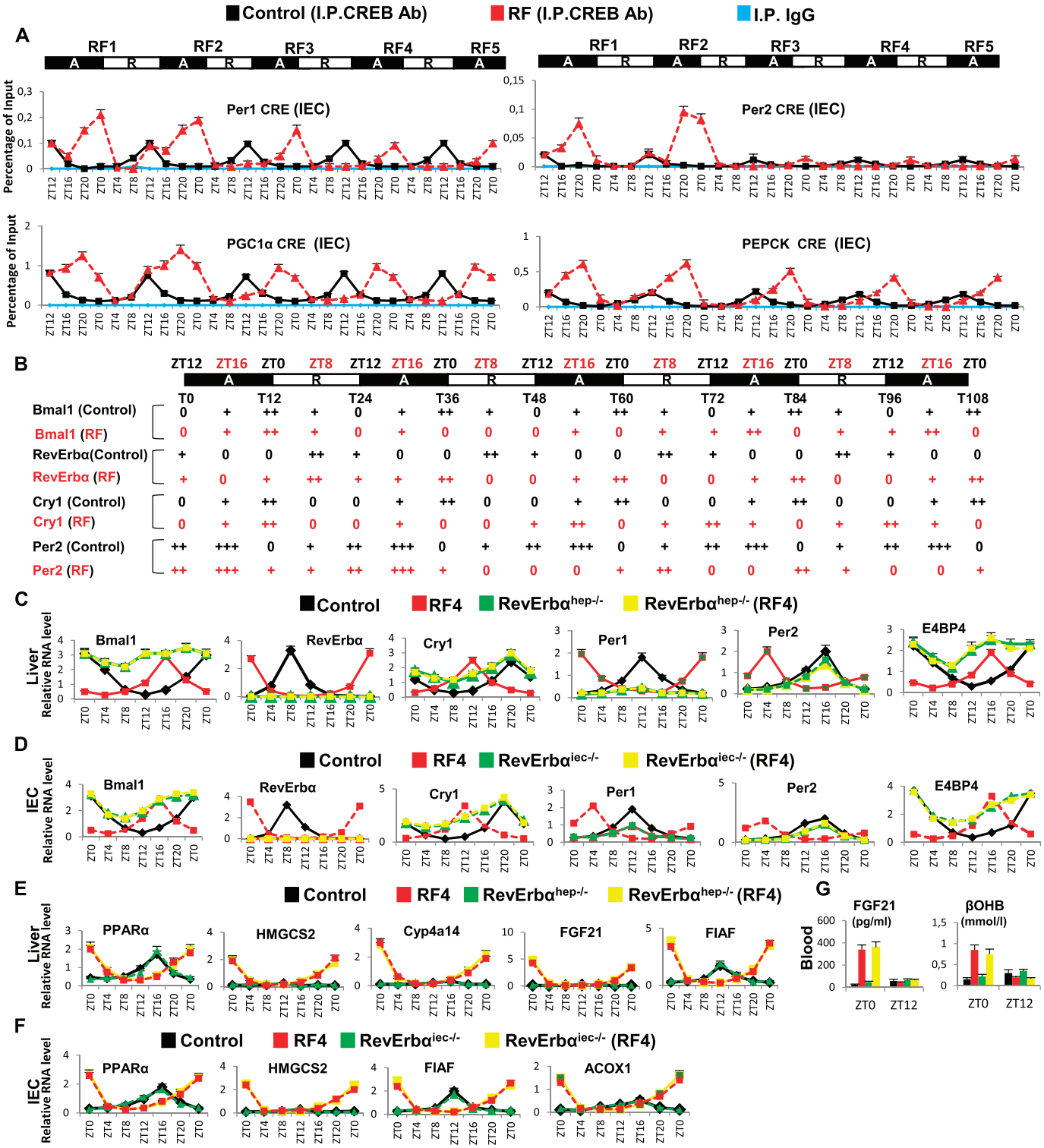

Fig. S5. Instrumental role of RevErbα in RF-induced CC shift. (*A*) ChIP-qPCR assays in IECs to analyze the CREB recruitment to the CRE DBSs present in genes as indicated. (*B*) Progressive shifts of the indicated clock genes during the first RF 108 h. 0, minimal transcript levels; +, ++, and +++, relative amount of detectable RNA transcripts. (*C*) RNA transcript levels of CC components in control and RF4 mice with or without a liver selective mutation of RevErbα (RevErbα$^{hep-/-}$). (*D*) RNA transcript levels of CC components in control and RF4 mice with or without an IEC selective mutation of RevErbα (RevErbα$^{iec-/-}$). (*E*) RNA transcript levels of genes, as indicated in control and RF4 mice with or without a liver-selective mutation of RevErbα (RevErbα$^{hep-/-}$). (*F*) RNA transcript levels of genes, as indicated in control and RF4 mice with or without an IEC-selective mutation of RevErbα (RevErbα$^{iec-/-}$). (*G*) Levels of FGF21 and βOHB in the blood of control and RF4 mice with or without a liver-selective mutation of RevErbα (RevErbα$^{hep-/-}$). All values are mean ± SEM.

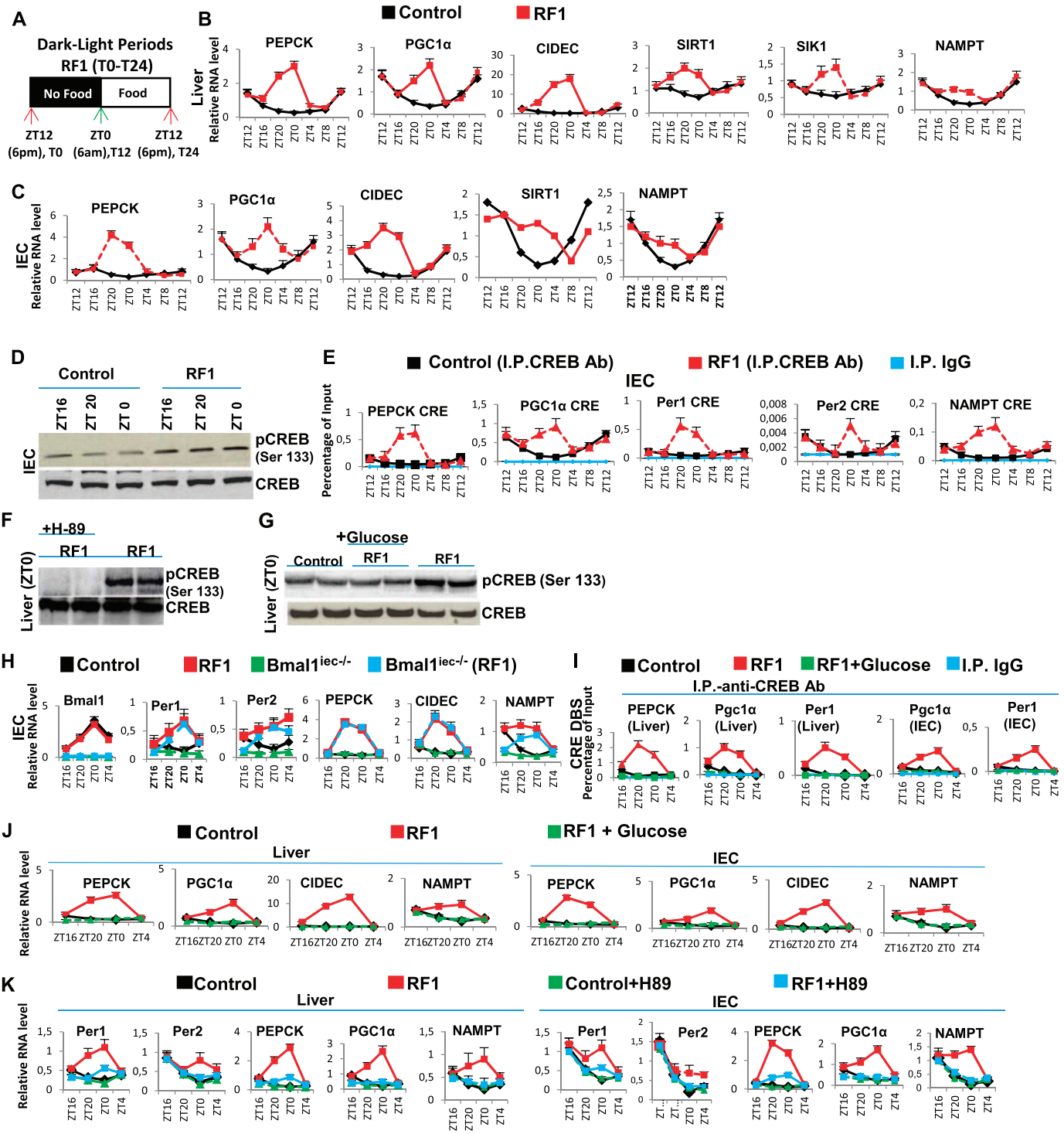

Fig. S6. RF-induced temporally aberrant CREB signaling participates in both gluconeogenesis and CC alterations. (*A*) A schematic representation of the RF1 experiment. (*B* and *C*) RNA transcript levels of indicated genes in liver (*B*) and IECs (*C*) of control and RF1 mice. (*D*) Immunoblot analyses of IECs from control and RF1 mice with pCREB and CREB antibodies. (*E*) ChIP-qPCR assays to analyze CREB binding to the CRE DBSs present in the indicated genes in IECs of control and RF1 mice. (*F*) Immunoblot analyses to detect CREB phosphorylation in liver of RF1 mice i.p. treated with or without the PKA inhibitor H-89. (*G*) Immunoblot analyses to detect CREB phosphorylation in liver of control, RF1, and RF1+Glucose mice. (*H*) RNA transcript analysis of genes, as indicated, in IECs of control and RF1 mice with or without an IEC selective mutation of Bmal1 (Bmal1$^{iec-/-}$). (*I*) ChIP-qPCR assays in livers and IECs of control, RF1, and RF1+Glucose mice to analyze CREB recruitment to the CRE DBSs present in genes as indicated. (*J*) RNA transcript levels of indicated genes in liver and IECs of control and RF1 and RF1+Glucose mice. (*K*) RNA transcript levels of indicated genes in RF1 liver and IECs on i.p. administration of the PKA inhibitor (H-89). All values are mean ± SEM.

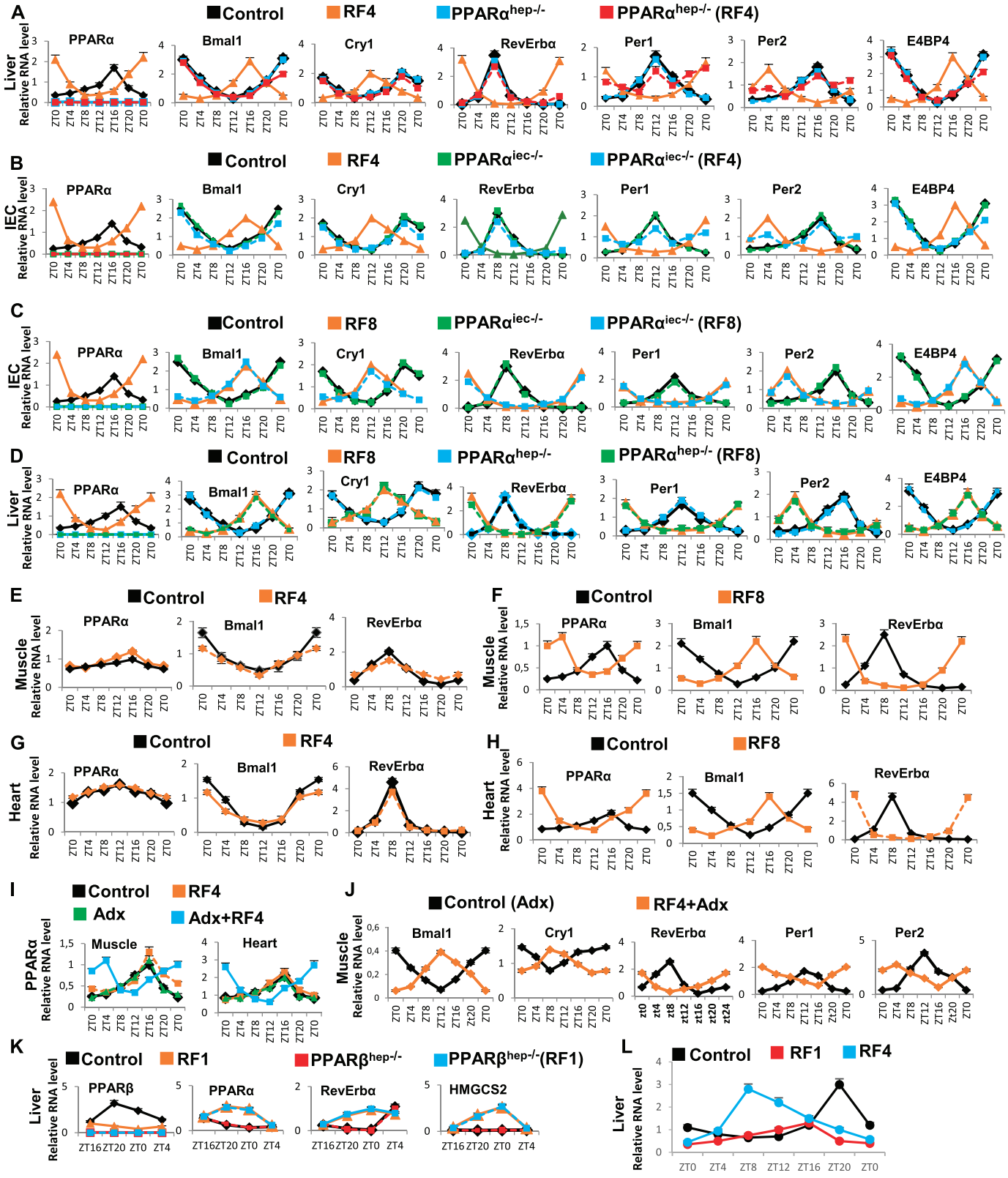

Fig. S7. RF-induced PPARα activation is delayed in muscles and heart compared with liver. (*A*) RNA transcript levels of CC components in control and RF4 mice with or without a liver selective mutation of PPARα (PPARα$^{hep-/-}$). (*B*) RNA transcript levels of CC components in control and RF4 mice with or without an IEC-selective PPARα mutation (PPARα$^{iec-/-}$). (*C*) As in *B*, but in RF8 mice. (*D*) As in *A*, but in RF8 mice. (*E*) RNA transcript levels of genes, as indicated, in muscles of control and RF4 mice. (*F*) As in *E*, but in RF8 mice. (*G*) RNA transcript levels of genes, as indicated, in heart of control and RF4 mice. (*H*) As in *G*, but in RF8 mice. (*I*) RNA transcript levels of PPARα in the muscle and heart of control and RF4 mice with or without adrenalectomy (Adx). (*J*) RNA transcript levels of CC components in muscles of Adx mice with or without RF4. (*K*) RNA transcript levels of genes, as indicated, in control and RF1 mice with or without a liver-selective PPARβ mutation (PPARβ$^{hep-/-}$). (*L*) RNA transcript levels of PPARβ in the liver of control, RF1, and RF4 mice. All values are mean ± SEM.

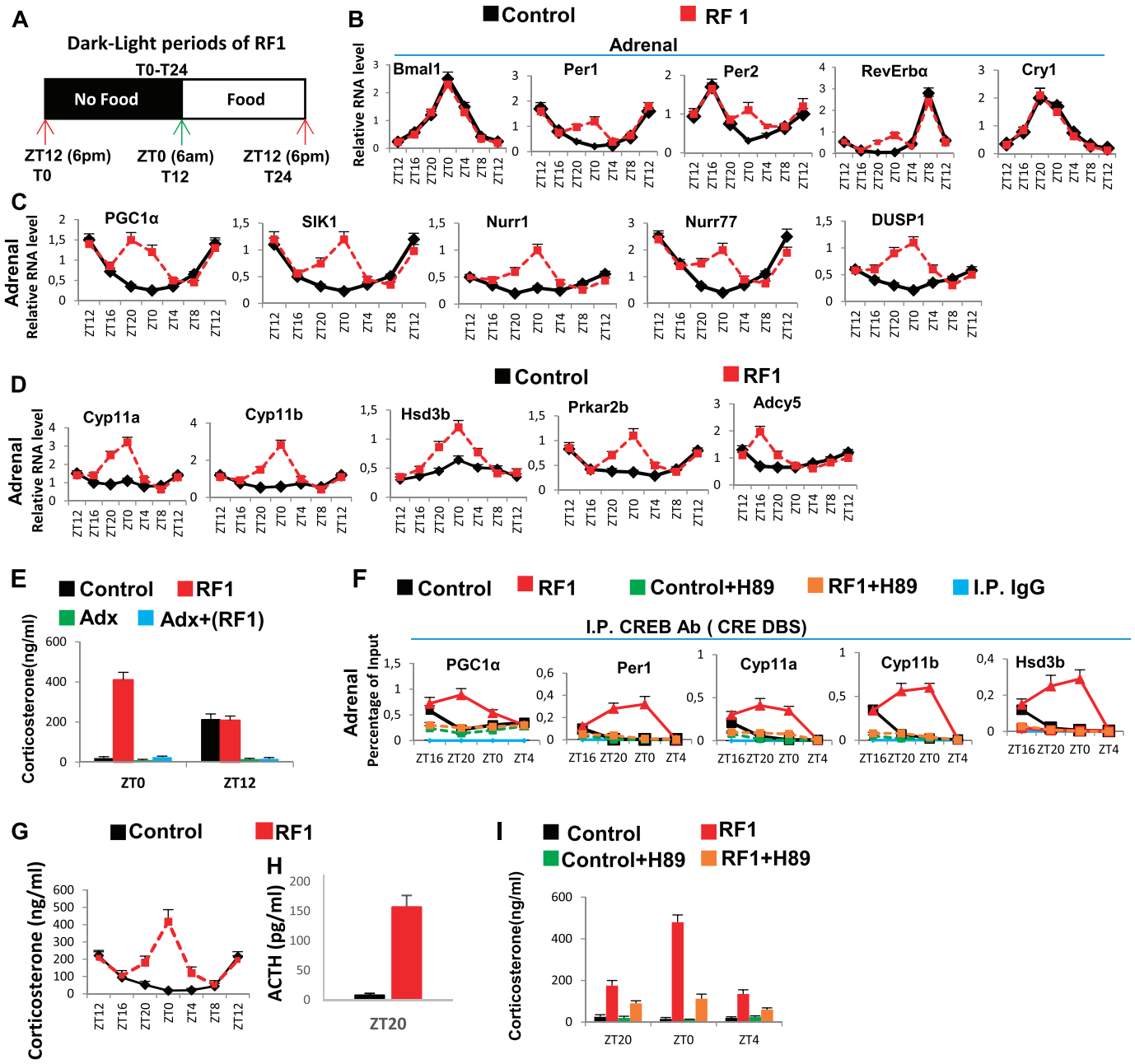

Fig. S8. RF-induced temporally aberrant increase in the CREB activity in the adrenal gland is instrumental in the extra-corticosterone production. (*A*) Schematic representation of the L/D period of RF1. (*B–D*) RNA transcript levels of genes, as indicated, in adrenal glands of RF1 mice. (*E*) Corticosterone levels in the blood of control and RF1 mice, with or without adrenalectomy (Adx). (*F*) ChIP-qPCR assays in adrenal glands to analyze CREB binding to the CRE DBSs present in the indicated genes in control and RF1 mice with or without i.p. administration of PKA inhibitor H-89. (*G*) Circadian corticosterone production in control and RF1 mice. (*H*) ACTH levels in the control and RF1 mice. (*I*) Corticosterone blood levels in control and RF1 mice with or without the administration of the PKA inhibitor H-89. All values are mean ± SEM.

Shifting eating to the circadian rest phase misaligns the peripheral clocks with the master SCN clock and leads to a metabolic syndrome

Atish Mukherji[a], Ahmad Kobiita[a], Manohar Damara[a], Nisha Misra[a], Hamid Meziane[b], Marie-France Champy[b], and Pierre Chambon[a,c,1]

[a]Institut de Génétique et de Biologie Moléculaire et Cellulaire, CNRS UMR7104, INSERM U964; [b]Institut Clinique de la Souris, Illkirch 67404, France; and [c]University of Strasbourg Institute for Advanced Study, Collège de France, Illkirch 67404, France

Contributed by Pierre Chambon, October 8, 2015 (sent for review September 13, 2015; reviewed by Gerard Karsenty and Paolo Sassone-Corsi)

The light-entrained master central circadian clock (CC) located in the suprachiasmatic nucleus (SCN) not only controls the diurnal alternance of the active phase (the light period of the human light-dark cycle, but the mouse dark period) and the rest phase (the human dark period, but the mouse light period), but also synchronizes the ubiquitous peripheral CCs (PCCs) with these phases to maintain homeostasis. We recently elucidated in mice the molecular signals through which metabolic alterations induced on an unusual feeding schedule, taking place during the rest phase [i.e., restricted feeding (RF)], creates a 12-h PCC shift. Importantly, a previous study showed that the SCN CC is unaltered during RF, which creates a misalignment between the RF-shifted PCCs and the SCN CC-controlled phases of activity and rest. However, the molecular basis of SCN CC insensitivity to RF and its possible pathological consequences are mostly unknown. Here we deciphered, at the molecular level, how RF creates this misalignment. We demonstrate that the PPARα and glucagon receptors, the two instrumental transducers in the RF-induced shift of PCCs, are not expressed in the SCN, thereby preventing on RF a shift of the master SCN CC and creating the misalignment. Most importantly, this RF-induced misalignment leads to a misexpression (with respect to their normal physiological phase of expression) of numerous CC-controlled homeostatic genes, which in the long term generates in RF mice a number of metabolic pathologies including diabetes, obesity, and metabolic syndrome, which have been reported in humans engaged in shift work schedules.

circadian clocks misalignment | shift work | diabetes | metabolic syndrome | mouse

Under physiological conditions, the light-entrained central master circadian clock (CC), which is located in the suprachiasmatic nucleus (SCN), synchronizes the ubiquitous peripheral CCs (PCCs) and generates a diurnal alternance of phases of activity and rest, both of which are at the origin of rhythmic variations of gene expression, which are essential to maintain metabolic and behavioral homeostasis (1–3). It is well established that shifting the feeding time in the mouse from the "active" to the "rest" phase [so-called restricted feeding (RF)] leads to a 12-h shift in the expression of PCC components (4). As the SCN CC is not affected during RF (4), this situation leads to a misalignment between the diurnal active and rest phases and the expression of PCC components. We recently unveiled in mice the origin and the identity of the molecular signals through which RF leads to this 12-h shift in the expression of PCC components (5). However, the molecular mechanisms that confer to the SCN CC an insensitivity to RF, as well as the consequences of the misalignment between the PCCs and the master SCN CC on homeostasis, are still largely unexplored (3, 6). In the present study, we elucidated, at the molecular level, how the SCN CC is protected against the RF-induced shift of PCCs, which is induced by metabolic alterations (5), and how the misalignment between the master SCN CC and the PCCs generates a metabolic syndrome-like pathology, similar to that exhibited by shift workers (3, 6–9).

Results and Discussion

The Glycogen Synthase Kinase 3β Plays a Crucial Role Both in the Long-Term Maintenance of the RF-Induced CC Shift and Its Reversal on Return to Normal Feeding. We recently elucidated (5) how the RF-induced decrease in insulin (INS) blood level during the active phase triggers an aberrant activation of nuclear receptor subfamily 1, group D, member 1 (Nr1d1/RevErbα) through phosphorylation by active glycogen synthase kinase 3β (GSK3β; Fig. 1*F*) (5). This RevErbα phosphorylation prevents its proteasome degradation (10) and is crucial for the repression of RORα/RevErbα response element (RORE)-DNA binding sequence (DBS)-containing genes (e.g., *Bmal1*, *Cry1*), which is a critical event in the initiation of the RF-induced shift of PCCs (5).

As this PCC shift is maintained in various tissues throughout the RF regime (Fig. 1*C* and Fig. S1 *C* and *D* and *In RF Mice, the Expression of PCC-Controlled Output Genes Is Shifted by 12 h with Respect to the Diurnal Active and Rest Phases Controlled by the Central SCN CC*), we explored the molecular basis of its maintenance and found that the active phase RF hypoinsulinemia is a recurring event during long-term RF regime (Fig. 1*A* and *In RF Mice, the Expression of PCC-Controlled Output Genes Is Shifted by 12 h with Respect to the Diurnal Active and Rest Phases Controlled by the Central SCN CC*), which, as expected (5, 11), leads to an increase in GSK3β-mediated phosphorylated RevErbα (pRevErbα) level at "*Zeitgeber*" (ZT) 0 (Fig. 1 *E* and *F* and Fig. S1*K*). Accordingly, in long-term RF mice, the level of pRevErbα bound to the RORE DBS of aryl hydrocarbon receptor nuclear translocator-like

Significance

Mounting epidemiological and genetic evidence suggests that the disruption of circadian rhythms is at the origin of pathologies. It is known that people who are engaged in shift work and exhibit a shifted feeding schedule often develop a cohort of metabolic pathologies including diabetes, obesity, and metabolic syndrome. However, the molecular mechanisms that are at the origin of these pathologies are poorly understood. Using mice, we now revealed at the molecular level how metabolic alterations generated on shifting the eating schedule from the normal active phase to the rest phase creates a misalignment' between the central and peripheral circadian clocks. Importantly, we demonstrate that this misalignment progressively induces a metabolic pathological syndrome similar to that observed in shift workers.

Author contributions: A.M. and P.C. designed research; A.M., A.K., M.D., and N.M. performed research; H.M. and M.-F.C. contributed new reagents/analytic tools; A.M., A.K., M.D., N.M., and P.C. analyzed data; and A.M. and P.C. wrote the paper.

Reviewers: G.K., Columbia University, NY; and P.S.-C., University of California, Irvine.

The authors declare no conflict of interest.

[1]To whom correspondence should be addressed. Email: chambon@igbmc.fr.

This article contains supporting information online at www.pnas.org/lookup/suppl/doi:10.1073/pnas.1519807112/-/DCSupplemental.

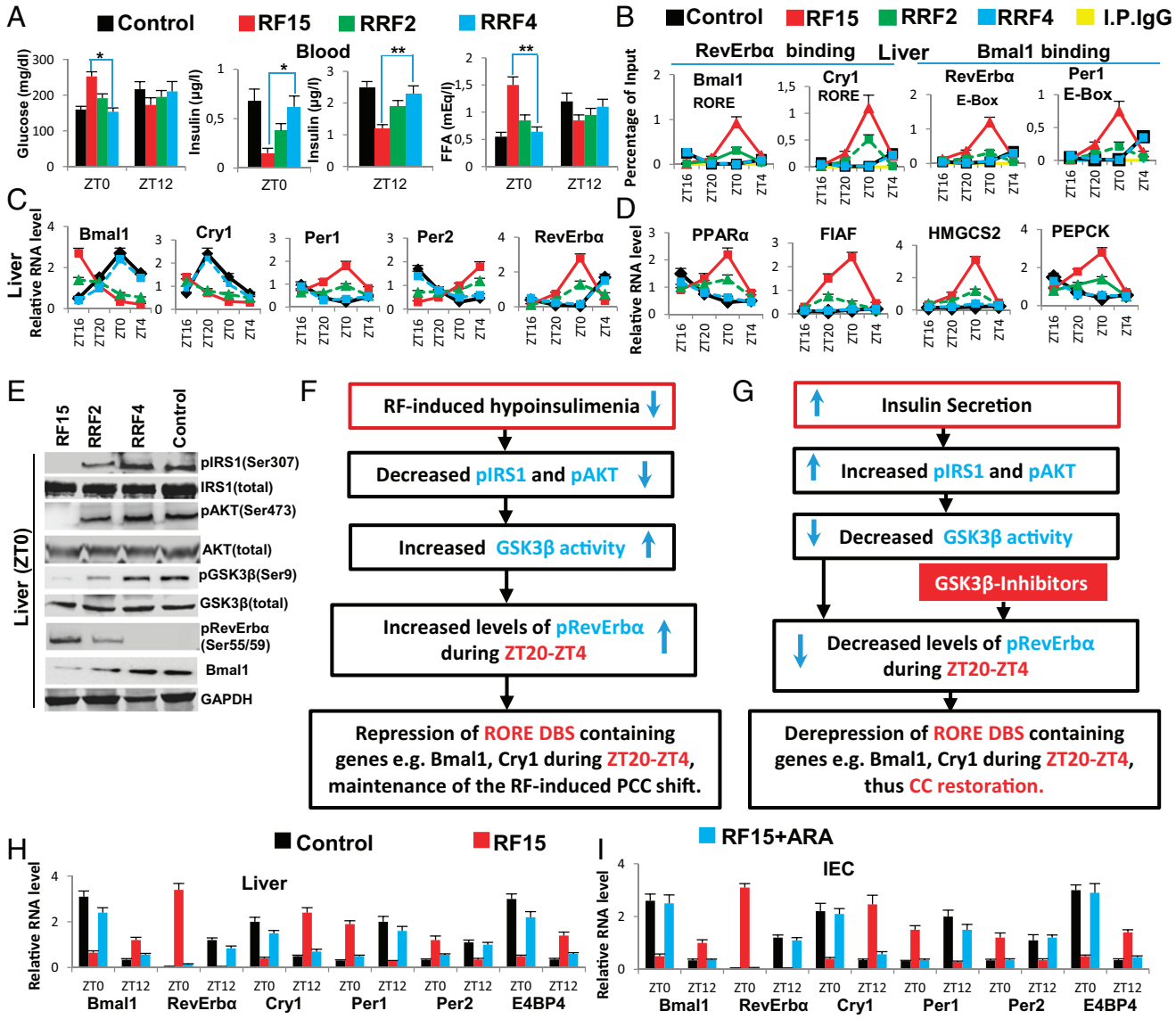

Fig. 1. GSK3β-dependent RevErbα phosphorylation is critical for maintaining the RF-induced CC shift. (*A*) Levels of blood components in control, RF15 mice, and in mice after 2 and 4 d of reversal of RF (RRF2 and RRF4). (*B*) ChIP-qPCR assays in liver to analyze the RevErbα and the Bmal1 recruitment to their respective DBSs in the genes as indicated. (*C*) RNA transcript levels of CC components in liver of control, RF15, RRF2, and RRF4 mice. (*D*) RNA transcript levels of genes, as indicated, in the liver of control, RF15, RRF2, and RRF4 mice. (*E*) Immunoblot analyses, at ZT0, of control, RF15, RRF2, and RRF4 livers with indicated antibodies. (*F*) A schematic representation of how RF-induced PCCs shift is maintained. (*G*) A schematic representation of how restoration of insulin signaling leads to the reversal of RF-induced PCCs shift. (*H*) RNA transcript levels of CC components in liver of control, RF15, and RF15+ARA mice. (*I*) RNA transcript levels of CC components in IEC of control, RF15, and RF15+ARA mice. All values are mean ± SEM. $*P < 0.05$, $**P < 0.01$.

protein 1 (*ARNTL1*/*Bmal1*) and cryptochrome 1 (*Cry1*) is permanently increased during the ZT20–ZT0 period (Fig. 1*B*), thereby leading to a permanent PCCs shift (Fig. 1*C* and Fig. S1 *C* and *D*).

Reciprocally, we found that, on a 4-day return to a normal active phase feeding after RF15 (RRF4 following RF15), the levels of several metabolic parameters (including INS) were normalized (Fig. 1 *A* and *D* and Fig. S1 *A* and *B*). Importantly, this treatment also normalized the expression of all CC components in liver, intestinal epithelial cells (IECs), and pancreas (Fig. 1*C* and Fig. S1 *C* and *D*). As expected (11), the RRF restoration of INS signaling during the active phase led to an increased level of pAKT, which through phosphorylation of GSK3β inhibited its activity, thereby reducing drastically the level of pRevErbα at ZT0 (Fig. 1 *E* and *G*). This RRF-induced decrease in pRevErbα level, which is correlated with its reduced binding to the RORE DBS of *Bmal1* and *Cry1* (Fig. 1*B*), then restored through derepression the normal (ZT20–ZT4) expression of these genes (5) and consequently the return to the original normal PCCs (Fig. 1*C* and Fig. S1 *C* and *D*). Most interestingly, we also found that increasing the INS blood level through administration of glucose for 4 consecutive d to RF30 mice at ZT18 (after removal of food at ZT12), activated pAKT (due to the INS increase) and led to a reduction in pRevErbα level at ZT0 (Fig. S1*L*), thereby normalizing the PCC (Fig. S1 *L* and *M*). Taken altogether, these experiments demonstrate that the restoration of INS signaling in RF mice during the active phase triggers the PCC normalization (Fig. 1 *A*, *E*, and *G*).

Even though, on RF cessation, RF mice do return to apparent normality in a few days (see above), it is noteworthy that such a return can also be achieved under continuous RF regime by administration of GSK3β inhibitors, which prevents RevErbα phosphorylation (Fig. 1*G*). Indeed, we found that pharmacological inhibition of GSK3β activity, through a 5-day administration to

RF mice (at ZT18) of either one of the two inhibitors of GSK3β activity, AR-A014418 (ARA) (12) and LiCl (10), is sufficient to prevent the RF-induced ZT0 binding of RevErbα to the RORE DBSs present in PCC components Fig. S1 *E* and *G*), thereby restoring normal PCCs under RF conditions (Fig. 1 *H* and *I* and Fig. S1 *F* and *H–J*). Most notably, as pharmacological inhibitors of GSK3β (e.g., LiCl and valproic acid, among others) are used in clinics to treat anxiety and mood disorders, it is tempting to speculate that, under shift work conditions, their use may prove to be beneficial to normalize the misalignment of circadian clocks, thereby preventing the progression of metabolic pathologies toward insulin resistance.

The Lack of PPARα and Glucagon Receptors Immunizes the SCN Central Clock Against RF-Induced Metabolic Perturbations. The SCN expression of Period 1 and 2 (*Per1* and *Per2*) was reported to be unaltered after 9 d of RF (RF9) (4). Of note, transcript analyses on RF15 and RF30 failed to detect any variation in the expression of not only *Per1* and *Per2*, but also of the other circadian clock components *RORα*, *Bmal1*, *Cry1*, and *RevErbα* (Fig. 2*A* and Fig. S2*A*). This raised the possibility that the SCN CC may either lack or be unresponsive (due to the absence of their transducers) to the RF metabolic signals triggering the shift of PCCs (5). Most notably, on quantitative RT-PCR (qRT-PCR) of microdissected SCN, we could not detect any transcripts for the peroxisome proliferator-activated receptor alpha (*PPARα*) and glucagon (subunit GαS) receptors, which orchestrate the CC shift in peripheral tissues (Fig. 2*B*) (5). Accordingly, in situ hybridization of SCN sections of both control and RF mice failed to reveal *PPARα* transcripts (Fig. 2*C*). In marked contrast, *PPARα* expression was readily detected in the hippocampus and paraventricular nucleus (PVN), in which a peripheral 12-h CC shift was also observed (Fig. 2*B* and Fig. S2 *B* and *C*). These CC shifts in PVN and hippocampus are noteworthy, as (*i*) the PVN, which is connected with the SCN via both afferent and efferent projections, has been proposed to function as a "relaying center" for SCN-generated signals (13), and (*ii*) the proper functioning of peripheral circadian clocks in the hippocampus is known to facilitate memory formation (14), which suggests that RF could interfere with memory processes (15).

Importantly and in keeping with the established role of the SCN in controlling the diurnal alternance of active (ZT12–ZT0) and rest (ZT0–ZT12) phases (1–3), analyses of the locomotor activity of RF mice revealed that, on RF, this alternance was unaffected (Fig. 2*D*). Thus, by excluding the expression of two transducers (PPARα and glucagon receptor) necessary to induce the PCC shift (5), the neurons of the SCN ensure the constancy of the master SCN CC during RF, as well as the proper control of the diurnal alternance of active and rest phases (1–3).

From the teleological perspective, this insensitivity of the SCN CC during a RF starvation-like state is an expected necessity, as the SCN-controlled active phase has to occur during the mouse dark cycle (the human light cycle), even though, due to the misalignment of the PCCs, this active period corresponds to the rest phase in peripheral tissues. This evolutionary design, which maintains the original active phase (wakefulness) in the SCN CC, as well as the rest phase (sleep) during RF-like conditions, is indeed advantageous as it provides the opportunity for a starving organism to efficiently look for food during the normal active phase, thereby increasing the chance to put an end to starvation and to readily realign the PCCs with the unchanged SCN master clock, as soon as feeding is restored.

It was previously suggested that the RF insensitivity of the SCN CC is related to the lack of the glucocorticoid (GC) receptor (GR) in SCN (16), as such a lack (that we confirmed; Fig. S2*D*) would prevent a SCN CC shift through an alteration of Per1/Per2 expression on RF extra-corticosterone production (16, 17). Our

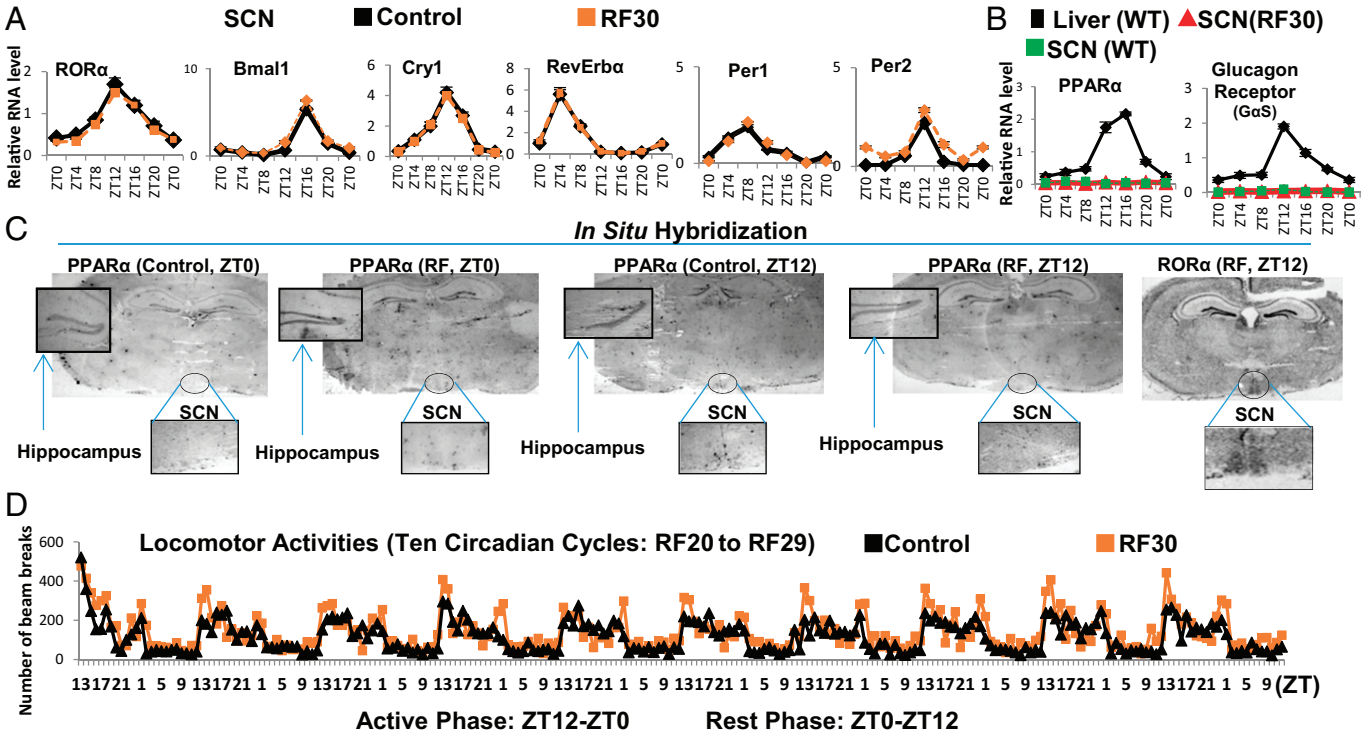

Fig. 2. The SCN CC is insensitive to the RF-induced metabolic alterations. (*A*) RNA transcript levels of CC components in the SCN of control and RF30 mice. (*B*) RNA transcript levels of PPARα and glucagon receptors in the SCN of control and RF30 mice. Expression of these genes in liver was evaluated as a control. (*C*) In situ hybridization of brain sections of control and RF mice with PPARα riboprobes. RORα expression was used as a marker for localizing the SCN. (*D*) Actimetric analyses of the circadian locomotor activity in control and RF30 mice. All values are mean ± SEM.

present results do not exclude this possibility. However, we found that the lacks of both PPARα and glucagon receptors in SCN are sufficient on their own to prevent a shift of the whole SCN CC on RF, as taken together they prevent the RF-induced CC shifts of RevErbα through PPARα increase and of Per1/Per2 through glucagon/CREB activation (5).

In RF Mice, the Expression of PCC-Controlled Output Genes Is Shifted by 12 h with Respect to the Diurnal Active and Rest Phases Controlled by the Central SCN CC. Under physiological conditions, the level of expression of nearly 10–15% of the genes expressed in mice is controlled by PCCs, such that specific sets of genes are selectively expressed during the active and rest phases, their expression being

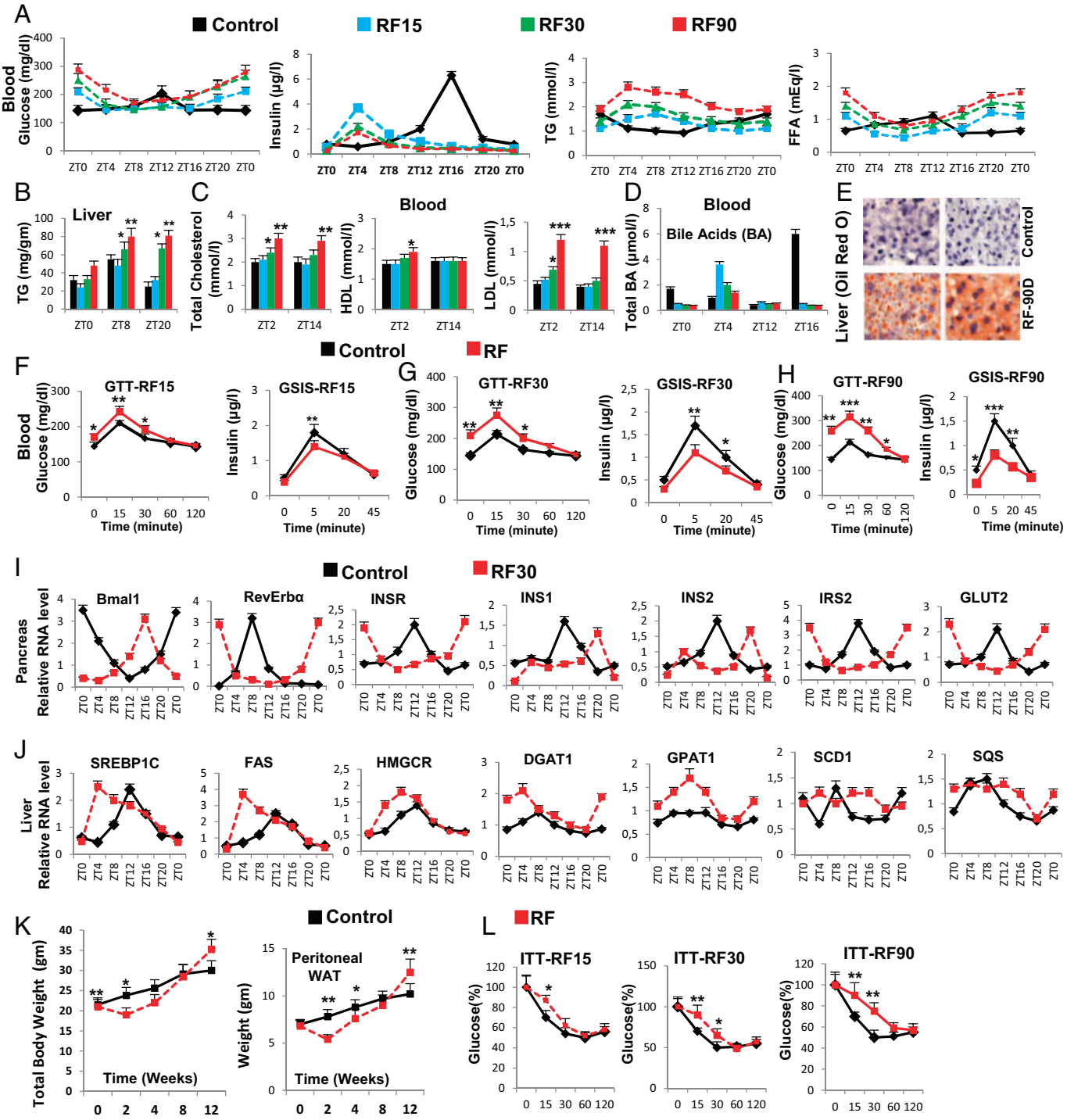

Fig. 3. Prolonged feeding during the rest phase leads to the development of diabetes and fatty liver. (*A*) Levels of blood components, as indicated, after RF15, RF30, and RF90. (*B*) As in *A*, but measuring TG levels in liver. (*C*) As in *A*, but measuring blood levels of total, HDL, and LDL cholesterol. (*D*) As in *A*, but measuring total bile acids. (*E*) Oil red O staining to detect TG deposition in control and RF90 liver. (*F–H*) Glucose tolerance tests (GTTs) and GSIS after RF15 (*F*), RF30 (*G*), and RF90 (*H*). (*I*) RNA transcript levels of genes, as indicated, in pancreas of control and RF30 mice. (*J*) RNA transcript levels of genes as indicated in liver of control and RF30 mice. (*K*) Total body weight and weight of the peritoneal adipose tissue in control and RF mice. (*L*) Insulin tolerance tests (ITT) after RF15, RF30, and RF90 days. All values are mean ± SEM. $*P < 0.05$, $**P < 0.01$, $***P < 0.001$.

directly controlled by CC components or indirectly by their output genes (1–3). Notably, it has been demonstrated that the normal expression of RORE DBS-bearing genes in different tissues is at their zenith during the circadian active phase (while at nadir during the rest phase), whereas E- and D-Box DBS-bearing genes are at their zenith during the circadian rest phase (18–20).

As the RF CC shifts occur in peripheral tissues, but not in SCN, we investigated whether the misalignment between the unchanged SCN CC-controlled genes expressed during the active and rest phases will lead to an "out of phase" expression of PCC-controlled output genes, i.e., whether the PCC active phase genes would be expressed during the SCN rest phase, whereas the PCC rest phase genes would be expressed during the SCN active phase. A bioinformatic search in the mouse genome for genes harboring D-Box DBS in their promoter-enhancer regions revealed numerous candidates, of which ~2,000 have human orthologs (Dataset S1 and *SI Methods*). Among these, we chose 40 D-Box–containing genes having known functions. We also chose 40 RORE DBS-containing genes all having known homeostatic functions (19). When analyzed at RF15 in liver and IECs the circadian expression of such RORE DBS- and D-Box–containing genes, which in WT mice also displayed a circadian variation (Tables S1–S4), confirmed a 12-h shift (misalignment) in the expression, such that the expression of the normally active phase-restricted RORE genes was shifted to the rest phase (Tables S1 and S2), whereas the initially rest phase-restricted D-Box genes were expressed during the active phase (Tables S3 and S4). Importantly, this misaligned expression of numerous CC-controlled output genes (Tables S1–S4), including those of endocrine factors (*INS*, *IGF1*, and *FGF21*), key transcription factors

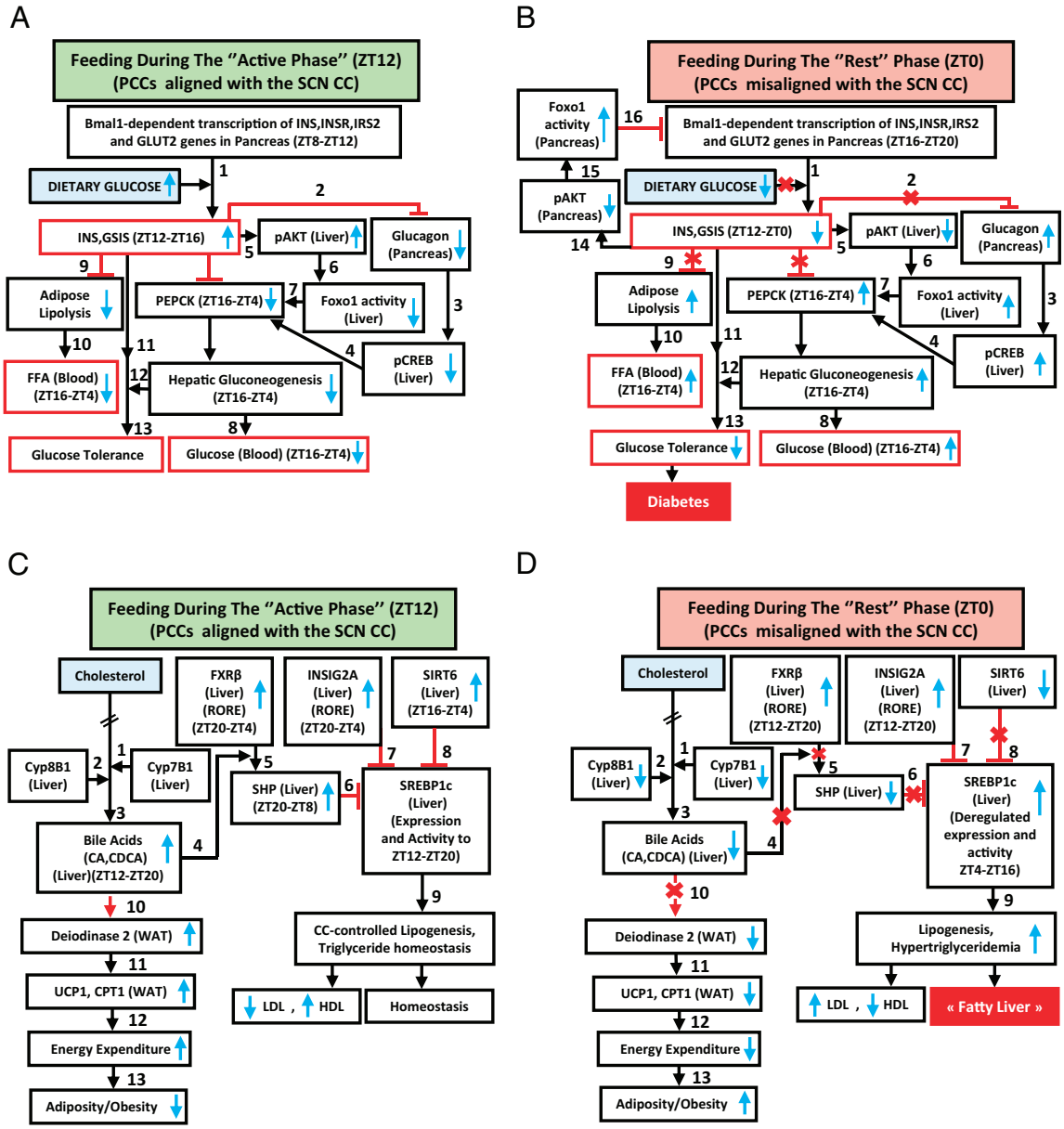

Fig. 4. A misalignment of PCCs with the SCN CC under RF regime progressively induces a metabolic syndrome. (*A*) Schematic representation of how PCCs alignment with the SCN CC maintains INS, glucose, and FFA homeostasis. (*B*) A schematic representation of how PCCs misalignment with the SCN CC in RF mice leads to hypoinsulinemia, hyperglycemia, and increased FFA level. (*C*) A schematic representation of how PCCs alignment with the SCN CC maintains lipogenesis and TG level and prevents adiposity. (*D*) A schematic representation of how PCCs misalignment with the SCN CC in RF mice leads to an increase in lipogenesis, hypertriglyceridemia, and adiposity.

(*c-Jun*, *IRF3*, *ATF5*, and *FXRβ*), critical enzymes (*NAMPT*, *Hsd3b5*, *FAS*, and *HMGCR*), receptors, and transporters (*INSR*, *IRS2*, *Glut2*, and *TLRs*), all controlling essential physiological homeostatic processes, sets the stage for the development of RF-associated pathologies (see below).

Mice Selectively Fed During the Rest Phase Display a Metabolic Syndrome-Like Pathology due to the Misalignment of the Peripheral Clocks with the Central SCN CC. The physiological alignment of PCCs with the master central SCN CC has emerged as an important factor for the homeostatic maintenance of an organism, as misalignments of PCCs with the SCN CC, such as those associated with shift work and RF, both of which correspond to activities performed during the SCN CC-controlled rest phase while being physiologically controlled and exerted during the SCN CC-controlled active phase, have been associated with increased risk of developing diabetes (hypoinsulinemia, hyperglycemia, reduced glucose tolerance), high free fatty acid (FFA) level, hypertriglyceridemia, obesity, and metabolic syndrome (6–9, 21–23). It is, however, largely unknown how these pathologies are mechanistically related to the PCC/SCN CC misalignments (3, 6–9). Most interestingly, our present study reveals, at the molecular level, that all of these metabolic pathologies eventually develop in RF mice, as a consequence of the RF-induced 12-h misalignment between the PCCs and rest and active phases of activity of the SCN CC.

A Misalignment-Induced Decrease in INS Production Leads to Diabetes in RF Mice. Under ad libitum feeding during the active phase (the ZT8–ZT12 period; Fig. 4*A*), the Bmal1 activity of the pancreatic CC transcribes *INS*, insulin receptor (*INSR*), insulin receptor substrate 2 (*IRS2*), and glucose transporter 2 (*GLUT2*) genes, thus aligning INS synthesis and signaling with the ZT12 feeding time (Fig. 3*I*) (24) and enabling maximal postprandial (ZT12–ZT16) glucose-stimulated INS secretion (GSIS) (Fig. 3*A*). This GSIS (step 1 in Fig. 4*A*), at the beginning of the active phase, is critical to prevent lipolysis within the adipose tissue (11), thereby decreasing the FFA blood level (Fig. 3*A* and steps 9–10 in Fig. 4*A*). Moreover, the INS blood increase (*i*) counteracts glucagon secretion to prevent pCREB activity in liver (steps 2–4 in Fig. 4*A*) and (*ii*) activates pAKT (Fig. 1*E* and Fig. S1*L*) to inactivate the FOXO1 protein in liver (11) (steps 5–7 in Fig. 4*A*). This combined decrease in pCREB and FOXO1 reduces the PEPCK expression in liver, thereby preventing hepatic gluconeogenesis (ZT16–ZT4) and maintaining the physiological glucose blood level (step 8 in Fig. 4*A*), which ensures glucose tolerance (steps 11–13 in Fig. 4*A*).

We found by RF7, that the CC shift was complete in pancreas, which resulted in a permanent misalignment in the expression of genes critically involved in insulin synthesis and signaling (see below) and led to a recurrent hypoinsulinemia (in RF mice) during the active phase, thereby accounting for all of the pathological metabolic features typically associated with diabetes (Fig. 4*B*). Due to this RF CC shift, Bmal1-dependent transcriptions in pancreas were shifted to the ZT16–ZT20 period (Fig. 3*I*), at a time where dietary glucose is unavailable due to the rest phase feeding at ZT0 (Fig. 4*B*).The ensuing RF-hypoinsulinemia (ZT12–ZT0; Fig. 3*A*) induced the FOXO1 activity in pancreas, as a consequence of a reduction in pAKT level (11, 25, 26), thus leading to a repression (25) of the transcription of the INS gene at ZT0 (steps 14–16 in Fig. 4*B* and Fig. 3*I*) and to a decreased postprandial GSIS in RF mice (Fig. 3*A*). Moreover, as a result of the RF hypoinsulinemia, there was an increase in *PEPCK* expression due to enhanced pCREB and FOXO1 activity (Fig. S3*D* and steps 2–7 in Fig. 4*B*), which resulted in RF hyperglycemia (Fig. 3*A* and step 8 in Fig. 4*B*). Taken together, this RF hypoinsulinemia and hyperglycemia account for the reduced glucose tolerance in RF mice (Fig. 3 *F–H* and steps 11–13 in Fig. 4*B*). However, even at RF90, an INS-resistant state was not achieved, although there was a progressive deterioration from RF15 to RF90 (Fig. 3*L*). Importantly, the reduction in INS level in RF mice also accounted for the inability of these mice to suppress lipolysis in adipose tissue and the resulting increase in FFA blood level (Fig. 3*A* and steps 9–10 in Fig. 4*B*).

In summary, taken together, our present results establish how an RF-induced misalignment of PCCs and SCN CC triggers the development of diabetes (hypoinsulinemia, hyperglycemia, reduced glucose tolerance) and increased FFA level through misexpression during the active phase of PCC genes normally expressed during the rest phase.

A Misalignment-Induced Increase in SREBP1c Leads to Hypertriglyceridemia and Hypercholesterolemia in RF Mice. Because, in addition to diabetes, shift workers also develop hypertriglyceridemia and hypercholesterolemia (6, 7, 22, 23), we investigated whether these

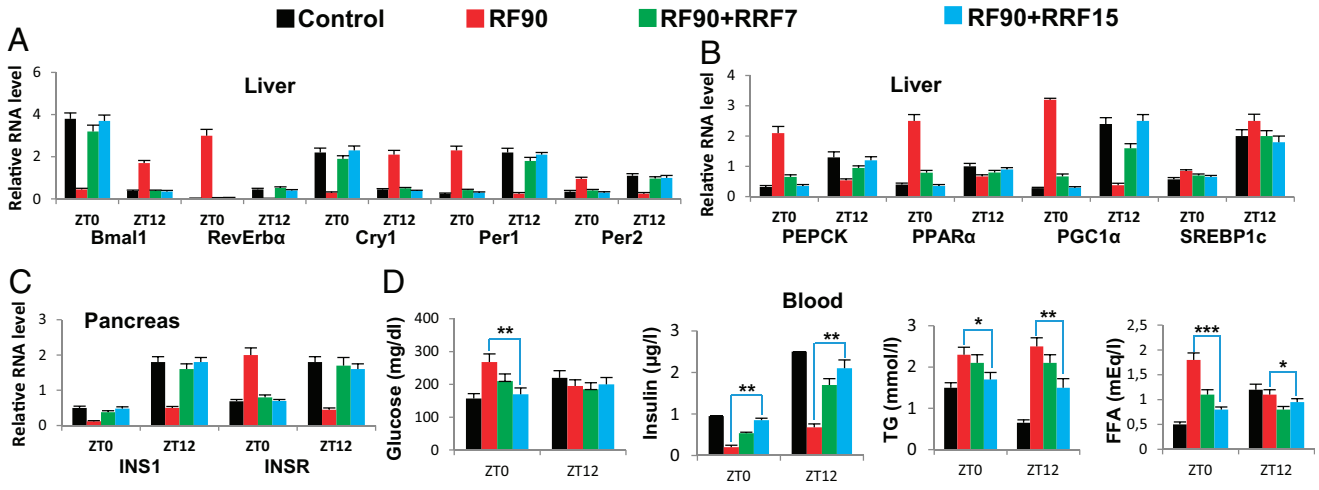

Fig. 5. Prolonged RF-induced metabolic alterations are reversible on returning to normal feeding regime. (*A*) RNA transcript levels of CC components in liver of control and RF90 mice, and in mice after reversal of RF (RRF7 and RRF15). (*B*) RNA transcript levels of genes, as indicated, in liver of control and RF90 mice, and in mice after reversal of RF (RRF7 and RRF15). (*C*) RNA transcript levels of genes, as indicated, in pancreas of control and RF90 mice, and in mice after reversal of RF (RRF7 and RRF15). (*D*) Levels of blood components, as indicated, in control and RF90 mice, and in mice after reversal of RF (RRF7 and RRF15). All values are mean ± SEM. $*P < 0.05$, $**P < 0.01$, $***P < 0.001$.

metabolic alterations could also originate from RF-induced clock misalignment. Under ad libitum feeding during the active phase (ZT12–ZT20; Fig. 4*C*), the liver CC components are involved in the control of expression and activity of SREBP1c, which is well known to act as the master transcriptional regulator of triglyceride (TG) synthesis and lipogenesis (2, 3, 27). Multiple mechanisms are involved in this regulation. (*i*) In liver, cholesterol is converted into bile acids (BAs), cholic acid (CA), and cheno deoxy-cholic acid (CDCA) through the action of two enzymes Cyp8B1 and Cyp7B1, respectively (steps 1–2 in Fig. 4*C*); this blood BA postprandial increase (Fig. 3*D* and step 3 in Fig. 4*C*) enables the RORE-controlled farnesoid X receptor (FXR) receptor (28) (Fig. S3*A*) to activate transcription of the small heterodimer partner (SHP) repressor during the ZT20–ZT8 period (Fig. S3*A* and steps 4–5 in Fig. 4*C*), which in turn inhibits the expression of SREBP1c (29) (step 6 in Fig. 4*C*). (*ii*) The nuclear import of SREBP1c from endoplasmic reticulum and Golgi vesicles is inhibited by INSIG2A (30), the expression of which is also controlled (30) by a RORE DBS (ZT20–ZT4, Fig. S3*A* and step 7 in Fig. 4*C*). (*iii*) The chromatin recruitment of SREBP1c to DBSs present in multiple genes is inhibited by SIRT6 (31) (step 8 in Fig. 4*C*). Taken together, these mechanisms ensure a circadian pattern for SREBP1c expression and activity, which maintains homeostatic TG levels in blood and tissues (steps 6–9 in Fig. 4*C*).

In contrast, we found that in RF liver there was a decrease in *Cyp7B1* and *Cyp8B1* expression (Fig. S3*A*; see above), which was correlated with a decrease in postprandial BA secretion (Fig. 3*D* and steps 1–3 in Fig. 4*D*). Moreover, as a consequence of the RF CC shift in liver (5), the RORE-dependent *FXRβ* expression was shifted to the ZT12–ZT20 period (Fig. S3*A*), which in conjunction with the reduced BA levels in RF mice decreased the FXR-dependent expression of *SHP* (Fig. S3*A* and steps 3–5 in Fig. 4*D*). Furthermore, the *SIRT6* expression was reduced in RF mice (Fig. S3*A* and step 8 in Fig. 4*D*), whereas the RORE-dependent expression of *INSIG2A* (Fig. S3*A* and step 7 in Fig. 4*D*) was shifted due to the permanent shift of RevErbα expression in RF liver (5). Thus, alterations of all of these SREBP1c negative regulators (2, 3, 32, 33) increased SREBP1c expression and activity in RF liver (Fig. 3*J* and steps 6–9 in Fig. 4*D*), which resulted in an induction of the genes critically involved in the lipogenesis (27) (i.e., *FAS*, *HMGCR*, *DGAT1*, *GPAT1*, *SCD1*, and *SQS*; Fig. 3*J*), thereby leading to an increase in hepatic de novo lipogenesis and finally to hypertriglyceridemia and hypercholesterolemia (Fig. 3 *B* and *C*).

By RF90, the expression pattern of CC genes in various tissues remained unchanged (compare Fig. S3*D* with Fig. S4*A*) (5). However, at this time, RF mice displayed a fatty liver phenotype, as revealed by an increase in hepatic TG levels and Oil red O staining (Fig. 3 *B* and *E*). This was accompanied in RF liver by a further up-regulation of SREBP1c-driven expression of lipogenic genes (Fig. S4*B*), which disrupted the normal circadian variation (2, 3) in liver and blood TG levels (2, 3) (Fig. 3 *A* and *B*; compare the progressive deteriorations from RF15 to RF90). Importantly, this RF increase in lipogenesis enhanced blood levels of both total and LDL cholesterol (Fig. 3*C*), whereas the HDL-LDL ratio was reduced (Fig. 4*D*), which is a hallmark of atherosclerosis (27) and is also associated with shift work (6, 23).

Of note, RF mice after an initial loss of weight, slowly started gaining weight, despite equal food intake, and by 12 wk of RF, weighed more than control mice, with a selective increase in the weight of visceral white adipose tissue (WAT; Fig. 3*K* and Fig. S4*C*). In keeping with this weight gain, transcript analyses of WAT revealed (*i*) an increase of the SREBP1c level, which is known to stimulate (34) the expression of adipogenic genes (*PPARγ2*, *FAS*, *SCD1*, *ACC1*, and *DGAT1*; Fig. S4*D*), and (*ii*) a decrease in BA-controlled expression of iodothyronine deiodinase 2 (DIO2) (29) and of the uncoupling protein 1 (UCP1) (Fig. S4*E* and steps 10–13 in Fig. 4*D*), which are known to increase energy expenditure (29). Remarkably, we also found that even after RF90, both the RF-induced CC shift and all of the above metabolic perturbations (Fig. 4 *A*–*D*) were still reversible within 15 d (RRF15) on return to the normal active phase feeding (Fig. 5 *A*–*D*).

In conclusion, it is striking that the pathological metabolic perturbations that are frequently observed in shift workers are similar to those occurring in mice on a prolonged RF-induced misalignment between the feeding time and the diurnal rest and active phases controlled by the master SCN clock, which validates the use of RF mice as a model for further studies on the consequences of shift work.

Methods

Mice and Treatments. Eight- to 12-wk-old C57BL6/J male WT mice (Charles River Laboratories) were used. Control mice were provided food and water ad libitum, under 12-h light (6:00 AM–6:00 PM) and 12-h dark (6:00 PM–6:00 AM) conditions. RF mice were provided food during the entire light period (4). Breeding, maintenance, and experimental manipulations were approved by the Animal care and Use Committee of Institut de Génétique et de Biologie Moléculaire et Cellulaire (IGBMC)/Institut Clinique de la souris (ICS).

Statistics. Data are represented as mean ± SEM of at least three independent experiments and were analyzed by SyStat and Microsoft Excel statistics software using the Student *t* test (RNA transcripts) and one-way ANOVA (blood metabolic analysis). $P < 0.05$ was considered significant.

ACKNOWLEDGMENTS. We thank the staffs of animal house facilities in Institut de Génétique et de Biologie Moléculaire et Cellulaire (IGBMC)/Institut Clinique de la souris (ICS) for help. This work was supported by the Centre national de la recherche scientifique (CNRS), Institut national de la santé et de la recherche médicale (INSERM), University of Strasbourg Institute for Advanced Studies, and the Association pour la Recherche a l'IGBMC (ARI). A.M., A.K., M.D., and N.M. were supported by fellowships from ARI.

1. Asher G, Schibler U (2011) Crosstalk between components of circadian and metabolic cycles in mammals. *Cell Metab* 13(2):125–137.
2. Bass J, Takahashi JS (2010) Circadian integration of metabolism and energetics. *Science* 330(6009):1349–1354.
3. Asher G, Sassone-Corsi P (2015) Time for food: The intimate interplay between nutrition, metabolism, and the circadian clock. *Cell* 161(1):84–92.
4. Damiola F, et al. (2000) Restricted feeding uncouples circadian oscillators in peripheral tissues from the central pacemaker in the suprachiasmatic nucleus. *Genes Dev* 14(23): 2950–2961.
5. Mukherji A, Kobiita A, Chambon P (2015) Shifting the feeding of mice to the rest phase creates metabolic alterations, which, on their own, shift the peripheral circadian clocks by 12 hours. *Proc Natl Acad Sci USA*, 10.1073/pnas.1519735112.
6. Paschos GK (2015) Circadian clocks, feeding time, and metabolic homeostasis. *Front Pharmacol* 6(112):112.
7. Leproult R, Holmbäck U, Van Cauter E (2014) Circadian misalignment augments markers of insulin resistance and inflammation, independently of sleep loss. *Diabetes* 63(6):1860–1869.
8. Esquirol Y, Bongard V, Ferrieres J, Verdier H, Perret B (2012) Shiftwork and higher pancreatic secretion: Early detection of an intermediate state of insulin resistance? *Chronobiol Int* 29(9):1258–1266.
9. McHill AW, et al. (2014) Impact of circadian misalignment on energy metabolism during simulated nightshift work. *Proc Natl Acad Sci USA* 111(48):17302–17307.
10. Yin L, Wang J, Klein PS, Lazar MA (2006) Nuclear receptor Rev-erbalpha is a critical lithium-sensitive component of the circadian clock. *Science* 311(5763):1002–1005.
11. Saltiel AR, Kahn CR (2001) Insulin signalling and the regulation of glucose and lipid metabolism. *Nature* 414(6865):799–806.
12. Ly PT, et al. (2013) Inhibition of GSK3β-mediated BACE1 expression reduces Alzheimer-associated phenotypes. *J Clin Invest* 123(1):224–235.
13. Moga MM, Weis RP, Moore RY (1995) Efferent projections of the paraventricular thalamic nucleus in the rat. *J Comp Neurol* 359(2):221–238.
14. Gerstner JR, Yin JC (2010) Circadian rhythms and memory formation. *Nat Rev Neurosci* 11(8):577–588.
15. Talani G, et al. (September 10, 2015) Enhanced glutamatergic synaptic plasticity in the hippocampal CA1 field of food-restricted rats: Involvement of CB1 receptors. *Neuropsychopharmacology*, 10.1038/npp.2015.280.
16. Balsalobre A, et al. (2000) Resetting of circadian time in peripheral tissues by glucocorticoid signaling. *Science* 289(5488):2344–2347.
17. Le Minh N, Damiola F, Tronche F, Schütz G, Schibler U (2001) Glucocorticoid hormones inhibit food-induced phase-shifting of peripheral circadian oscillators. *EMBO J* 20(24): 7128–7136.

18. Koike N, et al. (2012) Transcriptional architecture and chromatin landscape of the core circadian clock in mammals. *Science* 338(6105):349–354.
19. Mukherji A, Kobiita A, Ye T, Chambon P (2013) Homeostasis in intestinal epithelium is orchestrated by the circadian clock and microbiota cues transduced by TLRs. *Cell* 153(4):812–827.
20. Fang B, et al. (2014) Circadian enhancers coordinate multiple phases of rhythmic gene transcription in vivo. *Cell* 159(5):1140–1152.
21. Morris CJ, et al. (2015) Endogenous circadian system and circadian misalignment impact glucose tolerance via separate mechanisms in humans. *Proc Natl Acad Sci USA* 112(17):E2225–E2234.
22. Suwazono Y, et al. (2008) A longitudinal study on the effect of shift work on weight gain in male Japanese workers. *Obesity (Silver Spring)* 16(8):1887–1893.
23. Sookoian S, et al. (2007) Effects of rotating shift work on biomarkers of metabolic syndrome and inflammation. *J Intern Med* 261(3):285–292.
24. Marcheva B, et al. (2010) Disruption of the clock components CLOCK and BMAL1 leads to hypoinsulinaemia and diabetes. *Nature* 466(7306):627–631.
25. Kitamura T, et al. (2002) The forkhead transcription factor Foxo1 links insulin signaling to Pdx1 regulation of pancreatic β cell growth. *J Clin Invest* 110(12):1839–1847.
26. Inagaki T, et al. (2008) Inhibition of growth hormone signaling by the fasting-induced hormone FGF21. *Cell Metab* 8(1):77–83.
27. Horton JD, Goldstein JL, Brown MS (2002) SREBPs: Activators of the complete program of cholesterol and fatty acid synthesis in the liver. *J Clin Invest* 109(9):1125–1131.
28. Yang X, et al. (2006) Nuclear receptor expression links the circadian clock to metabolism. *Cell* 126(4):801–810.
29. Houten SM, Watanabe M, Auwerx J (2006) Endocrine functions of bile acids. *EMBO J* 25(7):1419–1425.
30. Le Martelot G, et al. (2009) REV-ERBalpha participates in circadian SREBP signaling and bile acid homeostasis. *PLoS Biol* 7(9):e1000181.
31. Masri S, et al. (2014) Partitioning circadian transcription by SIRT6 leads to segregated control of cellular metabolism. *Cell* 158(3):659–672.
32. Fu S, et al. (2012) Polysome profiling in liver identifies dynamic regulation of endoplasmic reticulum translatome by obesity and fasting. *PLoS Genet* 8(8):e1002902.
33. Kim HS, et al. (2010) Hepatic-specific disruption of SIRT6 in mice results in fatty liver formation due to enhanced glycolysis and triglyceride synthesis. *Cell Metab* 12(3):224–236.
34. Kim JB, Wright HM, Wright M, Spiegelman BM (1998) ADD1/SREBP1 activates PPARgamma through the production of endogenous ligand. *Proc Natl Acad Sci USA* 95(8):4333–4337.
35. Chotteau-Lelièvre A, Dollé P, Gofflot F (2006) Expression analysis of murine genes using *in situ* hybridization with radioactive and nonradioactively labeled RNA probes. *Methods Mol Biol* 326:61–87.
36. Mitsui S, Yamaguchi S, Matsuo T, Ishida Y, Okamura H (2001) Antagonistic role of E4BP4 and PAR proteins in the circadian oscillatory mechanism. *Genes Dev* 15(8): 995–1006.
37. Huang W, Sherman BT, Lempicki RA (2009) Systematic and integrative analysis of large gene lists using DAVID bioinformatics resources. *Nature Protocols* 4:44–57.

Supporting Information

Mukherji et al. 10.1073/pnas.1519807112

SI Methods

Mice. All experiments were performed under light-dark (L/D) conditions, with ZT0 being the start of the light period (6:00 AM) and ZT12 the start of the dark period (6:00 PM). Mice were killed at 4-h intervals starting from ZT12 or ZT0. Food was removed from the RF cages at 6:00 PM and reintroduced at 6:00 AM. Food intake was measured (in 12 control and 20 RF mice) by continuously measuring the weight of the food supplied for individual animals (individual pellets weighing 20 mg). Overall food intake was measured by determining the weight of consumed food in bins of 1 wk. All mice were fed the normal laboratory chow diet.

Isolation and Laser Capture Microdissection of SCN and PVN. The brains were isolated and frozen in iso-pentane (Sigma Aldrich) kept on dry ice and immediately stored at −70 °C. The frozen brains were fixed by Cryomatrix (Thermo Scientific), and 12-μm-thick sections were cut using a cryotome. The sections were mounted on PET-Membrane frame slides (Leica no. 11505151), which were first fixed in 70% (vol/vol) ethanol for 1 min and then stained in cresyl violet (Sigma Aldrich) for 3 min, followed by rinsing in 70% and 100% ethanol for 30 s each. Finally, the slides were air dried and used for laser capture microdissection. The locations of the SCN and PVN was confirmed using the brain atlas. The laser-cut SCN and PVN samples were collected in the caps of RNase-free 200-μL PCR tubes containing RLT buffer (a guanidine-thiocyanate–containing lysis buffer) (Qiagen). RNA was extracted using the RNeasy micro kit (Qiagen) following the manufacturer's instruction manual. A standard reverse transcription protocol was used to convert the isolated RNA into cDNA, and purity of SCN samples was verified by measuring the transcripts for arginine vasopressin (AVP) and vasoactive intestinal polypeptide (VIP), expressed relative to GAPDH.

In Situ Hybridization. In situ hybridization was performed using digioxigenin (DIG)-labeled riboprobes as previously described (35). PPARα and RORα cDNA was PCR amplified from mouse liver and subsequently cloned into the pGEM-T easy vector system (Promega) and sequenced to verify the gene identify. DIG-labeled sense and antisense riboprobes were synthesized using the in vitro transcription kit (Promega). Brain sections (14 μm thick) were cut and mounted on superfrost plus (Thermo Scientific) slides. The sections were stored at −80 °C. For in situ hybridization, the slides were first defrosted and then air dried at room temperature for 30 min. The sections were postfixed in ethanol gradation of 70%, 90%, and 100% for 5 min each and finally rinsed in PBS. The sections were hybridized overnight using 0.1 μg/mL RORα riboprobe and 1 μg/mL PPARα riboprobe in hybridization solution and incubated at 65 °C in a humidified chamber. The slides were washed in 5× SSC for 15 min followed by 0.2× SSC for 2 h at 72 °C. The blocking was performed for 2 h in blocking solution [maleic acid buffer (MAB), pH 7.5, Tween-20 0.1%, blocking reagent 2% (Roche), and 20% heat inactivated normal goat serum]. Next, alkaline phosphatase-conjugated anti-DIG Fab fragment (Roche) was added on the glass sides at a dilution of 1:2,000 in blocking solution and incubated overnight at 4 °C under glass coverslip. The slides were then washed five times in MAB with 10% Tween-20 for 5 min each and finally rinsed in alkaline phosphatase buffer. Nitro blue tetrazolium (NBT)/5-Bromo 4-chloro-3-indolyl phosphate (BCIP) (Roche) was used as staining solution for developing slides to detect alkaline phosphatase activity. The sections were incubated in dark for color development for 1 d (RORα) and 3 d (PPARα) at room temperature. After color development, the slides were rinsed in PBS, air dried, and mounted in PERTEX. Photographs were taken using Leica M420 macroscope and DMLB/DM4000B microscopes equipped with Photometrics digital cameras and CoolSnap imaging software (Roger Scientific). Primer sequences for the preparation of riboprobes are available on request.

RNA Transcript Determination. Freshly isolated IECs, liver, pancreas, and hippocampus samples were used for RNA isolation using TRI reagent (Molecular Research Center). Subsequent to the verification of RNA quality (gel electrophoresis), 1 μg total RNA (determined spectrophotometrically) was reverse transcribed using random hexamers and SuperScript II reagents (Invitrogen) per the manufacturer's instructions. The synthesized cDNA was used for qRT-PCR with SYBRgreen (QIAGEN) and expressed relative to the hypoxanthine phosphoribosyltransferase (HPRT) levels, as previously described (19). Primer sequences are available on request. For transcript determination, four control and four RF mice were killed at each time point, and each experiment was replicated three times.

Protein Immunoblots. Immunoblots from isolated liver were performed following standard SDS/PAGE procedures. Proteins were visualized following ECL (Pierce), and images were captured using CCD. The primary antibodies for IRS1 (2390), pIRS1 Ser307 (2381), pAkt Ser473 (4060), Akt (4685), pGSK3β Ser9 (5558), GSK3β (12456), and pRevErbα Ser55/59 (2129) were obtained from Cell Signaling Technology. RevErbα (ab115552) and Bmal1 (ab93806) antibodies were obtained from abcam. GAPDH antibody was from Millipore.

FGF21 Measurement. FGF21 was assayed from the plasma samples obtained from the blood of control and RF mice (eight animals were used per group), using the FGF21 quantikine ELISA kit (R&D; MF2100) per the manufacturer's instructions.

ChIP Assays. ChIP was performed as reported (19) with some minor modifications. Briefly, isolated IEC suspension in PBS was cross-linked with 1% formaldehyde for 15 min at room temperature; cross-linking was stopped by addition of 2 M glycine (0.125 M final concentration) at room temperature for 5 min. Cells were pelleted, and 500 μL lysis buffer was added in presence of protease inhibitors (Roche) on ice. For liver samples, identical lobes of liver from different groups of mice were disrupted using a dounce homogenizer; samples were then cross-linked and processed as described above. For adrenal glands, 12 adrenal glands were pulled and homogenized for each antibody per time point. Following cell lysis, the samples were sonicated (Bioruptor; Diagenode) to generate fragments of average length of 200–500 bp. Cellular debris were removed by centrifugation at 4 °C for 10 min (10,000 × *g*), and supernatant was precleared with Protein A/G-Sepharose (Roche) beads and preblocked with salmon DNA and BSA for 60 min at 4 °C. Beads were pelleted and discarded; 10% of the lysate was stored from each sample as the source of Input, and the remaining lysate was diluted eight times (five times for adrenal glands) in dilution buffer [16.7 mM Tris·HCl, pH 8.1, 0.01% (wt/vol) SDS, 1.1% (vol/vol) Triton X-100, 1.2 mM EDTA, 16.7 mM NaCl, protease inhibitor mixture] in the presence of different primary antibodies for 14 h at 4 °C, on a flip-flop rocker. Ninety microliters Protein A/G-Sepharose beads (preblocked with salmon DNA and BSA) was then added for 90 min at 4 °C. Immunecomplexes were recovered by centrifugation at 500 ×*g* for 1 min. Beads were washed extensively at 4 °C in low salt

buffer [20 mM Tris·HCl, pH 8.1, 0.1% (wt/vol) SDS, 1% (vol/vol) Triton X-100, 2 mM EDTA, 150 mM NaCl], in high salt buffer [20 mM Tris·HCl, pH 8.1, 0.1% (wt/vol) SDS, 1% (vol/vol) Triton X-100, 2 mM EDTA, 500 mM NaCl], in LiCl buffer [10 mM Tris·HCl, pH 8.1, 250 mM LiCl, 1% (vol/vol) Nonidet P-40, 1% (wt/vol) sodium deoxycholate, 1 mM EDTA], and finally in 1 mL TE buffer (10 mM Tris·HCl, pH 8.0, 1 mM EDTA). The bound chromatin was released from the beads by intermittent vortexing at room temperature in 200 μL elution buffer [1 (wt/vol) SDS and 100 mM $NaHCO_3$]. One milliliter of 10 mg/mL RnaseA and 5 M NaCl (200 mM final concentration) was added to the eluate and incubated overnight at 65 °C and then treated with Proteinase K for 1 h at 55 °C; DNA was purified using the QIAGEN PCR purification kit in a final volume of 50 μL. The qPCR was done using this eluted DNA and SYBRgreen reagent (QIAGEN). PCR cycles were verified to be within the linear range of amplification. Primer sequences are available on request.

Plasma Metabolic Analysis. Blood glucose, INS, TG, FFA, cholesterol (total, LDL, HDL), bile acids, and IGF1 levels were measured from control and RF mice (eight animals per group per time point) at indicated ZTs. Blood glucose levels were determined on blood collected from the tail vein using a handheld Accu-check active glucometer (Roche). For all other measurements, blood were collected by retro-orbital puncture in EDTA-coated vials, plasma was separated, and measurements were done in the metabolomics unit of the IGBMC/ICS.

GTTs and ITTs. GTTs and ITTs were performed after 15, 30, and 90 d of RF. Blood glucose was measured at the indicated times after i.p. administration of glucose (1 g/kg) of body weight. GSIS was also similarly studied after i.p. administration of glucose. ITTs were carried out after i.p. administration of 0.75 U INS/kg of body weight (Humulin R; EliLilly). INS level at the beginning of the experiment was considered as 100%. Eight to 10 control and RF mice were used for GTT and ITT experiments. GTT and GSIS were performed from the same animals. For glucose administration-dependent reversal of RF PCC shift, glucose (2 g/kg) was i.p. administered for 4 consecutive d at ZT18.

Pharmacological Inhibition of GSK3β. GSK3β activity was inhibited by i.p. administration of either LiCl (Merck) or AR-A014418 (ARA; Sigma Aldrich; 3230) at ZT18 to RF mice. LiCl (25 mEq/kg) was prepared in PBS, whereas ARA (8 mg/kg) was dissolved in DMSO (Sigma Aldrich) and diluted in PBS before injection. Both inhibitors were administered for 5 consecutive RF days (injected every day at ZT18). One group of RF mice were mock i.p. administered with DMSO + PBS.

Oil Red O Staining. Following death, liver samples were frozen in Cryomatrix and kept at −20 °C. Eight-micrometer sections were prepared and stained in 0.5% Oil red O stain (prepared in glycerol) for lipid (TG) and then in hematoxylin for 5 s, and images were captured.

Quantification of TG Levels in Liver. Hepatic TG levels were analyzed as per a previous report (33). Briefly liver extracts were prepared by homogenization in 0.25% sucrose with 1 mmol/L EDTA, and lipids were extracted using chloroform/methanol [2:1 (vol/vol)] and suspended with 5% fatty acid-free BSA. TG level was measured using triglyceride assay reagents (Sigma). The assay was performed in the metabolomics unit of ICS.

Circadian Locomotor Activity and Ingestive Behaviors. Spontaneous locomotor activity of control and RF mice in the front and rear portions of the cages were simultaneously recorded from 24 individual boxes equipped with infrared captors, connected to computers. The quantity of water and food consumed was measured during the test period using an automated pellet feeder and lickometer (Imetronic, Pessac, France). For RF cages, the automated pellet feeder was disconnected manually at 6:00 PM (ZT12), whereas it was connected back to the cages at 6:00 AM (ZT0). Mice were tested for 32 h to measure habituation to the apparatus, as well as nocturnal and diurnal activities, following which the locomotor activity data are recorded for 10 consecutive light-dark periods. Results are expressed per 1-h periods.

Bioinformatics Analysis. For identification of D-Box DNA binding sequences present across the human and mouse genome, human (hg19, Ensembl version: 67), downloaded from Ensembl and mouse (mm9, Ensembl version: 67; ftp://ftp.ensembl.org/pub/current_fasta/mus_musculus/dna/) repeat masked genome assembly was used. The database had 37,991 mouse genes and 57,945 human genes. The database was searched for D-Box–containing genes with the consensus sequence RT(G/T)AYGTAAY [where R is a purine and Y is a pyrimidine residue (36)] and no mismatch in both the DNA strands, within −20 kb upstream and +5 kb downstream of the transcriptional start sites for each genes using a JAVA-based homemade program to reveal gene annotation: Ensembl Gene ID, Associated Gene Name, Chromosome Name, Gene Start, Gene End, chromosome strand, and location. The analysis revealed 12,933 mouse genes and 18,311 human genes containing at least one D-Box sequence. The D-Box containing 2,110 ortholog genes between mice and humans was found using the table of gene orthology (Ensembl) with the help of biomart (www.biomart.org). Gene functional annotation was done using the DAVID program (37).

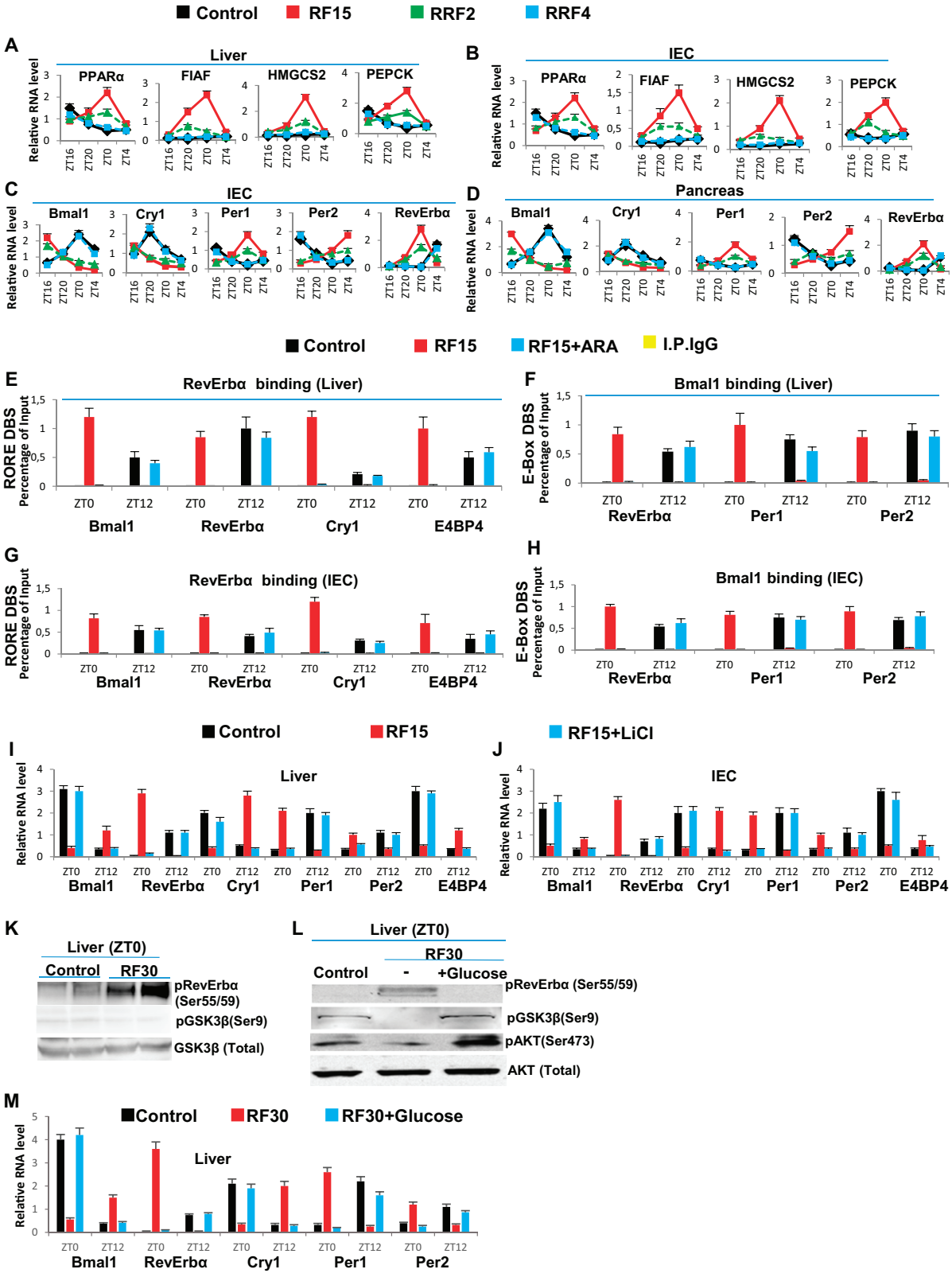

Fig. S1. RF-induced increase in GSK3β activity plays a critical role in maintaining the peripheral CCs shift. (*A* and *B*) RNA transcript levels of genes, as indicated, in liver (*A*) and IECs (*B*) of control, RF15, and reversal of RF (RRF; RRF2 and RRF4) mice. (*C* and *D*) RNA transcript levels of CC components genes in IECs (*C*) and pancreas (*D*) of control, RF15, RRF2, and RRF4 mice. (*E*) ChIP-qPCR analysis of RevErbα recruitment to RORE DBSs present in genes, as indicated, in liver of RF mice, with or without i.p. administration of the GSK3β inhibitor ARA. (*F*) ChIP-qPCR analysis of Bmal1 recruitment to E-box DBS present in genes, as indicated, in liver of RF mice, with or without i.p. administration of the GSK3β inhibitor ARA. (*G*) ChIP-qPCR analysis of RevErbα recruitment to RORE DBSs present in genes, as indicated, in IECs of RF mice, with or without i.p. administration of the GSK3β inhibitor ARA. (*H*) ChIP-qPCR analysis of Bmal1 recruitment to E-box DBS present in genes, as indicated, in IECs of RF mice, with or without i.p. administration of the GSK3β inhibitor ARA. (*I* and *J*) RNA transcript levels of CC components in liver (*I*) and IECs (*J*) of RF mice with or without i.p. administration of LiCl. (*K*) Immunoblot analyses, at ZT0, of control and RF30 livers, with indicated antibodies. (*L*) Immunoblot analyses, at ZT0, of RF30 livers treated with or without i.p. administration of glucose, with indicated antibodies. (*M*) RNA transcript levels of CC components in the liver of control, RF30, and RF30+Glucose mice. All values are mean ± SEM.

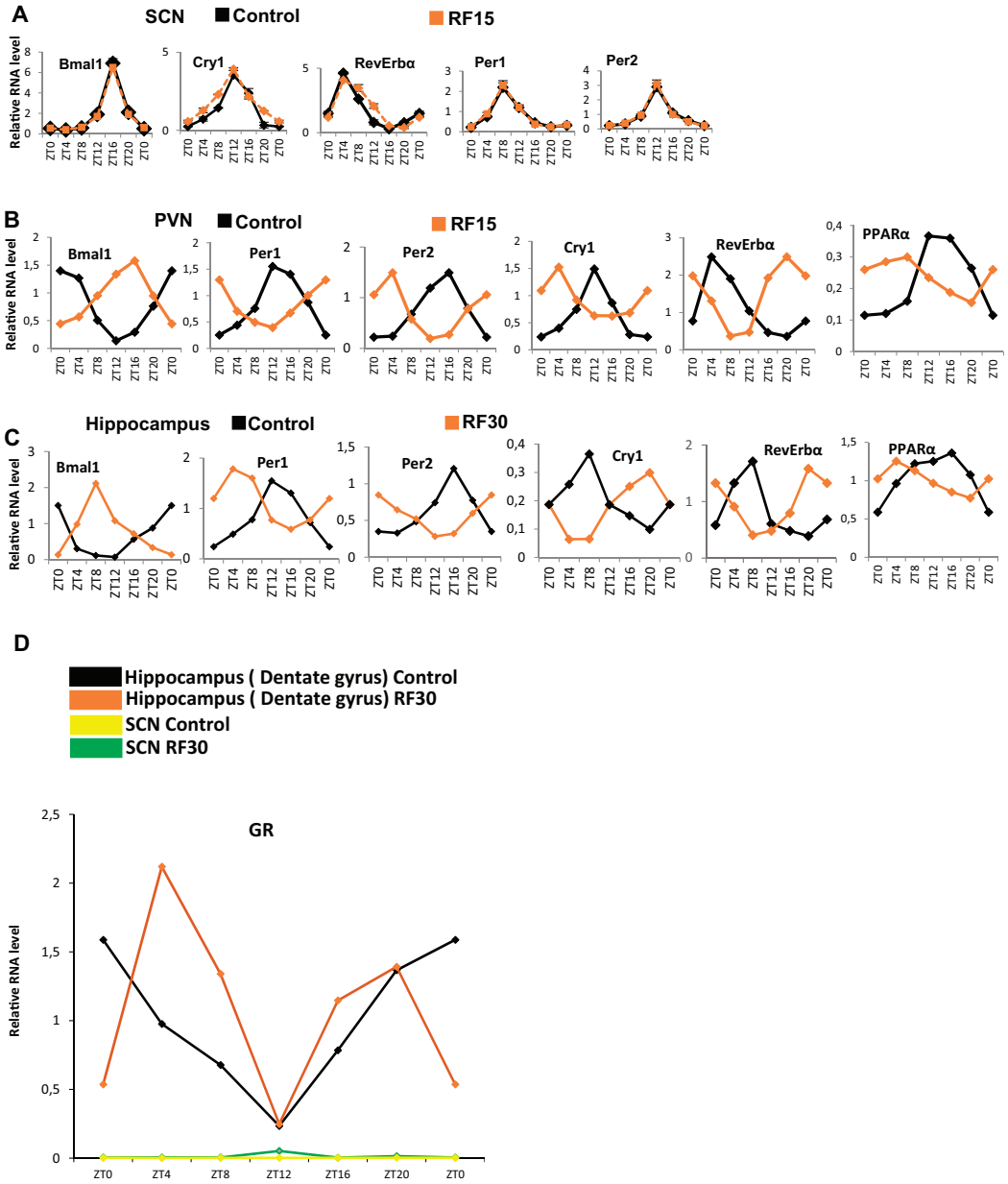

Fig. S2. The central SCN CC is unaffected by the RF. (*A*) RNA transcript levels of CC components in the SCN of control and RF15 mice. (*B*) RNA transcript levels of CC components in the PVN of control and RF15 mice. (*C*) RNA transcript levels of CC components genes in the hippocampus (dentate gyrus) of control and RF30 mice. (*D*) RNA transcript level of GR in the hippocampus (dentate gyrus) and SCN of control and RF30 mice. All values are mean ± SEM.

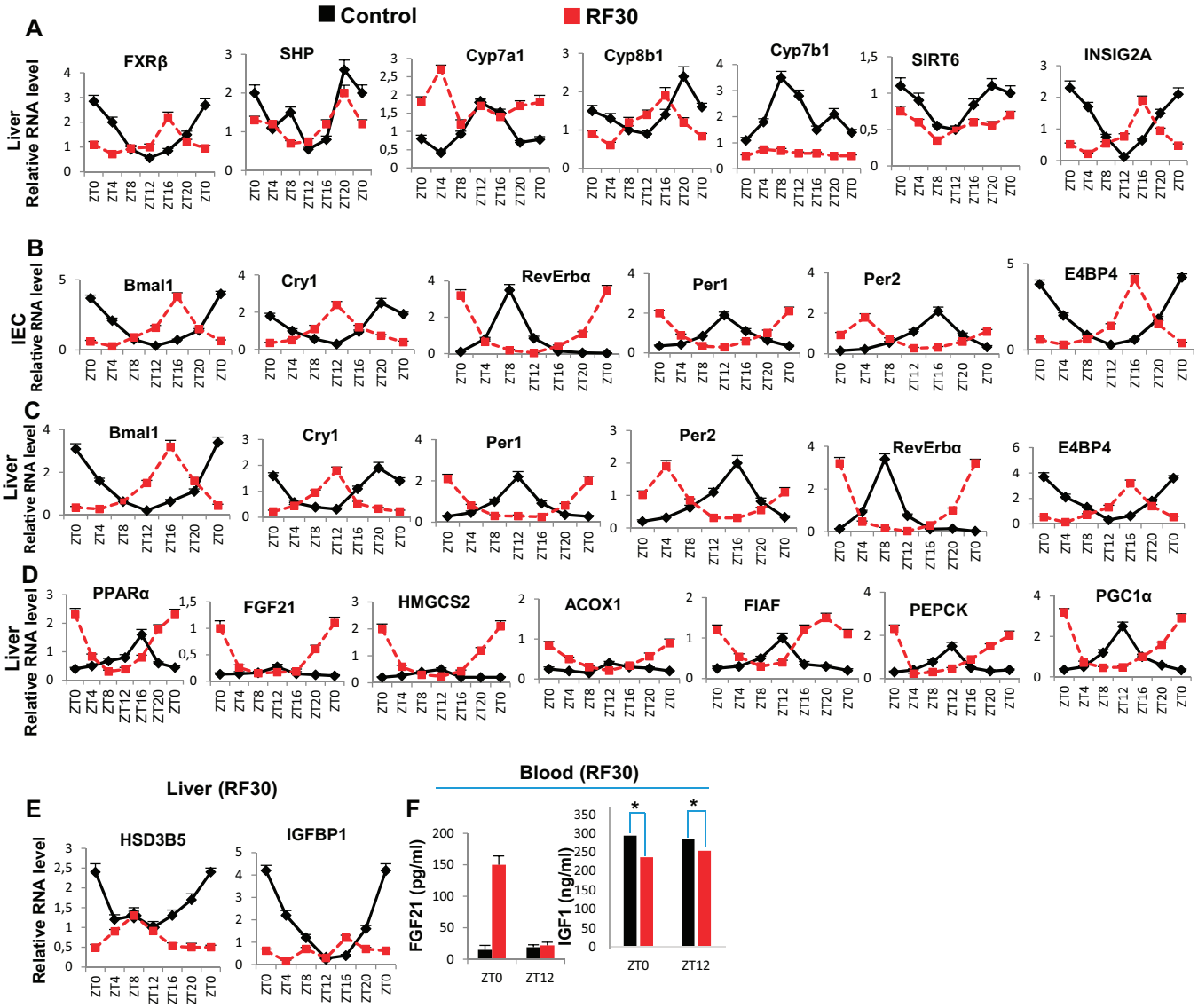

Fig. S3. Metabolic features of RF30 mice. (*A*) RNA transcript levels of genes, as indicated, in liver of control and RF30 mice. (*B*) RNA transcript levels of CC components in IECs of control and RF30 mice. (*C*) RNA transcript levels of CC components liver of control and RF30 mice. (*D*) RNA transcript levels of genes, as indicated, in liver of control and RF30 mice. (*E*) RNA transcript levels of HSD3B5 and IGFBP1 in liver of control and RF30 mice. (*F*) FGF21 and IGF1 levels in blood of control and RF30 mice. All values are mean ± SEM. $*P < 0.05$.

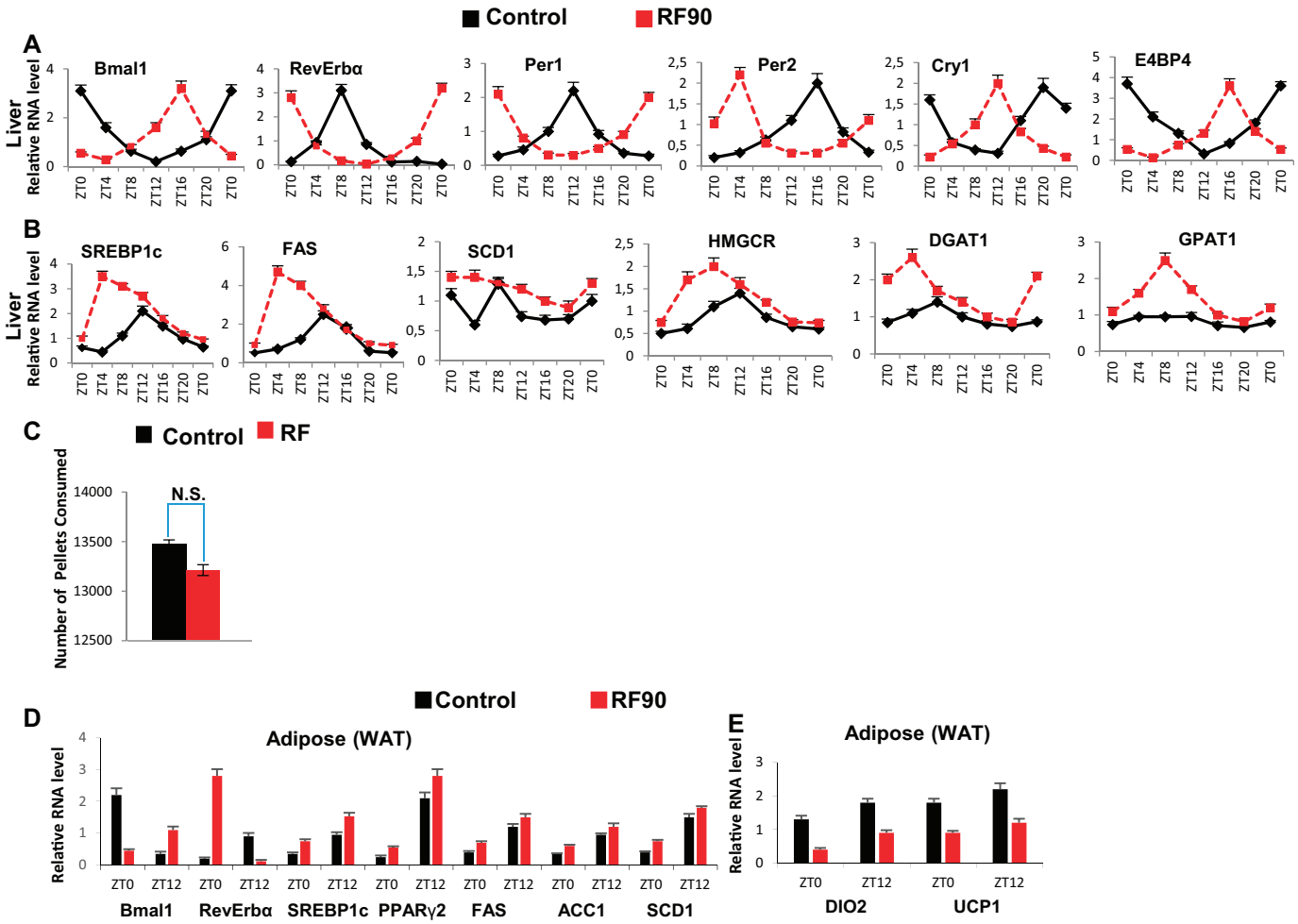

Fig. S4. Progressive deterioration of metabolism on prolonged RF. (*A*) RNA transcript levels of CC components in liver of control and RF90 mice. (*B*) RNA transcript levels of genes, as indicated, in liver of control and RF90 mice. (*C*) The total number of pellets consumed by control and RF90 mice. (*D* and *E*) RNA transcript levels of genes, as indicated, in WAT of control and RF90 mice. All values are mean ± SEM.

Table S1. Circadian expression of mouse liver genes containing RORE DBS after RF15

Genes	Function	Circadian expression	
		Ad libitum feeding (ZT20–4 > ZT12–16)	RF15 (ZT12–16 > ZT20–4)
ATF5	Transactivator	+	+
BAX	Apoptosis	+	+
c-Jun	Transactivator	+	+
CDC25c	Cell cycle regulator	+	+
CDKN1A	Cell cycle regulator	+	+
CDK8	Transcriptional coactivator	+	+
CHEK1	Regulator of DNA damage signaling	+	+
CREB1	Transactivator	=	=
CSNK2A1	Casein kinase2, α1 subunit	=	=
CSNK1D	Casein kinase1, δ subunit	=	=
CUL5	Ubiquitin ligase	=	=
CYFIP1	FMR1 interacting protein	+	+
CYP8B1	Bile acid synthesis	+	+
DAG1	Structural maintenance	+	+
DR5	Apoptosis	+	+
DLAT	Member of pyruvate dehydrogenase complex	=	=
ELOVL3	Fatty acid synthesis	+	+
FGF18	Osteocyte differentiation	=	=
GCK	Glucose metabolism	+	+
GCKR	Glucose metabolism	+	+
HSD3B5	Cholesterol metabolism	+	+
HIC53	Phosphatidic acid phosphatase	=	=
IGFBP4	IGF1 signaling	+	+
INSIG2A	Regulator of lipogenesis	+	+
IRF1	Transactivator	+	+
KLF15	Transactivator	+	+
LIPC	Lipoprotein metabolism	+	+
LRIG1	Regulator of ERBB signaling	=	=
MGA	Transactivator	=	=
NOD2	Receptor for inflammosome activation	+	+
PDK4	Glucose metabolism	+	+
PEX3	Peroxisomal biogenesis	+	+
PEX16	Peroxisomal biogenesis	+	+
POFUT1	Fucosyl transferase	+	+
RAF1	Regulator of MAPK signaling	=	=
RAB25	Endocytosis	=	=
ROCK2	Rho-associated kinase	=	=
U1	Spliceosome assembly	=	=
UBE2QL1	Ubiquitin conjugating enzyme	=	=
WDR5B	WD-40 repeat protein, subunit 5B	=	=

+, genes with circadian variation in the transcript levels; =, represent genes with no circadian variation in the transcript levels.

Table S2. Circadian expression of mouse IEC genes containing RORE DBS after RF15

Genes	Function	Circadian expression	
		Ad libitum feeding (ZT20–4 > ZT12–16)	RF15 (ZT12–16 > ZT20–4)
ATF5	Transactivator	=	=
BAX	Apoptosis	+	+
c-Jun	Transactivator	+	+
CDC25c	Cell cycle regulator	+	+
CDKN1A	Cell cycle regulator	+	+
CDK8	Transcriptional coactivator	+	+
CHEK1	Regulator of DNA damage signaling	+	+
CREB1	Transactivator	=	=
CSNK2A1	Casein kinase 2, α1 subunit	=	=
CSNK1D	Casein kinase 1, δ subunit	=	=
CUL5	Ubiquitin ligase	=	=
CYFIP1	FMR1 interacting protein	+	+
CYP8B1	Bile acid synthesis	+	+
DAG1	Structural maintenance	=	=
DR5	Apoptosis	+	+
DLAT	Member of pyruvate dehydrogenase complex	=	=
ELOVL3	Fatty acid synthesis	+	+
FGF18	Osteocyte differentiation	=	=
GCK	Glucose metabolism	+	+
GCKR	Glucose metabolism	+	+
HSD3B5	Cholesterol metabolism	+	+
HIC53	Phosphatidic acid phosphatase	=	=
IGFBP4	IGF1 signaling	=	=
INSIG2A	Regulator of lipogenesis	+	+
IRF1	Transactivator	+	+
KLF15	Transactivator	+	+
LIPC	Lipoprotein metabolism	+	+
LRIG1	Regulator of ERBB signaling	+	+
MGA	Transactivator	=	=
NOD2	Receptor for inflammosome activation	+	+
PDK4	Glucose metabolism	+	+
PEX3	Peroxisomal biogenesis	+	+
PEX16	Peroxisomal biogenesis	+	+
POFUT1	Fucosyl transferase	=	+
RAF1	Regulator of MAPK signaling	=	=
RAB25	Endocytosis	=	=
ROCK2	Rho-associated kinase	=	=
U1	Spliceosome assembly	=	=
UBE2QL1	Ubiquitin conjugating enzyme	=	=
WDR5B	WD-40 repeat protein, subunit 5B	=	=

+, genes with circadian variation in the transcript levels; =, represent genes with no circadian variation in the transcript levels.

Table S3. Circadian expression of mouse liver genes containing D-Box DBS after RF15

Genes	Function	Circadian expression	
		Ad libitum feeding (ZT20–4 > ZT12–16)	RF15 (ZT12–16 > ZT20–4)
AIF	Apoptosis	+	+
ATG14	Autophagy	+	+
CHERP	Calcium homeostasis	=	=
CGGBP1	CGG-binding protein	=	=
CLPTM1	Development of palate	=	=
DUSP12	Negative regulator of MAPK signaling	+	+
DUSP22	Negative regulator of MAPK signaling	+	+
ELP4	Regulator of transcriptional elongation	+	+
ELVOL7	Fatty acid synthesis	+	+
ERCC3	DNA-repair	+	+
FASL	Apoptosis	+	+
GCH1	GTP-hydrolysis	+	+
GSK3β	Signal transduction	=	=
HSF2	Transactivator	=	=
KDM3A	Lysine demethylase	=	=
LARP7	La ribonucleoprotein 7	+	+
MRPL1	Ribosome biogenesis	=	=
MRPL3	Ribosome biogenesis	=	=
MRC1	Mannose receptor, C-type	=	=
MTND3	Mitochondrial NAD dehydrogenase	+	+
MUT	Methylmalonyl CoA mutase	+	+
NDUFB9	NADH dehydrogenase subunit	+	+
NOL7	Nucleolar organizer	=	=
OSBP	Oxysterol binding	+	+
PAIP1	Regulator of transcription termination	+	+
PDK1	Glucose metabolism	+	+
PER3	Regulator of circadian clock	+	+
PHF17	Transcriptional regulation	+	+
PTEN	Negative regulator of PI3K signaling	=	=
RAP1GDS1	Rap1 GTP-GDP exchange stimulator	+	=
RPS27A	Ribosomal protein	+	+
SMAD5	Transactivator	=	=
SPT16	Suppressor of Ty16	+	+
SUMO2	Posttranslational modification	=	=
TEF	Transactivator	+	+
TGM1	Glutamine metabolism	=	=
TGFBR1	TGFβ receptor	=	=
TSG101	Tumor suppressor	+	+
VDBP	Vitamin (D3) metabolism	=	=
WEE1	Cell cycle regulator	+	+

+, genes with circadian variation in the transcript levels; =, represent genes with no circadian variation in the transcript levels.

Table S4. Circadian expression of mouse IEC genes containing D-Box DBS after RF15

Genes	Function	Circadian expression	
		Ad libitum feeding (ZT20–4 > ZT12–16)	RF15 (ZT12–16 > ZT20–4)
AIF	Apoptosis	+	+
ATG14	Autophagy	+	+
CHERP	Calcium homeostasis	=	=
CGGBP1	CGG-binding protein	+	+
CLPTM1	Development of palate	=	=
DUSP12	Negative regulator of MAPK signaling	+	+
DUSP22	Negative regulator of MAPK signaling	+	+
ELP4	Regulator of transcriptional elongation	=	=
ELVOL7	Fatty acid synthesis	=	=
ERCC3	DNA-repair	=	=
FASL	Apoptosis	+	+
GCH1	GTP-hydrolysis	=	=
GSK3β	Signal transduction	=	=
HSF2	Transactivator	+	=
KDM3A	Lysine demethylase	=	=
LARP7	La ribonucleoprotein 7	=	=
MRPL1	Ribosome biogenesis	=	=
MRPL3	Ribosome biogenesis	=	=
MRC1	Mannose receptor, C-type	=	=
MTND3	Mitochondrial NAD dehydrogenase	+	+
MUT	Methylmalonyl CoA mutase	+	+
NDUFB9	NADH dehydrogenase subunit	+	+
NOL7	Nucleolar organizer	=	=
OSBP	Oxysterol binding	+	+
PAIP1	Regulator of transcription termination	+	+
PDK1	Glucose metabolism	+	+
PER3	Regulator of circadian clock	+	+
PHF17	Transcriptional regulation	+	+
PTEN	Negative regulator of PI3K signaling	+	+
RAP1GDS1	Rap1 GTP-GDP exchange stimulator	+	+
RPS27A	Ribosomal protein	+	+
SMAD5	Transactivator	=	=
SPT16	Suppressor of Ty16	=	=
SUMO2	Posttranslational modification	=	=
TEF	Transactivator	+	+
TGM1	Glutamine metabolism	=	=
TGFBR1	TGFβ receptor	=	=
TSG101	Tumor suppressor	=	=
VDBP	Vitamin (D3) metabolism	=	=
WEE1	Cell cycle regulator	+	+

+, genes with circadian variation in the transcript levels; =, represent genes with no circadian variation in the transcript levels.

Other Supporting Information Files

Dataset S1 (XLS)

Cell

Homeostasis in Intestinal Epithelium Is Orchestrated by the Circadian Clock and Microbiota Cues Transduced by TLRs

Atish Mukherji,[1] Ahmad Kobiita,[1] Tao Ye,[1] and Pierre Chambon[1,*]
[1]Institut de Génétique et de Biologie Moléculaire et Cellulaire, CNRS UMR7104, Inserm U964, Institut d'Etudes Avancées de l'Université de Strasbourg, Collège de France, Illkirch 67404, France
*Correspondence: chambon@igbmc.fr
http://dx.doi.org/10.1016/j.cell.2013.04.020

SUMMARY

Alterations of symbiosis between microbiota and intestinal epithelial cells (IEC) are associated with intestinal and systemic pathologies. Interactions between bacterial products (MAMPs) and Toll-like receptors (TLRs) are known to be mandatory for IEC homeostasis, but how TLRs may time homeostatic functions with circadian changes is unknown. Our functional and molecular dissections of the IEC circadian clock demonstrate that its integrity is required for microbiota-IEC dialog. In IEC, the antiphasic expression of the RORα activator and RevErbα repressor clock output regulators generates a circadian rhythmic TLR expression that converts the temporally arrhythmic microbiota signaling into circadian rhythmic JNK and IKKβ activities, which prevents RevErbα activation by PPARα that would disrupt the circadian clock. Moreover, through activation of AP1 and NF-κB, these activities, together with RORα and RevErbα, enable timing homeostatic functions of numerous genes with IEC circadian events. Interestingly, microbiota signaling deficiencies induce a prediabetic syndrome due to ileal corticosterone overproduction consequent to clock disruption.

INTRODUCTION

A single layer of intestinal epithelial cells (IECs) provides the physical barrier that separates, from the underlying lamina propria and the rest of the body, $\sim 10^{14}$ microorganisms (mostly commensal bacteria) living in the intestinal lumen and termed gut microbiota. Studies on germ-free (GF) and antibiotic-induced microbiota-depleted (AIMD) mice have revealed that gut colonization by the microbiota is beneficial in many respects for mammalian host homeostasis (Hooper et al., 2001; Rakoff-Nahoum et al., 2004; Ivanov et al., 2009; Reikvam et al., 2011; Larsson et al., 2012). Rakoff-Nahoum et al. (2004) unveiled that commensal bacteria are recognized by IEC Toll-like receptors (TLRs), thus providing a new perspective on host-commensal symbiosis and raising the question of how the interaction of commensal bacterial products (microbiota-associated molecular patterns [MAMPS], e.g., LPS) with TLR members of the pattern recognition receptors (PRRs) could control at the molecular level many homeostatic processes in IECs (Abreu, 2010). Several intestinal functions (e.g., nutrient absorption, cell proliferation, motility, metabolic activities) are known to be rhythmically regulated in a circadian manner (Hussain and Pan, 2009), and it has been shown that core components of the circadian clock could be functional in mouse small intestine in which the expression of some TLR genes may also vary around the circadian day (Froy and Chapnik, 2007). To explore the possibility that such a clock (reviewed in Dibner et al., 2010; Asher and Schibler, 2011; Feng and Lazar, 2012; see below Figure 2 and Figure S2 available online) could be instrumental in the mechanism through which the microbiota may control homeostasis in IEC, we investigated in the mouse the effect of antibiotic-induced microbiota depletion on the clock. Interestingly, our study not only revealed the functional organization of this clock, but also demonstrated that it is critically involved in the molecular mechanism underlying the control of IEC homeostasis through TLR-mediated microbiota signaling.

RESULTS

Lack of Microbiota Affects Nuclear Receptors and Circadian Clock Components in IEC as well as Systemic Metabolism

Because many nuclear receptors (NRs) exhibit a circadian oscillatory expression in various tissues (Yang et al., 2006) and some of them are clock components (Asher and Schibler, 2011), we examined the transcript profiles of the 42 NRs expressed in ileum and colon of control and AIMD mice (AIMDM) (Figures 1A and 1B; data not shown). Upon antibiotic treatment, transcripts of RevErbα, PPARα, and CAR increased, and those of RORα, ERβ, and PPARβ decreased, whereas only CAR varied in liver (data not shown). As RORα (Sato et al., 2004) and RevErbα (Feng and Lazar, 2012; Cho et al., 2012) belong to the clock machinery, we examined the expression of clock components (see Figures 2 and S2) in AIMD IEC. The classical clock core was disrupted: Bmal1 and Cry1 transcripts decreased, whereas

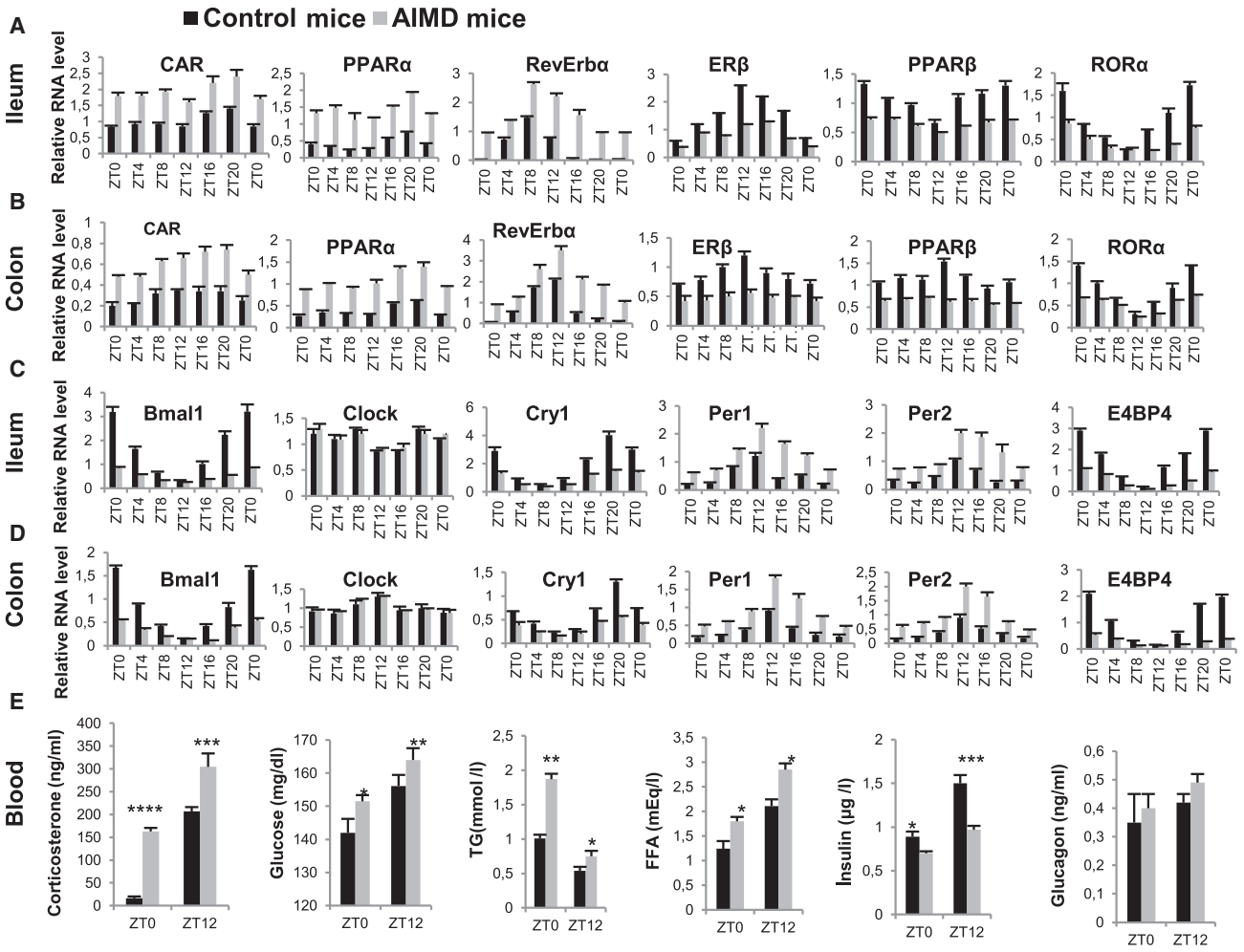

Figure 1. Effects of Lack of Microbiota on IEC Nuclear Receptors, Circadian Clock, and Systemic Metabolism

(A) RNA transcripts (Q-RT-PCR) of nuclear receptors (NRs) in ileal IEC of control and antibiotic-induced microbiota-depleted (AIMD) mice. ERβ is $\times 10^4$.

(B) As in (A), colonic IEC.

(C) As in (A), RNA transcripts of clock components in ileal IEC.

(D) As in (C), colonic IEC.

(E) Levels of blood components in ad lib fed control and AIMD mice at ZT0 and ZT12.

Values are mean ± SEM. *p < 0.05,**p < 0.01 and ***p < 0.001. See also Figures S1 and S3 and Tables S2, S5, and S6.

Per1 and Per2 transcripts increased, and those of Clock were unaffected (Figures 1C and 1D). Because germ-free (GF) mice exhibit increased triglycerides (TG) and hypoinsulinemia (Bäckhed et al., 2007; Figure S3M), we analyzed blood metabolic parameters in AIMDM at circadian cycle times ZT0 (6 a.m.) and ZT12 (6 p.m.). Significant increases in glucose, TG, free fatty acids (FFA), and corticosterone, and a decrease in insulin were found (Figure 1E). Reduction in *insulin* transcripts in AIMDM correlated with decreased insulin secretion in the glucose tolerance test (GTT) (Figures S1A–S1E). The AIMD increase in blood glucose was in keeping with those of liver PEPCK and G6Pase transcripts (Figure S1F). Moreover, expression of Hes1, a negative regulator of hepatic TG production (Lemke et al., 2008), decreased in AIMD liver (Figure S1F), in agreement with an increase in blood TG. Expression of Angptl4 (FIAF), necessary for conversion of TG to FFA, was also increased in AIMD ileum (Figure S1G), thus contributing to elevated blood FFA levels (Mandard et al., 2006) (see Figures 2 and S2).

Collectively, these results indicated an involvement of gut microbiota in controlling IEC expression of NRs and clock components, as well as systemic metabolism homeostasis. Importantly, all above AIMD variations were also found in GF mice (compare Figure 1 with Figures S1 and S3).

Lack of Microbiota Results in Corticosterone Overproduction in Ileal IEC, which Affects Clock Components and Systemic Metabolism

The ZT0 and ZT12 corticosterone increases in AIMDM led us to analyze blood adrenocorticotropic hormone (ACTH) levels. Undetectable at ZT0, ACTH was lower at ZT12 in AIMD and

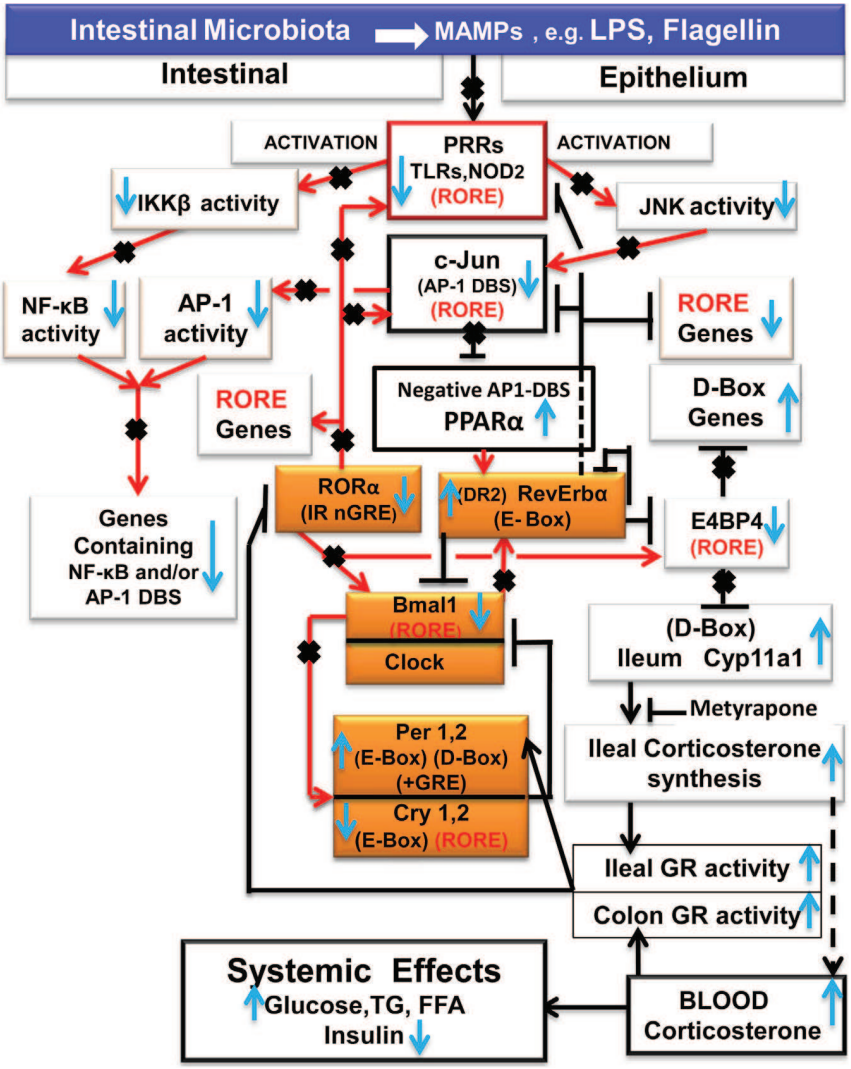

Figure 2. Orchestration of Homeostasis in Intestinal Epithelium by Clock-Controlled Circadian Expression of PRRs that Transduce MAMP Signals

The mammalian circadian clock (orange boxes) consists of two interlocked feedback loops. The first loop involves Bmal1 and Clock binding to the E-box elements present in *Per1*, *Per2*, and *Cry1*, *Cry2* genes, and the autorepression of Per and Cry genes by their own protein products. The second loop involves the RORα activator competing with the RevErbα repressor for binding to RORE DBS present in *Bmal1*. Remarkably, Bmal1 binding to the E box present in *RevErbα* activates its transcription, whereas the presence of a DR2 element in *RevErbα* mediates its transcriptional autorepression and its transcriptional activation by PPARα. Red arrows represent "activation" events; blunt black lines indicate "repression" events. The upward and downward blue arrows correspond to increase and decrease of the indicated components in AIMD mice. Black crosses (X) indicate impairment of activation or repression signaling events in AIMD mice. MAMPs, microbiota-associated molecular patterns; PRRs, pattern recognition receptors; TLRs, Toll-like receptors; NOD2, nucleotide oligomerization domain 2. See text and Figure S2 for additional descriptions and abbreviations.

GF mice than in controls (Figures 3A and S4A). Remarkably, adrenalectomy (Adx) of AIMDM had no effect on blood corticosterone at ZT0, whereas it was identical at ZT12 in Adx AIMD and control mice, indicating that there was no adrenal corticosterone synthesis at ZT0, whereas at ZT12 its extra-adrenal production was similar to that normally produced in control mice (Figure 3B). It has been reported that corticosterone synthesis may occur in ileal, but not in colonic IEC (Cima et al., 2004). Accordingly, Cyp11a1 transcripts and protein (the rate limiting enzyme in corticosterone synthesis) were present in control ileal IEC, and increased in ileal IEC of AIMD (Figures 3E and 3F) and GF mice (Figure S4D), whereas there was no increase in adrenals of AIMD and GF mice (Figures S4B, S4C, and S4E).

Interestingly, on its own, Adx did not generate the AIMD defects found in IEC clock components and in blood metabolic parameters (Figures 3C, 3D, S4F, and S4G), indicating that ileal corticosterone overproduction could be involved in the AIMD syndrome. That AIMD hypercorticosterolism was instrumental in generating the systemic metabolic and clock defects, was shown by treating AIMD mice with metyrapone (a Cyp11a1 competitive inhibitor) (Mueller et al., 2006; see Figure S4H) and by using the conditional GR mutants, *GRiec*$^{-/-}$ and *GRhep*$^{-/-}$, bearing a selective GR null mutation in IEC and liver, respectively. Metyrapone reversed the AIMD systemic alterations in blood (TG, FFA, insulin, and glucose), and in liver (Figures 3J, 3K, and S4K–S4O), as well as AIMD IEC clock defects (Figures 3G, 3H, S4I, and S4J). A treatment with the glucocorticoid (GC) antagonist RU486 similarly reversed systemic alterations (Figures S5B and S5C) and IEC clock defects in AIMD mice (Figure S5A). In this respect, note that there is an IR nGRE element in the *RORα* gene (see Figure S5D) and (+)GRE elements in *Per1* and *Per2* genes (So et al., 2009; Surjit et al., 2011). As expected, AIMDM *GRiec*$^{-/-}$ mutants did not exhibit alterations in RORα, Per1, and Per2 (Figures 3L, 3M, and S5E–S5H), nor the AIMD systemic increases in TG and FFA (Figures 3N, 3O, and S5I), whereas AIMDM *GRhep*$^{-/-}$ mutants lacked the systemic AIMD increase in glucose and TG (Figures 3P–3R).

RORα and RevErbα Play Key Roles in IEC Clock Function and Control of Corticosterone Synthesis in Ileal IEC

Ileal and colonic IEC RORα reached zenith expression and was maximally bound to *Bmal1* RORE at ZT0 (Figures 1A, 1B, 3T, and S7A), whereas Bmal1 expression drastically decreased at ZT0 in *RORαiec*$^{-/-}$ mutant mice (Figure 3U, and data not shown for colon). In contrast, a similar Bmal1 mutation (*Bmal1iec*$^{-/-}$)

had no effect on expression of RORα and Cry1 (even though the latter contains an E box) (Feng and Lazar, 2012), although, as expected, it decreased that of Per1 and Per2 (Figures 3V, 3W, and S6H). Due to competition with the RevErbα repressor (see below), RORα binding to *Bmal1* RORE decreased (Figures 1A and 3T) from ZT0 to ZT12. At this time (ZT12) corticosterone, which was the lowest at ZT0 was high both in blood (Figure 3B) and in ileal IEC (see below), and RORα expression was directly repressed through GR binding to its IR nGRE (Figures 3S and S5D, control panel), whereas Bmal1 expression was the lowest (compare RORα and Bmal1 in Figures 1A and 1B, with Figures 1C and 1D). Expressions of Cry1 and of the clock output regulator E4BP4 repressor (Asher and Schibler, 2011) were also RORα-dependent in IEC (Figures 2, S2, and S7A), as evidenced by their reduced expression at ZT0 in *RORαiec*$^{-/-}$ mice (Figure 3U), and RORα bindings to Cry1 and E4BP4 ROREs (Figures 3T and 4A) which, similarly to RORα binding to Bmal1 RORE, had their zenith and nadir at ZT0 and ZT12, respectively. As expected (Preitner et al., 2002), RevErbα reached its zenith at ZT8 and was triggered in control IEC through binding of Bmal1 to a *RevErbα* E-box element (see Figure 1A and the strong decrease in RevErbα expression in *Bmal1iec*$^{-/-}$ mice; Figures 3V and 3W). RevErbα expression was decreased after ZT8 due both to (1) an autorepression mediated through its binding to a DR2 element present in its promoter region (Duez and Staels, 2008), and (2) the antiphasic circadian binding of RORα and RevErbα (associated with the NCoR corepressor, not shown) (Feng and Lazar, 2012) on the Bmal1 RORE (Sato et al., 2004; Figure 3T).

Examination of the *Cyp11a1* promoter revealed a D-box-like DNA binding sequence (DBS) (Cowell, 2002) (5′GTTACGTGAC) for the E4BP4 repressor. In control ileal and colonic IEC, chromatin immunoprecipitation (ChIP) analysis showed antiphasic circadian binding of RORα and RevErbα (associated with NCoR) to the *E4BP4* RORE (Figure 4A, and data not shown). E4BP4 binding to the *Cyp11a1* D box exhibited a circadian profile in control ileal IEC (Figure 4C) in which the minimal and maximal E4BP4 recruitments, at the beginning (ZT12) and the end (ZT0) of the dark period (Figure 4C), coincided with maximal and minimal expression of Cyp11a1 transcripts, respectively (Figure 4E), and therefore to the highest and lowest ileal corticosterone synthesis. That in control mice, binding of RORα at ZT0 to the *E4BP4* RORE led to repression of Cyp11a1 and corticosterone synthesis, was demonstrated in IEC *RORαiec*$^{-/-}$ mutants in which Cyp11a1 transcripts were increased (Figure 3U). Importantly, and in keeping with the lack of corticosterone production, no binding of E4BP4 to the *Cyp11a1* D box was observed in colonic IEC (data not shown).

Circadian Corticosterone Synthesis in Ileal IEC and Adrenals Is Cophasic but Independently Regulated in Control and AIMD Mice

Mouse HPA axis-controlled corticosterolemia exhibited a nadir and a zenith around ZT0 and ZT10–ZT14, respectively (Figure 1E; Le Minh et al., 2001), similar to those of ileal IEC-produced corticosterone (Figure 3B). Accordingly, in control mouse liver, ileum, and colon, (+)GRE-containing gene expression was highest at ZT12 and lowest at ZT0, whereas IR nGRE-containing gene (Hes1) expression was highest at ZT0 and lowest at ZT12 (Figures 4P–4R and S6A–S6C), demonstrating that ileal IEC and adrenal corticosterone circadian synthesis were cophasic. Circadian profiles of ileal Cyp11a1, MT-I, MT-II, and Angptl4 transcripts in control and Adx mice further demonstrated that ileal corticosterone synthesis was not under HPA axis control (Figure 4S). Note that, in liver and colon that do not synthesize corticosterone or CYP11a1, Adx similarly affected corticosterone-induced gene expression (Figures 4P–4R).

Interestingly, in control and AIMD mice (AIMDM), (+)GRE gene expression exhibited similar circadian profiles in ileum, colon, and liver (Figures S6A–S6C). Similarly, in AIMD mice, repression of the IR nGRE *Hes1* gene was maximal and minimal at ZT12 and ZT0 respectively, in both ileum and liver (Figures S6A and S6B). Thus, ileal IEC and adrenal corticosterone circadian synthesis in AIMDM were also cophasic. Furthermore, in liver, ileum, and colon, Adx in AIMDM did not affect the increased expression of (+)GRE genes at ZT12, whereas it decreased that of Hes1 (Figures 4P–4R), thus indicating that ileal IEC was also the origin of the AIMD corticosterone surge and systemic effects. Finally, upon Adx in control mice, the increase and decrease in expression of the same genes were markedly affected at ZT12 in liver and colon, but not in ileum, indicating that under physiological conditions corticosterone produced in control mice by ileal IEC did not exert significant systemic effects (Figures 4P–4R).

Involvement of PPARα in Corticosterone Synthesis in Ileal IEC of AIMD Mice

In AIMD IEC, both RevErbα expression (Figures 1A and 1B) and its binding (with NCoR) increased on *E4BP4* RORE throughout the circadian cycle, whereas the binding of RORα decreased (compare Figures 4A and 4B). This "constitutive" repression, not only resulted in a marked decrease in E4BP4 transcripts in IEC (Figures 1C and 1D), but also led, in ileal IEC of AIMDM, to a permanent decrease of E4BP4 binding on the *Cyp11a1* D box (compare Figures 4C and 4D), and therefore to a constitutive expression of Cyp11a1 in ileal cells (Figure 4E) and to corticosterone hyperproduction (Figure 1E). Clearly, Bmal1 was not involved in increased expression of RevErbα in AIMDM (Figures 3V and 3W), and analysis of *Bmal1iec*$^{-/-}$ AIMD mice indicated that Bmal1 was not instrumental in alterations characteristic of the microbiota-less syndrome (Figures S6D–S6H). Of note, PPARα, which may also activate RevErbα expression (Duez and Staels, 2008), had no effect on this expression in control mice, as shown in ileal IEC of *PPARαiec*$^{-/-}$ mice (Figure 4G). However, the same mutation abrogated RevErbα overexpression in AIMDM (Figure 4G), thus suggesting that PPARα could be the critical activator of RevErbα expression through binding to the *RevErbα* promoter DR2 element that may mediate RevErbα autorepression (Duez and Staels, 2008). ChIP assays demonstrated that PPARα could bind this DR2 element (Figure 4N), and that this binding was increased throughout the circadian cycle in AIMDM (Figure 4O). Strikingly, all AIMD alterations in clock components (Bmal1, Cry1, Per1, Per2, RORα, RevErbα, E4BP4) disappeared in *PPARαiec*$^{-/-}$ AIMDM (Figures 4F and 4G), whereas corticosterone and metabolic blood parameters were restored to control levels (Figures 4H and 4I and S6I–S6N), thus demonstrating the crucial role of

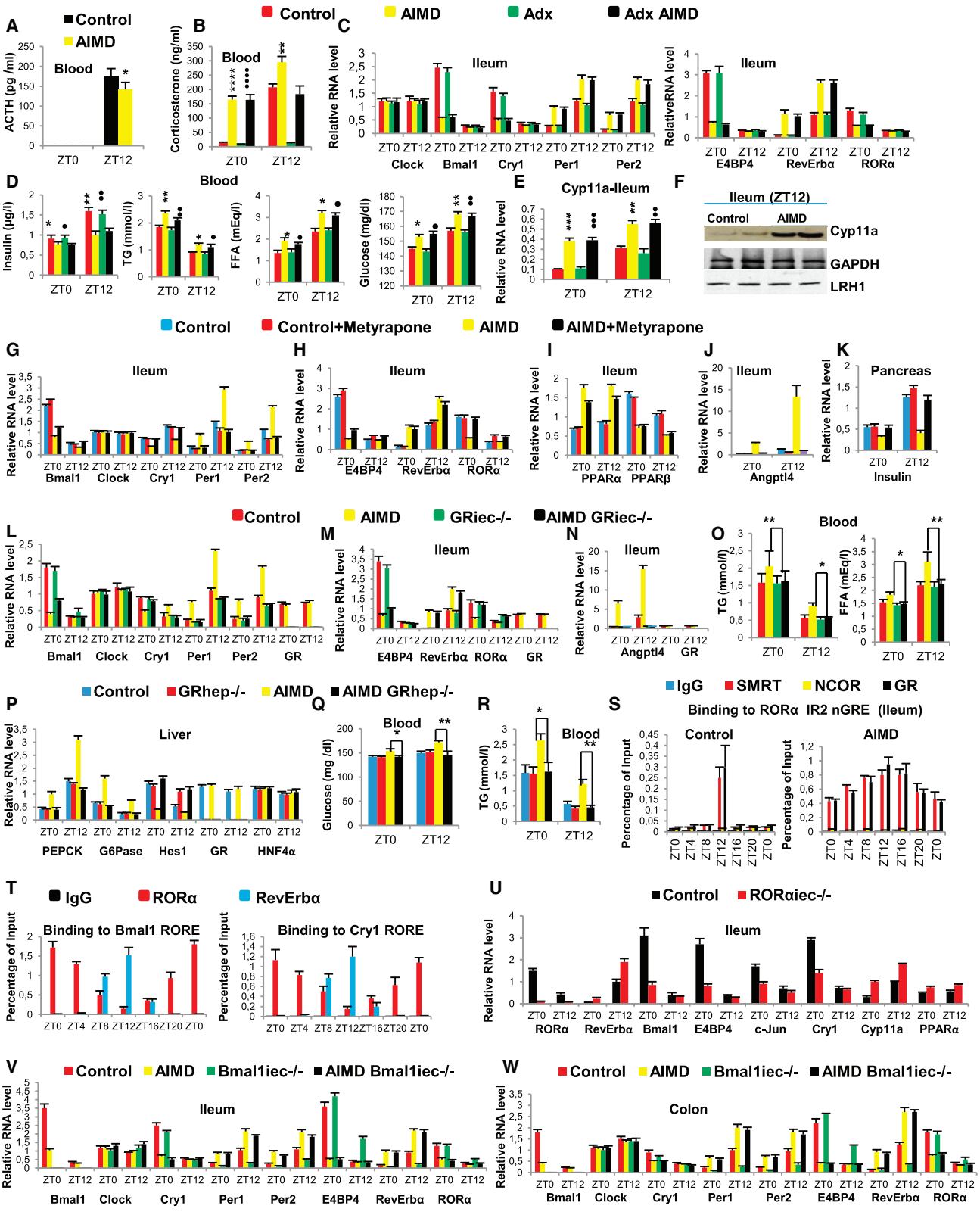

(legend on next page)

PPARα-induced RevErbα overexpression in generating the microbiota-less syndrome.

Normalization of IEC Cyp11a1 (Figures 4H and 4I) and blood corticosterone in *PPARαiec*$^{-/-}$ AIMD mice also confirmed the ileal origin of the corticosterone surge. Altered expression of metabolic genes in different tissues, either GC-induced (PEPCK, G6Pase, and Angptl4) or -repressed (Hes1 and Insulin), was normalized by the same *PPARαiec*$^{-/-}$ mutation (Figures 4J and 4K; data not shown), further pointing to IEC as the source of hypercorticosterolism.

PPARα Expression Is Controlled by JNK/c-Jun Signaling

How then, could PPARα expression be increased in intestinal epithelium of AIMD mice? We assumed that this increase could reflect the lack of a repressing activity that might be triggered in IEC by a microbial product, e.g., LPS that was previously shown to decrease PPARα expression when administered to control mice (Drosatos et al., 2011). As the binding of LPS leads to activation of IKKβ and JNK through their phosphorylation (Takeda and Akira, 2004), we speculated that the PPARα increase in AIMD mice could be related to a decrease in "activated" IKKβ and JNK in IEC. The activity of these two kinases (KA) were indeed decreased in ileal and colonic IEC of AIMDM, whereas it was restored upon LPS administration (Figures 5A and 5B; data not shown for colon) together with c-Jun transcripts (and protein; data not shown) that were also decreased in IEC of AIMD and GF mice (Figures 5C and 5D; see below). Interestingly, a cotreatment with a specific inhibitor of JNK activity (JI) abrogated the LPS-dependent decrease in PPARα transcripts, whereas an inhibitor of IKKβ activity (Bay-11-7085 [Bay]) had no effect on PPARα transcripts, indicating that a member of the AP-1 family could repress PPARα expression (Figure 5E) (in contrast both inhibitors were effective in decreasing LPS-induced IL-6 transcripts, see below). Analysis of the *PPARα* promoter region, revealed the existence of an AP-1 DBS (5′-TGACACA), and ChIP assays with ileal IEC from control mice indicated the presence of c-Jun (but not c-Fos) and NCoR on this AP-1 DBS (Figure 5G). Interestingly, this repressing complex was not present on the *PPARα* promoter region in AIMD mice, whereas it reappeared upon LPS administration (Figure 5G). Thus, gut microbiota appears to be mandatory in IEC to generate a c-Jun-repressing activity (Schreiber et al., 1999) that, by decreasing the expression of PPARα, also decreases that of RevErbα (Figure 5F), thereby preventing the appearance of a microbiota-less syndrome. Of note, LPS could substitute for microbiota in this mechanism. (Figure 5H).

Remarkably, the c-Jun-repressing activity exhibited a circadian profile (Figure 5G), as both the expression of c-Jun transcripts (but not of c-Fos) (Figure 5I), the c-Jun protein level and c-Jun protein phosphorylation by activated JNK (JNK1 and JNK2) (Figure 5J), as well as binding of c-Jun to the *c-Jun* promoter (Figure 5K) that is known to activate c-Jun transcription (Aguilera et al., 2011), were similarly temporally-controlled in IEC. Furthermore, we found a RORE DBS within the *c-Jun* promoter (5′-ACTTCTAGGTCA) that, in IEC, bound RORα and RevErbα in an antiphasic circadian manner (Figure 5L), in accordance with the expression pattern of c-Jun transcripts (compare Figures 5I and 5L).The functionality of this *c-Jun* RORE was demonstrated using IEC *RORαiec*$^{-/-}$ mutant mice (see Figure 3U). Collectively, these results raised the puzzling question of how the activation of JNK1 and JNK2 by phosphorylation (Aguilera et al., 2011) could be temporally-controlled in IEC like that of c-Jun (Figure 5N), whereas their transcripts and protein expression did not exhibit a circadian pattern (Figure 5M).

RORα/RevErbα-Induced Circadian Expression of TLRs and NOD2 Is Required for Microbiota-Induced Activation of JNK and IKKβ

Because in the absence of microbiota, JNK and IKKβ activities were restored by administration of LPS, we investigated in ileal IEC whether the expression pattern of its cognate Toll-like receptor (TLR4), as well as those of other TLRs (Takeda and Akira, 2004), could be affected in AIMD mice. Importantly, TLR1, TLR2, TLR3, TLR4, TLR5, and TLR9 (but not TLR6 and TLR7) transcript levels, which were significantly lower in AIMD mice than in control mice, were restored to control levels upon LPS administration (Figure 6A). Most interestingly, in control mice, TLR expression patterns throughout the circadian cycle revealed

Figure 3. Origin and Effects of Increased Synthesis of Corticosterone in AIMD Mice

(A) Blood ACTH in control and AIMDM at ZT0 and ZT12.
(B) Blood corticosterone in control, AIMD, Adx, and Adx AIMD mice.
(C) RNA transcripts for genes as indicated in ileal IEC of mice treated as in (B).
(D) Blood components in mice fed ad lib and treated as in (B). *Comparison between control and AIMD mice. •Comparison between Adx and Adx AIMD mice. *p < 0.05; •p < 0.05; **p < 0.01; ••p < 0.01. All values represent mean ± SEM.
(E) Cyp11a transcripts in ileal IEC of mice treated as in (B). *Comparison between control and AIMD mice. •Comparison between Adx and Adx AIMD mice. *p < 0.05; •p < 0.05; **p < 0.01; ••p < 0.01. All values represent mean ± SEM.
(F) Cyp11a and LRH1 immunoblot using ileal IEC of control and AIMD mice.
(G–J) RNA transcripts for genes as indicated in ileal IEC of control and AIMD mice treated with metyrapone.
(K) Insulin RNA transcripts in pancreas of mice treated as in (G).
(L–N) RNA transcripts in ileal IEC for genes as indicated in control and AIMD *GRiec*$^{-/-}$ mice.
(O) TG and FFA levels in blood of mice as in (L).
(P) RNA transcripts in liver for genes as indicated in control and AIMD *GRhep*$^{-/-}$ mice.
(Q and R) Blood glucose and TG level in mice fed ad lib as in (L).
(S) Recruitment (ChIP-Q-PCR assays) to the RORα IR2 nGRE region, using IEC of control and AIMD mice, and IgG, GR, SMRT, and NCoR antibodies.
(T) Recruitment (ChIP-Q-PCR assays) to the Bmal1 and Cry1 RORE regions, using IEC of control mice and IgG, RORα, and RevErbα antibodies.
(U) RNA transcripts of genes as indicated in IEC of control and *RORαiec*$^{-/-}$ mice. Cyp11a is ×5.
(V and W) RNA transcripts of genes as indicated in ileal (V) and colonic (W) epithelium of control and AIMD *Bmal1iec*$^{-/-}$ mice.
See also Figures S4 and S5 and Tables S2 and S5.

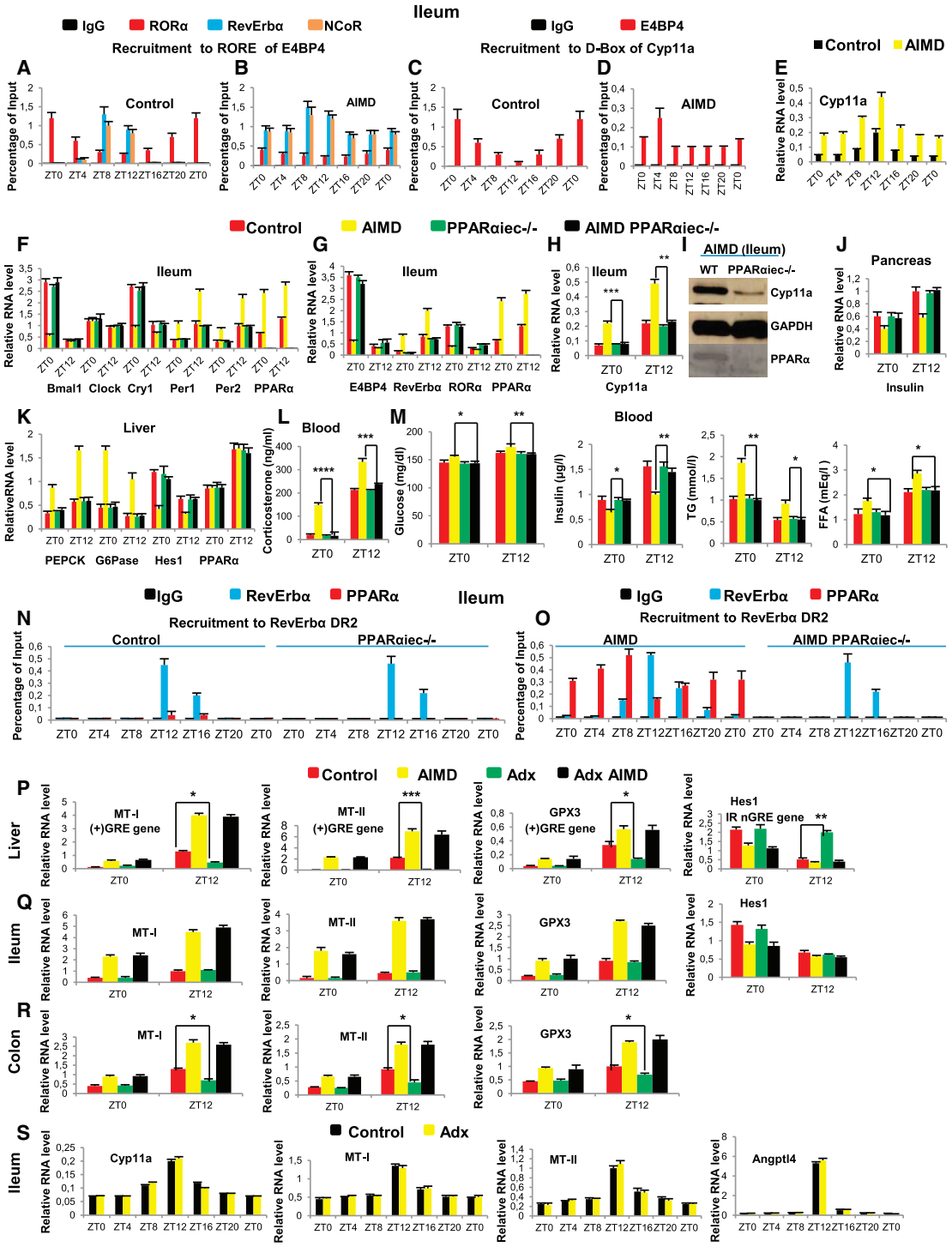

Figure 4. Critical Role of PPARα and RevErbα in Controlling Corticosterone Homeostasis in IEC

(A) Circadian ChIP-Q-PCR assays for recruitment to the E4BP4 RORE, using ileal IEC from control mice and RORα, RevErbα, and NCoR antibodies.

(B) As in (A), but from AIMD mice.

(C) ChIP-Q-PCR assays for recruitment to the D box of the Cyp11a promoter, using IEC of control mice and E4BP4 antibody.

(D) As in (C), but from AIMD mice.

(E) Cyp11a transcripts in IEC of control and AIMD mice.

(F–H) RNA transcript for genes as indicated in ileal IEC of control and AIMD *PPARαiec*$^{-/-}$ mice.

(legend continued on next page)

that TLR1–TLR5 and TLR9 (but not TLR6 and TLR7) transcripts exhibited a circadian-like profile with levels generally higher at ZT0 than at ZT12 (Figures 6B and S7B; similar data were obtained in GF mice, Figure S7C), in keeping with both the presence or absence (in TLR6 and TLR7) of an evolutionary-conserved RORE in their promoter region (Figure S7A) to which the bindings of the RORα activator and the RevErbα repressor exhibited antiphasic circadian profiles (ChIP assays in Figure 6C). These circadian recruitments were notably similar to those of RORα and RevErbα to the E4BP4 RORE (Figure 4A), the *c-Jun* RORE (Figure 5L), and the ROREs present in *Bmal1* and *Cry1* (Figure 3T). That RORα (Figure 6D), but not Bmal1 (Figure S7D), activated TLR transcription was demonstrated using *RORαiec*$^{-/-}$ mice, which resulted in decreased transcripts of TLRs at ZT0, similar to those of Bmal1, c-Jun, E4BP4, and Cry1 (Figure 3U). Note that, for all of these genes, as well as for TLRs, these reduced transcript levels in *RORαiec*$^{-/-}$ mice correlated with a drastically impaired RORα recruitment to ROREs present in their respective promoters (ChIP assays in Figures 6G and 6H), and with a RevErbα recruitment throughout the circadian cycle similar to that observed on the *E4BP4* RORE in AIMD mice (Figure 4B; data not shown). TLR transcripts were lower in AIMD than in control mice and their circadian expression profile was lost (Figures 6A and 6B), which resulted in loss of IKKβ and JNK activation (Figures 5A and 5B), followed by derepression of PPARα expression (Figures 1A, 1B, 5E, and 5F), and consequently to PPARα-induced DR2-mediated activation of RevErbα expression (Figures 4G and 4O). Collectively, these data (similar data were obtained in colonic IEC, not shown) demonstrated that TLRs (TLR1–TLR5 and TLR9) exhibited a circadian expression profile controlled by the opposing action of RORα and RevErbα, and revealed why, upon activation of TLRs by LPS and other MAMPs, activated JNKs and activated IKKβ could exhibit a circadian pattern of activity, even though the expression of unphosphorylated JNKs and IKKβ proteins did not display a circadian profile.

Interestingly, the *IRAK4* and *TIRAP* genes, whose proteins are known to transduce MAMP-induced TLR signaling and to activate JNK and IKKβ, contain a RORE (Figure S7A) and exhibited a decreased circadian expression in both AIMD and *RORαiec*$^{-/-}$ mice, whereas the expression of the RORE-less *TRAF6* and *MyD88* gene involved in TLR signaling (Takeda and Akira, 2004) was neither oscillatory nor decreased in AIMDM (Figures 6I and 6J). Of note, an IEC selective mutation of the TLR adaptor MyD88 that is mandatory for TLR signaling, but dispensable for TLR3 and TLR4 (Takeda and Akira, 2004), did not perturb the IEC circadian clock in *MyD88iec*$^{-/-}$ mice (Figure S7E; identical results were obtained in colon, data not shown) and did not affect the IEC expression of PPARα, c-Jun and Cyp11a1 (Figure S7F), nor the LPS-induced repression of PPARα and RevErbα (Figure S7G), in keeping with previous data (Larsson et al., 2012) showing that the expression of many microbiota-dependent genes does not require MyD88 in IEC (Table S6). In this respect, we note that the expression of the intracellular PRR NOD2, which activates JNK and IKKβ upon MAMPs binding (Kanneganti et al., 2007) and possesses a RORE DBS (Figure S7A) in its promoter region to which the bindings of RORα and RevErbα exhibited antiphasic circadian profiles (Figure 6F), was also impaired in AIMD mice (Figure 6E).

Of note, Silver et al. (2012) recently reported a circadian control of the oscillatory expression and function of TLR9 in macrophages, through binding of Bmal1 to a cognate E box present in the *TLR9* gene. We found a similar Bmal1 binding to the TLR9 E box in peritoneal macrophages (Figure S7H), but not in IEC where in contrast RORα did bind the *TLR9* RORE (Figure S7I; see also Figures 6D, 6G, 6H, and S7D), thus indicating that the activity of circadian clock output regulators could be cell-selectively modulated.

Microbiota-Dependent AP-1 and NF-κB Activities Are Required for Homeostatic Gene Expression in IEC

The role of microbiota in JNK, c-Jun, and IKKβ activities led us to investigate whether the homeostatic expression of genes bearing AP-1 and/or NF-κB DBS could be dependent on microbiota. "Active vitamin D3" (VD3) signaling plays an important role in intestinal homeostasis, and is generated in IEC by the 25-(OH)$D_3$1-α hydroxylase (Cyp27B1) (Cross et al., 2011), the promoter of which contains NF-κB and AP-1 sites (Figure 7A). Cyp27B1 expression was decreased in IEC of AIMD and GF mice (Figures 7B, 7C, and S7L–S7M), due to lack of recruitment of NF-κB (p65/p50) and AP-1 (c-Jun/c-Fos) to their DBS (Figures 7D and 7E). Microbiota requirement for VD3 synthesis was supported by decreased transcripts for Angiogenin 4 (Ang4), Claudins (Cldn) 2 and 12 (Cross et al., 2011), and TSLP (Surjit et al., 2011) (Figures 7B and S7L–S7N), known to be VD3 targets in IEC. ChIP assays showed that the VD3 receptor (VDR) assembled in control mice an activation complex (VDR/SRC2 and/or SRC3, requiring VD3) on *TSLP*, *Cldn2*, and *Cldn12* VDREs, whereas a repression complex (VDR/NCoR and/or SMRT, not requiring VD3) was assembled in IEC of AIMD mice (Figure 7F).

Among AP-1 and/or NF-κB DBS-bearing genes, the transcripts of which were previously shown to be decreased in AIMDM, we found that IL-1β, IL-6, TNFα, and KC-1 (Rakoff-Nahoum et al., 2004), Reg3γ (Reikvam et al., 2011), and STAT3

(I) Cyp11a Immunoblot analysis using ileal IEC from AIMD and AIMD *PPARαiec*$^{-/-}$ mice.
(J) Insulin transcripts in pancreas, for mice as in (F).
(K) RNA transcripts for genes as indicated, in liver, for mice as in (F).
(L and M) Blood levels for the indicated parameters at ZT0 and ZT12, using mice as in (F).
(N) ChIP-Q-PCR assays for recruitment to the RevErbα DR2 DBS, using ileal IEC of control and *PPARαiec*$^{-/-}$ mice, and IgG, RevErbα, or PPARα antibodies.
(O) As in (N), but with AIMD and AIMD *PPARαiec*$^{-/-}$ mice.
(P) RNA transcripts of genes as indicated in livers of control, AIMD, Adx, and Adx AIMD mice.
(Q) As in (P), but ileal IEC.
(R) As in (Q), but using colonic IEC.
(S) RNA transcripts of genes as indicated in ileal IEC of control and Adx mice.
Values represent mean ± SEM. *p < 0.05,**p < 0.01,***p < 0.001. See also Figure S6.

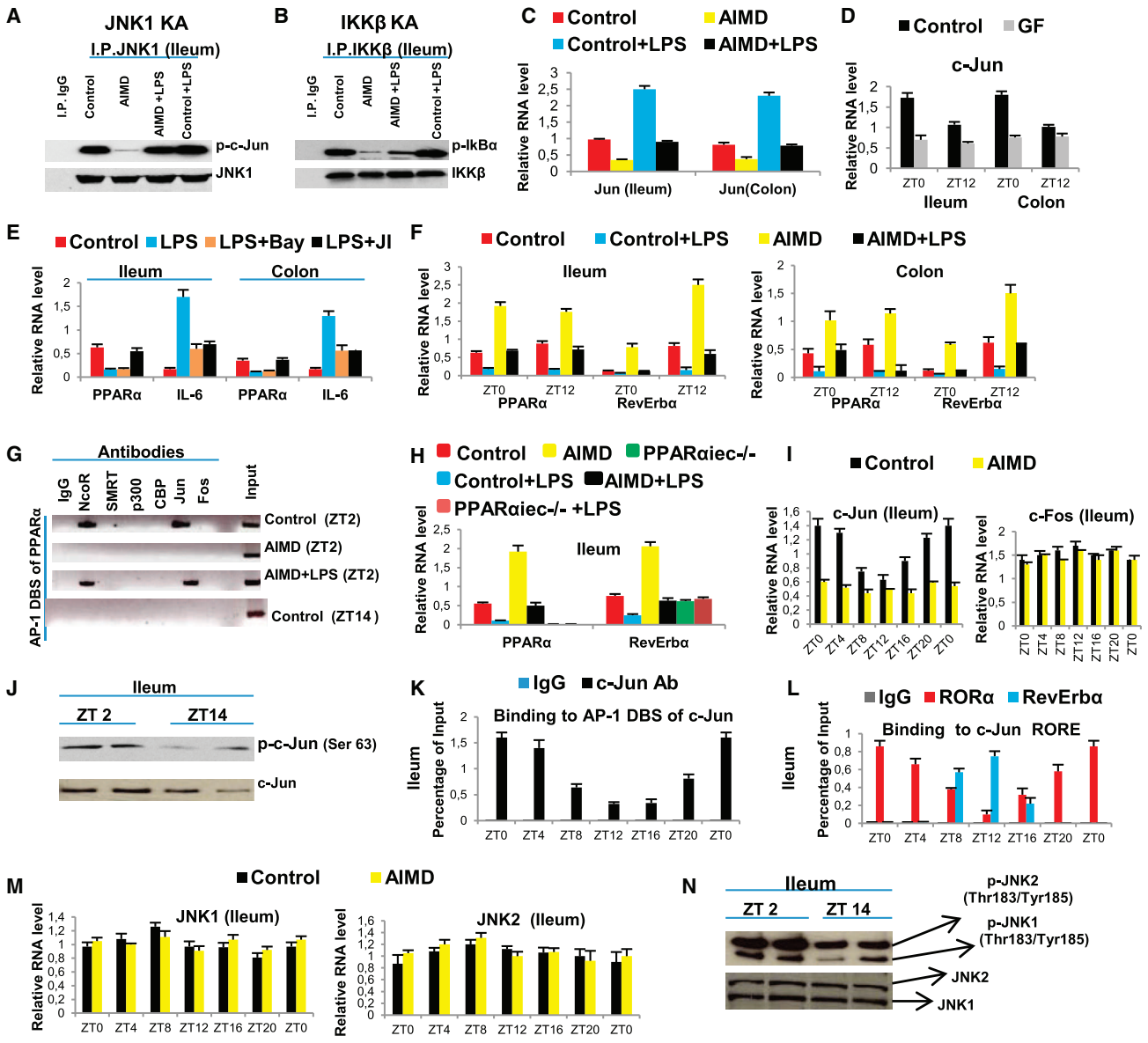

Figure 5. Reduction of c-Jun/JNK Activity in AIMD Mice Relieved the Repression of PPARα Expression

(A) Analysis of JNK1 kinase activity using ileal IEC of control and AIMD mice treated with or without LPS.

(B) As in (A), but for IKKβ kinase.

(C) c-Jun transcripts in ileal and colonic IEC of control and AIMD mice.

(D) As in (C), but for control and germ-free (GF) mice.

(E) RNA transcripts for genes as indicated following LPS treatment of control mice treated with or without Bay (IKKβ inhibitor) or JI (JNK inhibitor).

(F) RNA transcripts for genes as indicated in ileal and colonic IEC of control and AIMD mice following LPS treatment.

(G) ChIP assays using ileal IEC to analyze the recruitment of transcriptional factors to the AP-1 DBS of the PPARα gene.

(H) RevErbα transcripts in ileal IEC of control, AIMD, and *PPARαiec*$^{-/-}$ mice following LPS treatment.

(I) c-Jun and c-Fos transcripts in ileal IEC of control and AIMD mice.

(J) Immunoblot analysis of total and active Ser63-phosphorylated c-Jun in ileal IEC of control mice at ZT2 and ZT14.

(K) ChIP-Q-PCR assays for recruitment to the AP-1 DBS present in the c-Jun promoter using ileal IEC from control mice with IgG and c-Jun antibodies.

(L) As under (K), but using RORα and RevErbα antibodies to analyze the recruitment to the RORE present in the c-Jun promoter.

(M) JNK1 and JNK2 transcripts in ileal IEC from control and AIMD mice.

(N) Immunoblot analysis of total JNK1/2 and phosphorylated JNK1/2 (Thr183/Tyr185) in ileal IEC of control mice at ZT2 and ZT14. The same IEC extracts were used as in (J).

Values represent the mean ± SEM. See also Tables S2, S5, and S6.

transcripts could be restored through administration of LPS to AIMD mice (Figure 7G; note also the reduction in IL-1β and IL-6 blood levels in AIMD mice, Figures S7O and S7P). IL-1β, IL-6, Reg3γ, and TNFα transcripts exhibited in control mice a circadian oscillatory profile similar to that of TLRs (Figures 7I and S7J). Remarkably, in control mice, the circadian bindings of NF-κB and AP-1 to their cognate DBS on IL-6, IL1β, and Reg3γ genes (Figures 7K and 7L) had a profile similar to those of RORα bound to either *E4BP4*, *c-Jun*, *TLRs*, or Bmal1 ROREs (see Figures 3T, 4A, 5L, and 6C). In all cases, similar results were obtained in colonic IEC (not shown). Of note, among additional NF-κB and/or AP-1-dependent genes, the expression of which was decreased in IEC of GF mice (Hooper et al., 2001), several (pIgR, DAF, Sprr2a, Angiogenin 3, and CRP-A) exhibited a decreased expression in AIMD mice, which was restored upon LPS treatment (Figure 7G and Table S2A). Finally, we also found ROREs in the promoter region of *IL-6*, *Reg3γ*, *STAT3*, and *TNFα* genes (Figures 7H and S7A) to which the bindings of RORα and RevErbα were antiphasic (Figure 7J).

Numerous Genes Involved in IEC Homeostatic Functions Exhibit a Microbiota- and Clock-Controlled Circadian Expression through Antiphasic Binding of RORα and RevErbα to Cognate ROREs

A bioinformatics search revealed that the mouse and human genomes comprise several thousands of genes that contain potential consensus RORE DBS. A comparison between mouse and human ortholog genes showed that more than 2,000 of them contained a RORE (Table S3). Among 20 of them selected for their expression in IEC and known homeostatic functions (Table S1), 15 had a higher expression at ZT0 than at ZT12 (Tables S2A and S2B), as well as a lower expression in AIMD (Figure 7M) and in *RORαiec*$^{-/-}$ mice (Figure 7N), thus exhibiting a microbiota- and clock-controlled circadian expression. Moreover, six of them (taken at random), displayed the characteristic antiphasic binding of RORα and RevErbα to their RORE (ChIP assays in Figure 7O).

DISCUSSION

MAMPs Are Mandatory in Ileal and Colonic IEC for Homeostatic Maintenance of the Circadian Clock

Our present data (schematized in Figures 2 and S2) unveil the physiological sequence of events that define the circadian clock in IEC, as deduced from (1) the circadian temporal expression profiles of transcripts of relevant clock genes, (2) the effect of IEC-selective mutations of these genes, and (3) the selective bindings of proteins encoded in some of these genes with regulatory sequences present in promoter regions of their target genes. At ZT0 (6 a.m.), the level of corticosterone produced in ileal IEC is low, similar to that present in colonic IEC that originates from the HPA axis-controlled adrenal production of corticosterone. Thus, RORα expression in IEC is at zenith, as its IR nGRE-mediated repression by corticosterone-liganded GR is minimal. Consequently, the RORα-dependent RORE-mediated activation of expression of TLRs (TLR1–TLR5 and TLR9) and NOD2 is also at zenith, the MAMPs-induced PRR-mediated JNK and c-Jun activations are maximum (of note, c-Jun expression is also RORα-dependent), and the c-Jun-dependent "negative AP-1 DBS"-mediated repression of PPARα expression is therefore maximal. On the clock side, the RORα-dependent RORE-mediated expressions of Bmal1 and E4BP4 are at zenith, whereas Cyp11a1 expression that is repressed by E4BP4 is minimal, in keeping with a low level of ileal IEC corticosterone synthesis (as evidenced by the low transcript levels of GC-responsive genes in ileal IEC) (Figures S6A–S6C). At ZT8, the Bmal1-induced E-box-mediated expression of RevErbα, initiated at ZT4, is maximal. This results in repression of RORE-containing genes (including TLRs, NOD2, c-Jun, Bmal1) and also E4BP4. The repression of the latter then leads, through derepression of Cyp11a1, to increasing corticosterone production in ileal IEC, and consequently to IR nGRE-mediated repression of RORα that reaches its trough at ZT12, whereas the expression of the (+)GRE-containing *Per1* and *Per2* genes is at zenith. Subsequently, the level of ileal and colonic IEC corticosterone decreases, due (1) in ileum, to an increase in E4BP4 expression (upon autorepression of RevErbα expression, leading to repression of Cyp11a1 expression), and (2) in colon, to the cophasic circadian decrease in HPA axis-controlled adrenal corticosteroid production (Figures 4P–4R); these decreases then relieve the GR-mediated repression on RORα, and stimulate the RORE-dependent expression of Cry1, which by inhibiting the GR (Lamia et al., 2011) further decreases the expression of Per 1 and 2, thereby allowing the next circadian cycle to begin. Thus, not only RevErbα (Feng and Lazar, 2012; Cho et al., 2012), but also RORα are integral components of the IEC circadian clock. Of note, RORα was previously identified as an activator of Bmal1 expression and an integral component of the suprachiasmatic nucleus master clock (Sato et al., 2004).

In the absence of microbiota, the impairment of PRR signaling, and consequently of the activation of c-Jun expression and activity, leads to a permanent expression of PPARα, thereby resulting in the loss of all IEC events exhibiting a circadian rhythm. Indeed, the "constitutive" expression of PPARα in IEC results into a permanent increase of RevErbα expression and E4BP4 repression. This overexpression of the RevErbα repressor then leads, through competition for RORE binding, to repression of all RORE-mediated RORα-dependent transcription, in both ileum and colon, thereby resulting in disruption of TLR signaling due to repression of TLR expression, as well as in disruption of the circadian clock because Bmal1 and Cry1 expressions are no longer activated by RORα, while being repressed by RevErbα. In addition, the permanent increase in RevErbα expression in ileum leads, through E4BP4 repression, to a constitutive expression of Cyp11a1, leading to systemic hypercorticosterolism. Importantly, the decrease in expression of the E4BP4 repressor, also results into a general increased expression of numerous D-box-containing genes, the expression of which (high from ZT8 to ZT16) is clearly temporally distinct from that of RORE-containing genes (high from ZT20 to ZT4) (our data not shown; Asher and Schibler, 2011; see Figure S2). Moreover, the decrease in Cry1 expression results in an increase of GR activity (Lamia et al., 2011) that, together with the systemic hypercorticosterolism, causes a total disruption of the circadian clock in both ileal and colonic IEC, with a permanent increase in Per1 and Per2. Importantly, this AIMD hypercorticosterolism

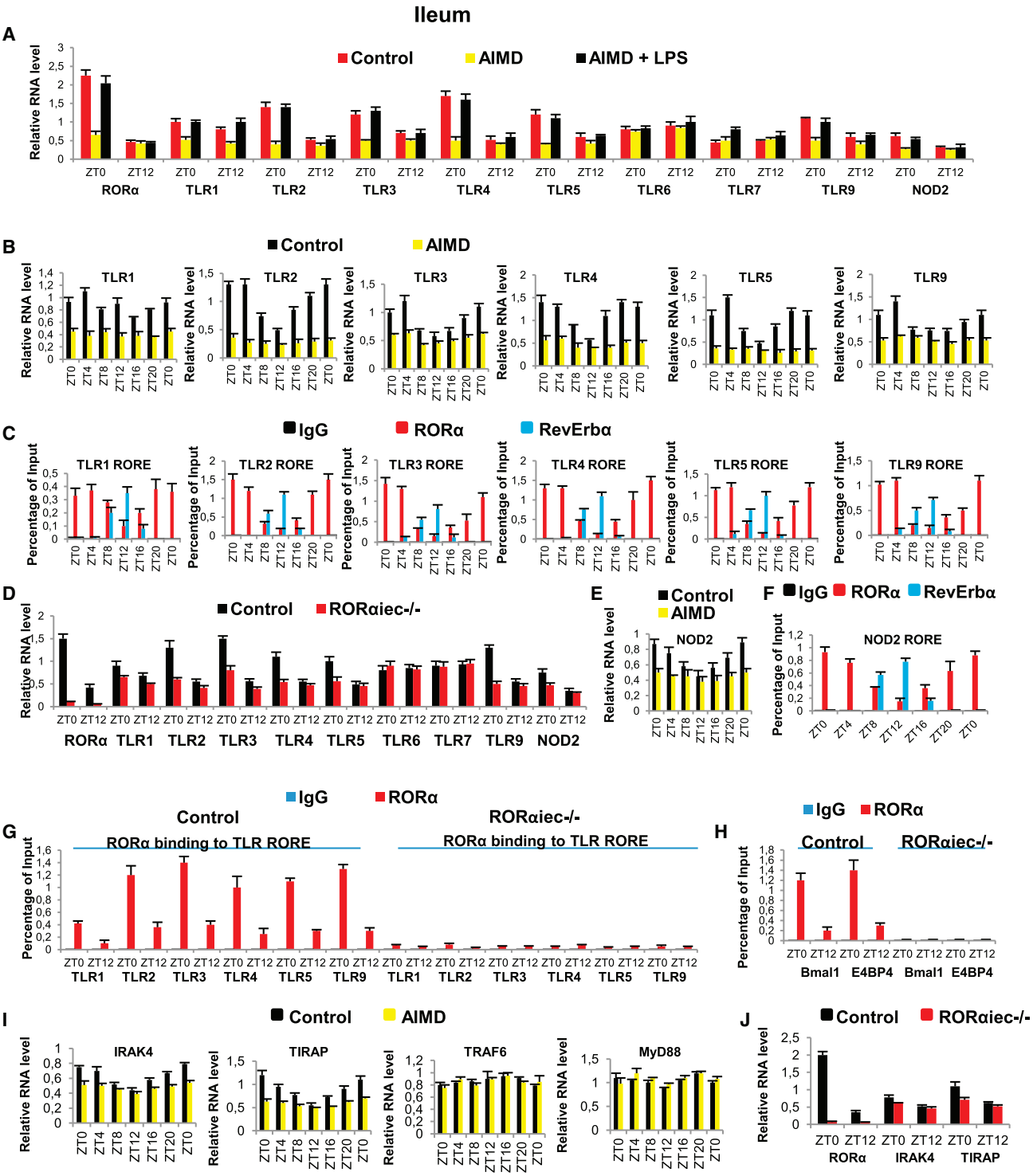

Figure 6. RORα Controls TLR Expression in IEC

(A) RNA transcripts for genes as indicated in ileal IEC from control and LPS-treated AIMD mice.

(B) TLR transcripts in ileal IEC of control and AIMD mice.

(C) ChIP-Q-PCR assays for recruitment to ROREs of TLR genes using ileal IEC and IgG, RORα, or RevErbα antibodies.

(D) RNA transcripts of genes as indicated in ileal IEC of control and *RORαiec*$^{-/-}$ mice.

(E) NOD2 transcripts in ileal IEC of control and AIMD mice.

(F) ChIP-Q-PCR assays for recruitment to RORE of NOD2 gene using ileal IEC and IgG, RORα and RevErbα antibodies.

(legend continued on next page)

generates systemic defects that have been previously correlated with microbiota impairment (see below). Of note, the IEC-selective abrogation of PPARα expression in control mice (*PPARαiec*$^{-/-}$ mice) had no deleterious effect on the function of the circadian cycle, nor on corticosterone production and blood parameters, whereas in AIMD mice the same mutation restored normality in IEC for clock components, corticosterone levels, and blood parameters. Thus, PPARα intervenes on the clock system to boost the production of corticosterone in ileal cells, only when microbiota is lacking or seriously impaired in its capacity to signaling through TLRs.

A Tight Connection between the IEC Circadian Clock, Ileal Corticosterone Synthesis, and the Microbiota-less Systemic Syndrome

Our study unveiled that, unique among peripheral organs but the adrenal glands, the ileal (but not the colonic) circadian clock is intimately associated with the ileal generation of a rhythmic production of corticosterone that under physiological conditions is cophasic with the HPA axis-controlled adrenal corticosterone production. This is important in two respects. First, as GCs possess the capability to reset circadian clocks (Balsalobre et al., 2000), corticosterone produced by ileal epithelial cells can act as a tissue-specific cue ensuring the temporal functional synchronization of these cells. Second, as adrenalectomy does not affect the ileal corticosterone production, ileal IEC unlike other tissues/organs is not dependent on adrenal HPA axis-controlled GC synthesis and may therefore normally perform GC-dependent homeostatic functions under pathophysiological conditions that either decrease GC blood level (e.g., chronic stress) or require an ileal corticosterone production in order to effectively combat an ileal inflammation (Noti et al., 2010).

On the other hand, we have shown here that a lack of microbiota results in a permanent ileal overproduction of corticosterone due to decreased expression of the D-box-binding E4BP4 repressor. This hypercorticosterolism generates systemic metabolic defects (hyperglycemia, insulin resistance, increased TG and FA) (Vegiopoulos and Herzig, 2007), which affect mainly the liver, the pancreas, and the HPA axis, leading to a prediabetic syndrome within a month of antibiotic treatment. It remains to be seen whether longer treatments may result in the numerous systemic debilitating effects known to occur upon long-term GC administration (affecting among others, skin, bone, muscle, CNS, and behavior) (Schäcke et al., 2002). Of note, studies on GF mice and on mice exposed to antibiotics strongly suggest a role for gut microbiota in regulation of anxiety, depression, and cognition (Cryan and Dinan, 2012). In fact, it is likely that physiological functions dependent on the control of gene expression by liganded GR (GRE-mediated transactivation, NF-κB/AP1 tethered transrepression, and IR nGRE-mediated direct transrepression; see Surjit et al. [2011] for references), can all be affected by the microbiota-less hypercorticosterolism.

As GF mice exhibit a hypercorticosterolism and systemic metabolic defects similar to those found in AIMD mice, it would be interesting to investigate whether the administration of current probiotics could normalize GF mice. It would also be interesting to investigate how the Cyp11a-like increased expression of numerous D-box-containing genes encoding homeostatic functions (data not shown) contributes to the microbiota-less syndrome in AIMD mice.

Microbiota Cues through the Circadian Clock Control Essential Homeostatic Functions in IEC

Our study reveals how the IEC clock and microbiota cues control, at the molecular level, the circadian oscillatory expression of genes, the promoter regions of which contain RORα/RevErbα-binding ROREs and/or DBS for AP1 and/or NF-κB. The absence of microbiota precludes PRR-mediated signaling, as well as the function of the clock, thus impairing in IEC the transcription of all genes, the expression of which is dependent on both PRRs and clock components (see above). Interestingly, many of these genes play important homeostatic functions either directly in IEC (e.g., gut innate immunity) or indirectly in the lamina propria (e.g., gut adaptive immunity). In innate immunity (Table S2A and references therein), this is the case for proteins well-known to (1) exhibit antibacterial effects: Reg3β, Reg3γ, Angiogenin 4, and Cryptidins, the IgA receptor (pIgR), and the complement factor DAF, (2) be crucial for gut barrier function: Claudin 2 and 12 for tight junctions, and Sprr2a for barrier fortification, (3) exhibit cytokine activity: IL-6, IL-1β, TNFα, and TSLP, (4) be required for induction of gene expression by IL-6 and IL-22: the Stat3 transcription factor, and (5) function as a cytokine receptor: HVEM (the IL-22 receptor). Of note, the expression of several genes involved in IEC innate immunity (Angiogenin 4, TSLP, and Claudins 2 and 12) requires the synthesis of active vitamin D3 by the "microbiota-dependent" Cyp27B1 enzyme (see above and Figures 2 and S2). Interestingly, a defective VDR signaling has been shown to increase the susceptibility to inflammatory bowel disease (IBD) and colitis (Cross et al., 2011). The development of the adaptive immune system in lamina propria, notably the differentiation of Th17 cells, a source of IL-17 and IL-22, has been shown to be microbiota-dependent (Ivanov et al., 2009). Thus, as IL-1β and IL-6 are required for Th17 cell differentiation (Hu et al., 2011), IEC also appears to be important for instructing the adaptive immune system in lamina propria.

Strikingly, more than 2,000 genes present in mice and humans contain a consensus RORE DBS (Tables S3 and S4). We found that, among 20 of them selected for known homeostatic functions and expression in IEC, 15 exhibited a microbiota-dependent and ZT0 > ZT12 clock-controlled circadian expression (Tables S1 and S2B), thus emphasizing the crucial role played by microbiota MAMPs, TLRs, and circadian clock output regulators in the control of IEC homeostatic functions. Two additional

(G) ChIP-Q-PCR assays for recruitment to TLR ROREs of control and *RORαiec*$^{-/-}$ mice using ileal IEC and RORα antibody.
(H) As in (F), but for Bmal1 and E4BP4 ROREs.
(I) RNA transcripts for genes as indicated in ileal IEC of control and AIMD mice.
(J) RNA transcripts of genes as indicated in ileal IEC of control and *RORαiec*$^{-/-}$ mice.
Values represent mean ± SEM. See also Figure S7 and Tables S2, S5, and S6.

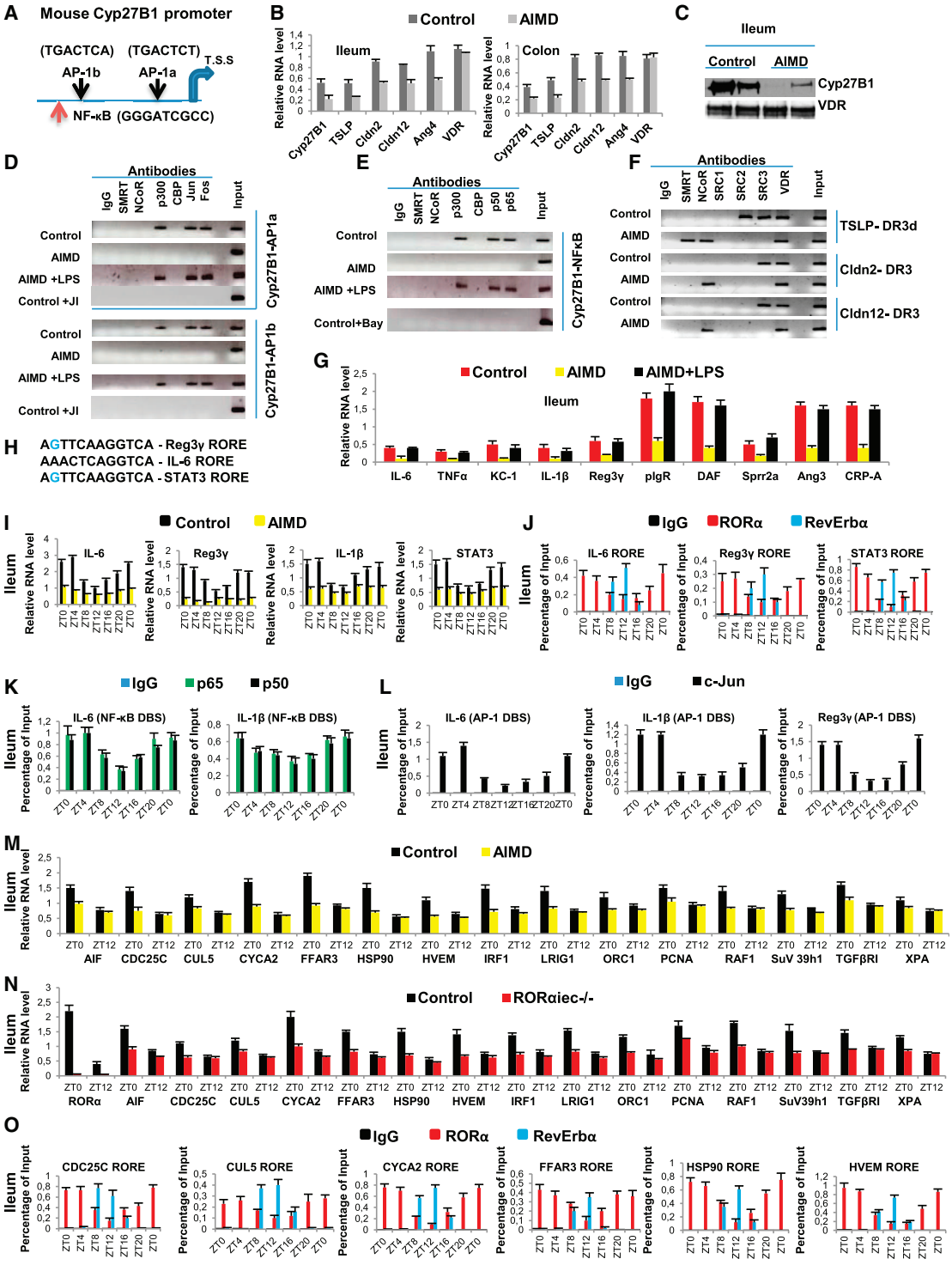

Figure 7. Microbiota Controls the Homeostatic Expression of NF-κB and AP-1-Dependent Genes in IEC

(A) Schematic organization of the Cyp27B1 promoter. TSS, transcription start site. Small arrows represent positions of AP-1a, AP-1b, and NF-κB DBS located at positions −524, −1,205, and −1,332, respectively, upstream to TSS.

(B) RNA transcripts of genes as indicated in ileal and colonic IEC of control and AIMD mice.

(C) Immunoblot for Cyp27B1 in ileal IEC of control and AIMD mice.

(D) ChIP assays for recruitments to AP-1a and AP-1b DBS of the Cyp27B1 gene using ileal IEC of control and AIMD mice, and antibodies as indicated. JNK inhibitor (JI) was injected intraperitoneally.

(legend continued on next page)

RORE-containing genes exhibiting a ZT0 > ZT12 circadian rhythm are worth mentioning (see Figures 6D–6F and 7M–7O; Table S2B). The PRR *NOD2* receptor gene, which belongs to the group of *NLR* intracellular receptors genes (Kanneganti et al., 2007), was the first susceptibility gene to be linked to Crohn's disease. It encodes an NLR that is important for the release of antibacterial Cryptidins by IEC Paneth cells, and its decreased expression in AIMD mice is known to heighten the intestinal susceptibility to inflammation and colitis (Maynard et al., 2012). We also found that the expression of the short chain fatty acid (SCFA) receptor (FFAR3 or GPR41), a GPCR that binds SCFA and may be implicated in adiposity and intestinal motility (Samuel et al., 2008), is controlled by RORα in a ZT0 > ZT12 circadian manner and is decreased in AIMD mice. Of note, these data extend the effects of microbiota signals on circadian gene expression in IEC to the expression of NLR intracellular receptors and GPCR membrane receptors.

CONCLUSIONS

Within the symbiotic dialog between the gut and the microbiota, we investigated here, at the level of gene expression, the role played by cues from commensal bacteria in the control of intestinal epithelial cell homeostasis. While dissecting the defects exhibited by these cells in microbiota-depleted mice, we discovered that this dialog not only involves external bacterial cues (MAMPs) interacting with epithelial cell PRRs (TLRs and NLRs) (Abreu, 2010), but also requires the integrity of their circadian clock that opens a temporal window during which MAMP signals can be transduced by PRRs. Indeed, thanks to the opposing transcriptional activities of the clock components and output regulators RORα and RevErbα, the temporally "even" arrhythmic bacterial signaling is converted into a circadian rhythmic activation of synthesis of cell membrane receptors (e.g., TLRs), which results in a temporally-controlled circadian activation of IKKβ and JNK activities in IEC. The rhythmic activation of IKKβ and JNK (see Figures 2 and S2) enables timing the IEC homeostatic functions of genes activated by AP1 and/or NF-κB with circadian events occurring at diurnal times ZT20-ZT4, which correspond to the mouse "active phase" (Dibner et al., 2010). In addition, the circadian pattern of IKKβ and JNK prevents in IEC the disruption of the circadian clock through inappropriate activation of RevErbα by PPARα. Together, these mechanisms ensure that, during the same ZT20-ZT4 active phase, the transactivating (RORα and Bmal1/Clock) and transrepressing (RevErbα/E4BP4) output regulator components of the clock can adequately control the temporal expression of RORE- and E-box-containing genes encoding IEC homeostatic functions. Importantly, by preventing the disruption of the circadian clock through activation of RevErbα by PPARα, the microbiota MAMPs also control the proper repression of the E4BP4 repressor, thereby allowing, at diurnal times ZT8–ZT16 that correspond to the mouse "rest phase" (Dibner et al., 2010), the expression of the numerous D-box-containing genes encoding IEC homeostatic functions (data not shown; see Figures 2 and S2).

Our study also raises important questions concerning the possible generality of our conclusions. For instance, could a variety of membrane or intracellular receptors, binding to nonmicrobial extra or intracellular cognate physiological ligands, be differently connected with peripheral circadian clocks in various cells/tissues to convert arrhythmic signals into circadian rhythmic outputs in order to time homeostatic functions with physiologically-relevant circadian events (e.g., food availability and intake, exposure to infection, diurnal variation in light and temperature) (Feng and Lazar, 2012; Dibner et al., 2010; Masri and Sassone-Corsi, 2010; Hussain and Pan, 2009)? Elucidating, in various cell types/tissues, the molecular mechanisms that underlie the sophisticated dialogs between ligands, their cognate membrane or intracellular receptors, and peripheral circadian clocks, in order to time homeostatic functions with circadian changes, may pave the way to new therapies aimed at treating multiple pathologies, the origin of which has to be found in disruption of these conversations.

EXPERIMENTAL PROCEDURES

Additional details on methods are available in Extended Experimental Procedures.

Mice and Treatments

C57BL6/J male wild-type and adrenalectomized mice (Charles River Laboratories) 8–12 weeks old were used. Germ-free mice of C57BL6/J background were obtained from CDTA, Orleans (France). Mice were provided food and water ad lib, under 12 hr light/12 hr dark conditions. Antibiotics-induced

(E) As in (D), but for recruitments to the NF-κB DBS of the Cyp27B1 gene. IKKβ inhibitor (Bay) was injected as in (D).
(F) ChIP assays for recruitments of VDR and other factors as indicated to DR3 elements in TSLP, Claudin2, and 12 genes using ileal IEC of control and AIMD mice, and antibodies as indicated.
(G) RNA transcripts of genes as indicated from ileal IEC of control and LPS-treated AIMD mice.
(H) RORE sequences identified in the promoter regions of Reg3γ, IL-6, and STAT3 mouse genes. The blue letters indicate one base mismatch with the consensus RORE2 in Bmal1 gene (see also Figure S7A).
(I) RNA transcripts of genes as indicated in ileal IEC of control and AIMD mice.
(J) ChIP-Q-PCR assays for recruitment of RORα and RevErbα to ROREs in genes as indicated using control mice ileal IEC, with IgG, RORα, and RevErbα antibodies.
(K) As in (J), but with IgG, p65, and p50 antibodies for recruitments to NF-κB DBS in genes as indicated.
(L) As in (J), but with IgG and c-Jun antibodies for recruitments to AP-1 DBS in genes as indicated.
(M) RNA transcripts of genes as indicated in ileal IEC of control and AIMD mice.
(N) RNA transcripts of genes as indicated in ileal IEC of control and *RORαiec*$^{-/-}$ mice.
(O) ChIP-Q-PCR assays for circadian recruitment of RORα and RevErbα to ROREs of genes as indicated using control mice ileal IEC, with IgG, RORα, and RevErbα antibodies.
Values represent mean ± SEM. See also Figure S7 and Tables S1, S2, S3, S4, S5, and S6.

microbiota depletion was conducted for 4 weeks as described (Rakoff-Nahoum et al., 2004).Applicable LPS was added together with antibiotic during the fourth week. In all instances, the bacterial depletion was more than 99%, irrespective of LPS addition, whether it was determined by bacterial count or by 16 s Q-PCR (Table S5). Breeding, maintenance, and experimental manipulations were approved by the Animal Care and Use Committee of IGBMC/ICS. Intestinal epithelial cells (IEC) were isolated as described (Cima et al., 2004).

ChIP Assays

Isolated IEC were crosslinked in 1% formaldehyde, followed by ChIP assay as described (Surjit et al., 2011).

Real-Time RNA Transcript Determination

RNA isolated from IEC and other organs were reverse transcribed using random hexamers, followed by Q-PCR, and expressed relative to the hypoxanthine-guanine phosphoribosyltransferase (HPRT) levels, as described (Surjit et al., 2011).

Blood Metabolic Analysis

Blood glucose was analyzed from tail vein using Accu-check glucometer (Roche). Other measurements were done using blood collected after retroorbital punction at the IGBMC-ICS Metabolomic Unit.

Statistics

Data are represented as mean ± SEM of at least three independent experiments, and were analyzed by SyStat and Microsoft Excel statistics software using Student's t test (RNA transcripts) and one-way ANOVA (blood metabolic analysis). $p < 0.05$ was considered as significant.

Bioinformatics Analysis

hg19 (human) and mm9 (mouse) repeat masked Ensembl genome assembly was used to determine genome-wide distribution of RORE containing genes. Gene functional annotation was performed using DAVID program.

SUPPLEMENTAL INFORMATION

Supplemental Information includes Extended Experimental Procedures, seven figures, and six tables and can be found with this article online at http://dx.doi.org/10.1016/j.cell.2013.04.020.

ACKNOWLEDGMENTS

We thank Dr. Daniel Metzger for discussions, Dr. Patricia Lopez (CDTA) for GF mice, and Mrs. Estelle Meyer for secretariat help. We are grateful to Marie-France Champy (ICS) for metabolism analysis, and Armelle Van Es for bacterial scoring. We are grateful to S. Akira for floxed MyD88 mice. We also thank the staff of the animal facilities of the IGBMC/ICS. This work was supported by the CNRS, the INSERM, the ANR (ANR 07-Physio 002-01), the University of Strasbourg Institute for Advanced Studies (USIAS), and the Association pour la Recherche à l'IGBMC (ARI). A.M. and A.K. were supported by ARI fellowships.

Received: October 19, 2012
Revised: December 24, 2012
Accepted: April 4, 2013
Published: May 9, 2013

REFERENCES

Abreu, M.T. (2010). Toll-like receptor signalling in the intestinal epithelium: how bacterial recognition shapes intestinal function. Nat. Rev. Immunol. *10*, 131–144.

Aguilera, C., Nakagawa, K., Sancho, R., Chakraborty, A., Hendrich, B., and Behrens, A. (2011). c-Jun N-terminal phosphorylation antagonises recruitment of the Mbd3/NuRD repressor complex. Nature *469*, 231–235.

Asher, G., and Schibler, U. (2011). Crosstalk between components of circadian and metabolic cycles in mammals. Cell Metab. *13*, 125–137.

Bäckhed, F., Manchester, J.K., Semenkovich, C.F., and Gordon, J.I. (2007). Mechanisms underlying the resistance to diet-induced obesity in germ-free mice. Proc. Natl. Acad. Sci. USA *104*, 979–984.

Balsalobre, A., Brown, S.A., Marcacci, L., Tronche, F., Kellendonk, C., Reichardt, H.M., Schutz, G., and Schibler, U. (2000). Resetting of circadian time in peripheral tissues by glucocorticoid signaling. Science *289*, 2344–2347.

Cho, H., Zhao, X., Hatori, M., Yu, R.T., Barish, G.D., Lam, M.T., Chong, L.-W., DiTacchio, L., Atkins, A.R., Glass, C.K., et al. (2012). Regulation of circadian behaviour and metabolism by REV-ERB-α and REV-ERB-β. Nature *485*, 123–127.

Cima, I., Corazza, N., Dick, B., Fuhrer, A., Herren, S., Jakob, S., Ayuni, E., Mueller, C., and Brunner, T. (2004). Intestinal epithelial cells synthesize glucocorticoids and regulate T cell activation. J. Exp. Med. *200*, 1635–1646.

Cowell, I.G. (2002). E4BP4/NFIL3, a PAR-related bZIP factor with many roles. Bioessays *24*, 1023–1029.

Cross, H.S., Nittke, T., and Kallay, E. (2011). Colonic vitamin D metabolism: implications for the pathogenesis of inflammatory bowel disease and colorectal cancer. Mol. Cell. Endocrinol. *347*, 70–79.

Cryan, J.F., and Dinan, T.G. (2012). Mind-altering microorganisms: the impact of the gut microbiota on brain and behaviour. Nat. Rev. Neurosci. *13*, 701–712.

Dibner, C., Schibler, U., and Albrecht, U. (2010). The mammalian circadian timing system: organization and coordination of central and peripheral clocks. Annu. Rev. Physiol. *72*, 517–549.

Drosatos, K., Drosatos-Tampakaki, Z., Khan, R., Homma, S., Schulze, P.C., Zannis, V.I., and Goldberg, I.J. (2011). Inhibition of c-Jun-N-terminal kinase increases cardiac peroxisome proliferator-activated receptor alpha expression and fatty acid oxidation and prevents lipopolysaccharide-induced heart dysfunction. J. Biol. Chem. *286*, 36331–36339.

Duez, H., and Staels, B. (2008). Rev-erb α gives a time cue to metabolism. FEBS Lett. *582*, 19–25.

Feng, D., and Lazar, M.A. (2012). Clocks, metabolism, and the epigenome. Mol. Cell *47*, 158–167.

Froy, O., and Chapnik, N. (2007). Circadian oscillation of innate immunity components in mouse small intestine. Mol. Immunol. *44*, 1954–1960.

Hooper, L.V., Wong, M.H., Thelin, A., Hansson, L., Falk, P.G., and Gordon, J.I. (2001). Molecular analysis of commensal host-microbial relationships in the intestine. Science *291*, 881–884.

Hu, W., Troutman, T.D., Edukulla, R., and Pasare, C. (2011). Priming microenvironments dictate cytokine requirements for T helper 17 cell lineage commitment. Immunity *35*, 1010–1022.

Hussain, M.M., and Pan, X. (2009). Clock genes, intestinal transport and plasma lipid homeostasis. Trends Endocrinol. Metab. *20*, 177–185.

Ivanov, I.I., Atarashi, K., Manel, N., Brodie, E.L., Shima, T., Karaoz, U., Wei, D., Goldfarb, K.C., Santee, C.A., Lynch, S.V., et al. (2009). Induction of intestinal Th17 cells by segmented filamentous bacteria. Cell *139*, 485–498.

Kanneganti, T.-D., Lamkanfi, M., and Núñez, G. (2007). Intracellular NOD-like receptors in host defense and disease. Immunity *27*, 549–559.

Lamia, K.A., Papp, S.J., Yu, R.T., Barish, G.D., Uhlenhaut, N.H., Jonker, J.W., Downes, M., and Evans, R.M. (2011). Cryptochromes mediate rhythmic repression of the glucocorticoid receptor. Nature *480*, 552–556.

Larsson, E., Tremaroli, V., Lee, Y.S., Koren, O., Nookaew, I., Fricker, A., Nielsen, J., Ley, R.E., and Bäckhed, F. (2012). Analysis of gut microbial regulation of host gene expression along the length of the gut and regulation of gut microbial ecology through MyD88. Gut *61*, 1124–1131.

Le Minh, N., Damiola, F., Tronche, F., Schütz, G., and Schibler, U. (2001). Glucocorticoid hormones inhibit food-induced phase-shifting of peripheral circadian oscillators. EMBO J. *20*, 7128–7136.

Lemke, U., Krones-Herzig, A., Berriel Diaz, M., Narvekar, P., Ziegler, A., Vegiopoulos, A., Cato, A.C.B., Bohl, S., Klingmüller, U., Screaton, R.A., et al. (2008).

The glucocorticoid receptor controls hepatic dyslipidemia through Hes1. Cell Metab. *8*, 212–223.

Mandard, S., Zandbergen, F., van Straten, E., Wahli, W., Kuipers, F., Müller, M., and Kersten, S. (2006). The fasting-induced adipose factor/angiopoietin-like protein 4 is physically associated with lipoproteins and governs plasma lipid levels and adiposity. J. Biol. Chem. *281*, 934–944.

Masri, S., and Sassone-Corsi, P. (2010). Plasticity and specificity of the circadian epigenome. Nat. Neurosci. *13*, 1324–1329.

Maynard, C.L., Elson, C.O., Hatton, R.D., and Weaver, C.T. (2012). Reciprocal interactions of the intestinal microbiota and immune system. Nature *489*, 231–241.

Mueller, M., Cima, I., Noti, M., Fuhrer, A., Jakob, S., Dubuquoy, L., Schoonjans, K., and Brunner, T. (2006). The nuclear receptor LRH-1 critically regulates extra-adrenal glucocorticoid synthesis in the intestine. J. Exp. Med. *203*, 2057–2062.

Noti, M., Corazza, N., Mueller, C., Berger, B., and Brunner, T. (2010). TNF suppresses acute intestinal inflammation by inducing local glucocorticoid synthesis. J. Exp. Med. *207*, 1057–1066.

Preitner, N., Damiola, F., Lopez-Molina, L., Zakany, J., Duboule, D., Albrecht, U., and Schibler, U. (2002). The orphan nuclear receptor REV-ERBalpha controls circadian transcription within the positive limb of the mammalian circadian oscillator. Cell *110*, 251–260.

Rakoff-Nahoum, S., Paglino, J., Eslami-Varzaneh, F., Edberg, S., and Medzhitov, R. (2004). Recognition of commensal microflora by toll-like receptors is required for intestinal homeostasis. Cell *118*, 229–241.

Reikvam, D.H., Erofeev, A., Sandvik, A., Grcic, V., Jahnsen, F.L., Gaustad, P., McCoy, K.D., Macpherson, A.J., Meza-Zepeda, L.A., and Johansen, F.E. (2011). Depletion of murine intestinal microbiota: effects on gut mucosa and epithelial gene expression. PLoS ONE *6*, e17996. http://dx.doi.org/10.1371/journal.pone.0017996.

Samuel, B.S., Shaito, A., Motoike, T., Rey, F.E., Backhed, F., Manchester, J.K., Hammer, R.E., Williams, S.C., Crowley, J., Yanagisawa, M., and Gordon, J.I. (2008). Effects of the gut microbiota on host adiposity are modulated by the short-chain fatty-acid binding G protein-coupled receptor, Gpr41. Proc. Natl. Acad. Sci. USA *105*, 16767–16772.

Sato, T.K., Panda, S., Miraglia, L.J., Reyes, T.-M., Rudic, R.D., McNamara, P., Naik, K.A., Fitzgerald, G.A., Kay, S.A., and Hogenesch, J.B. (2004). A functional genomics strategy reveals Rora as a component of the mammalian circadian clock. Neuron *43*, 527–537.

Schäcke, H., Döcke, W.D., and Asadullah, K. (2002). Mechanisms involved in the side effects of glucocorticoids. Pharmacol. Ther. *96*, 23–43.

Schreiber, M., Kolbus, A., Piu, F., Szabowski, A., Möhle-Steinlein, U., Tian, J., Karin, M., Angel, P., and Wagner, E.F. (1999). Control of cell cycle progression by c-Jun is p53 dependent. Genes Dev. *13*, 607–619.

Silver, A.C., Arjona, A., Walker, W.E., and Fikrig, E. (2012). The circadian clock controls toll-like receptor 9-mediated innate and adaptive immunity. Immunity *36*, 251–261.

So, A.Y., Bernal, T.U., Pillsbury, M.L., Yamamoto, K.R., and Feldman, B.J. (2009). Glucocorticoid regulation of the circadian clock modulates glucose homeostasis. Proc. Natl. Acad. Sci. USA *106*, 17582–17587.

Surjit, M., Ganti, K.P., Mukherji, A., Ye, T., Hua, G., Metzger, D., Li, M., and Chambon, P. (2011). Widespread negative response elements mediate direct repression by agonist-liganded glucocorticoid receptor. Cell *145*, 224–241.

Takeda, K., and Akira, S. (2004). TLR signaling pathways. Semin. Immunol. *16*, 3–9.

Vegiopoulos, A., and Herzig, S. (2007). Glucocorticoids, metabolism and metabolic diseases. Mol. Cell. Endocrinol. *275*, 43–61.

Yang, X., Downes, M., Yu, R.T., Bookout, A.L., He, W., Straume, M., Mangelsdorf, D.J., and Evans, R.M. (2006). Nuclear receptor expression links the circadian clock to metabolism. Cell *126*, 801–810.

Supplemental Information

EXTENDED EXPERIMENTAL PROCEDURES

Mice

Intestinal epithelial cells (IEC)-selective mutants of PPARα (*PPARαiec*$^{-/-}$), RORα (*RORαiec*$^{-/-}$), GR (*GRiec*$^{-/-}$), Bmal1 (*Bmal1iec*$^{-/-}$), Cyp27B1 (*Cyp27B1iec*$^{-/-}$), MyD88 (*MyD88iec*$^{-/-}$) were generated by crossing floxed female mice with the Villin-Cre floxed male mice. Hepatocyte-selective ablation of GR (*GRhep*$^{-/-}$) was achieved by crossing floxed GR with Albumin-CreERT^{2} floxed male mice (Schuler et al., 2004), and subsequent Tamoxifen injection for five days. Bmal1 floxed mice were obtained from Jackson Laboratories (B6.129S4 (Cg)-*Arntl*^{tm1Weit}/J). Floxed Cyp27B1 mice were as described (Dardenne et al., 2001). Floxed MyD88 mice were as described (Adachi et al., 1998). All other floxed mice were generated at IGBMC/ICS and maintained in either IGBMC and/or ICS animal house. Genotyping was performed by PCR on genomic DNA isolated from mouse tails. Mice were provided food and water *ad libitum*, and housed in cages under12 hr light (L) and 12 hr dark (D) conditions. All experiments were performed under Light-Dark (LD) conditions, with ZT0 being the start of the light period (6 a.m.) and ZT12 the start of the dark period (6 p.m.). Mice were sacrificed at 4 hr intervals starting from ZT0. Breeding, maintenance and experimental manipulations were approved by the Animal care and Use Committee of IGBMC/ICS.

Depletion of Gut Microbiota by Antibiotic Treatment and 16 s-QPCR for Bacterial Counting

Mice were provided drinking water containing Ampicillin (1gm/l), Vancomycin (500mg/l), Neomycin Sulfate (1g/l) and Metronidazole (1gm/l) for 30 days (Rakoff-Nahoum et al., 2004). Following this treatment feces were collected from both control and antibiotic-treated groups, under sterile conditions, vortexed and homogenized in thioglycollate and cultured for both aerobic and anaerobic bacterias, bacterial colonies were identified and counted (Table S5) following Grams staining, by the IGBMC animal house sanitary facility.

For 16 s Q-PCR of rRNA genes the feces from different groups of mice were collected directly in sterile eppendorfs and DNA was isolated using QIAmp DNA kit (QIAGEN) and concentration was determined by spectrophotometry at 260nm. Degenerate primers for V2 and V6 regions of bacterial 16 s genes as well as PCR conditions were as described (Reikvam et al., 2011).

Treatment of Antibiotic-Treated Mice with LPS

After 3 weeks of antibiotic treatment, mice were provided with water supplemented with purified LPS (E.Coli) (Sigma Aldrich), at a concentration of 50 μg/μl for one week concurrently with antibiotics. This dose was chosen based on LPS bioavailability (Rakoff-Nahoum et al., 2004).

Intestinal Epithelial Cells Isolation

Intestinal epithelial cells were isolated using a modification of a nonenzymatic protocol (Cima et al., 2004). Briefly, approximately 5-6cm long pieces of distal ileum and colon were separately excised, and placed in Petri dishes containing cold Hanks Balanced Salt Solution (HBSS) with 0.2% horse serum. Blood vessels and associated fat were removed, the intestine was opened longitudinally, gently cleared of feces, and extensively washed on ice in HBSS with 1mM DTT to remove mucus. The intestinal segments were placed in fresh PBS with 30mM EDTA, and shaken at 150 rpm (37°C for 5 min). The supernatant was transferred into a fresh tube, centrifuged (500 g, 5minutes at 4°C) and the pellet was either immediately processed for subsequent analysis, or snap frozen and stored at −70°C for future use. The viability and purity of samples were checked by trypan blue dye exclusion and by measuring the relative transcript levels of alkaline phosphatase, Lrig1, Lgr5 which are expressed selectively in IEC (Cima et al., 2004; Powell et al., 2012).

Macrophage Isolation

Peritoneal macrophages were isolated from wild-type (control) C57BL6/J mouse 3 days after thioglycollate I.P. administration by peritoneal lavage and processed as described (Silver et al., 2012).

Reagents

Metronidazole (M-1547), Vancomycin (V-8138), Neomycin (N-1142), Ampicillin (A-0166), Metyrapone (M-2696), PF-915275 (3291,Tocris). Dexamethasone (D-4902) and RU486 (M-8046) were from Sigma (Surjit et al., 2011). Jnk Inhibitor(II) and Bay-11-7085 were from Calbiochem. Antibodies to GR (Sc-1004x), p65 (Sc-372x), p50 (Sc-1192x), c-Jun (Sc-44x), RORα (Sc-6062x), SRC3 (Sc-9119x) and E4BP4 (Sc-74415x) were from Santa Cruz Biotechnology. Control rabbit IgG (ab 46450) and antibodies to SRC1 (ab 84) and PPARα (ab2779) were from Abcam. Antibodies against VDR, SMRT, NCoR and SRC2 generated at the IGBMC antibody facility were reported earlier (Surjit et al., 2011). Cyp11a (SH-A11435) and GAPDH antibodies were from NovateinBio and Millipore, respectively.

Kinase Assays

Epithelial cells were lysed in 50 mM Tris, pH 7.4, 150 mM NaCl, 25 mM β-glycerophosphate, 2 mM $NaPP_i$, 2 mM EDTA, 1 mM Na_3VO_4, 1% Triton X-100 and 10% glycerol, containing protease inhibitors (Roche), precleared with control preimmune sera and then immunoprecipitated with antibodies against JNK1 or IKKβ (Santa Cruz Biotechnology). Immunoprecipitates were washed three times in

RIPA buffer and finally in kinase assay buffer (50 mM HEPES, pH 7.4, 25 mM β-glycerophosphate, 25 mM $MgCl_2$, 0.1 mM Na_3VO_4 and 0.5 mM DTT ; Greten et al., 2004) and resuspended in 25 μl of the same buffer, to which 150ng of exogenous substrates (GST-c-Jun or GST-IkBα, Millipore), and 1 μCi of γ-P^{32}-ATP were added. The phosphorylation reaction was carried out at 30°C for 20 min. Following SDS-PAGE, the gel was transferred to a nitrocellulose membrane and exposed for autoradiography.

RNA Transcript Determination

Freshly isolated IEC, liver or pancreas samples were used for RNA isolation using TRI reagent (Molecular Research Center). Subsequent to the verification of RNA quality (gel electrophoresis), 1 μg of total RNA (determined spectrophotometrically), was reverse-transcribed using random hexamers and SuperscriptII reagents (Invitrogen) as per manufacturers instructions. The synthesized cDNA was used for Q-RT-PCR with SYBRgreen (QIAGEN) and expressed relative to the HPRT levels, as previously described (Surjit et al., 2011). Primer sequences are available upon request.

Protein Immunoblots

Immunoblots from isolated epithelial cells were performed following standard SDS-PAGE procedures. Proteins were visualized following enhanced chemiluminisence (ECL, Pierce).The primary antibodies used for protein detection were c-Jun (Sc-44), p-c-Jun (Ser63) (Cell Signaling Technology, 2361), pJnk1/2(Thr183/Tyr185) (Cell Signaling Technology, 4668). Other antibodies were as described in reagents section.

ChIP Assays

ChIP was performed as reported (Surjit et al., 2011) with some minor modifications. Briefly, isolated IEC suspension in PBS, was crosslinked with 1% formaldehyde for 15 min at room temperature; crosslinking was stopped by addition of 2M Glycine (0.125M final concentration) at room temperature for 5 min. Cells were pelleted and 500 μl of lysis buffer was added in presence of protease inhibitors on ice. For liver samples, identical lobes of liver from different groups of mice were disrupted using a dounce homogenizer; samples were then crosslinked and processed as described above. Following cell lysis, the samples were sonicated (Bioruptor, Diagenode) to generate fragments of average length of 200-500 base pairs. Cellular debris were removed by centrifugation at 4°C for 10 min (10,000 g) and supernatant was precleared with Protein A/G-Sepharose (Roche) beads, preblocked with salmon DNA and BSA for 30 min at 4°C. Beads were pelleted and discarded; 10% of the lysate was stored from each sample as the source of " Input," and the remaining lysate was diluted 8 times in dilution buffer (16.7 mM Tris-HCl, pH 8.1, 0.01% (w/v) SDS, 1.1% (v/v) Triton X-100, 1.2 mM EDTA, 16.7 mM NaCl, protease inhibitor cocktail), in presence of different primary antibodies for 14 hr at 4°C, on a flip-flop rocker. 70 μl of Protein A/G-Sepharose beads (preblocked with salmon DNA and BSA) were then added for 90 min at 4°C. Immune complexes were recovered by centrifugation at 500 g for 1 min. Beads were washed extensively at 4°C in Low salt buffer (20mM Tris-HCl, pH 8.1, 0.1% (w/v) SDS, 1% (v/v) Triton X-100, 2mM EDTA,150mM NaCl), in High salt buffer (20mM Tris-HCl, pH 8.1, 0.1% (w/v) SDS, 1% (v/v) Triton X-100, 2mM EDTA, 500mM NaCl), and in LiCl buffer (10mM Tris-HCl, pH 8.1, 250mM LiCl, 1% (v/v) NP-40, 1% (w/v) sodium deoxycholate, 1mM EDTA), and finally in 1ml of TE buffer (10mM Tris-HCl, pH 8.0, 1mM EDTA). The bound chromatin was released from the beads by intermittent vortexing at romm-temperature in 200 μl elution buffer (1w/v SDS and 100mM NaHCO3). 1 μl of 10mg/ml RnaseA and 5M NaCl (200mM final concentration) was added to the eluate and incubated O/N at 65°C, and then treated with Proteinase K for 1 hr at 55°C; DNA was purified using QIAGEN PCR purification kit in a final volume of 50 μl. The DNA was either PCR-amplified (separated by agarose gel electrophoresis, stained with ethidium bromide and photographed with UV illuminator equipped with digital camera) or Q-PCR was done using SYBRgreen reagent (QIAGEN). PCR cycles were verified to be within the linear range of amplification. Primer sequences are available upon request.

Plasma Metabolic Analysis

Blood glucose, Insulin, Corticosterone, TG and FFA levels were measured from ad libitum fed mouse at ZT0 and ZT12. Blood glucose levels were determined on blood collected from tail vein using a hand held Accu-check active glucometer (Roche). For all other measurements blood were collected by retroorbital puncture, in EDTA coated vials, plasma was separated and measurements done in the metabolomics unit of the IGBMC/ICS.

Glucose and Insulin Tolerance Tests

Glucose tolerance tests were performed at ZT0 and ZT14, after a 14 hr fast. Blood glucose was measured at the indicated times after intraperitoneal (IP) administration of glucose (2g/kg) of body weight. Glucose-stimulated insulin secretion was also similarly studied after an IP administration of glucose (ZT0 and ZT14). Insulin tolerance tests were carried out after a 4 hr fasting (ZT0 and ZT14), where mice were IP administered with 0 .75units of insulin/kg of body weight (Humulin R, EliLilly). Insulin level at the beginning of the experiment was considered as 100%.

siRNA Treatment

ON-TARGET PLUS SMART POOL siRNAs (DHARMACON) against E4BP4 (NFIL3) (L-063246-00-0050) were transfected into mouse CICL2 (mCICL2) cells in culture, following manufacturers instructions using DHARMAFECT transfection reagent. Cells were

maintained in charcoal-treated FCS-containing medium for 72 hr, and then processed for RNA isolation and transcript determination, protein immunoblot analysis and ChIP assays.

Bioinformatics Analysis

For identification of RORE sequences present across the human and mouse genome, Human [hg19, Ensembl version: 67], downloaded from Ensembl and mouse [mm9, Ensembl version: 67 (ftp://ftp.ensembl.org/pub/current_fasta/mus_musculus/dna/] repeat masked genome assembly was used. The database had 37991 mouse genes and 57945 genes. The database was searched for RORE containing genes with the consensus sequence WAWNTRGGTCA (Preitner et al., 2002) and no mismatch in both the DNA strands, within −20kb upstream and +5kb downstream of the transcriptional start sites for each genes using a JAVA based homemade program to reveal- gene annotation: Ensembl Gene ID, Associated Gene Name, Chromosome Name, Gene Start, Gene End, chromosome strand and location. The analysis revealed 12933 mouse genes and 18311 human genes contain at least one RORE sequence. The RORE containing 2510 ortholog genes between mouse and human were found using the table of gene orthology (Ensembl) using the help of biomart (http://www.biomart.org). Gene functional annotation was done using DAVID program (Huang et al., 2009).

SUPPLEMENTAL REFERENCES

Adachi, O., Kawai, T., Takeda, K., Matsumoto, M., Tsutsui, H., Sakagami, M., Nakanishi, K., and Akira, S. (1998). Targeted disruption of the MyD88 gene results in loss of IL-1- and IL-18-mediated function. Immunity *9*, 143–150.

Banerjee, H., Das, A., Srivastava, S., Mattoo, H.R., Thyagarajan, K., Khalsa, J.K., Tanwar, S., Das, D.S., Majumdar, S.S., George, A., et al. (2012). A role for apoptosis-inducing factor in T cell development. J. Exp. Med. *209*, 1641–1653.

Dardenne, O., Prud'homme, J., Arabian, A., Glorieux, F.H., and St-Arnaud, R. (2001). Targeted inactivation of the 25-hydroxyvitamin $D_{(3)}$-1(α)-hydroxylase gene (CYP27B1) creates an animal model of pseudovitamin D-deficiency rickets. Endocrinology *142*, 3135–3141.

Den, R.B., and Lu, B. (2012). Heat shock protein 90 inhibition: rationale and clinical potential. Ther. Adv. Med. Oncol. *4*, 211–218.

Greten, F.R., Eckmann, L., Greten, T.F., Park, J.M., Li, Z.-W., Egan, L.J., Kagnoff, M.F., and Karin, M. (2004). IKKβ links inflammation and tumorigenesis in a mouse model of colitis-associated cancer. Cell *118*, 285–296.

Grummt, I., and Ladurner, A.G. (2008). A metabolic throttle regulates the epigenetic state of rDNA. Cell *133*, 577–580.

Huang, da W., Sherman, B.T., and Lempicki, R.A. (2009). Systematic and integrative analysis of large gene lists using DAVID bioinformatics resources. Nat. Protoc. *4*, 44–57.

Kamura, T., Maenaka, K., Kotoshiba, S., Matsumoto, M., Kohda, D., Conaway, R.C., Conaway, J.W., and Nakayama, K.I. (2004). VHL-box and SOCS-box domains determine binding specificity for Cul2-Rbx1 and Cul5-Rbx2 modules of ubiquitin ligases. Genes Dev. *18*, 3055–3065.

Kang, T.-H., Reardon, J.T., and Sancar, A. (2011). Regulation of nucleotide excision repair activity by transcriptional and post-transcriptional control of the XPA protein. Nucleic Acids Res. *39*, 3176–3187.

Massagué, J., and Xi, Q. (2012). TGF-β control of stem cell differentiation genes. FEBS Lett. *586*, 1953–1958.

Müller, G.A., and Engeland, K. (2010). The central role of CDE/CHR promoter elements in the regulation of cell cycle-dependent gene transcription. FEBS J. *277*, 877–893.

Pickert, G., Neufert, C., Leppkes, M., Zheng, Y., Wittkopf, N., Warntjen, M., Lehr, H.A., Hirth, S., Weigmann, B., Wirtz, S., et al. (2009). STAT3 links IL-22 signaling in intestinal epithelial cells to mucosal wound healing. J. Exp. Med. *206*, 1465–1472.

Powell, A.E., Wang, Y., Li, Y., Poulin, E.J., Means, A.L., Washington, M.K., Higginbotham, J.N., Juchheim, A., Prasad, N., Levy, S.E., et al. (2012). The pan-ErbB negative regulator Lrig1 is an intestinal stem cell marker that functions as a tumor suppressor. Cell *149*, 146–158.

Reardon, C., Lechmann, M., Brüstle, A., Gareau, M.G., Shuman, N., Philpott, D., Ziegler, S.F., and Mak, T.W. (2011). Thymic stromal lymphopoetin-induced expression of the endogenous inhibitory enzyme SLPI mediates recovery from colonic inflammation. Immunity *35*, 223–235.

Schuler, M., Dierich, A., Chambon, P., and Metzger, D. (2004). Efficient temporally controlled targeted somatic mutagenesis in hepatocytes of the mouse. Genesis *39*, 167–172.

Segatto, O., Anastasi, S., and Alemà, S. (2011). Regulation of epidermal growth factor receptor signalling by inducible feedback inhibitors. J. Cell Sci. *124*, 1785–1793.

Shui, J.W., Larange, A., Kim, G., Vela, J.L., Zahner, S., Cheroutre, H., and Kronenberg, M. (2012). HVEM signalling at mucosal barriers provides host defence against pathogenic bacteria. Nature *488*, 222–225.

Stillman, B. (2008). DNA polymerases at the replication fork in eukaryotes. Mol. Cell *30*, 259–260.

Ubeda, C., and Pamer, E.G. (2012). Antibiotics, microbiota, and immune defense. Trends Immunol. *33*, 459–466.

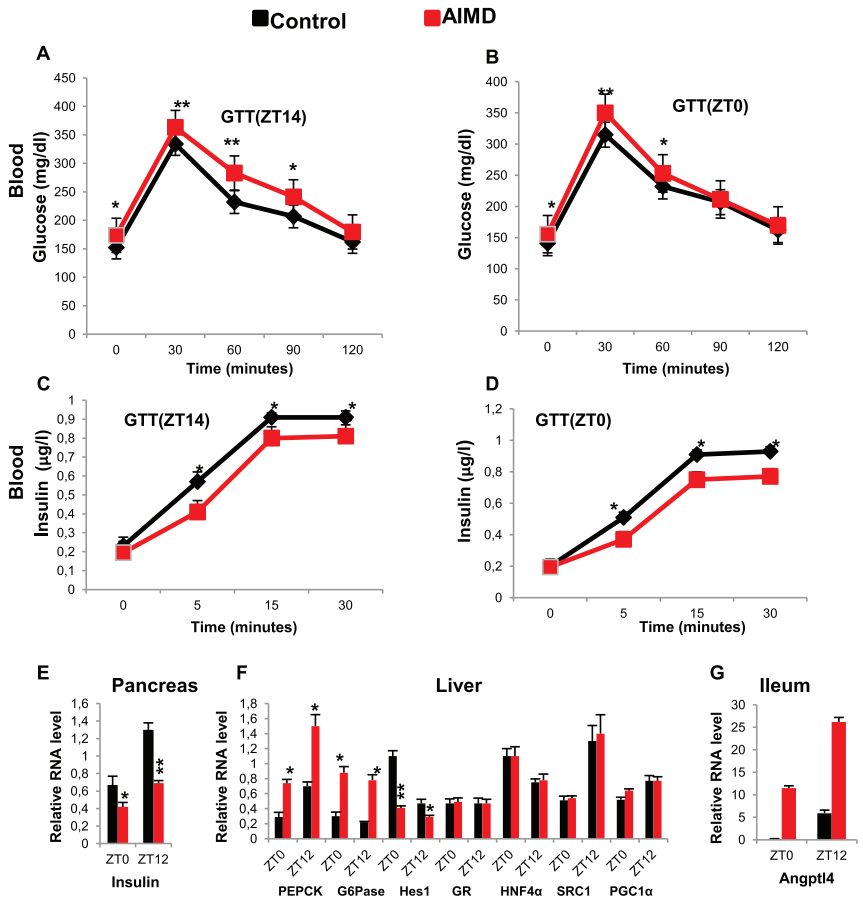

Figure S1. Hyperglycemia and Hypoinsulinemia in AIMD Mice, Related to Figure 1

(A) Glucose Tolerance Test (GTT) measuring blood glucose levels at ZT14 in control and AIMD mice, following a 4 hr fasting and I.P. administration of Glucose.

(B) GTT as in (A), but at ZT0.

(C) GTT as in (A), but measuring blood insulin levels at ZT14.

(D) GTT as in (C), but at ZT0.

(E) Relative insulin RNA transcript level in pancreas of control and AIMD mice at ZT0 and ZT12.

(F) Relative transcript level of gluconeogenic genes and their regulators, as well as that of Hes1, in livers of control and AIMD mice at ZT0 and ZT12.

(G) Relative Angptl4 transcript level in ileal epithelium of control and AIMD mice.

All values represent mean ± SEM n = 8–10 mice for (A)–(D) and n = 4 mice per time point per group for (E)–(G). *p < 0.05,**p < 0.01.

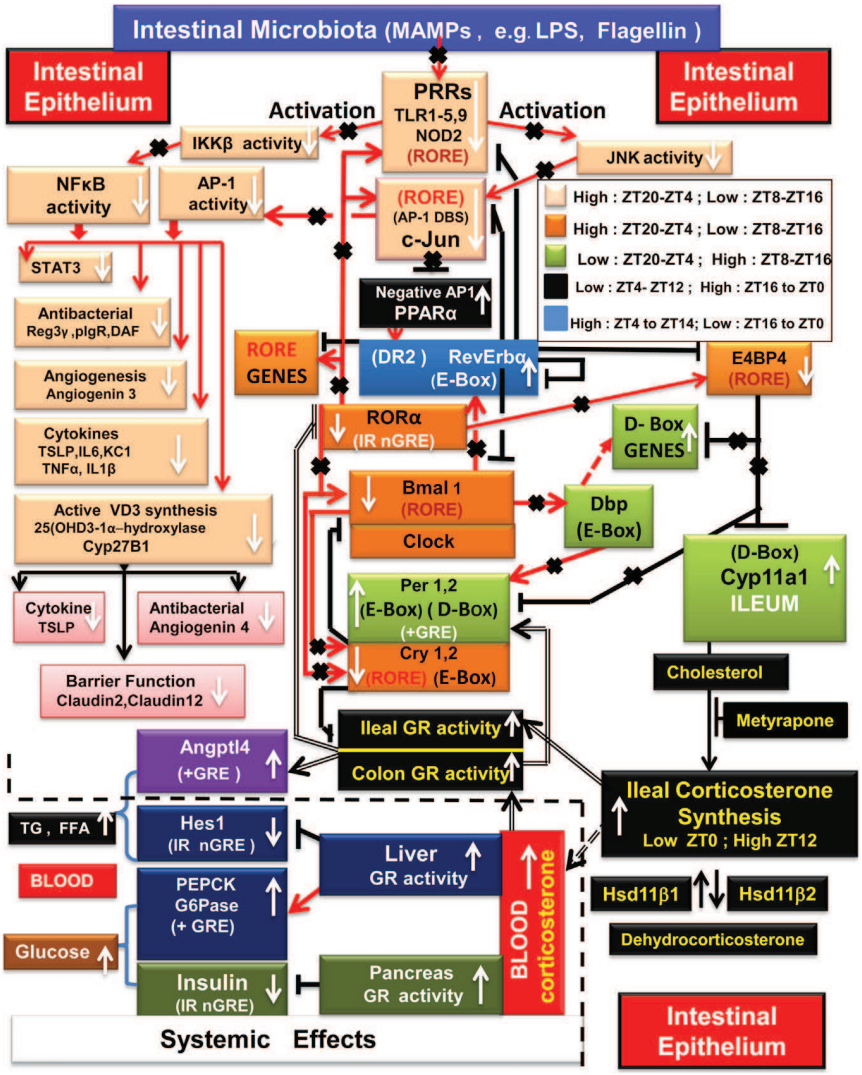

Figure S2. Orchestration of Homeostasis in Intestinal Epithelium by Clock-Controlled Circadian Expression of Pattern Recognition Receptors that Transduce MAMP Signals, Related to Figure 2 and Discussion

The mammalian circadian clock consists of two interlocked feedback loops. The major loop involves the transcriptional activation of the E-box-containing Per1, Per2 and Cry1,Cry2 genes by the E-box-binding transcription factors Clock and Bmal1, and the autorepression of Per and Cry genes by their own protein products. Importantly, Per1 and Per2 contain a GR DBS (+GRE) and a D box to which the E4BP4 repressor can bind. A second feedback loop involves the RORα activator which competes with the RevErbα repressor for binding to RORE DBS present in Bmal1 and in the E4BP4 output regulator. Remarkably, in this second feedback loop Bmal1 binds to the E box present in RevErbα to activate its transcription, while the presence of a DR2 element in RevErbα mediates its autorepression, as well as its transcriptional activation by PPARα. The transcript activator DBP (D-box-binding protein) is another E-box-containing gene, the transcription of which is driven by Bmal1/Clock through E-box elements in its promoter. DBP and E4BP4 (a transcriptional repressor) competes for binding to D-box elements present in numerous genes, the expression of which, during the diurnal "active phase," is antiphasic to that of RORE- containing genes (Asher and Schibler, 2011). Red arrowheads represent "activation" events; blunt black lines indicate "repression" events; black double lines refer to corticosterone and/or GR-dependent events. Black crosses (X) indicate impairment of activation or repression signaling events in AIMD mice. The upward and downward white arrows correspond to increase and decrease of the indicated components in AIMD mice. ROREs are DNA Binding Sites (DBS) for RORα and RevErbα; (+GRE) and IR nGRE are DBS for GR-mediated transcriptional activation and direct transcriptional repression, respectively. E box and D box are DBS for Bmal1 and DBP/E4BP4, respectively. DR2 is a DBS on the RevErbα promoter for RevErbα autorepression and for activation of RevErbα transcription by PPARα. MAMPs: Microbiota Associated Molecular Patterns; TLRs: Toll-Like Receptors; NOD2: Nucleotide Oligomerization Domain2. The small colored boxes (inset) indicate the time [ZT0 (6A.M) to ZT24] of expression of clock genes and of diverse classes of microbiota- and clock- controlled genes in IEC. For general references, see Asher and Schibler (2011) Crosstalk between Components of Circadian and Metabolic Cycles in Mammals. Cell Metab. 13,125–137. For additional abbreviations, see main text.

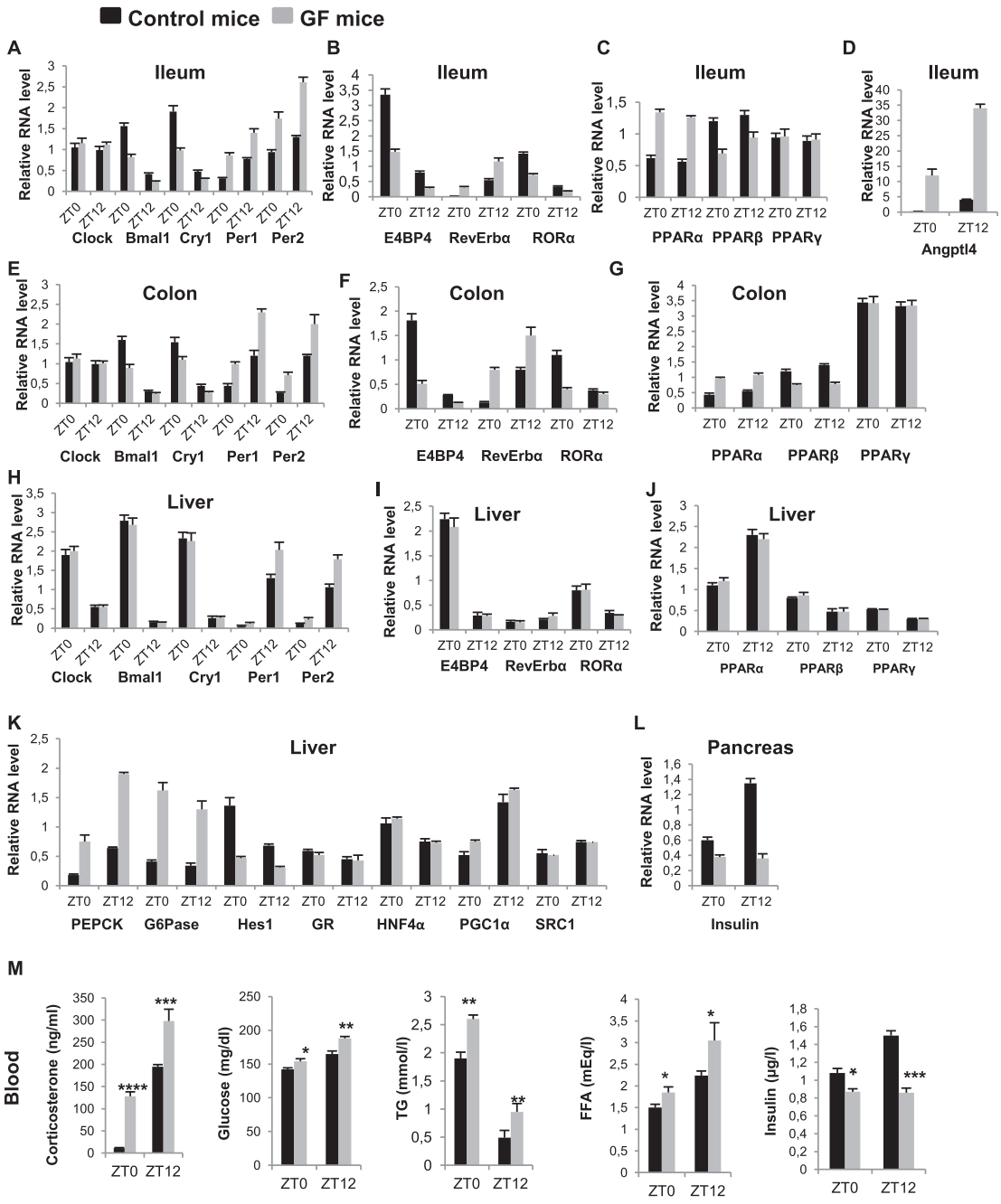

Figure S3. Alterations in NRs, Circadian Clock, and Systemic Metabolism in Germ-free Mice, Related to Figure 1

(A–D) RNA transcript levels of genes as indicated in ileal epithelium of control and germ-free (GF) mice at ZT0 and ZT12.

(E–G) RNA transcript levels of genes as indicated in colonic epithelium of control and GF mice at ZT0 and ZT12.

(H–K) RNA transcript levels of genes as indicated in liver of control and GF mice at ZT0 and ZT12.

(L) Relative insulin RNA transcript level in pancreas of control and GF mice at ZT0 and ZT12.

(M) Levels of indicated blood components in *ad libitum* fed control and GF mice at ZT0 and ZT12.

All values are mean ± SEM n = 4 mice per time point per group (A)–(L). n = 8–10 mice per time point per group in (M). *p < 0.05,**p < 0.01 and ***p < 0.001.

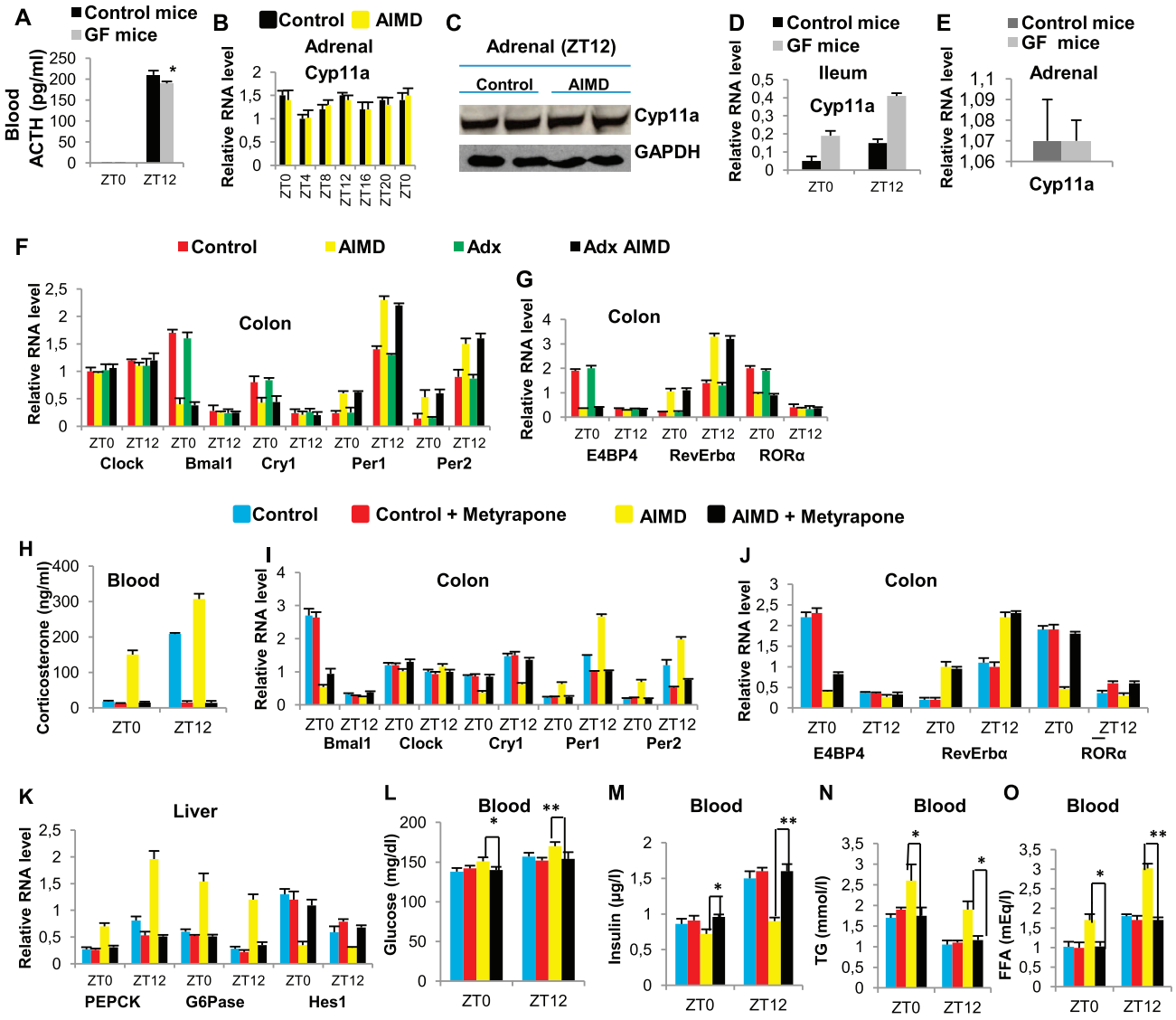

Figure S4. Intestinal Epithelium Is the Source of Increased Corticosterone Synthesis in AIMD Mice, Related to Figure 3

(A) Blood ACTH levels in control and Germ-Free (GF) mice at ZT0 and ZT12 (see also Figure 3A).

(B) RNA transcript level of Cyp11a involved in corticosteroid synthesis in adrenal glands of control and AIMD mice.

(C) Immunoblot analysis of Cyp11a in adrenals of control and AIMD mice.

(D) Relative Cyp11a RNA transcript level in ileal epithelial cells of control and GF mice at ZT0 and ZT12.

(E) RNA transcript level of Cyp11a in adrenal glands of control and GF mice at ZT12.

(F and G) RNA transcript levels of circadian clock components at ZT0 and ZT12 in colonic epithelium of sham-operated control, AIMD, adrenalectomized (Adx) and adrenalectomized-microbiota-depleted (Adx AIMD) mice.

(H) Blood Corticosterone level in control and AIMD mice with or without Metyrapone treatment at ZT0 and ZT12.

(I and J) RNA transcript levels of circadian clock genes in colonic epithelium of control and AIMD mice with or without Metyrapone treatment.

(K) RNA transcript levels for genes (as indicated) in liver of mice treated as in (H).

(L–O) Blood levels of indicated parameters in control and AIMD mice at ZT0 and ZT12 with or without Metyrapone treatment.

All values represent mean ± SEM n = 8–10 mice per time point per group (A, H, L–O). n = 4 mice per time point per group (B, D–G, I–K). Note that the same mice were used for analyses presented in (H) and (L)–(O).

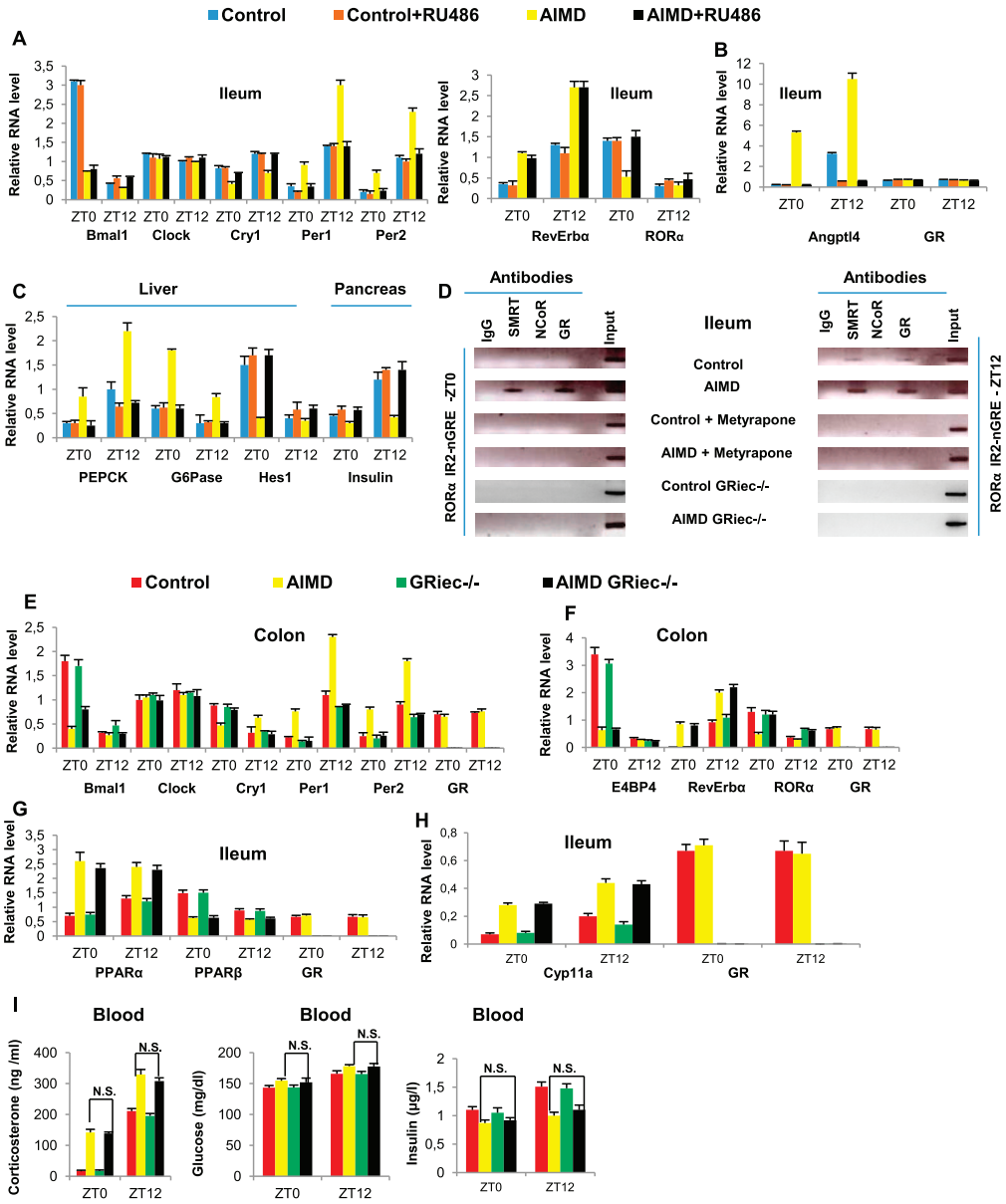

Figure S5. Inhibition of GR Activity Suppresses AIMD Defects, Related to Figure 3

(A) RNA transcript levels at ZT0 and ZT12 for indicated genes from ileal epithelium following RU486 administration to control and AIMD mice.

(B) As above (A), but for Angptl4 and GR.

(C) RNA transcript levels at ZT0 and ZT12 for indicated genes from liver and pancreas following RU486 administration to control and AIMD mice.

(D) ChIP analysis with ileal epithelial cells from mice (as indicated) for recruitment of IgG, GR, NCoR and SMRT to the IR2 nGRE of the RORα gene at ZT0 and ZT12.

(E) Relative RNA transcript levels of circadian clock components from colonic epithelial cells of control, IEC selective GR null mutant (*GRiec*$^{-/-}$), AIMD and microbiota-depleted *GRiec*$^{-/-}$ (AIMD *GRiec*$^{-/-}$) mice at ZT0 and ZT12.

(F) As above (E), but for additional clock components.

(G) As above (E), but for PPARα and PPARβ transcripts in ileal epithelium.

(H) As above (E), but for Cyp11a transcripts in ileal epithelium.

(I) Blood levels of indicated parameters from *ad libitum* fed mice, in groups as in (E) (see also Figure 3O).

All values represent mean ± SEM n = 4 mice per time point per group (A–C, E–H). n = 8–10 mice per time point per group for (I). The same mice were used for experiments in Figure 3O and (I).

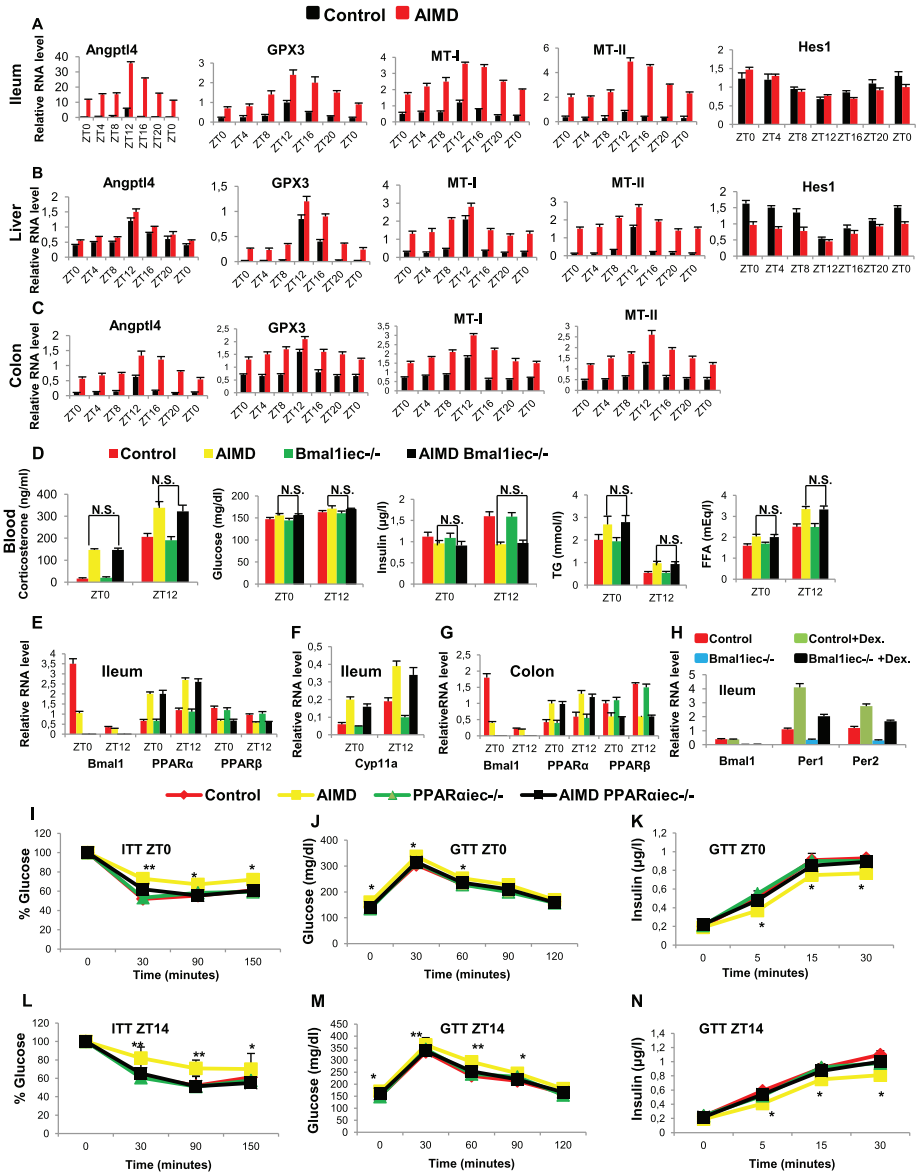

Figure S6. Reduction in Bmal1 Level Is Not Responsible for the Generation of AIMD Defects, Related to Figure 4

(A–C) Circadian profiles of RNA transcripts of corticosterone-induced genes in ileum (A), liver (B) and colon (C), from control and AIMD mice.

(D) Blood levels at ZT0 and ZT12 of indicated parameters in control and AIMD mice with or without IEC-selective Bmal1 null mutation (*Bmal1iec*$^{-/-}$).

(E and F) RNA transcript levels of PPARα, PPARβ and Cyp11a from ileal epithelium at ZT0 and ZT12, in mice as indicated under (D).

(G) RNA transcript levels for PPARα and PPARβ from colonic epithelium, in mice as indicated under (D).

(H) RNA transcript levels of Per1 and Per2, in ileal epithelium of control and *Bmal1iec*$^{-/-}$ mice with or without Dexamethasone (Dex) intraperitoneal injection.

(I) Insulin tolerance test (ITT), following intraperitoneal injection of insulin to control, AIMD, *PPARαiec*$^{-/-}$ and AIMD *PPARαiec*$^{-/-}$ mice at ZT0. The initial blood glucose levels prior to injection were considered as 100%.

(J) Glucose tolerance test (GTT), measurement of blood glucose levels following glucose injection at ZT0, in groups of mice as described under (I).

(K) GTT, measurement of insulin levels following glucose injection at ZT0, in the groups of mice described in (I).

(L) As above in (I), but at ZT14.

(M) As above in (J), but at ZT14.

(N) As above in (K), but at ZT14.

All values represent mean ± SEM n = 8–10 mice per time point per group (D). n = 4 mice per time point per group (A–C, E–H).Note that the same mice were used in (I) and (J), while different set of mice were used for (J), (K), (M), and (N). *p < 0.05,**p < 0.01. The data correspond to three independent experiments.

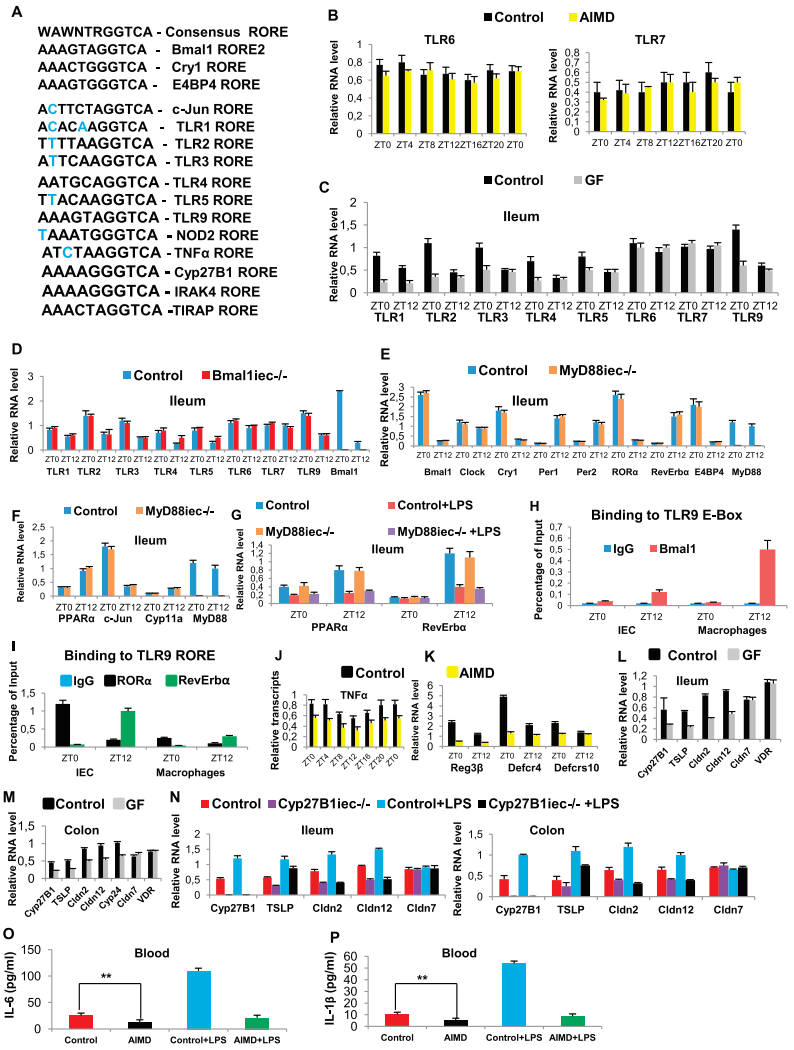

Figure S7. Microbiota- and RORE-Dependent, but MyD88- and Bmal1-Independent, TLR Expression in IEC, Related to Figures 6 and 7

(A) RORE sequences identified in mouse Cry1, E4BP4, c-Jun, TLR1/2/3/4/5/9, NOD2, TNFα, Cyp27B1, IRAK4 and TIRAP gene promoters. Bmal1 RORE2 was identified in Preitner et al. (2002). The consensus RORE sequence is based on the Bmal1 RORE2 sequence. The blue colored letters indicate nonconsensus nucleotides. W = A or T, R = A or G, N = any nucleotide.

(B) RNA transcript levels of TLR6 and TLR7 in ileal epithelium of control and AIMD mice.

(C) RNA transcript levels of indicated genes from ileal epithelium cells of control and GF mice, at ZT0 and ZT12 (see also Figures 6A and 6B).

(D) RNA transcript levels of TLR genes in ileal IEC of control and *Bmal1iec*$^{-/-}$ mice.

(E) RNA transcript levels of core clock components and clock output regulators in ileal IEC of control and *MyD88iec*$^{-/-}$ mice at ZT0 and ZT12.

(F) RNA transcript levels of PPARα, c-Jun and Cyp11a in ileal IEC of control and *MyD88iec*$^{-/-}$ mice.

(G) RNA transcript levels of indicated genes in ileal IEC of control and *MyD88iec*$^{-/-}$ mice treated with or without LPS.

(H) ChIP analysis for Bmal1 recruitment to E-box element in TLR9 promoter at ZT0 and ZT12, in ileal IEC and peritoneal macrophages of control mice.

(I) ChIP analysis of RORα and RevErbα recruitment to TLR9 RORE at ZT0 and ZT12 in ileal IEC and peritoneal macrophages of control mice.

(J) Circadian RNA transcript levels of TNFα from ileal IEC of control and AIMD mice.

(K) RNA transcript levels of indicated genes from ileal IEC of control and AIMD mice, at ZT0 and ZT12.

(L and M) RNA transcript levels of indicated genes in ileal (L) and colonic (M) IEC from control and GF mice.

(N) RNA transcript levels of indicated genes in ileal and colonic IEC of control and IEC- selective Cyp27B1 null mutant (*Cyp27B1iec*$^{-/-}$) mice treated with or without LPS.

(O) Blood levels of IL-6 in control and AIMD mice with or without LPS treatment.

(P) As above (O), but for blood levels of IL-1β.

All values represent mean ± SEM n = 4 mice per time point per group in (A)–(G) and (J)–(N). n = 6–8 mice per time point per group (O and P).

Table S1. Selected RORE-Containing Genes with Their Essential Homeostatic Functions and Identified RORE Sequences

Gene Name	Function	RORE Sequence
Apoptosis Inducing Factor (AIF)	**Apoptosis**	TATGTAGGTCA
Cell Division Cycle 25C (CDC25c)	**Control of Cell Cycle**	AATATGGGTCA
Cullin 5 (CUL5)	**Ubiquitin Ligase**	AAAATAGGTCA
Cyclin A2 (CYCA2)	**Control of Cell Cycle**	TATTTGGGTCA
Free Fatty Acid Receptor 3 (FFAR3/GPR41)	**Short Chain Fatty Acid receptor**	AAACTGGGTCA
Heat Shock Protein 90kDa (HSP90)	**Chaperone**	AAACTAGGTCA
Herpes Virus Entry Modulator (HVEM)	**Signal Transduction**	AATCTGGGTCA
Interferon Response Factor 1(IRF1)	**Transcription Regulator**	AAATTGGGTCA
Leucine-rich Repeats and Immunoglobulin-like domains 1(LRIG1)	**Pan ERB Inhibitor (Tumor suppressor)**	TAACTAGGTCA
Origin Recognition Complex1 (ORC1)	**DNA Replication**	TAAATGGGTCA
Proliferating Cell Nuclear Antigen (PCNA)	**DNA Replication**	AAACTAGGTCA
v-Raf-leukemia viral oncogene 1(RAF1)	**Signal Transduction**	AATTTGGGTCA
Suppressor of Variegation 3-9 homolog 1 (SuV39h1)	**Transcription Regulator**	TATGTAGGTCA
Transforming Growth Factor Beta, Receptor I (TGFβRI)	**Signal Transduction**	TATTTAGGTCA
Xeroderma Pigmentosum, Complementation group A (XPA)	**DNA Repair**	AAAATAGGTCA

Note that, of 20 genes selected from the list of 2000, consensus RORE containing mouse genes (Table S3) with essential homeostatic functions, these 15 genes showed both circadian- (ZT0>ZT12) and microbiota-dependent expressions in IEC (Tables S2A and S2B).

Table 2A. Microbiota-Dependent Expression of Genes with Known Essential Homeostatic Functions in IEC

Genes	Function	Transcriptional regulation (DBS)			Circadian Expression ZT0>ZT12	Decreased Expression in AIMD mice	Relevant Figures	References[2]
		AP-1 and/or NF-κB	RORE	VDRE				
	Innate Immunity							
Reg3β	Antibacterial	+			+	+	S7K	Ubeda and Pamer, 2012; Reikvam et al.,2011
Reg3γ		+	+		+	+	7H,7I, 7J	
Cryptidins (Defcr4 and Defcr 10)		+			+	+	S7K	
Angiogenin 4				+	— [1]	+	7B	
DAF	Complement factor	+			— [1]	+	7G	Hooper et al., 2001
Claudin 2	Gut Barrier Function			+	— [1]	+	7B, 7F	Cross et al., 2008
Claudin 12				+	— [1]	+	7B, 7F	
Sprr2a		+			— [1]	+	7G	Hooper et al., 2001
IL-6	Cytokines	+	+		+	+	7H,7I,7J	Rakoff-Nahoum et al., 2004
IL-1β		+			+	+	7G,7I, 7L	
TNFα		+	+		+	+	7G	
TSLP		+		+		+	7B, 7F	Reardon et al., 2011
HVEM	Cytokine Receptor	+	+		+	+	7M, 7N, 7O	Shui et al., 2011
STAT3	Transcription Regulators		+		+	+	7H, 7I, 7J	Pickert et al., 2009
IRF-1			+		+	+	7M, 7N	
pIgR	IgA receptor	+				+	7G	Hooper et al., 2001
Cyp27B1	Active VD3 synthesis	+	+		+	+	7B, 7D, 7E	Cross et al., 2011
IL-6	**Adaptive Immunity**	+	+		+	+	7H, 7I, 7J	Rakoff-Nahoum et al., 2004
IL-1β		+			+	+	7G,7I, 7L	
TSLP		+		+	— [1]	+	7B, 7F	Reardon et al., 2011
Angiogenin 3	**Gut Angiogenesis**	+				+	7G	Hooper et al., 2001

Table S2B. Microbiota-Dependent Expression of Genes with Known Essential Homeostatic Functions in IEC

Genes	Function	Transcriptional regulation (DBS)			Circadian Expression ZT0>ZT12	Decreased Expression in AIMD mice	Relevant Figures	References[2]
		AP-1 and/or NF-κB	RORE	VDRE				
Bmal1	Circadian Clock		+		+	+	1C,1D 3T, 3U	Bugge et al., 2012
Cry1			+		+	+	1C, 1D 3T, 3U	
E4BP4			+		+	+	1C, 1D, 4A, 4B	
TLR1, 2, 3, 4, 5, 9	Pattern Recognition Receptors (PRRs)		+		+	+	6A,6B, 6C,6D	Takeda and Akira, 2004
NOD2			+		+	+	6A, 6D, 6E,6F	
IRAK4 TIRAP	PRR signal transducers	+	+		+	+	6I, 6J	
CycA2	Control of cell cycle		+		+	+	7M, 7N, 7O	Muller and Engeland, 2010
Cdc25c			+		+	+	7M, 7N, 7O	
AIF (apoptosis inducing factor)	Apoptosis		+		+	+	7M, 7N	Banerjee et al., 2012
ORC1	DNA replication		+		+	+	7M, 7N	Stillman, 2008
PCNA			+		+	+	7M, 7N	
XPA	DNA repair		+		+	+	7M, 7N	Kang et al., 2011
HSP90	Chaperone		+		+	+	7M, 7N, 7O	Den and Lu, 2012
CUL5	Ubiquitin ligase		+		+	+	7M, 7N, 7O	Kamura et al. 2004
Suv 39h1	Transcription regulator		+		+	+	7M, 7N	Grummt and Ladurner, 2008
LRIG1	panERB inhibitor (tumor suppressor)		+		+	+	7M, 7N	Segatto et al., 2011
TGFβRI	Growth factor receptor		+		+	+	7M, 7N	Massague and Xi, 2012
RAF 1	Signal Transduction		+		+	+	7M, 7N	Davis, 2000
SCFA receptor (FFAR3 or GPR41)	Receptor for short chain fatty acid		+		+	+	7M, 7N, 7O	Samuel et al., 2008

— [1]: For these genes the lack of circadian oscillatory expression may reflect a longer half-life of the RNA transcripts

— [2]: See references in the main text and in Supplemental data

Table S5. Measurements of Bacterial Population following Antibiotic Treatment

Note that: The numbers represent the average value of bacterial counts from 8 independent experiments for Control mice and AIMD mice, and 3 independent experiments from AIMD mice treated with LPS in drinking water (as described in Extended Experimental Procedures).

Treatment	Total Bacterial Count	% of Bacteria (16s-QPCR)	Total Aerobic Bacteria	Total Anaerobic Bacteria
Control Mice	$1.3x10^{10}$	100	$0.45x10^{10}$	$0.78x10^{10}$
AIMD Mice	12±22	0.0001	3±6	17±8
AIMD Mice + LPS (in water)	15±20	0.0001	4±8	14±9

Table S6. MyD88-Independent but Microbiota-Dependent Expression of Genes in IEC

Note that: Some of the microbiota dependent genes which have been analysed here, have been previously identified independently by Reikvam et al. 2011 (in antibiotic induced microbiota depleted mice , Hooper et al., 2001 (Germ Free mice) and Larsson et al., 2012 (Germ Free and MyD88 genomic knock out mice) through unbiased microarray analysis.

Genes	Circadian Expression	Expression in AIMD mice	Expression in MyD88iec-/- mice	References
Bmal1	+	Decreased	Unaffected	Figures 1C, 1D, S7E
Cry1	+	Decreased	Unaffected	1C, 1D, S7E
RORα	+	Decreased	Unaffected	1A, 1B, S7E
E4BP4	+	Decreased	Unaffected	1C, 1D, S7E
RevErbα	+	Increased	Unaffected	1A, 1B, S7E
PPARα	+	Increased	Unaffected	1A, 1B, S7F
c-Jun	+	Decreased	Unaffected	5C, 5I, S7F
Cyp11a	+	Increased	Unaffected	3E, 4E, S7F
NOD2	+	Decreased	Unaffected	6A, 6D, 6E
TLR4	+	Decreased	Unaffected	6A, 6B, 6D
FFAR3/GPR41	+	Decreased	Unaffected	7M,7N
Cyp4B1	+	Increased	Unaffected	Reikvam et al.
Cyp2C55	+	Increased	Unaffected	Reikvam et al.
Tef	+	Increased	Unaffected	Reikvam et al.
Caspase14	+	Increased	Unaffected	Reikvam et al.
MT-I	+	Increased	Unaffected	Reikvam et al., Hooper et al.
MT-II	+	Increased	Unaffected	Reikvam et al., Hooper et al.
Cyp27a	+	Increased	Unaffected	Reikvam et al., Hooper et al.
FABP	+	Increased	Unaffected	Reikvam et al., Hooper et al.
GPX2	+	Increased	Unaffected	Reikvam et al.
TGM2	+	Decreased	Unaffected	Reikvam et al.

General discussion and Prospects

Recent studies have established that switching the feeding time in mice from the "active" phase to the "rest" phase, Restricted Feeding (RF), overrides the suprachiasmatic nucleus circadian clock (SCN CC)-derived signals and acts as a *"Zeitgeber"* for peripheral CCs (PCCs), leading to a 12-hour shift in the time at which components of PCCs are expressed. Numerous studies have shown that under homeostatic conditions, the functions of PCCs and metabolism are tightly linked and that perturbations in their interactions lead to metabolic pathologies. The identity of some of the molecular pathways that couple PCCs to metabolism are known, but it is largely unknown how environmental cues, e.g., altered feeding schedules, may directly perturb the expression of individual CC components, thereby leading to obesity and a metabolic syndrome-like pathology. In my thesis work, I have described how in mice a RF regime alters the metabolism due to an initial hypoinsulinemia, which creates a starvation-like state during the "active" phase. Importantly, this hypoinsulinemia leads to an increase in adipose tissue lipolysis leading to a systemic increase in FFA level. There is then a FFA-induced PPARα activation, which not only further reprograms the metabolism, but also results in a temporally aberrant activation of RevErbα expression during the ''active'' phase. Also, this hypoinsulinemia induces an increase in the activity of the GSK3β kinase, which further activates RevErbα. In turn, this aberrant RevErbα activity creates a 12-hour shift of the peripheral circadian clocks, which explains at the molecular level how the feeding time may act as a *"Zeitgeber"* for peripheral clocks. In contrast, the RF-induced early increase in glucagon level during the "active" phase plays a minor role in the PCC shift, through a CREB-induced increase of Per1 and Per2 expression. Most importantly, we found that a glucose administration to RF mice at the beginning of the "active" phase by blocking the reduction of insulin prevented both the metabolic alterations and the PCC shift, thereby establishing that it is the creation of a fasting state which is in fact at the ''origin'' of the RF PCC shift. In this work, I also elucidated the molecular mechanism underlying the RF-induced extra corticosterone production during the "rest" phase, and demonstrated that this "extra corticosterone" indirectly controls PPARα activation in muscle and heart, thereby accounting for the "delayed" of the CCs shift in these tissues. Importantly, through microdissection and in situ hybridization (ISH) techniques, we have demonstrated that the PPARα and glucagon receptors are not expressed in the SCN, thus revealing why the SCN central clock in contrast to the peripheral clocks is not shifted by the RF-altered metabolism. This SCN-insensitivity to RF-generated metabolic alterations leads to

a state of “misalignment” between the timing of expression of the numerous genes which are controlled by the peripheral CCs, and the diurnal “active” and “rest” phases controlled by the SCN CC: the peripheral CC “active” phase genes being expressed during the SCN “rest” phase, whereas the peripheral “rest” phase genes are expressed during the SCN “active” phase. This insensitivity of the SCN CC during a RF starvation-like state is an expected necessity, as the SCN-controlled active phase has to occur during the mouse dark cycle (the human light cycle), even though, due to the misalignment of the PCCs, this active period corresponds to the rest phase in peripheral tissues. This evolutionary design, which maintains the original active phase (wakefulness) in the SCN CC, as well as the rest phase (sleep) during RF-like conditions, is indeed advantageous as it provides the opportunity for a starving organism to efficiently look for food during the normal active phase, thereby increasing the chance to put an end to starvation and to readily realign the PCCs with the unchanged SCN master clock, as soon as feeding is restored. Moreover, we have also elucidated at the molecular level how a prolonged “circadian misalignment” under RF creates metabolic impairments in insulin, TG, FFA, cholesterol, and bile acid metabolism, thereby leading to a metabolic syndrome-like pathological state, consisting of type II diabetes, hypercholesterolemia, hypertriglyceridemia and obesity. Most interestingly all of these alterations are similar to those found in shift workers.

Alterations of the symbiosis between microbiota and intestinal epithelial cells (IEC) are known to be associated with intestinal and systemic pathologies. Interactions between bacterial products (MAMPs) and Toll-like receptors (TLRs) are known to be mandatory for IEC homeostasis, but how TLRs may time homeostatic functions with circadian changes is unknown. Our functional and molecular dissections of the IEC circadian clock demonstrate that its integrity is required for microbiota-IEC dialog. During the first part of my thesis work, I have compared temporal gene expression profiles in IECs from control, Germ-Free (GF) and Antibiotic-Induced Microbiota-Depleted mice (AIMD). Intestinal epithelial cells (IECs) from AIMD mice showed a disrupted circadian expression of several nuclear receptors, including PPARα, RevErbα and RORα, and of components of the circadian clock machinery. Notably, AIMD mice also led to systemic metabolic effects, with mice showing increased blood levels of glucose, triglycerides and free fatty acids, and decreased production of insulin. In this study, I showed that these metabolic disturbances resulted from increased corticosterone synthesis by ileal IECs, which was caused by an increased PPARα expression in these cells. Indeed, AIMD mice with an IEC PPARα selective mutation showed normal regulation of circadian clock

components and did not show any metabolic disturbances. Moreover, I found that the expression of some of the TLRs is under circadian control in IECs. This explains how the microbiota can activate JNK and JUN and represses PPARα in a circadian manner, which acts on the core circadian clock in IECs to disrupt its functioning. The temporal expression of TLRs in IECs was shown to be activated and repressed by the alternate binding of RORα or RevErbα, respectively, to a RORE DBS on their promoters. We also found that a large number of genes that are expressed by IECs contain RORα and RevErbα RORE DBS. Many of these genes involved in homeostatic IEC responses are controlled in a microbiota-dependent circadian fashion. This shows a key role for the microbiota and TLRs in controlling circadian responses in IECs. Such circadian control of IEC responses could be important for coordinating homeostatic IEC functions with behavioral activities in mice. Our study leaves us with several important questions. Firstly is the different type of intestinal epithelial cells, such as enterocytes, Paneth cells and stem cells differ in their regulation of the circadian clock in absence of the microbiota? Is there a specific population of the microbiota which is more specifically involved in the control of the circadian clock in these IECs? What is the physiological importance of corticosterone production in the intestine and its relevance to metabolic alterations associated with its disruption? Recently, Thaiss et al., 2014 demonstrated that the diurnal oscillations for both the composition and the function of the intestinal microbiota are governed by food consumption rhythmicity. Together this work and our study in microbiota suggest that a feedback loop may exist between the diurnal rhythmicity of the host (IEC) and the microbiota with mutual cross regulation of interdependent functions.

Résumé

La séquence des événements moléculaires engendrés par des perturbations de signaux externes qui peuvent affecter les horloges circadiennes, et en conséquence générer des pathologies restait largement inconnue à la fin du 20ème siècle. Durant mon travail de thèse, j'ai démontré au niveau moléculaire, comment déplacer l'horaire de l'alimentation chez la souris en inversant la prise de nourriture de la phase ''active'' à la phase de ''repos'' (Restricted Feeding : RF), conduit à une altération du métabolisme à la suite d'une hypoinsulinémie immédiatement au début de la phase ''active'', ce qui provoque une libération accrue d'acides gras libres (FFA) dans le sang et une activation du récepteur nucléaire PPARα qui reprogramme à la fois le métabolisme et l'expression de RevErbα. En outre, une hypoinsulinémie permanente crée une activation aberrante de la kinase GSK3β qui stabilise la protéine RevErbα, en la phosphorylant, pendant la phase '' active''. Il s'en suit une répression de l'expression des gènes contenant des éléments de liaison DNA RORE notamment des gènes codant pour des protéines appartenant à l'horloge circadienne, qui de ce fait est décalée de 12 heures dans les tissus périphériques.
Nous avons notamment montré qu'en raison de l'absence de PPARα dans les neurones du noyau suprachiasmatique (NSC) de l'hypothalamus l'horloge centrale est ''immunisée'' contre un tel décalage, ce qui explique qu'elle ne soit décalée durant le régime alimentaire ''RF''. Ainsi, les phases d''activité'' et de ''repos'' de la souris qui sont contrôlées ne sont pas ''alignées'' par l'horloge centrale et l'expression des gènes contrôlée par les horloges périphériques pendant un régime ''RF'' prolongé. Ce non-alignement crée un syndrome métabolique pathologique similaire à celui observé chez des individus soumis à des horaires de travail décalés.

Horloge circadienne, Régime alimentaire décalé, Altérations métaboliques, RevErbα, PPARα, Non-alignement des horloges circadiennes, Travail décalé, Syndrome métabolique

Abstract

The sequence of molecular events through which alterations in externals cues may impinge on circadian clocks, and generate pathologies, was mostly unknown at the end of the 20th century. During my thesis work, I have molecularly deciphered, how switching feeding in mice, from the "active" to the "rest" phase, immediately alters the metabolism through hypoinsulinemia during the "active" phase, leading to increased FFA levels and PPARα activity, thereby reprograming both metabolism and RevErbα expression. Moreover, the hypoinsulinemia aberrantly activates the GSK3β activity that, through phosphorylation, stabilizes RevErbα during the "active" phase, thereby maintaining a CC-shift. This results in transrepression of RORE DBS containing genes, including of CC components, consequently leading to a 12 hours circadian clock-shift in peripheral tissues.
Most notably, we also found that the lack of PPARα expression in the neurons of the suprachiasmatic nuclei (SCN) in hypothalamus prevents a shift of the central circadian clock. Similarly, the "activity" and "rest" phases are not shifted during a RF regime. Thus, the "active" and "rest" diurnal phases controlled by the SCN central circadian clock and gene expression controlled by the peripheral circadian clocks (PCCs) are misaligned during a long-term Restricted Feeding (RF). Most interestingly, this misalignment generates a metabolic syndrome-like pathology, similar to that associated with shiftwork schedules.

Circadian clocks, Shifted eating, Metabolic alterations, RevErbα, PPARα, Circadian clocks misalignment, Shift work, Metabolic syndrome